JUSTUS-LIEBIG-
UNIVERSITÄT
GIESSEN

Spatiotemporal regulation of polar flagellar assembly, chemotaxis and c-di-GMP-dependent signaling in γ-proteobacteria

---

Dissertation

zur Erlangung des Doktorgrades der Naturwissenschaften

(Dr. rer. nat.)

vorgelegt von

Lisa Marie Schmidt

angefertigt am Institut für Mikrobiologie und Molekularbiologie

Fachbereich 08 - Biologie und Chemie

der Justus-Liebig-Universität Giessen

Giessen, März 2026

1. Reviewer **Prof. Dr. Kai M. Thormann**
Institute for Microbiology and Molecular Biology
Faculty 08, Biology and Chemistry, Justus Liebig University Giessen

2. Reviewer **Prof. Dr. Till F. Schäberle**
Institute for Insect Biotechnology
Faculty 09, Agricultural Sciences, Nutritional Sciences, and Environmental Management, Justus Liebig University Giessen

Table of contents

I. Publications

Selected results from this doctoral work have been published in the following publications:

*Dornes, Anita; ***Schmidt, Lisa Marie**; Mais, Christopher-Nils; Hook, John C,; Pané-Farré, Jan; Kressler, Dieter; Thormann, Kai; Bange, Gert (2024) Polar confinement of a macromolecular machine by an SRP-type GTPase. *Nature Communications* 15:5797. DOI: 10.1038/s41467-024-50274-4.

***Schmidt, Lisa Marie**; *Pulido-Sánchez, Marta; Treuner-Lange, Anke; Zehner, Lukas; López-Sánchez, Aroa; Cava, Felipe, Govantes, Fernando; Thormann, Kai M. (2026) Functional characterization of the polar organizer FimV in *Pseudomonas putida*. *Journal of Bacteriology* 208:2. DOI: 10.1128/jb.00497-25.

*equal contribution

II. Abbreviations

aa	Amino acids
Amp	Ampicillin
AP	Alkaline phosphatase
APS	Ammonium peroxydisulfate
ATP	Adenosine triphosphate
ATPase	Adenosine triphosphatase
AU	Arbitrary units
BACTH	Bacterial adenylate cyclase two-hybrid
c-di-GMP	Bis-(3'-5')-cyclic dimeric guanosine monophosphate
C-ring	Cytoplasmic ring
Cam	Chloramphenicol
CCW	Counterclockwise
cGMP	Cylic guanosine monophosphate
CV	Column volumes
CW	Clockwise
DAP	2,6-diaminopimelic acid
ddH_2O	Double distilled water
DGC	Diguanylate cyclase
DMSO	Dimethyl sulfoxide
DNA	Deoxyribonucleic acid
EDTA	Ethylenediaminetetraacetic acid
EtOH	Ethanol
fT3SS	Flagellar type III secretion system
fwd	Forward
GDP	Guanosine diphosphate
Gent	Gentamycin
GLB domain	Immunoglobulin-like domain
GMP	Guanosine monophosphate
GTP	Guanosine triphosphate
GTPase	Guanosine triphosphatase
I-box	Insertion box
IPTG	Isopropyl-β-D-thiogalactopyranosid
ipTM	Interface predicted template modeling
Kan	Kanamycin
L-ring	Lipopolysaccharide ring
LB	Lysogeny broth
LysM	Lysin motif
MCP	Methyl-accepting chemotaxis protein
min	Minutes
OD_{600}	Optical density at 600 nm
P-ring	Peptidoglycan ring
PAC	PAS-associated C-terminal
Par system	Partitioning system
PAS	Per-Arnt-Sim
PCR	Polymerase chain reaction
PDE	Phosphodiesterase
pGpG	5' phosphoguanylyl-(3'-5')-guanosine

PI	Isoelectric point
pLDDT	Predicted local distance difference test
pTM	Predicted template modeling
PVDF	Polyvinylidene difluoride
REC	Receiver
rev	Reverse
rpm	Rounds per minute
SDS	Sodium dodecyl sulphate
sec	Seconds
SRP	Signal recognition particle
Strep	Streptomycin
TEMED	Tetrametyl ethylendiamine
TPR	Tetratricopeptide
v/v	volume per volume
w/v	weight per volume
X-Gal	X-galactosidase

III. Abstract

Bacterial motility is a fundamental trait that enables cells to explore their environment and respond to, as well as relocate to, more favorable growth conditions. In many species, motility is achieved by rotating flagellar filaments whose activity is controlled by the chemotaxis system, allowing bacteria to navigate along chemical gradients. In addition to this planktonic lifestyle, bacteria can transition to a sessile state, characterized by surface attachment and biofilm formation. This transition is generally regulated by intracellular second messenger molecules, such as c-di-GMP, with elevated levels promoting a sessile lifestyle by stimulating biofilm formation while simultaneously repressing motility. Consequently, coordination between chemotaxis and second messenger signaling is crucial for balancing motility and surface-associated growth in these bacteria.

In this work, the spatiotemporal regulation of polar flagellar assembly, chemotaxis, and c-di-GMP-dependent signaling was investigated in species of the genera *Shewanella* and *Pseudomonas*. In *S. putrefaciens*, polar flagellar assembly was shown to depend on an interaction between the polar landmark protein FlhF and the flagellar C-ring component FliG, mediated by the N-terminal domain of FlhF, termed FID. Furthermore, FlhF was demonstrated to restrict FliG recruitment to the cell pole, through its simultaneous interaction with FliG and HubP. In addition, the function of the HubP homolog FimV was investigated in *P. putida*. FimV was shown to localize to the cell pole, depending on the presence of both a LysM-like domain and an immunoglobulin-like domain. While deletion of *fimV* did not affect flagellation, chromosome segregation, or pilus-mediated motility, FimV was required for correct positioning of the chemotaxis system and efficient swimming motility in *P. putida*. Domain exchange experiments between HubP and FimV from *S. putrefaciens* and *P. putida* revealed species-specific functions, indicating distinct adaptations to their respective environments. Moreover, the interaction between the histidine kinase CheA and the phosphodiesterase Pch was investigated in *P. putida*. Both proteins exhibited polar localization, and their interaction was shown to be mediated by the EAL domain of Pch and a specific region within the unstructured linker region of CheA. While the polar localization of Pch strongly depended on CheA, CheA localization depended on FlhF, PocB, and ParP, and, to a lesser extent, on FimV. Sequence conservation analysis revealed a specialized amino acid sequence of the Pch EAL domain compared to canonical EAL domains, as well as five highly conserved regions within the CheA linker region. This suggests an evolutionarily conserved interaction interface between CheA and Pch, linking chemotaxis and c-di-GMP signaling.

Collectively, these results provide new insights into the spatiotemporal organization of flagellar assembly and chemotaxis signaling, highlighting the role of polar organizer proteins and signaling components in coordinating bacterial motility and transitions between motile and sessile states.

IV. Zusammenfassung

Die bakterielle Motilität ist eine grundlegende Eigenschaft, die es Zellen ermöglicht, ihre Umgebung zu erkunden und auf veränderte Bedingungen zu reagieren. Bei vielen Arten wird die Motilität durch rotierende Flagellen vermittelt, deren Aktivität von dem Chemotaxis-System gesteuert wird, wodurch Bakterien entlang chemischer Gradienten navigieren können. Zusätzlich zu dieser planktonischen Lebensweise können Bakterien in einen sessilen Zustand übergehen, der durch Oberflächenanheftung und Biofilmbildung gekennzeichnet ist. Dieser Übergang wird im Allgemeinen durch intrazelluläre Sekundärbotenstoffe wie c-di-GMP reguliert, wobei erhöhte Konzentrationen eine sessile Lebensweise fördern, indem sie die Biofilmbildung stimulieren und gleichzeitig die Motilität unterdrücken. Folglich ist die Koordination zwischen Chemotaxis und c-di-GMP-abhängiger Signalübertragung entscheidend für das Gleichgewicht zwischen Motilität und oberflächengebundenem Wachstum bei diesen Bakterien.

In dieser Arbeit wurde die räumliche und zeitliche Organisation der Flagellen-Bildung, Chemotaxis und c-di-GMP-abhängigen Signalübertragung bei Spezies der Gattungen *Shewanella* und *Pseudomonas* untersucht. Bei *S. putrefaciens* zeigte sich, dass der Aufbau der polaren Flagellen von einer Interaktion zwischen dem polaren „*landmark protein*“ FlhF und der flagellaren C-Ring-Komponente FliG abhängt, die durch die als FID bezeichnete N-terminale Domäne von FlhF vermittelt wird. Außerdem wurde nachgewiesen, dass FlhF die Rekrutierung von FliG an den Zellpol bindet, indem es gleichzeitig mit FliG und HubP interagiert. Darüber hinaus wurde die Funktion des HubP-Homologs FimV in *P. putida* untersucht. Es zeigte sich, dass sich FimV am Zellpol anreichert, was sowohl von der Anwesenheit einer LysM-ähnlichen Domäne, als auch einer Immunoglobulin-ähnlichen Domäne abhängt. Während die Deletion von *fimV* weder die Flagellierung, noch die Chromosomensegregation oder die Pilus-vermittelte Motilität beeinträchtigte, war FimV für die korrekte Positionierung des Chemotaxis-Systems und die effiziente Schwimmmotilität in *P. putida* erforderlich. Experimente, bei denen Domänen zwischen HubP und FimV aus *S. putrefaciens* und *P. putida* ausgetauscht wurden, zeigten artspezifische Eigenschaften beider Proteine, was auf eine Anpassung an unterschiedliche Umweltbedingungen hindeutet. Außerdem wurde die Interaktion zwischen der Histidinkinase CheA und der Phosphodiesterase Pch in *P. putida* untersucht. Beide Proteine wiesen eine polare Lokalisierung auf, und es zeigte sich, dass ihre Interaktion durch die EAL-Domäne von Pch und eine spezifische Region innerhalb der unstrukturierten Linker-Region von CheA vermittelt wurde. Während die polare Lokalisierung von Pch stark von CheA abhängig war, hing die Lokalisierung von CheA von FlhF, PocB und ParP sowie in geringerem Maße von FimV ab. Eine Sequenzkonservierungsanalyse ergab eine, im Vergleich zu kanonischen EAL-Domänen, spezialisierte Aminosäuresequenz der Pch-EAL-Domäne, sowie fünf hochkonservierte Regionen innerhalb der Linker-Region von CheA. Dies deutet auf eine evolutionär konservierte

Interaktionsschnittstelle zwischen CheA und Pch hin, die Chemotaxis und c-di-GMP-Signalweg miteinander verbindet.

Diese Ergebnisse geben neue Einblicke in die zeitlich-räumliche Organisation von Flagellenaufbau und Chemotaxis-Signalübertragung und zeigen, wie polare Organisator-Proteine und Signalproteine die bakterielle Motilität sowie den Übergang zwischen einem motilen und sessilen Lebensstil koordinieren.

1. Introduction

Motility is one of the fundamental characteristics of living organisms. It enables cells to respond to environmental stimuli, for example by moving toward favorable conditions or away from harmful ones. In bacteria, motility allows cells to navigate chemical gradients and locate optimal habitats while avoiding toxic compounds. In addition, motility plays an important role in bacterial pathogenicity and, therefore, represents a potential target for antibacterial therapies.

1.1 Motility in bacteria

Bacterial cells are widespread, colonizing diverse environments ranging from extreme habitats such as the deep sea to the tissues of humans and other living organisms. Motility is a fundamental adaptive trait that enables bacteria to actively navigate their surroundings in response to chemical and physical stimuli. This capability is crucial for nutrient acquisition, host colonization, and avoidance of harmful conditions [1,2]. While such traits can be beneficial - for instance, microbial symbionts play essential roles in the human gut microbiome and overall health [3] - bacterial motility also poses significant challenges. In many pathogenic species, motility contributes directly to virulence [4]. For example, the motility of uropathogenic *Escherichia coli* enhances the progression of urinary tract infections [5], and colonization of the human stomach by *Helicobacter pylori* heavily depends on its motility [6]. Understanding the mechanisms underlying bacterial motility is, therefore, critical for identifying potential targets for interventions against pathogenesis.

In their free-living state, bacteria primarily exhibit two types of motility. Firstly, swimming motility allows cells to move through liquid environments. Secondly, surface-associated motility enables movement across solid substrates, often through a variety of mechanisms [7,8]. Many bacterial species possess multiple of these motility mechanisms, allowing them to dynamically respond to changing environmental conditions.

1.2 Flagellum-mediated swimming motility

The most widespread mechanism of bacterial motility is mediated by a long, thin, helical appendage known as the flagellum. Flagella are complex rotary nanomachines that convert ion gradients into mechanical rotation [9]. This rotation of the flagellum propels the bacteria forward while simultaneously causing a counter-rotation of the cell body, which guides the bacteria through liquid environments and enables directed movement along chemical gradients.

1.2.1 Bacterial flagellation variety

Bacterial flagellation exhibits a wide variety of patterns, differing in both the number and spatial arrangement of flagella (**Figure 1A**). Many bacteria, such as *Pseudomonas aeruginosa*, possess a single flagellum, a configuration known as monotrichous flagellation. This flagellum is typically

located at one end of the cell, referred to as a polar flagellum, though it can occasionally appear at non-polar positions [10]. Other bacteria harbor multiple flagella, either clustered at one pole (lophotrichous flagellation), as observed in *Pseudomonas putida*, or at both poles (amphitrichous flagellation), as seen in *Campylobacter jejuni* [11,12]. In contrast, *E. coli* displays peritrichous flagellation, with several flagella distributed randomly along the cell body [13].

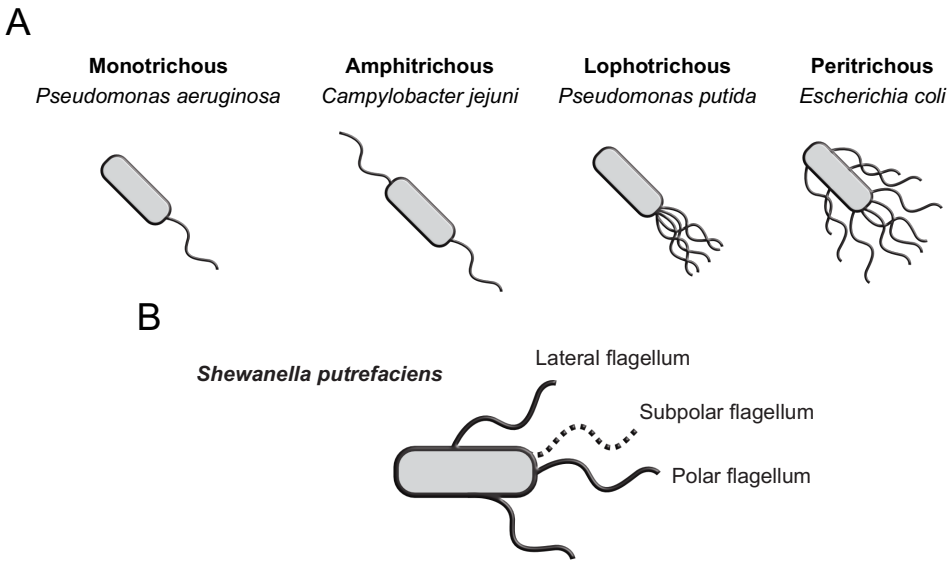

Figure 1. Bacterial flagellation patterns. A Schematic representation of common bacterial flagellation patterns and representative example organisms. Monotrichous flagellation is characterized by a single flagellum, typically located at one end of the cell (cell pole), as observed in *P. aeruginosa*. Amphitrichous flagellation describes the presence of flagella at both cell poles, independent of the total number of flagella, and is found, for example, in *C. jejuni*. *P. putida* exhibits a lophotrichous flagellation pattern, characterized by multiple flagella located at one cell pole. In contrast, peritrichous flagellation, typical for *E. coli*, consists of several flagella distributed around the entire cell body. **B** Flagellation of *S. putrefaciens*. Under standard conditions, *S. putrefaciens* cells possess a single polar flagellum that enables swimming motility. If the flagellum assembles adjacent to the pole, this positioning is referred to as subpolar localization. Under certain conditions, cells can additionally produce multiple lateral flagella, which facilitate movement through more complex or structured environments. Adapted from [14].

Some bacteria exhibit combinations of the flagellation patterns described above. For instance, the marine bacterium *Shewanella putrefaciens* possesses two distinct flagellar systems [15]. Under standard conditions, such as liquid cultivation of *S. putrefaciens*, cells produce a single polar flagellum, enabling swimming motility in this environment [16]. In more structured environments, such as those with increased viscosity, the bacterium can develop up to five lateral flagella, which enhance swimming performance by improving directional persistence [17,18]. Occasionally, the polar flagellum is positioned slightly off the cell pole, a configuration referred to as subpolar flagellation (**Figure 1B**).

Apart from extracellular flagella, some bacteria possess flagella located within the periplasmic space. These endoflagella, characteristic of spirochetes, rotate internally and generate a corkscrew-like motion of the entire cell [19]. This unique motility is crucial for virulence, as it enables spirochetes to penetrate host tissues, disseminate systemically, and establish infections [20,21].

1.2.2 Structure of the bacterial flagellum

The bacterial flagellum can be generally divided into three main structural components [8,22]. Firstly, the basal body, which is embedded in the cell membranes. Secondly, the hook, acting as a universal joint; and finally, the filament, which forms the long, helical propeller (**Figure 2**).

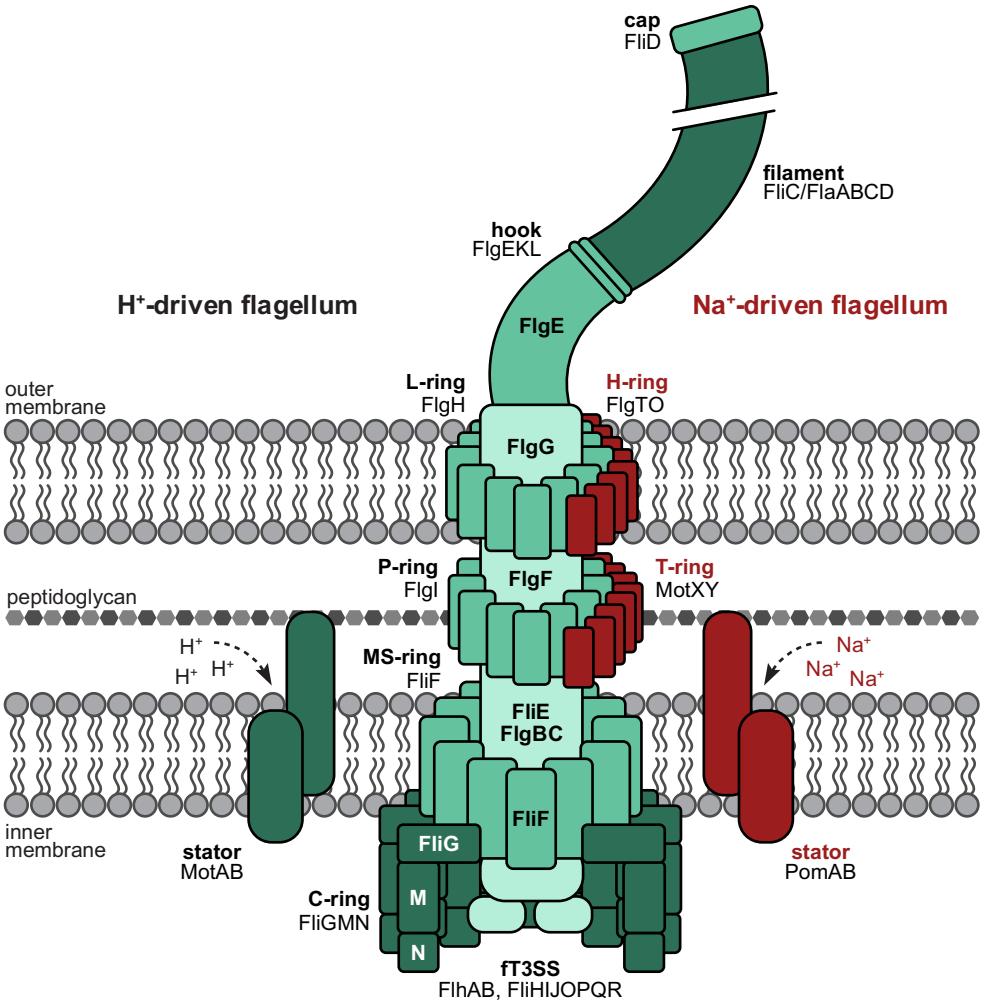

Figure 2. Structure of the bacterial flagellum. Schematic representation of the bacterial flagellum, including its ring structures and associated proteins. Components specific to Na+-driven flagellar motors are highlighted in red. fT3SS: flagellar type III secretion system. Adapted from [23,24].

Starting with the basal body, it serves as the engine of the entire flagellar machinery and has been best studied in *E. coli* and *Salmonella enterica*. It is composed of a cytoplasmic ring (C-ring), an oligomeric structure formed by the proteins FliG, FliM and FliN [25], which enables rotation of the flagellum in either counterclockwise (CCW) or clockwise (CW) directions [26]. The C-ring is connected to the membrane/supramembrane ring (MS-ring), which is composed of multiple copies of FliF anchored in the cytoplasmic membrane [27,28]. Surrounding the MS-ring are inner membrane-embedded, ion-specific stator units that use the electrochemical potential to create a torque and drive flagellar rotation by transferring the torque to the C-ring. For instance, rotation can be powered by protons (H^+), as is common in *E. coli* or *Salmonella* via the MotA and MotB stators [29–32]. Some species, such as *P. aeruginosa*, contain a second H^+-dependent stator complex,

MotC and MotD, which provide more stable motor speed [33]. Alternatively, certain bacteria, including *Vibrio* and *Shewanella* species, use the sodium (Na^+)-driven stators PomA and PomB [34–36].

Moreover, the basal body contains a rod composed of FliE, FlgB, FlgC, FlgF and FlgG, which spans the entire periplasm and is connected to a ring embedded in the peptidoglycan (P-ring) as well as a lipopolysaccharide ring (L-ring) embedded in the outer membrane in Gram-negative bacteria [37]. The LP-rings, formed by FlgH and FlgI, act as a molecular bushing that stabilizes the flagellar rod, allowing rapid rotation with minimal friction within the bacterial cell envelope [38]. Some bacterial species with Na^+-driven flagellar motors, such as *Vibrio* and *Salmonella*, possess additional rings, the H- and T-rings, that further stabilize the flagellar motor and facilitate proper stator assembly and torque generation. The H-ring, composed of FlgT and FlgO, assists in outer membrane penetration [39], whereas the T-ring, formed by MotX and MotY, interacts with the stator units to enable high-speed rotation [40]. This structural arrangement allows *Vibrio* to reach rotational speeds of up to 1700 Hz, compared to approximately 300 Hz in *Salmonella* [41,42].

For the assembly and export of flagellar components outside the cell, the basal body contains a flagellar protein-export apparatus, which is based on a type III secretion system (fT3SS) [43]. This apparatus forms a narrow channel of approximately 2.5 nm in diameter and is composed of a transmembrane export complex, including FlhA, FlhB, FliO, FliP, FliQ and FliR, together with a cytoplasmic adenosine triphosphatase (ATPase) complex, consisting of FliI, FliH and FliJ [23,44,45].

The flexible hook is composed of multiple copies of the FlgE protein, which transmits torque from the basal body to the filament, together with the hook-associated proteins FlgK and FlgL, forming the structural junction between hook and filament [46,47]. The length of the hook is controlled by the proteins FlhB and FliK [48]. The flagellar filament is a hollow helical structure approximately 20 nm in diameter and 10-15 µm in length, consisting of around 20,000 copies of flagellin proteins [45,49,50]. While species such as *E. coli* or *Pseudomonas* contain a single flagellin, FliC, other bacteria, including *Vibrio cholerae* and *S. putrefaciens*, possess multiple flagellins that can form the filament [51–54]. At the tip of the filament, the FliD protein forms a cap that promotes filament elongation by facilitating the incorporation and polymerization of flagellin subunits [55,56].

1.2.3 Transcriptional control of flagellar assembly

Production and operation of flagella represent a substantial investment for the bacterial cell. To coordinate this complex and energy-intensive network, at least 50 genes are involved in this tightly regulated transcriptional control. Flagellar assembly follows a strict hierarchical order, with the temporal expression of genes coupled to the progress of flagella biogenesis [57]. Components

required in later stages are therefore only expressed once earlier assembly steps are completed. This sophisticated regulatory network is best characterized in peritrichously flagellated species such as *E. coli* and *Salmonella typhimurium* [58]. While the general hierarchy of gene expression is broadly conserved, distinct differences exist among bacterial species. For instance, *E. coli* and *S. typhimurium* employ a three-tiered gene expression program, whereas flagellar biogenesis in *P. aeruginosa* follows a four-stage regulatory cascade [58,59]. The genes responsible for flagellar assembly are organized in operons and controlled by distinct classes of promoters, allowing differential transcription initiation through the activity of alternative sigma factors [60]. Initially, genes encoding regulatory proteins are expressed, which orchestrate the overall flagellar regulon. Transcription of these early genes is typically mediated by transcriptional activators, such as FlrA in *S. putrefaciens* (referred to as FleQ in *Pseudomonas*), in conjunction with sigma factor σ^{54}. Subsequently, genes encoding structural components of the basal body, hook and the fT3SS are expressed. Finally, genes are transcribed that encode flagellin proteins and, in some species other than *Shewanella*, motor-stator components and chemotaxis proteins. Expression of these late genes is generally dependent on sigma factor σ^{28}, also known as FliA [53,57].

In most bacteria, the number of flagella is tightly controlled by the MinD-type ATPase FlhG (referred to as FleN in *Pseudomonas*), which links assembly of the flagellar C-ring to transcriptional regulation [61]. FlhG interacts with the motor switch protein FliM independently of its nucleotide-bound state. In addition, the transcriptional activator FlrA/FleQ binds to the ATP-bound FlhG homodimer, stimulating its ATPase activity. By coordinating transcriptional regulation with the progress of flagellar assembly, this regulatory mechanism ensures the precise numerical control of flagellar biogenesis.

1.2.4 Differences in bacterial swimming behaviors

As previously mentioned, bacteria exhibit a variety of flagellation patterns, and the composition of their flagellar machineries can differ between species. Consequently, swimming behaviors and speeds vary widely, depending on the number and structure of the flagella. For instance, actively predatory *Bdellovibrio bacteriovorus* cells, which possess a single polar flagellum, can reach swimming speeds of up to 160 µm per second, whereas peritrichously flagellated *E. coli* cells typically swim at 25-35 µm per second [62,63]. Moreover, *E. coli* exhibits the characteristic run-and-tumble behavior, alternating between straight runs and random reorientation events (called “tumbles”) that occur when the flagellar rotation switches from CCW to CW, disrupting the flagellar bundle [64]. In contrast, monotrichously flagellated species such as *Vibrio* perform run-reverse-flick motility, in which a forward run is followed by motor reversal driving backward movement, and a subsequent rapid flick, caused by buckling of the flagellar hook, reorients the cell into a new direction [65].

1.3 Surface-associated motility types

In addition to swimming in liquid environments, many bacteria are capable of moving across solid surfaces, a process referred to as surface motility. This type of movement relies on specialized mechanisms, including swarming, twitching, or gliding motility, which depend on different extracellular structures or compounds produced by the cells. Surface motility is crucial for processes such as biofilm formation, host colonization, and adaptation to environmental conditions [8,66].

1.3.1 Flagellum-mediated swarming motility

One example of flagella-mediated surface motility is swarming. Swarming motility is a rapid, collective movement of cells across a surface and was first described in *E. coli*. This type of motility typically occurs under highly viscous conditions, such as agar concentrations above 0.45%, whereas swimming motility predominates at lower concentrations [7]. Cells transitioning from swimming to swarming often exhibit changes in morphology or flagellation [8,66]. In most species, swarming also relies on the production of surface-active agents (short: surfactants), such as rhamnolipids in *P. aeruginosa* [67,68]. Surfactants are amphipathic molecules that reduce surface tension and facilitate rapid surface movement. However, surfactant production is not universally required for swarming, as some species can swarm on media where surfactants are already present in the agar or not needed, depending on the agar composition [69,70].

1.3.2 Type IV pilus-mediated twitching motility

Twitching motility describes a surface-attached, jerky type of movement exhibited by individual bacterial cells. Forward movement is achieved through the extension, attachment and retraction of protein fibers, known as type IV pili [71,72]. While twitching has been studied in several model organisms, *P. aeruginosa* remains the best-characterized system. Twitching occurs on solid surfaces, as can be observed on agar with concentrations of at least 1%. Here, cells generally move at slow velocities that depend on nutrient availability, surface hydrophobicity or medium viscosity. For instance, *P. aeruginosa* develops a twitching zone of roughly 2 cm in diameter after 20 hours of incubation, corresponding to an average velocity of around 1 mm per hour [71,73,74].

1.3.2.1 Structure of the type IV pilus

Generally, type IV pili are dynamic, filamentous structures approximately 5-7 nm in width that can extend several µm in length and are often localized at the bacterial cell pole [75]. Their architecture closely resembles that of the type II secretion system, which translocates proteins from the periplasm to the extracellular space [76]. In the case of pili, pilin subunits are similarly exported and assembled outside the cytoplasmic membrane, analogous to the secretion and polymerization of flagellin subunits during flagellum formation.

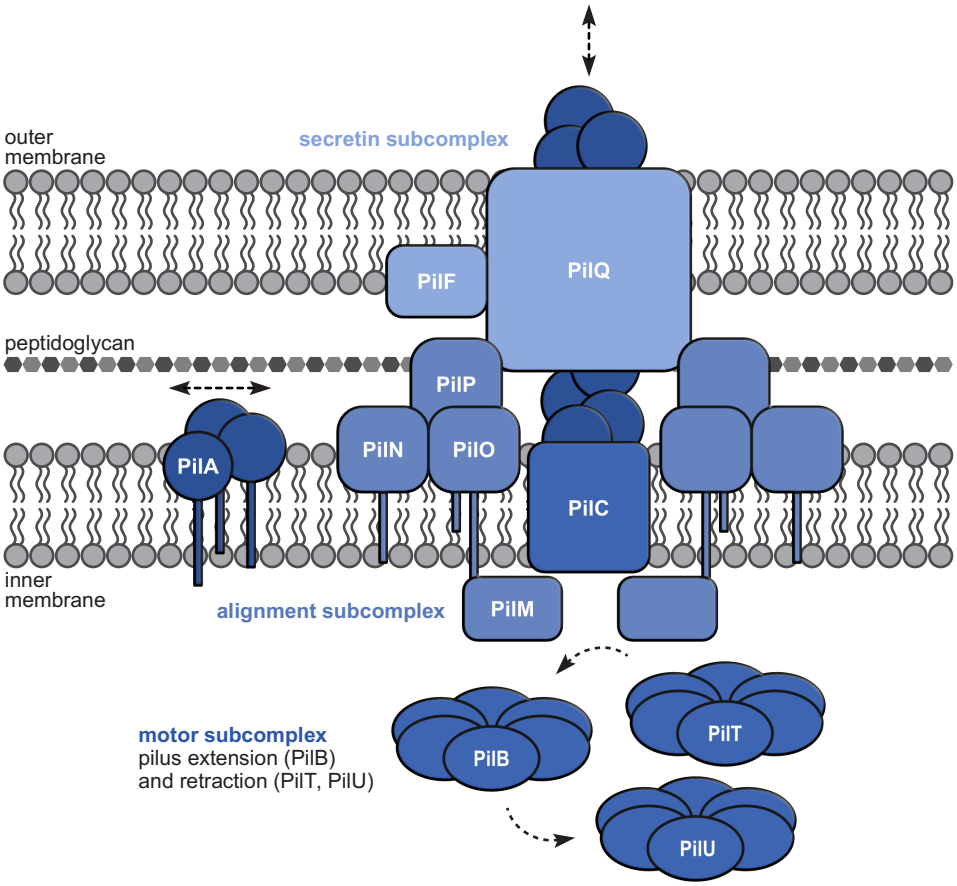

Figure 3. Structure of the bacterial type IVa pilus from *P. aeruginosa*. Schematic representation of the bacterial type IVa pilus. Proteins are color-coded according to the subcomplex to which they belong. The extension and retraction of the pilus is mediated by the dynamic exchange of the ATPases PilB and PilT/PilU engaged to PilC. Adapted from [71,77,78].

Type IV pili are classified into type IVa and type IVb subclasses, which differ in pilin structure, genetic organization, and function. Type IVa pili are primarily involved in twitching motility and deoxyribonucleic acid (DNA) uptake, whereas type IVb pili are mainly associated with host colonization and virulence [79–81]. The type IVa pilus machinery consists of four main components (**Figure 3)**. The first component is the secretin subcomplex in the outer membrane, comprising the PilQ pore, through which the pilus is assembled and disassembled, together with the lipoprotein PilF that tethers PilQ to the outer membrane [82,83]. The second component is the motor subcomplex in the inner membrane, consisting of the platform protein PilC and the cytoplasmic hexameric ATPases PilB and PilT/PilU, which convert chemical energy to mechanical work to drive pilus extension and retraction, respectively [84–87]. As the third component the cage-like alignment subcomplex, composed of PilM, PilN, PilO and PilP, connects the secretin to the motor through interaction of PilP with PilQ [88,89]. The final component is the helical pilus filament, which is primarily built from inner membrane-anchored major pilin subunits such as PilA, with additional minor pilin-like proteins contributing to filament assembly and function, like PilE or FimU in *P. aeruginosa* [90–93]. Those subunits are inserted as precursor pilins into the inner membrane and are processed by the prepilin peptidase PilD to mature pilin subunits [77,94]. In addition to the core structural components, a

further noteworthy signaling complex, composed of the proteins PilG, PilH, PilI, PilJ, PilK and PilL, enables cells to regulate twitching motility in response to environmental cues [95–98].

1.3.3 Other surface-dependent motility types

Besides twitching and swarming, bacteria exhibit additional surface-dependent types of motility, such as sliding and gliding. In the case of sliding, no extracellular structures appear to be involved in this type of surface translocation; rather, it is driven by the expansive forces of growing bacterial cultures [7]. Gliding, in contrast, is defined as the movement of non-flagellated cells and is thought to be facilitated by several mechanisms, including specialized motor structures or the production of surface compounds [66,99]. Moreover, some forms of motility do not fit neatly into these categories. For instance, a pilus-dependent motility was observed in *P. putida*, occurring only between 18-28°C, below the organism's optimal growth temperature of 30°C. This motility is phenotypically similar to swarming but has also been reported in *fliC* deletion mutants [100].

1.4 The bacterial chemotaxis system

Besides self-propulsion, the ability to sense and respond to environmental stimuli is equally important. The bacterial chemotaxis system enables cells to navigate chemical gradients, moving toward favorable conditions while avoiding harmful stimuli, and has been best characterized in *E. coli*. This behavior is mediated by a highly conserved signal transduction pathway that links environmental sensing to changes in flagellar rotation [101,102]. Most of these pathways are based on two-component systems, such as the histidine-aspartate phosphorelay, which consists of a dimeric histidine kinase and at least one response regulator.

The process is initiated by the uptake of chemoattractants or repellents through porins into the periplasmic space (**Figure 4**). Signal recognition is mediated by membrane-bound methyl-accepting chemotaxis proteins (MCPs), which span the inner bacterial membrane [103]. These homodimeric transmembrane proteins consist of periplasmic ligand-binding domains and cytoplasmic signaling domains [102,104,105]. MCPs are frequently organized into "trimers of dimers" that cluster at the cell pole, with the number of different MCPs varying among species - from five in *E. coli* to over 60 in *Magnetospirillum magnetotacticum* [106–108]. Upon ligand binding, MCPs perceive external stimuli and transmit signals to the cytoplasmic histidine kinase CheA, which is associated with MCPs via the adaptor protein CheW. At high attractant concentrations, CheA is maintained in a non-phosphorylated, inactive state. Simultaneously, the constitutively active methyl transferase CheR increases methylation of the MCPs, enhancing their capacity to stimulate CheA autophosphorylation [109,110].

If attractant binding decreases, autophosphorylation of a conserved histidine residue of CheA is stimulated. The resulting phosphoryl group can then be transferred to two different response

regulators: CheB or CheY [111]. CheB functions as a methylesterase that controls the adaption of the MCPs. Phosphorylation of CheB increases its methylesterase activity, leading to enhanced demethylation of the MCPs [112,113]. As a result, MCPs exhibit a reduced ability to stimulate CheA autophosphorylation, even at low attractant concentrations, allowing fine-tuned regulation of the system [114,115]. Alternatively, the phosphoryl group can be transferred to CheY, a protein that interacts with the flagellar motor. Phosphorylated CheY binds to the flagellar switch proteins FliM and FliN, inducing a switch in flagellar rotation from CCW to CW [116–119]. This CW rotation ultimately leads to tumbling or reverse-flick behavior, enabling the bacterial cells to reorient [64,65]. Spontaneous dephosphorylation of CheY is facilitated by the phosphatase CheZ [120].

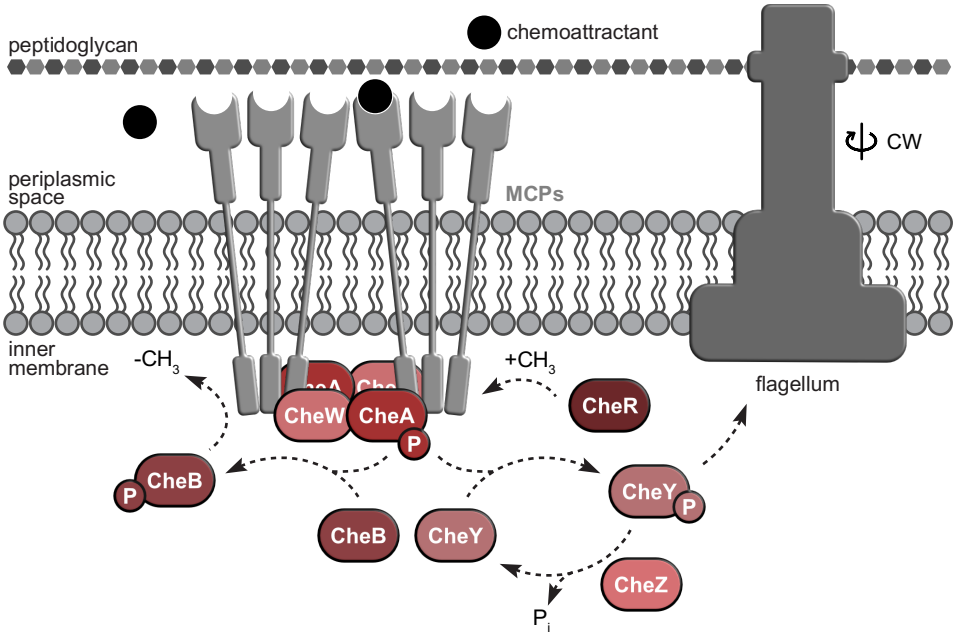

Figure 4. Chemotaxis signaling pathway of *E. coli*. Schematic representation of chemotaxis signal transduction under low chemoattractant concentrations. Following autophosphorylation of CheA, the phosphoryl group is transferred either to CheB, which demethylates the methyl-accepting chemotaxis proteins (MCPs), or to CheY. Phosphorylated CheY subsequently interacts with the flagellar motor switch complex and induces a change from counterclockwise to clockwise (CW) rotation. CheR constitutively methylates MCPs, whereas CheZ dephosphorylates CheY. Adapted from [101,121].

Although the chemotaxis system of many bacterial species is broadly similar to that of *E. coli*, some species possess significantly more complex systems due to an increased number of involved proteins and receptors. For instance, several bacteria encode multiple *cheA* homologs within their genomes [122–124].

1.4.1 Histidine kinase CheA

The histidine kinase CheA is a dimeric kinase that forms a central component of the chemotaxis receptor complex, acting as the main signal transducer in the pathway. Upon stimulation of the receptors, CheA autophosphorylates at a conserved histidine residue and subsequently transfers the phosphoryl group to the response regulators CheY and CheB. This phosphorylation cascade regulates both flagellar motor switching and receptor adaptation, allowing bacterial cells to navigate chemical gradients effectively [102,104].

The canonical CheA is composed of five main structural domains. The P1 domain, also called the histidine phosphotransfer (Hpt) domain, contains the conserved phosphorylatable histidine residue H48. The P2 domain binds response regulators and, in some species, features an unstructured linker region. The P3 domain mediates dimerization of the protein, while the P4 domain encompasses the catalytic histidine kinase activity. Finally, the P5 domain, also referred to as the CheW-like or regulatory domain, controls kinase activity and binds to MCPs [101,125,126].

It has been shown that a CheA variant lacking the histidine phosphorylation site is still capable of supporting phosphorylation of a second CheA variant with a defective histidine kinase domain, thereby revealing the mechanism of trans-autophosphorylation in CheA [127]. Following autophosphorylation, the phosphoryl group is transferred to the flagellar motor-binding protein CheY. CheA interacts with CheY via its P2 domain, bringing CheY into close proximity to the phosphorylated histidine residue, which enables transfer of the phosphoryl group to the conserved aspartate residue at position 57 in *E. coli* CheY [128,129].

1.5 Polarity in bacteria

As previously mentioned, some bacteria exhibit a distinct localization of their flagella at the cell pole, referred to as polar localization. Similar spatial organization can also apply to the chemotaxis machinery and type IV pili. In many species, including *S. putrefaciens* and *Pseudomonas*, the flagellar and chemotaxis systems co-localize at the cell pole, a pattern that is also observed for the type IV pilus machinery [130–132]. This specific localization requires strict spatiotemporal regulation mediated by a series of proteins commonly referred to as “landmark” proteins. These proteins ensure correct positioning of cellular structures and contribute to distinguishing between the “old” and “new” cell pole that arises during cell division [133].

1.5.1 Landmark proteins HubP and FimV

Several years ago, the polar landmark protein HubP (“hub of the pole”) was identified and shown to be conserved among *Vibrio* species [134]. Homologs of HubP have also been found in other bacteria, including *S. putrefaciens* [132], where the protein is capable of localizing to the cell pole independently. HubP is involved in multiple cellular processes: in its absence, both chemotaxis and flagellar motility are impaired, and the chromosomal origin of replication fails to localize properly to the cell poles [132,134,135].

A potential homolog of HubP in *Pseudomonas* species is FimV. Similar to HubP, FimV localizes to the flagellated cell pole, with most cells also displaying a smaller cluster at the opposite pole. In addition, both proteins accumulate at midcell during cell division, specifically at the cell division plane [131,132,134]. Like HubP, FimV in *P. putida* is required for normal flagellar function, although it does

not affect flagellar positioning. In contrast, deletion of *fimV* in *P. aeruginosa* does not impair flagellar function or swimming motility but abolishes twitching motility [136]. Both HubP and FimV interact with multiple cellular partners, including the regulator of flagellar number FlhG/FleN, proteins of the type IV pilus machinery, and enzymes involved in cell wall remodeling, thereby recruiting these components to the cell pole [131,136–139]. Notably, whereas HubP is strictly required for the polar localization of the chemotaxis system and the chromosomal origin of replication in *S. putrefaciens* and *Vibrio* species, its homolog FimV has not yet been shown to participate in these processes in *Pseudomonas*.

Besides some functional similarities, HubP and FimV also share a comparable protein architecture. Both proteins contain a transmembrane domain that separates the proteins into a periplasmic N-terminal region and a cytoplasmic C-terminal region. Within the N-terminal periplasmic region, both proteins harbor a lysin motif (LysM). LysM-like domains were first identified in the peptidoglycan-degrading lysozyme of *Bacillus* phage ϕ29 and are conserved across all domains of life [140–143]. These domains bind to N-acetylglucosamine-containing carbohydrates, such as chitin or peptidoglycan, the major component of the bacterial cell wall. Consistent with this function, FimV from *P. aeruginosa* was shown to bind peptidoglycan in a LysM-dependent manner. Furthermore, both HubP and FimV display aberrant localization patterns away from the cell pole when the LysM domain is absent, demonstrating its importance for proper polar positioning of the proteins [132,134,136,139]. In contrast, the cytoplasmic C-terminal region of these proteins is highly diverse in both length and amino acid composition among different species, even between closely related organisms such as *Shewanella oneidensis* and *S. putrefaciens* [132]. While the cytoplasmic region of HubP proteins contains several imperfect repeats enriched in acidic amino acids, these repeats appear to be absent in FimV homologs [132,134]. Nevertheless, HubP and FimV share another characteristic structural feature: a conserved tetratricopeptide (TPR) motif at the extreme C-terminus. This region, termed the “FimV domain” due to its structural similarity to the C-terminal region of *P. aeruginosa* FimV, is present in various bacterial species, including *Pseudomonas*, *Shewanella, Neisseria* and *Vibrio* [144]. Notably, the secondary structure is highly conserved across these organisms. The FimV domain mediates several protein-protein interactions, for example with FimL, an activator of a major adenylate cyclase in *P. aeruginosa* [145].

1.5.2 GTPase FlhF

Another widely conserved and well-characterized landmark protein is FlhF. Together with Ffh and FtsY, FlhF belongs to the signal recognition particle (SRP)-type guanosine triphosphatase (GTPase) family, a class that comprises three protein members in bacteria [146]. These proteins are involved in regulating protein targeting and membrane association. The signal sequence-binding protein Ffh recognizes the signal peptides of nascent membrane proteins at the ribosome and delivers them to

the cytoplasmic membrane-bound SRP receptor FtsY. Subsequently, the ribosome-protein-complex engages a membrane-embedded protein-conducting pore of the Sec pathway, made up of SecY, SecE and SecG that mediates co-translational insertion or translocation of proteins across the membrane [147]. In contrast to Ffh and FtsY, FlhF represents the third SRP-like GTPase member that is involved in the spatial organization of flagellar assembly rather than protein secretion [148].

Upon GTP-binding, the guanosine diphosphate (GDP)-bound FlhF monomer dimerizes to form a GTP-bound FlhF homodimer, coordinated through interactions within the NG-domains, similar to the SRP proteins Ffh and FtsY [149–151]. The FlhF protein consists of three major domains: the B-, N- and G-domains, with the NG-domains shared with the other two members of the SRP family (**Figure 5**). The N-terminal B-domain is largely structurally disordered and is thought to participate in protein-protein interactions [152]. The conserved N-domain, located in the central region of the protein, comprises four α-helices and contributes to regulation of the GTPase activity by stabilizing the NG-domain complex. The G-domain represents the catalytic unit of the protein and harbors the GTPase activity. Similar to the G-domains of other SRP family members, it contains five conserved nucleotide-binding motifs, referred to as G-elements, which are essential for proper GTPase function [150,151,153,154]. The G1-element, also known as the phosphate-binding loop, mediates nucleotide binding through formation of an oxyanion hole [155]. The G2-element contains a conserved threonine residue involved in nucleotide binding as well as an arginine residue that facilitates GTP hydrolysis [156–158]. Together with the G2-element, the G3-element coordinates the positioning of a magnesium ion and three structured water molecules with a threonine residue from the G1-element in the GTP-bound FlhF homodimer. Nucleotide-specificity is conferred by the G4-element, whose conserved aspartate residue interacts with the guanine base of the nucleotide through the formation of two hydrogen bonds. Finally, the G5-element forms a third hydrogen bond with the guanine base via a conserved threonine residue and contributes to enclosing the nucleotide-binding site [146,150,151]. Between these conserved motifs, FlhF contains an insertion box (I-box), characterized by an α-β-α-fold. This structural element contributes to the overall GTPase function of FlhF and is conserved among all members of the SRP-type GTPase family [159].

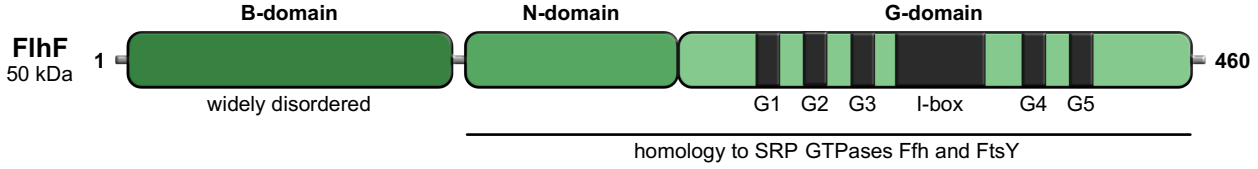

Figure 5. Domain organization of the GTPase FlhF from *S. putrefaciens*. Schematic representation of the domain architecture of FlhF. The protein consists of an N-terminal B-domain, followed by the N-domain and a C-terminal G-domain containing the GTPase activity. Conserved G-elements and the insertion box (I-box) are indicated by black boxes. The N- and C-termini are labeled with corresponding amino acid positions. Adapted from [149].

In general, FlhF exhibits polar localization and has been shown to be essential for polar placement of flagella in several bacterial species, including *S. putrefaciens, P. putida, P. aeruginosa* and *V. cholerae* [132,152,160–162]. In *P. putida*, the landmark protein FimV was found to stabilize the interaction of FlhF with the cell pole, although it does not directly contribute to its initial polar targeting [131]. Deletion of *flhF* in the aforementioned species results in reduced numbers of flagella and/or mislocalized flagellar filaments as well as severely impaired swimming behavior. Furthermore, FlhF in *P. putida* was shown to be required for full expression and fT3SS-dependent secretion of class III flagellar genes. In *P. aeruginosa*, FlhF has also been implicated in the polar localization of the chemotaxis machinery [130,163].

A prominent feature of FlhF is its interaction with the flagellar number regulator FlhG. Upon interaction of these two proteins, the GTPase activity of the GTP-bound FlhF homodimer is stimulated, resulting in its dissociation into a GDP-bound monomer [132,158,164]. This interaction inhibits the stable homodimer formation of FlhF at the cell pole and thereby contributes to the spatial and numerical control of flagellar biogenesis. Accordingly, the B-domain of FlhF has been implicated in recruiting the earliest flagellar assembly component, the MS-ring protein FliF, to the cell pole [152].

1.5.3 Other polar organization coordinators

Beyond HubP and FlhF, several additional proteins contribute to polar organization within the cell. One notable example is the recently identified FlhF-interaction partner A, FipA. FipA is widely conserved among polarly flagellated bacteria and has been shown to influence FlhF localization, thereby ensuring proper flagellar positioning and function in *V. parahaemolyticus*, *P. putida*, and, to a lesser extent, in *S. putrefaciens* [165].

Moreover, in *Pseudomonas* species, the membrane-associated Poc complex is required for the polar positioning of FlhF, as well as the flagellar and pilus machineries [166,167]. In addition to a TonB-homolog, the complex comprises two proteins, the polar organelle coordinators PocA and PocB, which are diffusely distributed within the cell. Deletion of either component leads to delocalization of FlhF and the flagellar filament, although the underlying molecular mechanism remains unclear.

Another prominent complex involved in the intracellular spatiotemporal organization of bacterial cells is the partitioning (Par) system. A well-characterized example is the ParABS system, a conserved ATP-dependent machinery that mediates chromosome and plasmid segregation through the coordinated action of the ATPase ParA, the DNA-binding protein ParB, and *parS* centromere-like DNA sequences near the chromosomal origin of replication [168]. Beyond this system, several bacteria utilize the ParA-like positioning system composed of ParC and ParP to spatially organize chemotaxis signaling arrays. In *Vibrio* species, ParC acts as cell pole determinant, with its polar localization dependent on the polar landmark protein HubP, whereas ParP interacts with chemotaxis

components such as CheA, thereby linking the Par machinery to the positioning of polar chemoreceptor clusters [135,169,170].

Besides FlhF and HubP, other homologous systems based on polar landmark proteins exist in diverse bacteria. For instance, the α-proteobacterium *Caulobacter crescentus* possesses a single flagellum, which is assembled at the cell pole generated during the previous cell division. This polar localization depends on the landmark protein TipN, which marks the newly formed cell pole and subsequently recruits TipF, a key flagellar assembly factor required for proper polar flagellation [171–173].

Notably, comparative genomic analyses have revealed that in several polar-flagellated bacteria, including *Pseudomonas*, *Shewanella*, and *Vibrio* species, core chemotaxis genes are located within or adjacent to the major flagellar gene cluster, together with polar organizer proteins [174–177]. This genomic arrangement suggests a coordinated regulation of motility and chemotactic signaling (**Figure 6**). However, such genomic linkage is not universally conserved across all bacteria.

Figure 6. Gene cluster encoding flagellar assembly, chemotaxis and polar organizer proteins in *P. putida*. Schematic representation of the genomic region containing genes involved in polarity, flagellar assembly, chemotaxis and regulatory functions. Genes are color-coded according to their respective functional categories. Adapted from *Pseudomonas* Genome DB and [178].

1.6 The sessile lifestyle of bacteria

Motility allows bacteria to rapidly respond to environmental changes and reach favorable niches. However, upon surface attachment, many species abandon active movement and transition to a sessile lifestyle, characterized by the formation of biofilms, in which cells are embedded in a self-produced extracellular matrix [179].

1.6.1 Biofilms

Biofilms are either single- or multi-species bacterial communities, in which cells differ from free-living, planktonic cells and are embedded in a specialized matrix primarily composed of exopolysaccharides, proteins and extracellular DNA. This structured environment protects bacteria from external threats while supporting community expansion [179]. Within biofilms, gradients of nutrients and oxygen give rise to cells with varying metabolic activity, enhancing bacterial tolerance and resistance to antibiotics [180]. Due to these properties, biofilms are clinically relevant, often contributing to persistent infections and promoting antimicrobial resistance [181,182].

Nevertheless, biofilms can also play beneficial roles, for instance in mutualistic relationships. The soil bacterium *P. putida* forms biofilms on diverse surfaces, including plant roots. Here, root exudates supply nutrients to the bacteria, while the bacteria enhance plant growth by improving nutrient availability and suppressing plant pathogens [183].

The transition between motile and sessile lifestyles is tightly regulated and often controlled by intracellular second messengers such as bis-(3'-5')-cyclic dimeric guanosine monophosphate (c-di-GMP), which promote biofilm formation while simultaneously repressing motility [184].

1.6.2 Second messenger c-di-GMP

Environmental signals are perceived by dedicated sensory systems and transmitted to downstream regulatory pathways. In many cases, this signal transduction involves small intracellular signaling molecules, known as second messengers, which allow rapid and coordinated responses to environmental changes [185]. By integrating multiple inputs, second messengers can regulate complex cellular processes, including motility, virulence, and biofilm formation [186].

The second messenger c-di-GMP is a soluble molecule that, for example, promotes the biosynthesis of adhesins and exopolysaccharide matrix components, while simultaneously inhibiting various forms of motility. As such, it governs the transition between the motile, planktonic and the sessile, biofilm-associated state in bacteria [184,186–190]. In addition, c-di-GMP has been implicated in pathogenesis and virulence of animal and plant pathogens as well as in cell cycle regulation in *C. crescentus* [191–195].

c-di-GMP is synthesized from two molecules of GTP by enzymes called diguanylate cyclases (DGCs, **Figure 7**). An active DGC functions as a dimer, with each subunit containing a GGDEF domain, which is catalytically responsible for c-di-GMP formation. The name GGDEF derives from a highly conserved amino acid motif (glycine, glycine, aspartic acid, glutamic acid, and phenylalanine) located in the active site, and point mutations in this motif (except aspartic acid to glutamic acid) abolish DGC activity [196–200]. Once synthesized, the second messenger c-di-GMP binds to downstream effectors such as riboswitches, transcription factors, or regulatory proteins, thereby influencing cellular behavior [185].

Conversely, c-di-GMP is degraded by specific phosphodiesterases (PDEs) into 5' phosphoguanylyl-(3'-5')-guanosine (pGpG), which is subsequently split up into two molecules guanosine monophosphate (GMP, **Figure 7**). Active PDEs typically contain one of two domains that facilitate c-di-GMP hydrolysis. The most widespread is the EAL domain, characterized by a conserved EAL motif (glutamic acid, alanine and leucine) and requiring Mg^{2+} or Mn^{2+} as a cofactor [201–203]. While most EAL domains exhibit enzymatic activity, some degenerate EAL proteins lack the key residues

necessary for catalysis and instead function in ligand or protein binding, often regulating processes such as transcription or RNA degradation without hydrolyzing c-di-GMP [203–206]. Another PDE domain, HD-GYP, can also degrade c-di-GMP directly into two GMP molecules, but is less widespread than the EAL domain [186,192].

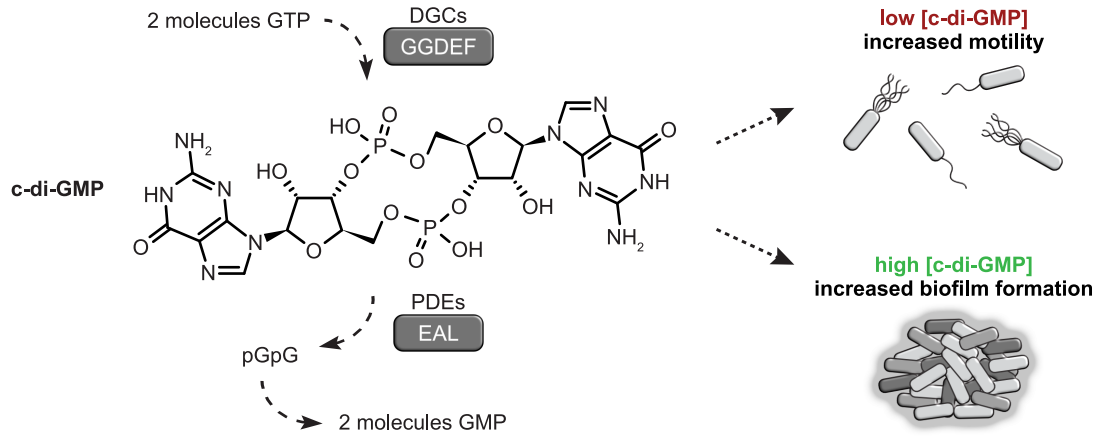

Figure 7. Second messenger c-di-GMP signaling pathway. Schematic representation of the c-di-GMP signaling pathway. The second messenger is synthesized from two GTP molecules by GGDEF domain-containing diguanylate cyclases (DGCs) and degraded into pGpG and subsequently into two GMP molecules by EAL domain-containing phosphodiesterases (PDEs). High intracellular c-di-GMP levels promote a sessile lifestyle and biofilm formation, whereas motile cells typically exhibit low c-di-GMP levels. Adapted from [186,190].

While most bacteria encode moderate numbers of GGDEF and EAL domain-containing proteins in their genome (for instance, *E. coli* possesses 19 GGDEF and 17 EAL domain proteins), some species completely lack these enzymes. One notable example is *H. pylori*, which does not encode a single GGDEF or EAL domain protein [188,207]. GGDEF and EAL domains may occur in separate proteins or within the same multidomain protein. However, proteins containing both domains typically exhibit either DGC or PDE activity, and only rarely possess both activities simultaneously [186].

1.6.3 Structure of canonical PDEs and Pch

EAL domain-containing PDEs are typically multidomain proteins, often fused to sensory input domains. One common sensory domain is the Per-Arnt-Sim (PAS) domain, which monitors changes in light, oxygen, the cellular energy state, small ligand concentrations and redox potential. PAS domains were first described in *Drosophila* proteins and are frequently extended by a PAS-associated C-terminal (PAC) motif, which contributes to the characteristic PAS fold [208–211]. Another well-characterized input domain is the receiver (REC) domain, commonly found in response regulators of two-component systems. In these proteins, a phosphoryl group is transferred to a conserved aspartate residue within the REC domain, activating enzymatic functions such as those observed in CheY or CheB in chemotaxis signaling [212]. Additionally, GAF domains, named after their presence in cyclic guanosine monophosphate (cGMP)-specific PDEs, adenylate cyclases and the transcriptional activator FhlA, serve as ligand-binding modules for small molecules like cGMP and share a structural fold similar to PAS domains [213–215].

At present, several c-di-GMP-specific PDEs are well characterized regarding their structure and regulatory function. For instance, the proteins RocR and BifA have been shown to influence virulence gene expression and biofilm formation in *P. aeruginosa* [216,217]. Similarly, the PDE PdeB directly interacts with the C-terminal FimV domain of the polar landmark protein HubP via its GGDEF domain, resulting in its polar recruitment in *S. putrefaciens* [218]. Consistent with these findings, the FimV homolog in *P. aeruginosa* has also been implicated in regulating intracellular c-di-GMP levels [136,145,219].

Nevertheless, another PDE has attracted particular attention: the phosphodiesterase determinant of c-di-GMP heterogeneity, named Pch [163]. Pch displays a prominent multidomain architecture, comprising two PAS domains, a GAF, domain, and both GGDEF and EAL domains. Moreover, the protein exhibits PDE activity, whereas no DGC activity could be detected, likely due to alterations in the GGDEF motif [220]. The protein was shown to associate with the membrane and to participate in regulating flagellar motility as well as biofilm dispersion [220,221], and is therefore also referred to as dispersion-induced phosphodiesterase A (DipA). Of particular interest, Pch was found to co-elute with the histidine kinase CheA in co-immunoprecipitation assays, suggesting a potential mechanistic link between chemotaxis and c-di-GMP-dependent signaling [163]. However, the precise details of this interaction remain incompletely characterized. Notably, Pch exhibits polar localization, which appears to depend on FlhF and CheA [163].

1.7 Model organisms *S. putrefaciens* and *P. putida*

To investigate the mechanisms underlying polar flagellar assembly, chemotaxis and c-di-GMP-dependent signaling, the model organisms *Shewanella putrefaciens* CN-32 and *Pseudomonas putida* KT2440 were employed. Both species are Gram-negative, polarly flagellated bacteria that display robust swimming motility, making them ideal models to study the assembly and regulation of polar flagella. Furthermore, both species possess well-defined chemotaxis systems. Similar to *S. putrefaciens* with around 36 predicted MCPs [132,222], the common rhizosphere inhabitant *P. putida* also exhibits remarkable metabolic diversity and encodes approximately 27 MCP-encoding genes in its genome [223]. They are, therefore, particularly interesting model organisms for studying bacterial signaling pathways. In addition, both organisms possess conserved regulatory components, including the GTPase FlhF, FipA and the ATPase FlhG (or FleN in *P. putida*), which are essential for controlling polar localization and flagellar number [132,165,224].

The marine bacterium *S. putrefaciens* serves as an experimentally tractable model for studying polar flagellar positioning. Its single Na^+-driven polar flagellum provides motility in the planktonic lifestyle, guiding the bacteria through marine environments [15,18]. Additionally, *S. putrefaciens* possesses a secondary H^+-driven flagellar system, allowing the formation of multiple lateral flagellar that

facilitate movement through more viscous or structured environments [17]. The flagellar filaments are generally composed of two flagellins: the minor flagellin FlaA and the major flagellin FlaB [16]. These features make *S. putrefaciens* an excellent model for dissecting regulatory mechanisms specific to each flagellar system. Indeed, it has been previously employed to investigate the role of polar landmark proteins, such as HubP, FipA and FlhF, in flagellar assembly [18,52,132].

In contrast, the chemotaxis system, as well as the c-di-GMP signaling network that coordinate motility and biofilm formation have been extensively studied in *Pseudomonas* species [163,221]. Especially *P. putida* serves as an important workhorse for genetic, physiological and biotechnology studies [225]. The bacterium displays a lophotrichous flagellation, with multiple H^+-driven flagella localized at the cell pole, composed of a single flagellin, FliC [51,226]. Together with *S. putrefaciens*, these two organisms enable the investigation of conserved mechanisms of polar flagellar assembly and chemotactic organization, while also providing insight into species-specific regulatory adaptations.

1.8 Project aim

The bacterial flagellum is a well-studied bacterial nanomachine. Nevertheless, many questions remain, including the precise spatiotemporal organization of proteins responsible for proper polar flagellar assembly. It is established that the polar landmark proteins FlhF and HubP play crucial roles in initiating and recruiting flagellar components to the cell pole, for instance in *S. putrefaciens* [132]. However, the exact recruitment cascade has not been fully elucidated. Therefore, this study aims to investigate the extent to which FlhF and HubP contribute to the recruitment of early flagellar components, with a particular focus on the interaction between FlhF and the C-ring protein FliG.

In addition, the potential HubP homolog FimV in *P. putida* will be characterized in greater detail and compared with HubP from *S. putrefaciens*. To date, FimV has primarily been associated with twitching motility and the localization of the type IV pilus apparatus, whereas HubP is involved in several critical cellular processes in *S. putrefaciens* and *V. cholerae* [137,139,144,227,228]. Therefore, this study aims to determine whether FimV in *P. putida* performs functions similar to those of HubP.

Since HubP and FlhF have been implicated in the polar recruitment of the chemotaxis system in several organisms [132,134,163], the chemotaxis machinery was also examined in greater detail. In particular, this study focuses on the polar localization and interaction of the histidine kinase CheA and the phosphodiesterase Pch, as well as the extent to which this interaction connects chemotaxis signaling with c-di-GMP-dependent signaling pathways.

2. Results

Cellular organization represents one of the most intricate molecular mechanisms exhibited by bacteria. Although several studies have uncovered complex intracellular pathways, key questions remain, particularly concerning polar flagellar assembly and the role of polar organizer proteins and their associated interaction networks. The aim of this study was, therefore, to investigate the localization and interactions of proteins involved in polarity, chemotaxis and overall intracellular organization in *S. putrefaciens* or *P. putida*. Accordingly, the work is organized into three main chapters:

I) Polar flagellar assembly in *S. putrefaciens* - focusing on the detailed characterization of the interaction between the proteins FlhF and FliG.
II) Functional characterization of the polar organizer protein FimV in *P. putida* - describing the localization and functional properties of the polar landmark protein FimV.
III) Interaction between the PDE Pch and histidine kinase CheA in *P. putida* - analyzing the polarity and interaction of these proteins and additional partners in greater detail.

2.1 Polar flagellar assembly in *S. putrefaciens*

This chapter focuses on the interaction between the GTPase FlhF and the flagellar C-ring component FliG, which is putatively responsible for restricting flagellar assembly to a single cell pole in *S. putrefaciens*. To elucidate the mechanisms underlying the polar restriction, the interaction was investigated using *in vitro* pulldown assays, *in vivo* yeast two-hybrid analysis and fluorescence microscopy. All yeast two-hybrid experiments and *in vitro* downstream analyses were performed by Anita Dornes at Philipps University in Marburg. Results from this chapter have been published in Dornes, Schmidt et al. [14].

2.1.1 FlhF interacts with FliG from the polar system

FlhF has been suggested to directly interact with the MS-ring protein FliF [152,229]. As shown before (**Figure 5**), the FlhF protein of *S. putrefaciens* can be divided into an N-terminal B-domain, followed by a C-terminal NG-domain, responsible for GTP/GDP-binding and hydrolysis (**Figure 8A**). To investigate potential interactions of FlhF with other proteins, particularly the C-ring protein FliG, yeast two-hybrid assays were performed using either full-length FlhF or the isolated B-domain fused to the Gal4 DNA-binding domain as bait together with flagellar proteins as prey.

As previously reported, FlhF interacts with the ATPase FlhG and forms a homodimer, as indicated by growth on -HLT and -ALT plates (**Figure 8B**). Furthermore, an interaction with FliG, restricted to the polar flagellar system, was observed. No interaction of FlhF with the cytoplasmic part of FliF (FliF-C) or with the other C-ring proteins, FliM and FliN, could be detected. When only the B-domain

of FlhF was used as bait, the interaction with FliG was maintained, indicating that this domain is sufficient for the interaction. In contrast, removal of the NG-domain abolished both the interaction with FlhG and FlhF homodimer formation observed previously. The results indicate that FlhF directly interacts with FliG from the polar system, while it does not directly interact with the MS-ring protein FliF.

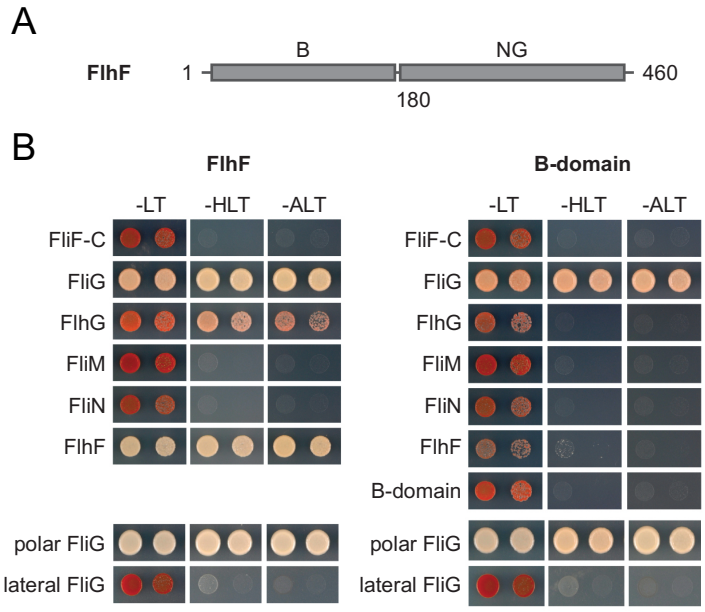

Figure 8. FlhF interacts with FliG from the polar system. A Schematic representation of the *S. putrefaciens* FlhF protein, showing the N-terminal B-domain followed by the C-terminal NG-domain. Amino acid positions of the respective domains are indicated. **B** Yeast two-hybrid analysis, performed by Anita Dornes (Philipps University in Marburg). Full-length FlhF (left) or the isolated B-domain (right) were fused to Gal4 DNA-binding domain as bait, while prey proteins were fused to Gal4 activation domain. Growth on plates lacking leucine and tryptophan (-LT) indicates stable plasmid maintenance. Weak to moderate protein-protein interactions are detected on plates lacking histidine, leucine and tryptophan (-HLT, *HIS3* reporter) while only strong interactions support growth on plates lacking adenine, leucine and tryptophan (-ALT, *ADE2* reporter). FliF-C: cytoplasmic region of FliF. Adapted from [14].

2.1.1.1 FlhF contains a structured N-terminal domain

Next, the specific structural elements within the B-domain responsible for mediating the interaction with FliG were investigated. Pulldown assays were performed using sequential StrepII-tagged B-domain mutants to delineate the interaction interface. As shown in **Figure 9A**, only the B-domain variant containing the first 60 amino acids was able to interact with FliG, whereas no interaction was observed in variants lacking the first 10, 20 or 30 amino acids.

A more detailed structural analysis of the FlhF protein by X-ray crystallography revealed a well-defined domain at the N-terminus, encompassing the first 44 amino acids of the B-domain. This domain consists of a single α-helix and three β-strands (**Figure 9B**). It is connected via a short linker to the remaining NG-domain, which contains the GTP/GDP-binding site. Because it is likely responsible for mediating the interaction with FliG, this N-terminal domain was named FID for FliG Interaction Domain.

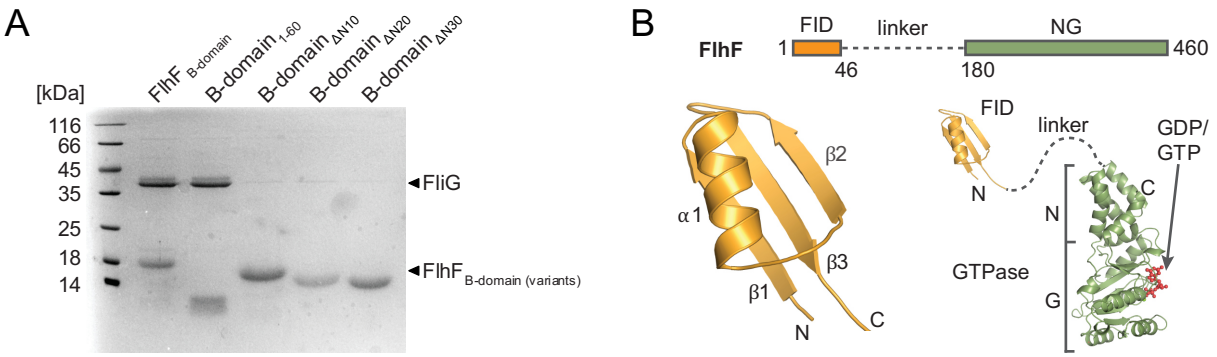

Figure 9. FlhF contains an N-terminal structured domain. A Coomassie-stained SDS-PAGE of an *in vitro* pulldown assay, performed by Anita Dornes (Philipps University in Marburg). StrepII-tagged FlhF B-domain and truncation variants were used as bait (amino acids numbers are indicated) and full-length FliG served as prey. **B** Upper panel: revised schematic representation of the domain architecture of FlhF, highlighting the FliG interaction domain (FID, orange) connected via a flexible linker (dashed line) to the NG-domain (green). Domains are drawn to scale and amino acids are indicated. Lower panel: X-ray crystal structure of the FlhF FID domain, consisting of one α-helix and three β-strands (this study), shown together with the GDP-bound NG-domain of *S. putrefaciens* FlhF (PDB-ID: 8R9R). Adapted from [14].

2.1.1.2 The N-terminal FID domain of FlhF interacts with the middle and C-terminal regions of FliG

To determine whether the N-terminal FID domain of FlhF is responsible for the interaction with FliG, the specific region of FliG required for the binding was investigated. Two FliG variants were generated: one comprising the N-terminal and middle regions ($FliG_{NM}$) and the other comprising the middle and C-terminal regions ($FliG_{MC}$) of the protein (**Figure 10A**). StrepII-tagged FlhF was used as bait and full-length FliG or its variants as prey in pulldown assays. While full-length FlhF interacted with full-length FliG, only the $FliG_{MC}$ variant exhibited a comparable stoichiometric interaction, whereas the interaction with $FliG_{NM}$ appeared sub-stoichiometric. Taken together, the data indicate that FliG interacts with FlhF via its middle and C-terminal regions.

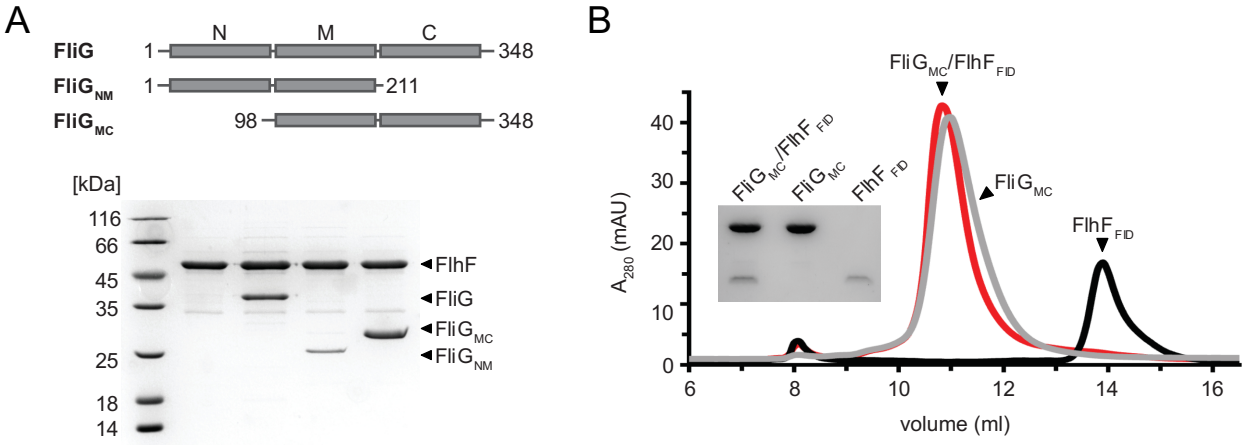

Figure 10. The N-terminal FID domain interacts with middle and cytoplasmic regions of FliG. A Upper panel: schematic representation of the domain architecture of full-length FliG and its truncation variants, indicating the respective domain organization ($FliG_{NM}$ and $FliG_{MC}$, respectively). Amino acid positions of the respective domains are indicated. Lower panel: coomassie-stained SDS-PAGE of an *in vitro* pulldown assay. StrepII-tagged FlhF was used as bait and full-length FliG and its two variants were used as prey. **B** Chromatograms from analytical size-exclusion chromatography experiments of the FlhF FID domain ($FlhF_{FID}$, black), the middle and C-terminal domains of FliG ($FliG_{MC}$, grey) and their complex ($FliG_{MC}/FlhF_{FID}$, red). Inner panel: Coomassie-stained SDS-PAGE of peak fractions from each run. Experiments were performed by Anita Dornes (Philipps University in Marburg). Adapted from [14].

After identifying the region of FliG responsible for its interaction, its binding to the N-terminal FID domain was tested using size-exclusion chromatography. Interaction between the proteins alters their individual chromatograms, providing evidence for complex formation. To this end, chromatography experiments were conducted on the N-terminal FID domain, the $FliG_{MC}$ variant or both proteins together. Size-exclusion chromatography confirmed the interaction between the two proteins, as the formation of a protein complex lead to a shift in the chromatographic elution profile, with both proteins co-eluting in the same fractions (**Figure 10B**).

2.1.2 FlhF bridges FliG and HubP

Following the confirmation of the interaction between the GTPase FlhF and C-ring protein FliG, the underlying mechanism by which this interaction contributes to polar flagellar assembly was investigated. This included an analysis of potential interactions with the polar landmark protein HubP, which has been described as a key factor for proper flagellar function in *S. putrefaciens* [132].

2.1.2.1 FlhF interacts with its NG-domain with the cytoplasmic region of HubP

As previously described, HubP comprises an N-terminal signal sequence, followed by a LysM-like domain and transmembrane segment, as well as a cytoplasmic region of approximately 70 kDa containing a TPR motif, also referred to as the FimV domain due to its structural homology to the C-terminal region of the *P. aeruginosa* FimV protein (**Figure 11A**). To identify the HubP region mediating the interaction with FlhF, *in vitro* pulldown assays were performed using three truncated variants as StrepII-tagged baits. However, production of those variants was only possible starting from amino acid 860 to the extreme C-terminus of the protein: a variant with a part of its cytoplasmic region (HubP-C), a variant lacking the FimV domain (HubP-$C_{\Delta FimV}$), and the isolated FimV domain (FimV).

While the B-domain of FlhF, specifically the FID domain, mediates the interaction with FliG and does not interact with HubP *in vitro*, the NG-domain of FlhF was confirmed to be responsible for the interaction with HubP (**Figure 11B**). Moreover, this interaction is detected only when the cytoplasmic region of HubP is present, whereas no interaction was observed with the isolated C-terminal FimV domain variant (**Figure 11C**). Together, these findings indicate that FlhF interacts via its NG-domain and that this interaction required the cytoplasmic region of HubP, but not the FimV domain.

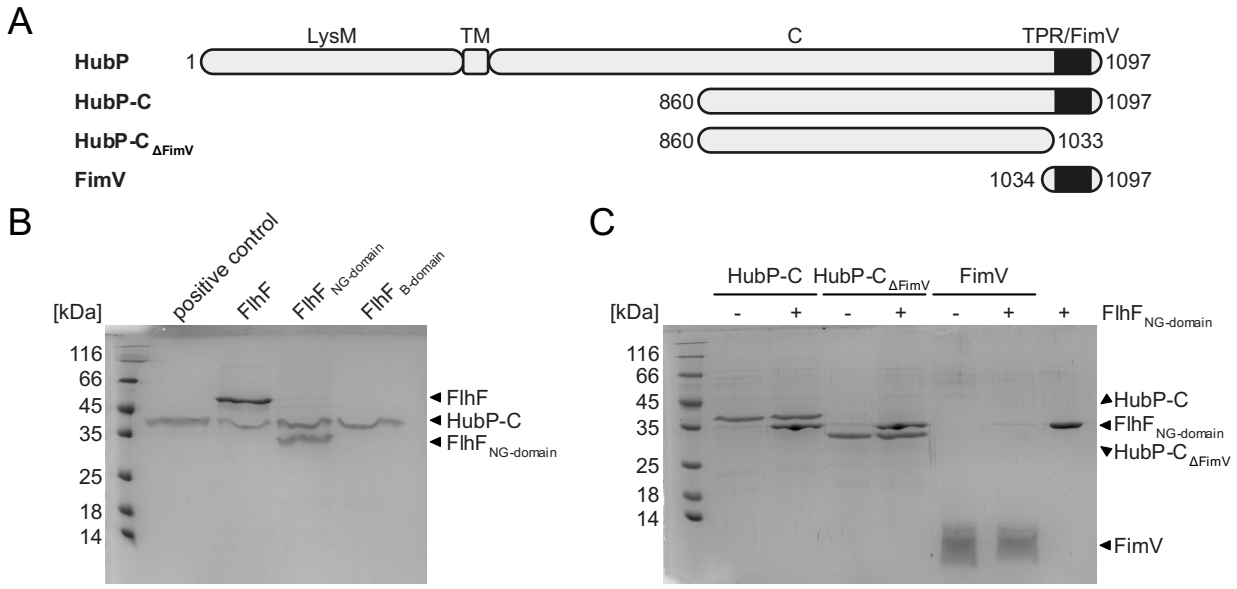

Figure 11. FlhF interacts via its NG-domain with the cytoplasmic region of HubP. A Schematic representation of the domain architecture of HubP and its truncations variants: full-length HubP containing a LysM-like domain (LysM), a transmembrane segment (TM) and a cytoplasmic region of approximately 70 kDa (C) comprising a tetratricopeptide repeat-like domain, also referred to as FimV domain (TPR/FimV); a variant comprising only part of the cytoplasmic region (HubP-C, aa 860-1097); a HubP-C variant lacking the C-terminal FimV domain (HubP-$C_{\Delta FimV}$, aa 860-1033) and the isolated FimV domain (FimV, aa 1034-1097). **B** Coomassie-stained SDS-PAGE of an *in vitro* pulldown assay. StrepII-tagged HubP-C was used as bait, while full-length FlhF, its NG-domain ($FlhF_{NG\text{-}domain}$) or its B-domain ($FlhF_{B\text{-}domain}$) served as prey. StrepII-tagged HubP-C was loaded as positive control. **C** Coomassie-stained SDS-PAGE of an *in vitro* pulldown assay. StrepII-tagged HubP variants were used as bait and $FlhF_{NG\text{-}domain}$ served as prey. Experiments were performed by Anita Dornes (Philipps University in Marburg). Adapted from [14].

2.1.2.2 FliG-bound FlhF interacts with HubP

After demonstrating that FlhF interacts via its N-terminal FID domain with the C-ring protein FliG and via its NG-domain with the cytoplasmic region of the polar landmark protein HubP, the question was whether these two interactions can occur simultaneously to restrict flagellar assembly to the cell pole. To address this, pulldown assays were performed using StrepII-tagged HubP-C as bait and FliG and FlhF as full-length prey proteins.

Since both FliG and FlhF co-eluted with StrepII-tagged HubP-C (**Figure 12**), these results suggest that FlhF is able to interact simultaneously with HubP and FliG, indicating a potential scaffolding role that links the polar landmark protein HubP to the flagellar C-ring component FliG.

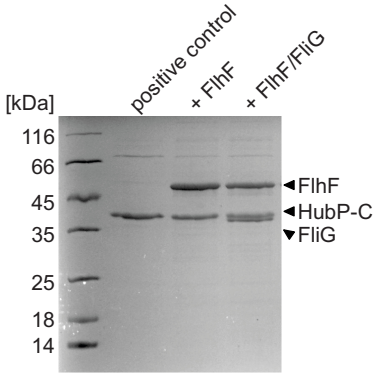

Figure 12. FlhF bridges HubP and FliG *in vitro*. Coomassie-stained SDS-PAGE of an *in vitro* pulldown assay, performed by Anita Dornes (Philipps-University in Marburg). StrepII-tagged cytoplasmic region of HubP (HubP-C) was used as bait and full-length FliG and FlhF served as prey. StrepII-tagged HubP-C was loaded as positive control. Adapted from [14].

2.1.3 FlhF restricts flagellar assembly to the cell pole

Since FlhF was shown to interact with the C-ring protein FliG and the polar landmark protein HubP *in vitro*, these interactions were further investigated in the context of intracellular protein organization. To this end, fluorescence microscopy was employed to analyze the subcellular localization of the respective proteins and to assess whether the observed interactions correlate with their spatial distribution within the cell.

2.1.3.1 FlhF localizes polarly independent of its FID domain

The aim of this part of the study was to generate a FlhF mutant whose interaction with FliG is disrupted while retaining the ability to interact with HubP. Through this preserved interaction, FlhF is expected to be recruited to the cell pole, whereas flagellar assembly should no longer be restricted to the pole due to the loss of FliG binding. As a first step, the subcellular localization of a FlhF-mVenus fusion protein, lacking the first N-terminal 44 amino acids ($FlhF_{\Delta FID}$), was analyzed in *S. putrefaciens* to confirm its polar localization. Furthermore, FlhF's ability to localize to the cell pole in the absence of its interaction partner FliG was tested, using two FliG variants, either lacking the N-terminal ($FliG_{\Delta N}$) or C-terminal ($FliG_{\Delta C}$) region of the protein. All fusion proteins are stably produced as shown by western blot analysis (Supplementary figure 1).

Fluorescence microscopy of wild-type FlhF-mVenus revealed monopolar localization in approximately 90% of cells displaying fluorescent FlhF foci (**Figure 13A**). In contrast, deletion of either the N- or C-terminal regions of FliG reduced the monopolar localization of FlhF to around 60%, while a bipolar localization was observed in nearly 40% of cells. Deletion of the first N-terminal 44 amino acids, corresponding to the FID domain of FlhF, decreased the proportion of monopolar FlhF foci to about 70%. However, this deletion did not alter the overall polar localization pattern. Deletions of either the N- or C-terminal regions of FliG significantly increased the intensity of FlhF foci at a single cell pole, while cells displayed a non-motile phenotype in soft-agar swimming assays (**Figure 13B,C**). Accordingly, a FlhF mutant lacking the FID domain phenocopied a *flhF* deletion mutant in terms of swimming ability. It can, therefore, be suggested that, although the interaction with FliG is abolished, FlhF is still properly recruited to the cell pole through its interaction with HubP via the remaining NG-domain.

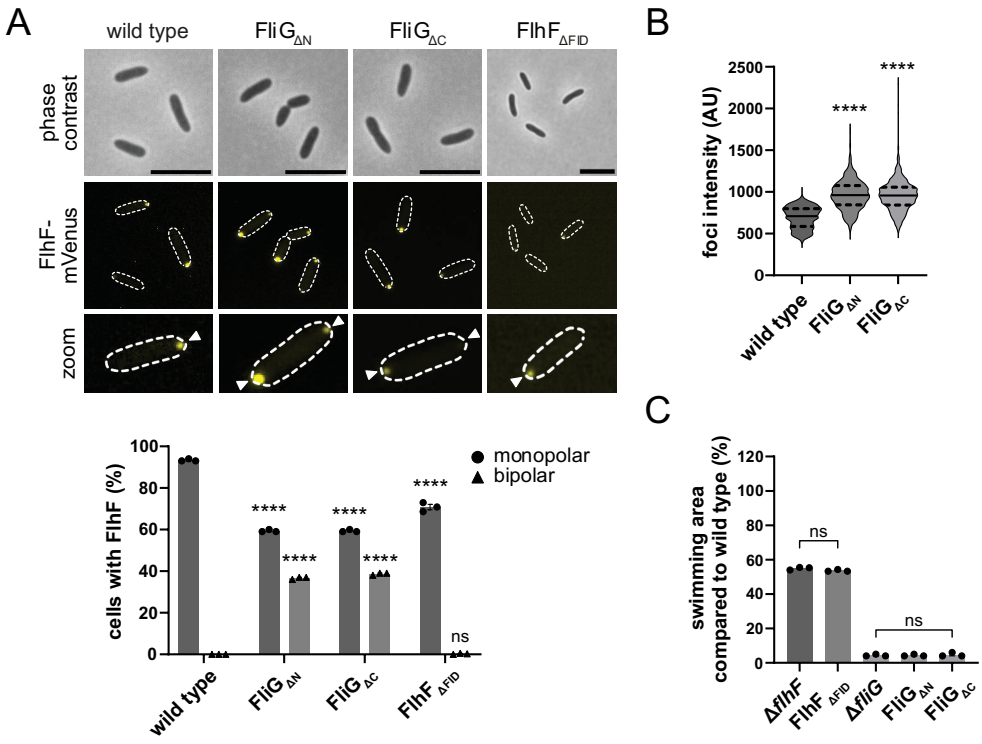

Figure 13. FlhF localizes polarly independent of its FID domain. A Upper panel: fluorescence microscopy images of the FlhF-mVenus fusion protein in *S. putrefaciens* wild-type cells, cells lacking the N-terminal or C-terminal regions of FliG (FliG$_{\Delta N}$ and FliG$_{\Delta C}$, respectively) and cells lacking the FID domain of FlhF (FlhF$_{\Delta FID}$). The upper row shows phase contrast images, the middle row shows the corresponding mVenus fluorescence (yellow) and the lower row shows magnified regions of the fluorescence images. Polar FlhF foci are indicated by white arrows. Scale bar equals 3 µm. Lower panel: quantification of FlhF-mVenus localization pattern in *S. putrefaciens* cells, classified as monopolar or bipolar. Data from three independent experiments, with more than 300 cells analyzed per replicate, are shown as mean with standard error of the mean. Statistical analysis was performed using two-way ANOVA (****p<0.0001, ns = non-significant; here: p=0.9663). **B** Quantification of FlhF-mVenus fluorescence intensity in arbitrary units (AU). Data from three independent experiments, with more than 300 cells analyzed per replicate, are shown. Statistical analysis was performed using two-way ANOVA (****p<0.0001). **C** Swimming motility of *S. putrefaciens* mutants compared to wild-type cells (set to 100%). Strains were spotted onto the same plate to ensure direct comparison. Data from three independent experiments are shown as mean with standard error of mean. Statistical analysis for Δ*flhF* and FlhF$_{\Delta FID}$ was performed using Welch's t-test (ns = non-significant; here: p=0.0888). Statistical analysis for Δ*fliG* and FliG variants was performed using one-way ANOVA (ns = non-significant; here p>0.999 and p=0.8399, respectively). Adapted from [14].

2.1.3.2 Interaction with FliG is required for proper polar flagellar assembly

After confirming the polar localization of FlhF lacking its FID domain, the localization of the flagellar apparatus itself was analyzed. To this end, a threonine-to-cysteine substitution at position 183 in the flagellar hook protein FlgE$_1$ was introduced (FlgE^{T183C}), enabling the covalent coupling of a maleimide-conjugated fluorescent dye [218]. Using this strain, the effects of deleting the FID domain or full-length FlhF on flagellar localization could be assessed.

In almost 80% of *S. putrefaciens* wild-type cells, the flagellar assembly was detected at the cell pole, whereas deletion of *flhF* reduced polar flagellar assembly to less than 10% of cells (**Figure 14**). In this mutant background, flagellar structures were observed at subpolar positions in approximately 30% of cells, while no flagellar assembly was detected in the remaining 60%. Absence of the N-terminal FID domain of FlhF resulted in a highly similar phenotype: polar flagellar assembly is

observed in only 10% of cells, whereas roughly 40% displayed subpolar flagellar structures. Taken together, these results demonstrate that disruption of the FlhF-FliG interaction by deletion of the FID domain uncouples proper polar flagellar assembly from the polar localization of FlhF itself. This indicates that, while FlhF can still be recruited to the cell pole via its interaction with HubP, the FID domain is essential to spatially restrict flagellar assembly to the pole.

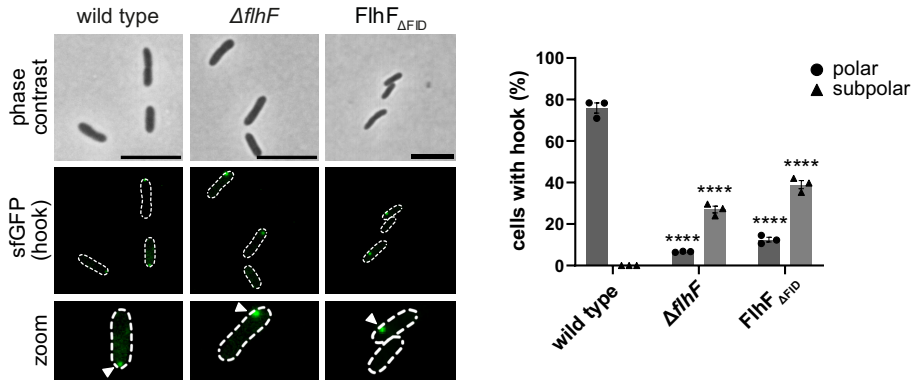

Figure 14. The FID domain of FlhF is required for proper flagellar assembly. Left panel: fluorescence microscopy images of stained hook structures in *S. putrefaciens* $FlgE^{T183C}$ cells labeled with Alexa Fluor 488-C5-maleimide-conjugated fluorescent dye in the Δ*flhF* mutant and a FlhF variant lacking the FID domain ($FlhF_{\Delta FID}$). The upper row shows phase contrast images, the middle row shows the corresponding sfGFP fluorescence (green) and the lower row shows magnified regions of the fluorescence images. Fluorescent hook structures are indicated by white arrows. Scale bar equals 3 µm. Right panel: quantification of hook localization pattern in *S. putrefaciens* cells, classified as polar or subpolar. Data from three independent experiments, with more than 300 cells analyzed per replicate, are shown as mean with standard error of the mean. Statistical analysis was performed using two-way ANOVA (****p<0.0001). Adapted from [14].

2.1.4 Flagellar recruitment cascade can be rebuilt in a heterologous host

Previous results presented in this chapter demonstrate that the interaction between FlhF and FliG, mediated by the N-terminal FID domain of FlhF (**Figure 10**), is essential for restricting flagellar assembly to the cell pole, while polar recruitment of FlhF remains HubP-dependent (**Figure 13**). These findings suggest a hierarchical recruitment cascade, in which HubP positions FlhF at the cell pole and FlhF in turn recruits FliG to spatially coordinate polarity with flagellar assembly.

To test whether this proposed recruitment hierarchy is sufficient to drive polar organization independently of the native cellular context, the behavior of these proteins should be investigated in a heterologous system. Specifically, the *Shewanella* proteins HubP (*Sp*HubP), FlhF (*Sp*FlhF) and FliG (*Sp*FliG) were fused to fluorescent proteins and expressed from plasmids in *E. coli*, which lacks HubP and FlhF orthologues. This approach allows direct visualization of their subcellular localization and interaction dynamics in a simplified background, thereby providing an experimental test of whether the hypothesized HubP-FlhF-FliG recruitment cascade is intrinsically encoded in the proteins themselves. Stability and expression of the fusion proteins was confirmed by western blot analysis (Supplementary figure 1).

When *Sp*HubP fused to sfGFP was expressed in *E. coli*, it preferentially localized to the cell poles and the cell division plane (**Figure 15**, left panel), consistent with previous observations [132]. In addition, *Sp*HubP fluorescence outlined the cell periphery. Expression of *Sp*FlhF-mVenus alone resulted in the formation of distinct monopolar foci in approximately 80% of the cells, while the remaining 20% of the cells displayed subpolar localization (**Figure 15**, middle panel). In the presence of *Sp*HubP, *Sp*FlhF localization shifted markedly: more than 60% of cells exhibit bipolar foci, a localization pattern that was never observed in the absence of *Sp*HubP. Moreover, *Sp*FlhF was now also recruited to the cell division plane. Next, the localization of mVenus-*Sp*FliG was analyzed. When expressed alone, no detectable fluorescent signal was observed (**Figure 15**, right panel). However, upon co-expression with *Sp*FlhF, monopolar *Sp*FliG foci became visible in approximately 50% of cells, while 20% showed bipolar or subpolar localization. Co-expression of *Sp*HubP together with *Sp*FlhF lead to a localization pattern of *Sp*FliG that closely resembled that of *Sp*FlhF. In nearly 70% of cells, *Sp*FliG localized bipolarly and was additionally recruited to the division plane. Taken together, these results obtained in a heterologous *E. coli* system strongly support the proposed HubP-FlhF-FliG recruitment cascade.

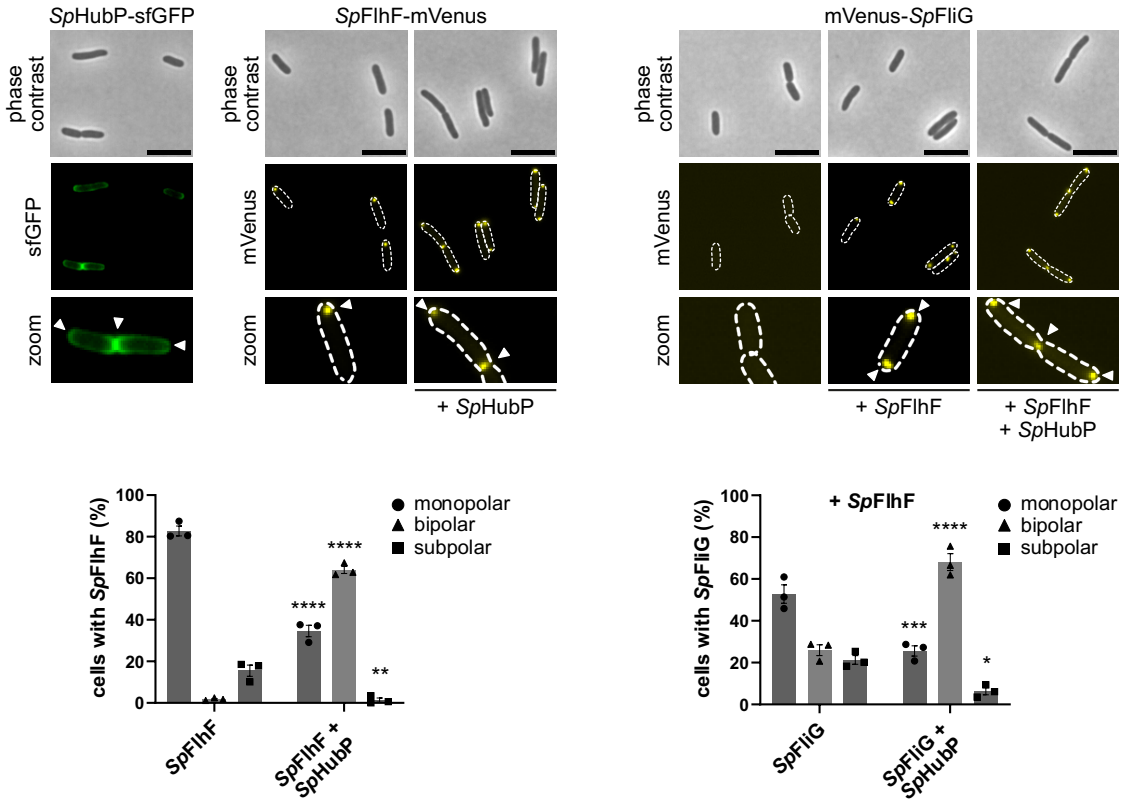

Figure 15. The flagellar HubP-FlhF-FliG recruitment cascade can be rebuilt in *E. coli*. Upper panel: fluorescence microscopy images of *Sp*HubP-sfGFP (left), *Sp*FlhF-mVenus (middle) and mVenus-*Sp*FliG (right) fusion proteins expressed in *E. coli*. The upper row shows phase contrast images, the middle row shows the corresponding sfGFP (green) or mVenus fluorescence (yellow) and the lower row shows magnified regions of the fluorescence images. Fluorescent *S. putrefaciens* proteins are indicated by white arrows. Scale bar equals 3 µm. Lower panel: quantification of *Sp*FlhF-mVenus (left) or mVenus-*Sp*FliG (right) localization patterns in *E. coli* cells, classified as monopolar, bipolar or subpolar. Data from three independent experiments, with more than 300 cells analyzed per replicate, are shown as mean with standard error of the mean. Statistical analysis was performed using two-way ANOVA (****p<0.0001, ***p=0.0001, **p=0.0011, *p=0.0141). Adapted from [14].

In conclusion, this chapter identified the molecular interaction between FlhF and FliG as a key determinant for polar flagellar assembly in *S. putrefaciens*. The N-terminal FID domain of FlhF is required to couple polar localization of FlhF to correct positioning of the flagellar apparatus, while recruitment of FlhF to the cell pole remains HubP-dependent. Expression of the *S. putrefaciens* proteins in *E. coli* further supports a hierarchical HubP-FlhF-FliG recruitment cascade that does not rely completely on species-specific factors. Together, these results provide a mechanistic basis for understanding how polarity information is translated into spatially controlled flagellar assembly.

2.2 Functional characterization of the polar organizer protein FimV in *P. putida*

The previous chapter focused on the polar landmark protein HubP and its role in organizing polar flagellar assembly in *S. putrefaciens*. Similar organizing principles are expected to exist in other bacteria. In *Shewanella* and *Vibrio* species, HubP functions as a central polar organizer involved in multiple cellular processes, including the spatial control of polar flagellar assembly [14] as well as the polar positioning of chromosome segregation and chemotactic machinery [132,134]. In *Pseudomonas* species, a putative functional homolog of HubP is the FimV protein, which was originally identified in *P. aeruginosa* as a protein required for twitching motility [144]. Although FimV is not a structural component of the type IV pilus itself, its presence is essential for correct polar localization and function of the motility machinery, and cells lacking FimV are unable to twitch [136,138,230]. In *P. putida*, however, twitching motility has not been reported yet, and the function of FimV remains largely unexplored. Functional homologies between FimV in *P. putida* and HubP in *Shewanella* or *Vibrio* species have not yet been established.

The following chapter therefore focuses on the functional characterization of the polar organizer protein FimV in *P. putida* KT2440, aiming to define its role in cellular organization and polarity and to investigate whether FimV represents a true functional homolog of the HubP protein found in *Shewanella* or *Vibrio* species. To address this, a series of phenotypic screening assays were performed using *P. putida* cells lacking FimV. In addition, *in vitro* studies with purified FimV from *P. putida* KT2442, a spontaneous rifampicin-resistant mutant of KT2440, were conducted by Marta Pulido-Sánchez at Universidad Pablo de Olavide in Seville, to assess its potential involvement in peptidoglycan binding. All further characterizations were performed in a *P. putida* KT2440 strain that allows staining of flagellar filaments ($FliC^{S267C}$). Furthermore, FimV from *P. putida* and HubP from *S. putrefaciens*, or selected domains of these proteins, were exchanged to test whether they are functionally interchangeable or instead perform species-specific roles. Results from this chapter have been published in Schmidt, Pulido-Sánchez et al. [231].

2.2.1 Structural characterization of the FimV protein

The investigation of *P. putida* FimV (*Pp*FimV) was initiated by a detailed analysis of its protein properties in comparison with *P. aeruginosa* FimV (*Pa*FimV) as well as the putative HubP homologs from *S. putrefaciens* (*Sp*HubP) and *V. cholerae* (*Vc*HubP).

*Pp*FimV is predicted to comprise 911 amino acids with a molecular mass of 96.9 kDa, making it highly similar in size to *Pa*FimV (919 amino acids, **Figure 16A**). *Pp*FimV contains an N-terminal signal peptide (SP, amino acids 1-24), followed by a periplasmic region (amino acids 25-387). Within this region, AlphaFold predicts the presence of an immunoglobulin-like (GLB) domain (amino acids 24-135, **Figure 16B**), which is directly located downstream of the signal peptide, as well as a LysM-

like domain (LysM, amino acids 152-206). A single transmembrane helix (TM, amino acids 388-408) separates the periplasmic region from the 503 amino acid long cytoplasmic region. The cytoplasmic region contains the hallmark TPR motif, also referred to as the FimV domain, located at the extreme C-terminus (TPR/FimV, amino acids 863-910). In addition, a second TPR repeat is predicted within this cytoplasmic region (amino acids 487-556).

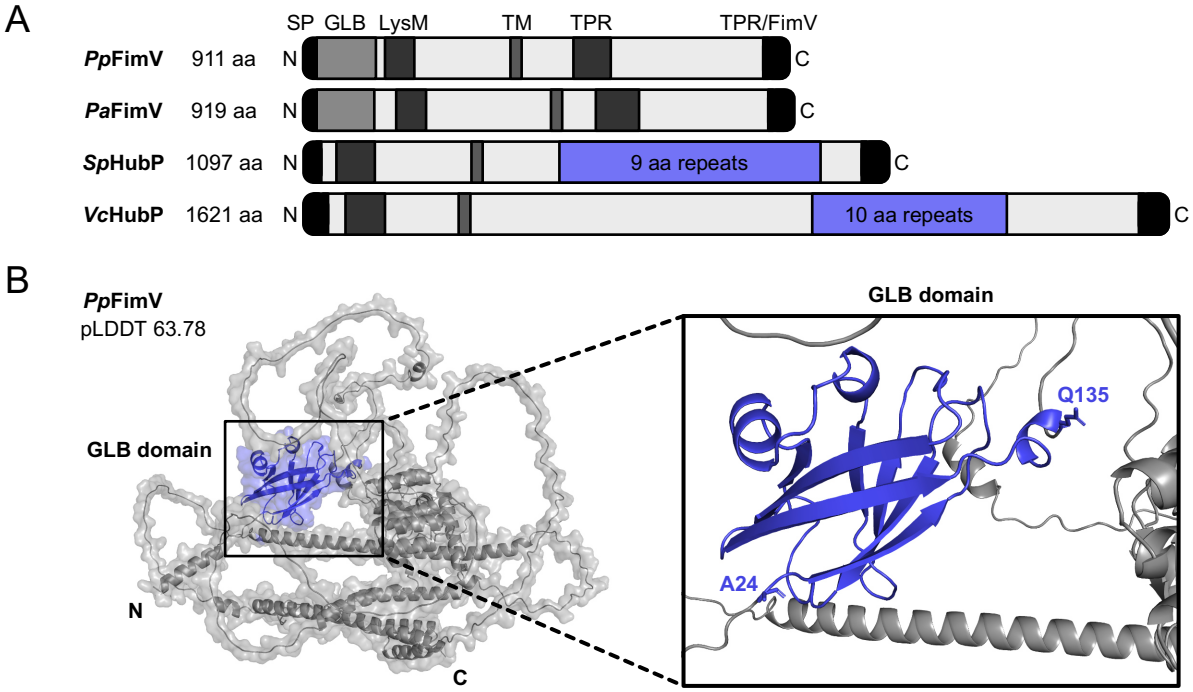

Figure 16. Structural domain organization of FimV and HubP homologs. A Schematic representation of the domain architectures of FimV from *P. putida* (*Pp*FimV) and *P. aeruginosa* (*Pa*FimV) and HubP from *S. putrefaciens* (*Sp*HubP) and *V. cholerae* (*Vc*HubP). Protein sizes (in amino acids) and C- and N-terminal orientation are indicated. The following abbreviations are used: signal peptide (SP), immunoglobulin-like domain (GLB), LysM-like domain (LysM), transmembrane region (TM), FimV domain with TPR motif (TPR/FimV). Regions, enriched in acidic amino acid repeats present in HubP variants are indicated in blue. **B** Left panel: AlphaFold structure prediction of *Pp*FimV (overall calculated pLDDT 63.78) with the GLB domain highlighted in blue. Right panel: Isolated structure of GLB domain spanning alanine 24 to glutamine 135. Structures were created using the AlphaFold Monomer v2.0 pipeline. Alphafold Database ID: AF-Q88LE1-F1-v6. Adapted from [231].

Despite the overall similarity in domain organization, the HubP proteins from *S. putrefaciens* (1097 amino acids) and *V. cholerae* (1621 amino acids) lack the predicted GLB domain within their periplasmic regions (**Figure 16**). In contrast to FimV, both HubP proteins contain multiple imperfect repeats enriched in acidic amino acid residues within their cytoplasmic regions. Notably, the C-terminal region of *Pp*FimV is also highly enriched in acidic residues (25%, 61 aspartate and 64 glutamate residues), resulting in a predicted isoelectric point (PI) of 3.75, comparable to that of *Sp*HubP (3.51). In summary, FimV and HubP share a similar overall domain architecture consistent with a conserved role as polar organizer proteins. However, distinct structural differences, particularly in their periplasmic and cytoplasmic regions, suggest potential species-specific adaptations and divergent interaction networks.

2.2.2 The LysM domain of FimV is essential for its peptidoglycan-binding properties

As mentioned above, FimV and HubP homologs possess a LysM-like domain, which is known to bind N-acetylglucosamine (NAG) residues in peptidoglycan [232], the major structural component of the bacterial cell wall (**Figure 17A**). It was therefore investigated whether FimV from *P. putida* binds to peptidoglycan and whether the LysM-like domain is required for this interaction. To address this, co-precipitation assays were performed using purified FimV-GFP and isolated peptidoglycan sacculi. Unless stated otherwise, FimV refers to *Pp*FimV throughout this study.

Western blot analysis revealed that FimV-GFP co-precipitated *in vitro* with insoluble *P. putida* peptidoglycan sacculi (**Figure 17B**, upper panel). In contrast, deletion of the LysM-like domain abolished this interaction, suggesting that this domain is essential for the peptidoglycan-binding properties of FimV (**Figure 17B**, middle panel). Confocal fluorescence microscopy showed that FimV predominantly localized to the cell pole, whereas deletion of the LysM-like domain lead to a dispersed localization along the cell periphery (**Figure 17C**). Furthermore, FimV-GFP also co-precipitated with peptidoglycan sacculi isolated from *E. coli*, indicating that FimV binds peptidoglycan in a non-species-specific manner (**Figure 17B**, lower panel). Collectively, these findings show that peptidoglycan binding by FimV is mediated by its LysM-like domain and occurs independently of the bacterial species origin.

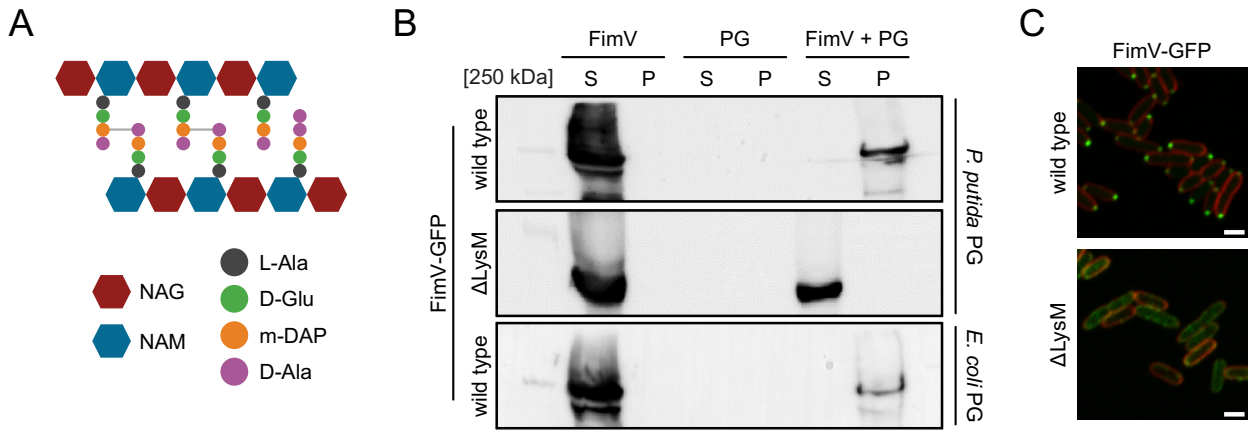

Figure 17. The LysM-like domain of FimV is essential for peptidoglycan binding. A Schematic representation of the peptidoglycan structure composing of alternating glycan strands made of N-acetylglucosamine (NAG) and N-acetylmuramic acid (NAM). Every NAM glycan strand comprises one peptide chain composing of the amino acids L-alanine (L-Ala), D-glutamate (D-Glu), meso-diaminopimelic acid (m-DAP) and D-alanine (D-Ala). The newest muropeptides incorporated into the cell wall carry another D-Ala (see right side in upper panel). Crosslinks between peptide chains (between m-DAP and D-Ala) are denoted by a grey line. **B** Western blot analysis of peptidoglycan binding assay with purified wild-type FimV-GFP or a truncation variant lacking the LysM-like domain (ΔLysM) and isolated peptidoglycan sacculi from either *P. putida* (upper panels) or *E. coli* (lower panel). An anti-GFP antibody was used to detect the fusion proteins. Molecular weight marker shows ~250 kDa. The following abbreviations are used: soluble fraction (S), pellet fraction (P), peptidoglycan (PG). **C** Confocal fluorescence microscopy images of wild-type *P. putida* cells carrying either a P*sal-fimV-gfp* or P*sal-fimV-ΔlysM-gfp* transposon integrated at the *att7* locus (green) are shown. The membrane was stained with FM^{TM} 4-64 (red). Images represent maximum intensity projections of seven Z-sections of the GFP channel, merged with the red channel depicting the cell contour at the focal plane. Scale bar equals 2 µm. Experiments were performed by Marta Pulido-Sánchez (Universidad Pablo de Olavide in Seville). Adapted from [231].

2.2.3 The GLB domain is required for correct polar placement of FimV

Because *Pseudomonas* FimV proteins contain a predicted N-terminal GLB domain that is absent in potential HubP homologs, the function of this domain was investigated in more detail. To address this, *fimV* was translationally fused to *mCherry* to generate a FimV-mCherry fusion protein, which was stably expressed in *P. putida* cells (Supplementary figure 2).

Fluorescence microscopy revealed distinct polar foci formation, with FimV forming one large cluster at one cell pole and a smaller cluster at the opposite pole, as well as localizing to the cell division plane (**Figure 18A**). In contrast, deletion of the GLB domain (FimV$_{\Delta GLB}$) abolished the distinct polar clustering and resulted in a speckled fluorescence pattern, with small clusters distributed along the cell envelope in proximity to one cell pole. Quantification of fluorescent foci, by measuring their relative distance to the cell center, revealed a median value of approximately 0.75 compared to 1 in wild-type cells (**Figure 18A**, right panel). Moreover, deletion of the GLB domain reduced swimming motility in soft-agar to approximately 70% of wild-type levels (**Figure 18B**), whereas a complete deletion of *fimV* resulted in a more pronounced reduction to around 50%. Altogether, these results indicate that, in addition to the LysM-like domain, the GLB domain contributes to proper localization of FimV and is therefore important for its function in supporting swimming motility *P. putida*.

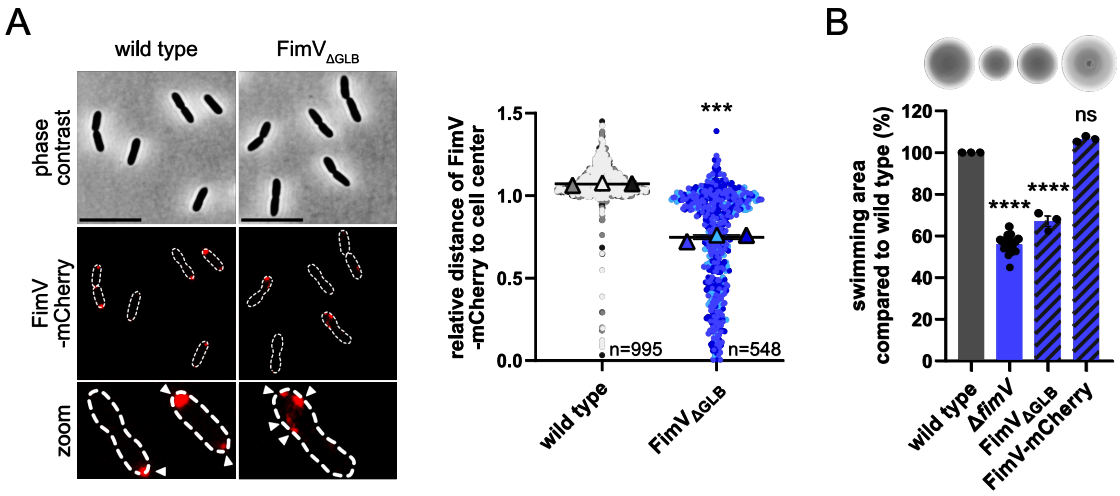

Figure 18. The immunoglobulin-like domain is required for correct polar placement of FimV. A Left panel: fluorescence microscopy images of the FimV-mCherry fusion protein expressed in *P. putida* wild-type cells or in cells lacking the immunoglobulin-like domain of FimV (FimV$_{\Delta GLB}$). The upper row shows phase contrast images, the middle row shows the corresponding mCherry fluorescence (red) and the lower row shows magnified regions of the fluorescence images. Fluorescent FimV foci are indicated by white arrows. Scale bar equals 5 µm. Right panel: quantification of the relative distance of FimV-mCherry to the cell center in *P. putida* wild type and FimV$_{\Delta GLB}$. The relative distance was calculated by dividing the distance between a fluorescent FimV cluster and the cell center (in µm) by the half cell length. Values close to 1 indicate polar localization, whereas values close to 0 correspond to midcell localization. Quantification was performed using the Fiji plugin MicrobeJ. Data from three independent experiments, with total number of cells, are shown as mean values (triangles) together with the mean of the means (horizontal line) and the standard error of the mean. Statistical analysis was performed using a Welch's t-test (***p=0.0006). **B** Swimming motility of the *fimV* deletion mutant, FimV$_{\Delta GLB}$ and FimV-mCherry compared to wild-type cells (set to 100%). Strains were spotted onto the same plate to ensure direct comparison. Data from at least three independent experiments are shown as mean with standard error of the mean. Statistical analysis was performed using one-way ANOVA (****p<0.0001, ns = non-significant; here: p=0.2609). Adapted from [231].

2.2.4 Loss of FimV does not alter cell morphology or flagellation but leads to increased biofilm formation

Reduced swimming motility can result from several cellular processes. To assess whether deletion of *fimV* affects flagellation or cell morphology, these parameters were analyzed in *P. putida.* Transmission electron microscopy revealed the presence of a polar bundle of flagella, consisting of approximately three to five filaments approximately 15 nm in width, in both wild-type cells and the *fimV* deletion mutant (**Figure 19A**). In addition, no notable differences in cell size or overall morphology were observed, as both strains exhibited a mean cell length of approximately 2.3 µm (**Figure 19B**).

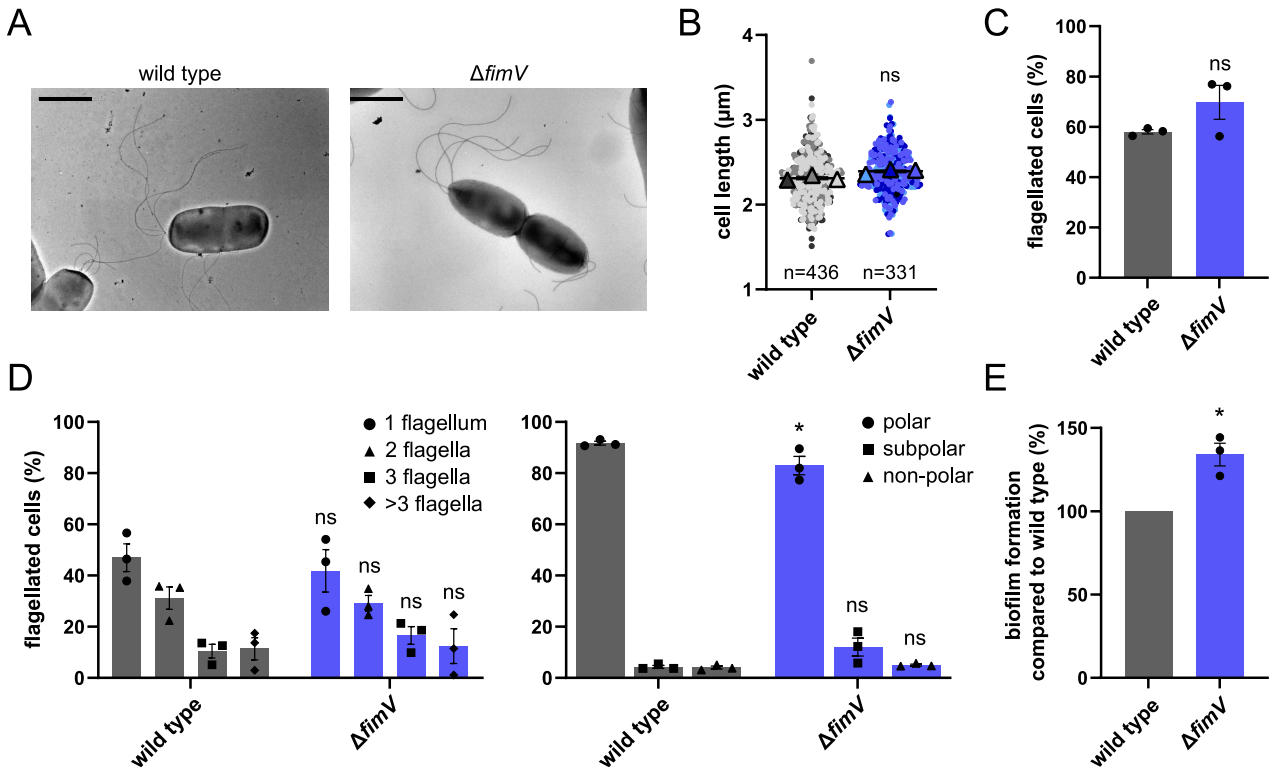

Figure 19. Loss of FimV does not alter cell morphology or flagellation but leads to increased biofilm formation. A Transmission electron microscopy images of *P. putida* wild-type cells and the *fimV* deletion mutant. Scale bar equals 2 µm. **B** Quantification analysis of the cell length (in µm) of *P. putida* wild-type cells and the *fimV* deletion mutant performed using the Bacstalk software. Data from three independent experiments, with total number of cells, are shown as mean values (triangles) together with the mean of the means (horizontal line) and the standard error of the mean. Statistical analysis was performed using a Mann-Whitney test (ns = non-significant; here p=0.1). **C** Quantification analysis of flagellated cells in *P. putida* FliC^{S267C} wild-type cells or in a *fimV* deletion mutant. Flagellar filaments were stained using Alexa Fluor 488-C5-maleimide-conjugated fluorescent dye. Data from three independent experiments, with more than 300 cells analyzed per replicate, are shown as mean with standard error of the mean. Statistical analysis was performed using Welch's t-test (ns = non-significant; here: p=0.2244). **D** Quantification analysis of the number of flagella (left panel) and localization pattern (right panel) of flagellated cells, classified as polar, subpolar or non-polar. Data from three independent experiments, with more than 300 cells analyzed per replicate, are shown as mean with standard error of the mean. Statistical analysis was performed using two-way ANOVA (*p=0.0364, ns = non-significant; here p>0.05). **E** Quantification analysis of biofilm formation of the *fimV* deletion mutant compared to *P. putida* wild-type cells (set to 100%). Biofilms were stained with 0.5% (w/v) crystal violet and absorption was measured at 580 nm using a Tecan plate reader. Data from three independent experiments are shown as mean with standard error of the mean. Statistical analysis was performed using Welch's t-test (*p=0.0377). Adapted from [231].

Further quantification of flagellation was performed by staining of flagellar filaments. To this end, a serine-to-cysteine substitution at position 267 in the flagellar filament protein FliC (FliC^{S267C}) was

introduced [12], enabling the covalent coupling of a maleimide-conjugated fluorescent dye. Fluorescent staining revealed that approximately 60% of wild-type cells and up to 80% of *fimV*-deficient cells were flagellated (**Figure 19C**). Among these cells, about 90% displayed polar flagellar localization. More than 40% of cells carried a single flagellum, whereas fewer than 20% possessed three or more flagella (**Figure 19D**). Because reduced motility can sometimes be associated with a shift from a motile to sessile lifestyle, biofilm formation was investigated. Analysis of biofilm formation in the *fimV* deletion mutant revealed a statistically significant increase to approximately 145% compared to wild-type cells (**Figure 19E**). Taken together, these results indicate that deletion of *fimV* does not affect the flagellar number, localization or overall cell morphology, but leads to enhanced biofilm formation.

2.2.5 Bacterial growth is not affected by deletion of FimV

In *Vibrio vulnificus,* HubP has been reported to recruit a positive regulator of flagellar assembly in a carbon source-dependent manner, thereby linking motility to environmental nutrient conditions [228]. To investigate whether nutrient availability similarly influences FimV-dependent motility, swimming assays were performed in M9 minimal medium supplemented with different carbon sources (glucose, L-arginine and L-glutamine).

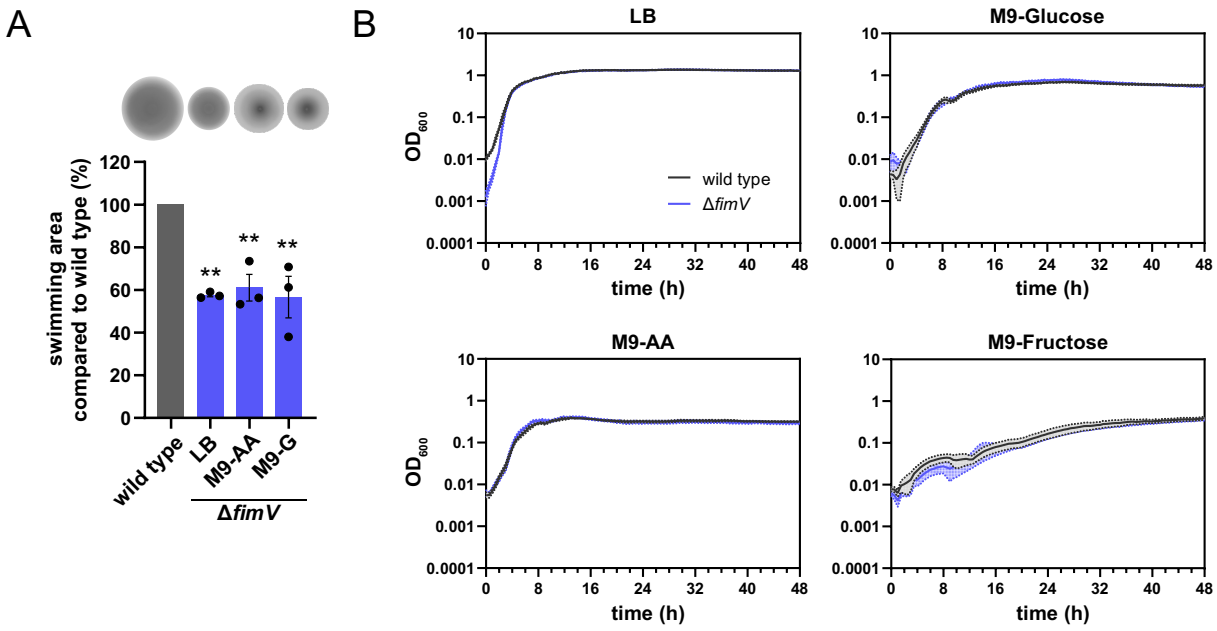

Figure 20. Bacterial growth is not affected by deletion of FimV. A Swimming motility of the *fimV* deletion mutant compared to *P. putida* wild-type swimming (set to 100%) in LB medium and M9 minimal medium supplemented with different carbon sources: L-arginine and L-glutamine (M9-AA, 5 mM each) or glucose (M9-G, 0.4%). Strains were spotted onto the same plate to ensure direct comparison. Data from three independent experiments are shown as mean with standard error of the mean. Statistical analysis was performed using one-way ANOVA (**p<0.01). **B** Growth curves of the *fimV* deletion mutant and *P. putida* wild type measured as OD_{600} in LB medium and M9 minimal medium, supplemented with the carbon sources mentioned above, as well as fructose (M9-Fructose, 0.4%). Data from three independent experiments are shown as mean with standard error of the mean. Adapted from [231].

No differences in swimming behavior of the *fimV* deletion mutant were detected between minimal medium and rich LB medium conditions (**Figure 20A**). Because altered growth can also influence swimming behavior in soft-agar, growth curves were recorded in both LB and M9 minimal medium. However, no significant differences in growth were detected between the *fimV* deletion mutant and wild-type cells under either condition (**Figure 20B**). In summary, deletion of *fimV* does not affect growth or nutrient-dependent swimming motility in *P. putida*.

2.2.6 FimV may contribute to the accurate placement of the chemotaxis machinery

After excluding growth, cell morphology and flagellation as causes of the altered swimming behavior, it was investigated whether changes in localization of the chemotaxis machinery affect motility in *P. putida*. To address this, CheA, the main histidine kinase of the chemotaxis system, was fused to mCherry creating a stably produced CheA-mCherry fusion protein in *P. putida* (Supplementary figure 2). The fusion protein retained partial functionality, as cells exhibit approximately 70% swimming ability compared to wild-type cells (**Figure 21A**).

In both, the wild type and *fimV* deletion strains, approximately 70% of cells displayed fluorescent CheA foci (**Figure 21B**). Combined staining of flagellar filaments revealed that CheA was localized in small, distinct clusters at the flagellated cell pole in *P. putida* (**Figure 21C**). Quantitative analysis confirmed polar localization of CheA, with a relative distance to cell center close to 1 (**Figure 21D**). In the absence of FimV, CheA localization appeared less distinct, often occurring near, but not directly at the cell pole and was occasionally split into multiple smaller foci (**Figure 21C**).

Since FlhF has previously been described to play a role in proper polar positioning of the chemotaxis and flagellar machinery in *P. aeruginosa* [163], deletion of *flhF* was also analyzed. In contrast to wild-type and *fimV* deletion cells, deletion of *flhF* reduced the proportion of cells displaying CheA foci to approximately 20% (**Figure 21B**). Moreover, CheA and flagella were no longer co-localized at the cell pole but were instead distributed along the cell body (**Figure 21C**). Consistently, the relative distance of CheA foci to the cell center was significantly reduced to approximately 0.8 in the *flhF* deletion mutant (**Figure 21D**).

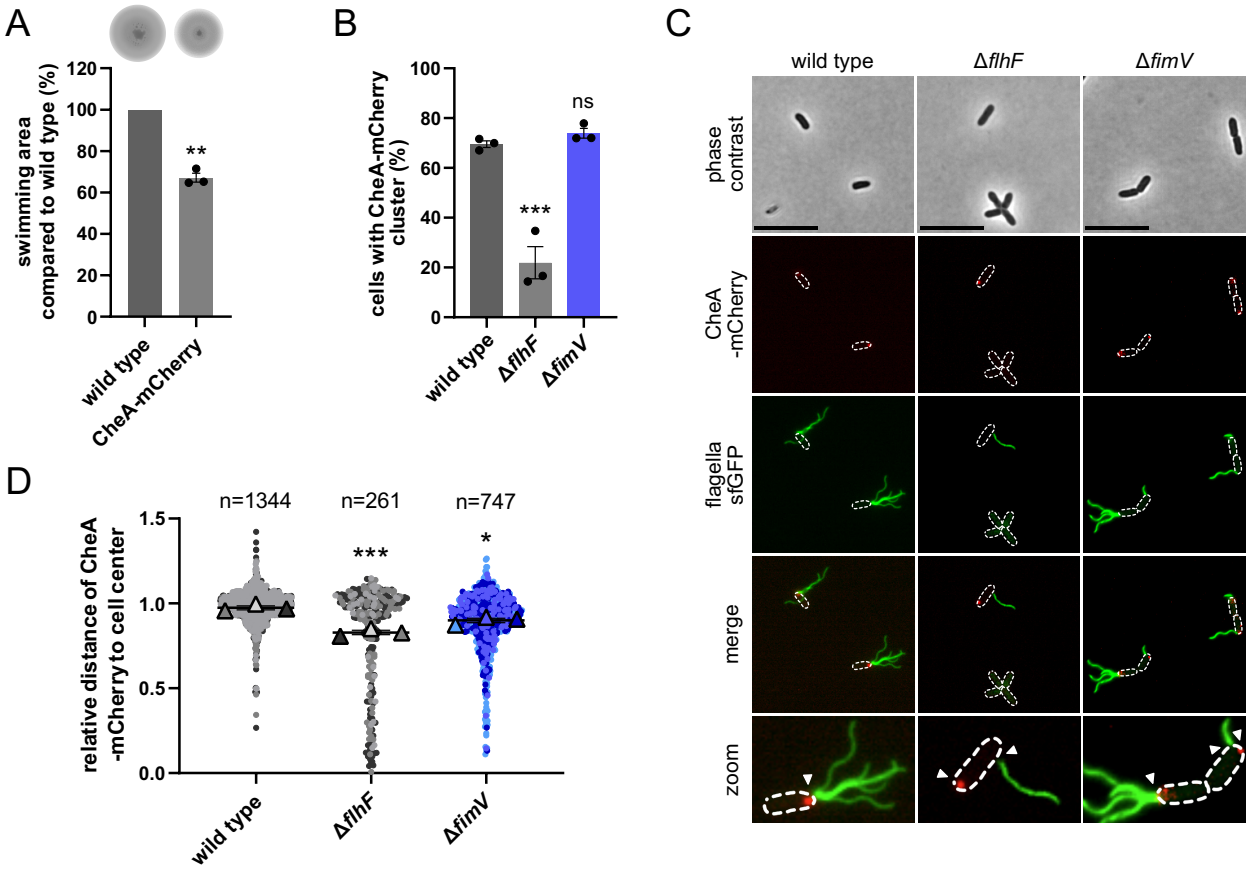

Figure 21. FimV may contribute to the accurate placement of the chemotaxis system. A Swimming motility of cells harboring the CheA-mCherry fusion protein compared to wild-type cells (set to 100%). Strains were spotted onto the same plate to ensure direct comparison. Data from three independent experiments are shown as mean with standard error of the mean. Statistical analysis was performed using Welch's t-test (**p=0.0043). **B** Quantification of cells exhibiting fluorescent CheA-mCherry cluster (percentage) of *P. putida* wild-type cells and *flhF* or *fimV* deletion mutants. Data from three independent experiments are shown as mean with standard error of the mean. Statistical analysis was performed using one-way ANOVA (***p=0.0003, ns = non-significant; here: p=0.4609). **C** Fluorescence microscopy images of CheA-mCherry expressed in *P. putida* wild-type cells and in *flhF* or *fimV* deletion mutants. The upper row shows phase contrast images, followed by the corresponding mCherry fluorescence (red) and the sfGFP fluorescence of stained flagellar filaments (green). Flagella were stained using Alexa Fluor 488-C5-maleimide-conjugated dye in *P. putida* FliC^{S267C}. The merged images show an overlay of the mCherry and sfGFP channels. The lower row shows magnified regions of the merged fluorescence images. Fluorescent CheA foci and flagellar filaments are indicated by white arrows. Scale bar equals 5 µm. **D** Quantification of the relative distance of CheA-mCherry cluster to the cell center in *P. putida* wild type and *flhF* and *fimV* deletion mutants. The relative distance was calculated by dividing the distance between a fluorescent CheA cluster and the cell center (in µm) by the half cell length. Values close to 1 indicate polar localization, whereas values close to 0 correspond to midcell localization. Quantifications were performed using the Fiji plugin MicrobeJ. Data from three independent experiments, with total number of cells, are shown as mean values (triangles) together with the mean of the means (horizontal line) and the standard error of the mean. Statistical analysis was performed using one-way ANOVA (*p=0.0111, ***p=0.0004). Adapted from [231].

Additionally, bacterial two-hybrid assays were performed to test for interactions between the aforementioned proteins. In contrast to its homolog HubP in *S. putrefaciens*, FimV did not interact with FlhF in *P. putida* (**Figure 22A**). Moreover, no direct interaction of FlhF and the histidine kinase CheA was detected (**Figure 22B**). Consistent with the fluorescence microscopy observations, FimV showed an interaction with CheA in the bacterial two-hybrid assays, at least when the T25 fragment was fused to the C-terminus of FimV (**Figure 22C**). Taken together, these results indicate that while FlhF is essential for proper polar positioning of the chemotaxis and flagellar machinery, FimV appears to play a more subtle role, likely contributing to the accuracy of polar placement, assembly

or function of the chemotaxis machinery. This notion is supported by bacterial two-hybrid assays, which revealed an interaction between FimV and the chemotaxis kinase CheA, suggesting a potential role of FimV in fine-tuning chemotaxis complex positioning or stability.

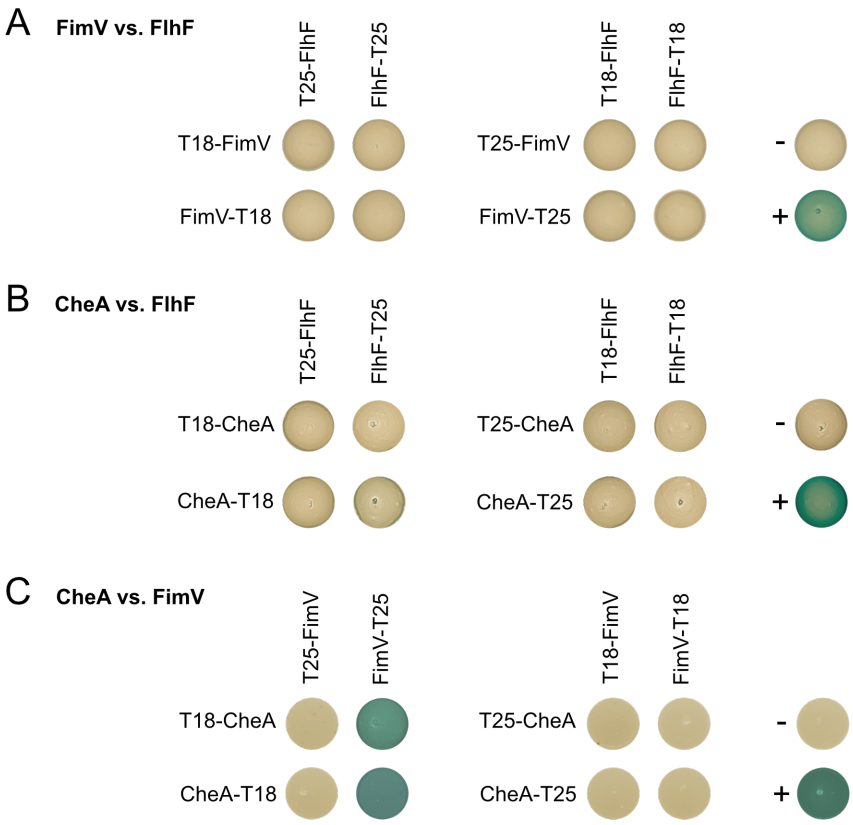

Figure 22. The histidine kinase CheA interacts with FimV. Bacterial two-hybrid analysis showing interactions between **A** FimV and FlhF, **B** CheA and FlhF and **C** CheA and FimV. Proteins were fused either N- or C-terminally to the T18 or T25 fragment of the catalytic domain of *Bordetella pertussis* adenylate cyclase. Blue coloration of colonies indicates reconstitution of adenylate cyclase activity and subsequent conversion of X-Gal, thereby indicating protein-protein interaction. "+" indicates the positive control and "-" the negative control. Data from at least two independent experiments are shown.

2.2.7 Loss of FimV does not affect chromosome segregation

As previously mentioned, the potential FimV homolog HubP is involved in correct placement of chromosome segregation in *S. putrefaciens* and *V. cholerae* [132,134]. To test whether this function is conserved in *P. putida*, the centromere-binding protein ParB, which binds to the *parS* site near the origin of replication, was fused to sfGFP. The stably produced fusion protein (Supplementary figure 2) was used to analyze the effect of a *fimV* deletion on chromosome segregation in *P. putida*.

Fluorescence time-lapse microscopy of cells expressing both FimV-mCherry and sfGFP-ParB revealed that FimV localized monopolar, bipolar or to the cell division plane during the cell cycle, consistent with previous observations (**Figure 23A**). In contrast, ParB formed several small, dynamic clusters that repositioned throughout the cell cycle in accordance with chromosome segregation.

When ParB localized toward the cell pole, it did not reach the extreme pole but remained at a distance of approximately 10-20% from the cell pole. Furthermore, the relative distance of sfGFP-ParB foci to the cell pole was not altered in the *fimV* deletion mutant compared to wild-type cells (**Figure 23B**). Collectively, these observations indicate that, in contrast to its proposed homolog HubP, FimV does not appear to play a role in chromosome segregation in *P. putida*.

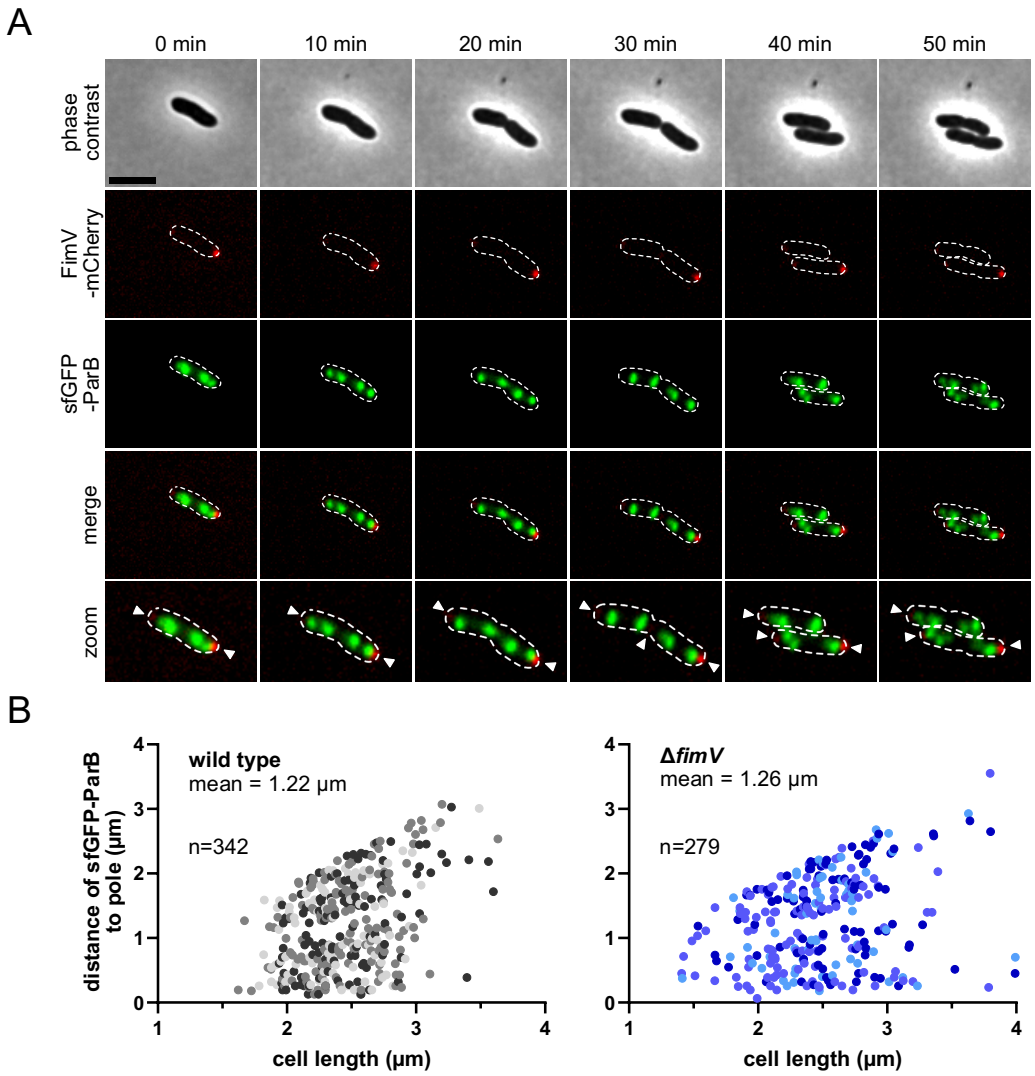

Figure 23. Loss of FimV does not affect chromosome segregation. A Fluorescence time-lapse microscopy images of FimV-mCherry and sfGFP-ParB expressed in *P. putida* wild-type cells. The upper row shows phase contrast images, followed by the corresponding mCherry fluorescence (FimV, red) and the sfGFP fluorescence (ParB, green). The merged images show an overlay of the mCherry and sfGFP channels. The lower row shows magnified regions of the merged fluorescence images. Fluorescent FimV foci are indicated by white arrows. Scale bar equals 2 µm. **B** Distance of sfGFP-ParB cluster to the cell pole (in µm) plotted relative to cell length (in µm) in *P. putida* wild type (left panel) and the *fimV* deletion mutant (right panel). Quantification was performed using the Bacstalk software. Data from three independent experiments are shown, including individual cells (colored by replicate) and mean values. Adapted from [231].

2.2.8 FimV is not required for pilus-mediated surface motility

While FimV was previously shown to be indispensable for twitching motility in *P. aeruginosa* [136,230] and its potential homolog HubP has also been implicated in twitching motility in

S. putrefaciens [132], this type of surface motility has not yet been demonstrated for *P. putida*. Notably, although orthologues of most core components of the *P. aeruginosa* type IV pilus system can be identified in *P. putida*, no clear homologs of the ATPases PilB/PilU and PilK are present (Table 1).

Table 1. Gene homologs. Gene homologs and corresponding gene numbers of *P. putida* and *P. aeruginosa pil* genes. Adapted from [231].

Gene name	*P. putida*	*P. aeruginosa*
pilA	PP_0634	PA4525
pilB	no documented homolog	PA4526
pilC	PP_0633	PA4527
pilD	PP_0632	PA4528
pilE	PP_0611	PA4556
pilF	PP_0851	PA3805
pilG	PP_4992	PA0408
pilH	PP_4991	PA0409
pilI	PP_4990	PA0410
pilJ	PP_4989	PA0411
pilK	no documented homolog	PA0412
pilM	PP_5083	PA5044
pilN	PP_5082	PA5043
pilO	PP_3480	PA5042
pilP	PP_5081	PA5041
pilQ	PP_5080	PA5040
pilT	PP_5093	PA0395
pilU	no documented homolog	PA0396

To test whether a comparable phenotype could be observed, twitching assays were performed following protocols established for *P. aeruginosa* (see Materials and Methods section 5.1.7). To exclude any contribution of flagella to surface motility, a strain lacking *fliC*, encoding the main flagellin, was used.

All tested strains, including the *fimV* deletion mutant and a *pilA* deletion mutant lacking the major pilin of the type IV pilus, still exhibited motile behavior (**Figure 24A**). These results indicate that the observed spreading is likely independent of both flagella and type IV pili, and therefore does not allow any conclusions regarding a role of FimV in twitching motility. Consistently, transmission electron microscopy on *P. putida* cells lacking FimV revealed only very rare pilus-like structures of approximately eight nm in width (less than 1 in 1,000 cells, **Figure 24B**).

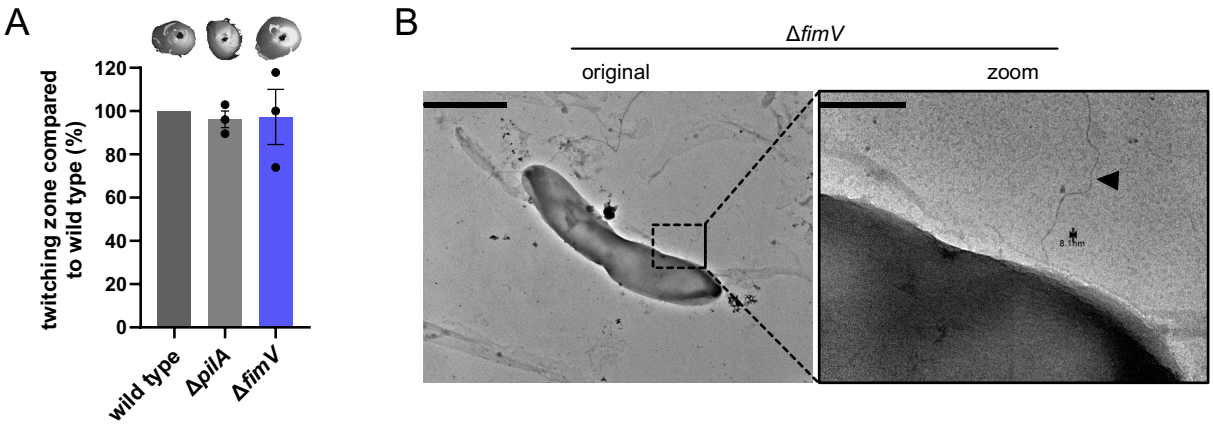

Figure 24. The *fimV* deletion mutant exhibits pilus-like structures. A Putative twitching motility of a *pilA* and *fimV* deletion mutant compared to wild-type cells (set to 100%). Strains were spotted onto the same plate to ensure direct comparison. Data from three independent experiments are shown as mean with standard error of the mean. **B** Transmission electron microscopy images of the *fimV* deletion mutant showing a pilus-like structure of approximately 8 nm, indicated by the arrow. Scale bar equals 2 µm (original) and 500 nm (zoom), respectively. Adapted from [231].

However, a different form of pilus-mediated surface motility has previously been described [100] and was therefore applied to further assess the potential involvement of FimV in pilus-dependent motility in *P. putida*. For this assay, *P. putida* cells were spotted onto PG-agar plates and incubated at 25°C for three days, including a transfer step of the motile population from the spreading edge onto a new plate. As shown in **Figure 25A**, wild-type cells displayed surface spreading comparable to that of the *fimV* deletion mutant, whereas deletion of the major pilin (*pilA*) abolished any detectable motility on these plates. Transmission electron microscopy of *fimV* deficient cells from the outer edge of the spreading area revealed pronounced hyper-flagellation and loss of polar identity in many cells (**Figure 25B**, left panel). Cells exhibited flagellar filaments with approximately 14 nm in width. In contrast, cells from the inner region of the plate often appeared more rounded and were either completely non-flagellated or carried several flagella distributed around the cell body (**Figure 25B**, right panel). In addition, numerous sheared-off flagellar filaments were detected in the surrounding area.

Because this phenotype was hypothesized to arise from emerging genetic variants rather than physiological adaptation [100], motile cells from the edge of the spreading zone were isolated and re-tested in pilus-mediated surface spreading assays. Using these evolved strains, surface spreading behavior became more regular and pronounced (data not shown). Since loss of flagellar polarity and hyper-flagellation are frequently associated with mutations in *flhF* or *flhG* (*fleN* in *Pseudomonas*), these genes were sequenced in the evolved strains to determine whether genetic alterations were responsible for the observed hyper-motile phenotype. However, sequencing did not reveal any mutations in either *flhF* or *fleN*.

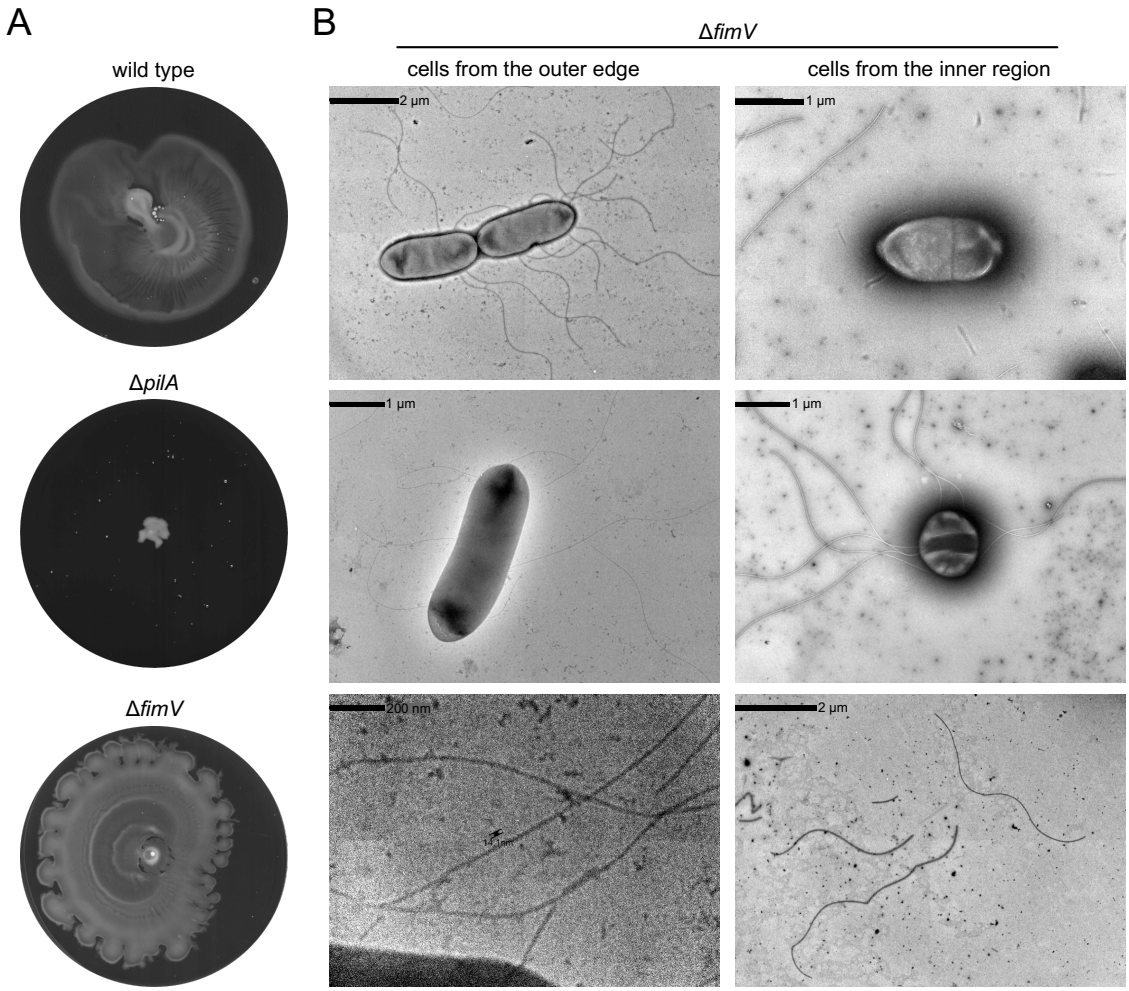

Figure 25. FimV is not required for pilus-mediated surface motility. A Representative images of pilus-mediated surface motility of *P. putida* wild-type cells and *pilA* and *fimV* deletion mutants on 0.5% PG-agar plates. Images shown are from at least three independent experiments. **B** Transmission electron microscopy images of *fimV* deletion mutants, isolated either from the outer edge (left panel) or the inner region (right panel) of PG-agar plates. Scale bar sizes are indicated in the images. Adapted from [231].

To further investigate whether alterations in these genes could reproduce the observed phenotype, an *flhF fleN* double deletion mutant was constructed. As previously shown, a *flhF* deletion mutant only rarely contained flagella, whereas a *fleN* deletion mutant exhibited hyper-flagellation that remained predominantly polar (**Figure 26A**). Consistent with the electron microscopy observations, the double mutant also displayed hyper-flagellation, with flagella distributed around the cell body. However, in contrast to the evolved strains, these flagella were considerably shorter and the double mutant exhibited a non-motile phenotype in soft-agar swimming assays. For comparison, swimming motility in cells lacking *flhF* was reduced to approximately 20%, whereas the *fleN* deletion mutant retained about 50% of wild-type motility (**Figure 26B**). In summary, these results suggest that FimV does not play a major role in pilus-mediated motility in *P. putida*. Nevertheless, a subtle contribution of FimV to the polar placement or activity of type IV pili cannot be fully excluded. Moreover, although a genetic basis for the observed hypermotile phenotype appears likely, no mutations were detected in *flhF* or *fleN*.

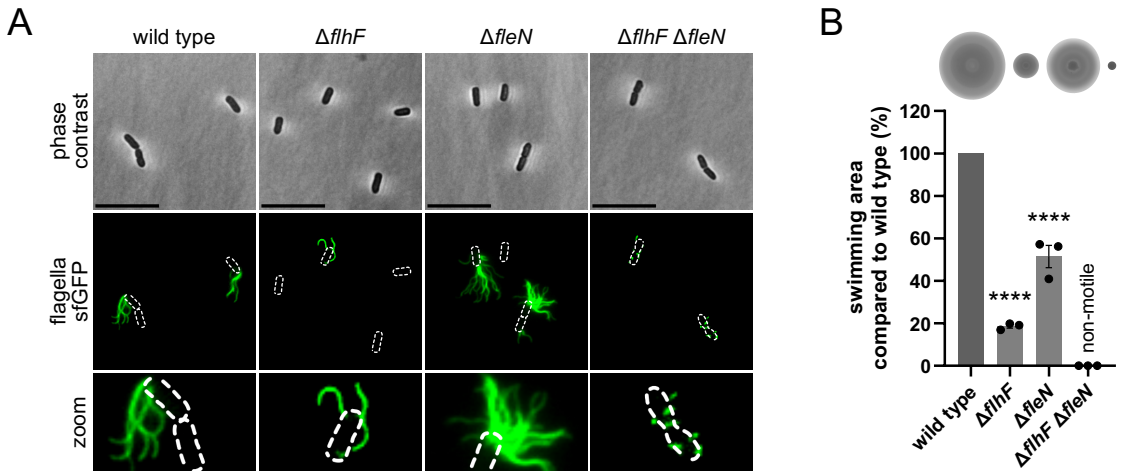

Figure 26. Deletion of *flhF* and *fleN* does not lead to hyper-motile phenotype. A Fluorescence microscopy images of stained flagellar filaments of *P. putida* wild-type cells and *flhF*, *fleN* or the double deletion mutant. The upper row shows phase contrast images, followed by the corresponding sfGFP fluorescence of stained flagellar filaments (green). Flagella were stained using Alexa Fluor 488-C5-maleimide-conjugated dye in *P. putida* FliC^{S267C}. The lower row shows magnified regions of the fluorescence images. Scale bar equals 5 µm. **B** Swimming motility of *flhF*, *fleN* and the double deletion mutant compared to wild-type cells (set to 100%). Strains were spotted onto the same plate to ensure direct comparison. Data from three independent experiments are shown as mean with standard error of the mean. Statistical analysis was performed using one-way ANOVA (****p<0.0001).

2.2.8.1 *P. putida* shows swarming-like motility on PG-agar

During the execution of pilus-mediates surface motility assays, a second type of a motility was occasionally observed, although all experiments were performed using identical experimental conditions. This alternative motility phenotype differed in several aspects from the previously described surface spreading (**Figure 25**) and instead resembled the flower-like pattern characteristic of swarming motility in *P. aeruginosa* PA14 [233]. Consistently, control experiments using *P. aeruginosa* PAO1 confirmed that swarming motility can occur on PG-agar plates, although the more circular swarming pattern of this strain differed from the tendril-like pattern of PA14 (**Figure 27A**, [233]). Notably, the appearance of this putative swarming motility occurred approximately one day later than the pilus-mediates surface spreading described above.

This swarming-like motility was observed in wild-type cells as well as in *fimV* and *pilA* deletion mutants, indicating that this behavior is independent of type IV pili (**Figure 27B**). In contrast, this phenotype was never observed in strains lacking the major flagellar filament protein FliC, hypothesizing its dependence on flagella (Supplementary figure 3). Transmission electron microscopy revealed that cells at the spreading edge occasionally possessed lateral flagella and that polar identity was less strictly maintained (**Figure 27C**). In addition, cells frequently contained prominent intracellular vesicle-like structures that were not observed at similar frequencies in earlier experiments and the agar background often appeared more structured. Moreover, further passaging of a *fimV* deletion strain resulted in the emergence of a comparable swarming-like pattern as observed for PAO1 after two generations (**Figure 27D**). Altogether, these observations indicate the presence of a second motility mode on PG-agar plates that resembles swarming motility previously

described for *P. aeruginosa*. Again, FimV does not appear to influence this type of motility in *P. putida*.

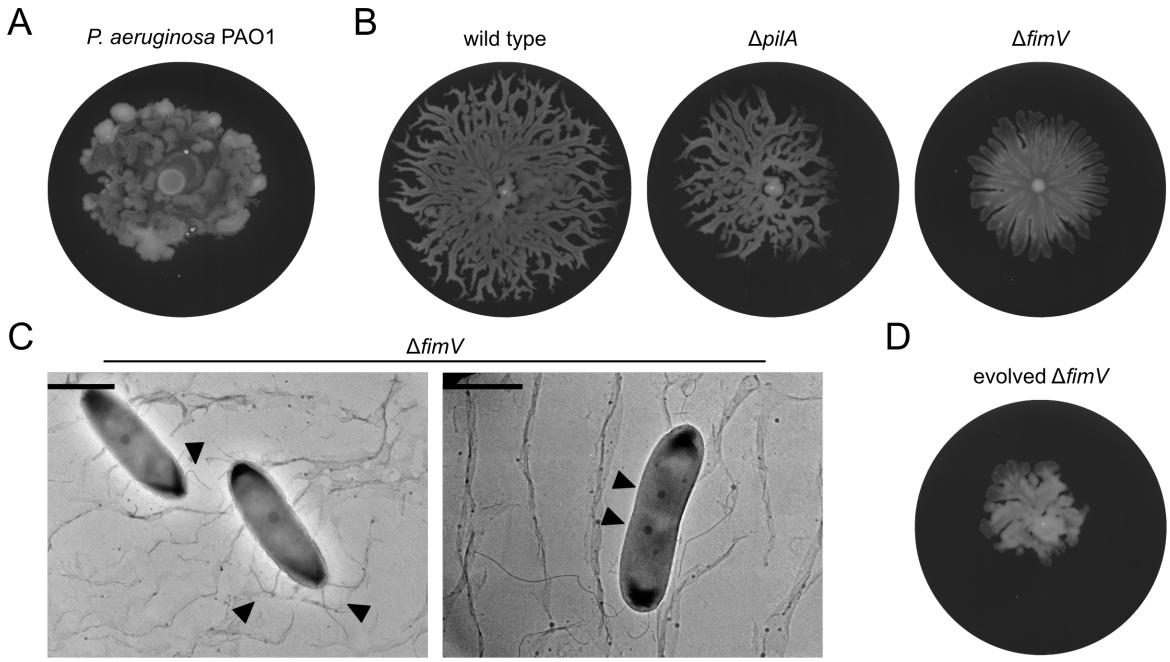

Figure 27. *P. putida* shows swarming-like behavior on PG-agar. A Swarming motility of *P. aeruginosa* PAO1 on 0.5% PG-agar plates. **B** Swarming-like motility of *P. putida* wild-type cells and *pilA* and *fimV* deletion mutants on 0.5% PG-agar plates. **C** Transmission electron microscopy images of *P. putida fimV* deletion mutants, isolated from the outer edge of 0.5% PG-agar plates. Scale bar equals 2 µm. Arrows indicate flagella and vesicle-like structures. **D** Swarming-like motility of evolved *P. putida fimV* deletion mutant on 0.5% PG-agar plate after two generations. Representative images from at least three independent experiments are shown.

2.2.9 FimV deletion cannot be functionally complemented by *Sp*HubP or its domains

Since *Sp*HubP and *Pp*FimV share a similar structural domain organization, their potential functional interchangeability was investigated. To this end, full-length proteins as well as domain-swapped versions of *Sp*HubP and *Pp*FimV were expressed in *P. putida* or *S. putrefaciens*, and their ability to restore swimming motility was assessed.

While plasmid-based expression of *fimV* partially restored the motility defect of a *fimV* deletion mutant, reintegration of *fimV* at its native locus fully restored the wild-type phenotype (**Figure 28A**). Prior to functional complementation assays, *Sp*HubP and *Pp*FimV were fused to sfGFP and introduced into the heterologous host to assess protein stability and localization. Both proteins were stably expressed and localized to the cell pole in the non-native host, however, fluorescent signals were detectable only in a small subpopulation of cells (**Figure 28B**, Supplementary figure 2).

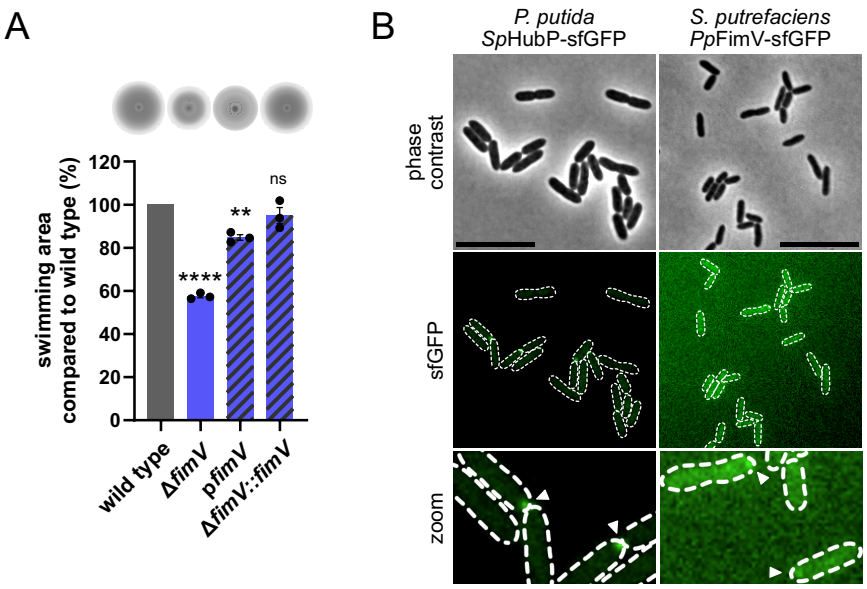

Figure 28. *Sp*HubP and *Pp*FimV show polar localization in their heterologous host. A Swimming motility of the *fimV* deletion mutant and plasmid-based complementation from cumate-inducible system (pBBR1-MCS2-cym, *p*fimV) or reintegration of *fimV* into its native locus (Δ*fimV*::*fimV*) compared to wild-type cells (set to 100%). Strains were spotted onto the same plate to ensure direct comparison. Data from three independent experiments are shown as mean with standard error of the mean. Statistical analysis was performed using one-way ANOVA (****p<0.0001, **p=0.0017, ns = non-significant; here: p=0.2476). **B** Fluorescence microscopy images of *Sp*HubP-sfGFP expressed in *P. putida* and *Pp*FimV-sfGFP expressed in *S. putrefaciens*. The upper row shows phase contrast images, followed by the corresponding sfGFP fluorescence. The lower row shows magnified regions of the fluorescence images. Fluorescent *Sp*HubP or *Pp*FimV foci are indicated by white arrows. Scale bar equals 5 µm. Adapted from [231].

Functional complementation assays revealed that neither full-length *Sp*HubP expressed in *P. putida* nor full-length *Pp*FimV expressed in *S. putrefaciens* were able to restore wild-type swimming motility. In *P. putida*, expression of *Sp*HubP resulted in swimming motility of approximately 50%, comparable to the *fimV* deletion mutant, while expression of *Pp*FimV in *S. putrefaciens* resulted in motility of around 20%, resembling the *hubP* deletion phenotype (**Figure 29**).

To further dissect domain-specific contributions, chimeric proteins were constructed, in which individual domains were exchanges between *Pp*FimV and *Sp*HubP. Exchange of the FimV domain from *P. putida* into *Sp*HubP did not restore swimming motility, resulting in approximately 80% motility, comparable to a *Sp*HubP variant lacking its FimV domain (**Figure 29B**). Conversely, insertion of the *S. putrefaciens* FimV domain into *Pp*FimV increased swimming motility to approximately 110%, similar to a *Pp*FimV variant lacking its native FimV domain (**Figure 29A**). Exchange of the cytoplasmic regions revealed stronger effects. Introduction of the *Sp*HubP cytoplasmic region into *Pp*FimV resulted in a phenotype comparable to the *fimV* deletion mutant, whereas insertion of the *Pp*FimV cytoplasmic region into *Sp*HubP lead to an intermediate phenotype with approximately 50% swimming ability. Swapping the periplasmic regions caused more moderate effects. Insertion of the *Sp*HubP periplasmic region into *Pp*FimV decreased swimming motility to around 70% (**Figure 29A**). In contrast, replacement of the *Sp*HubP periplasmic region with that of *Pp*FimV caused a minor reduction in swimming motility of approximately 10% (**Figure 29B**). Taken

together, these results show that although *Sp*HubP and *Pp*FimV share a similar overall domain organization, they are not interchangeable. In particular, the cytoplasmic regions appear to have species-specific functionality, while the FimV domain itself is not essential for swimming motility in either organism.

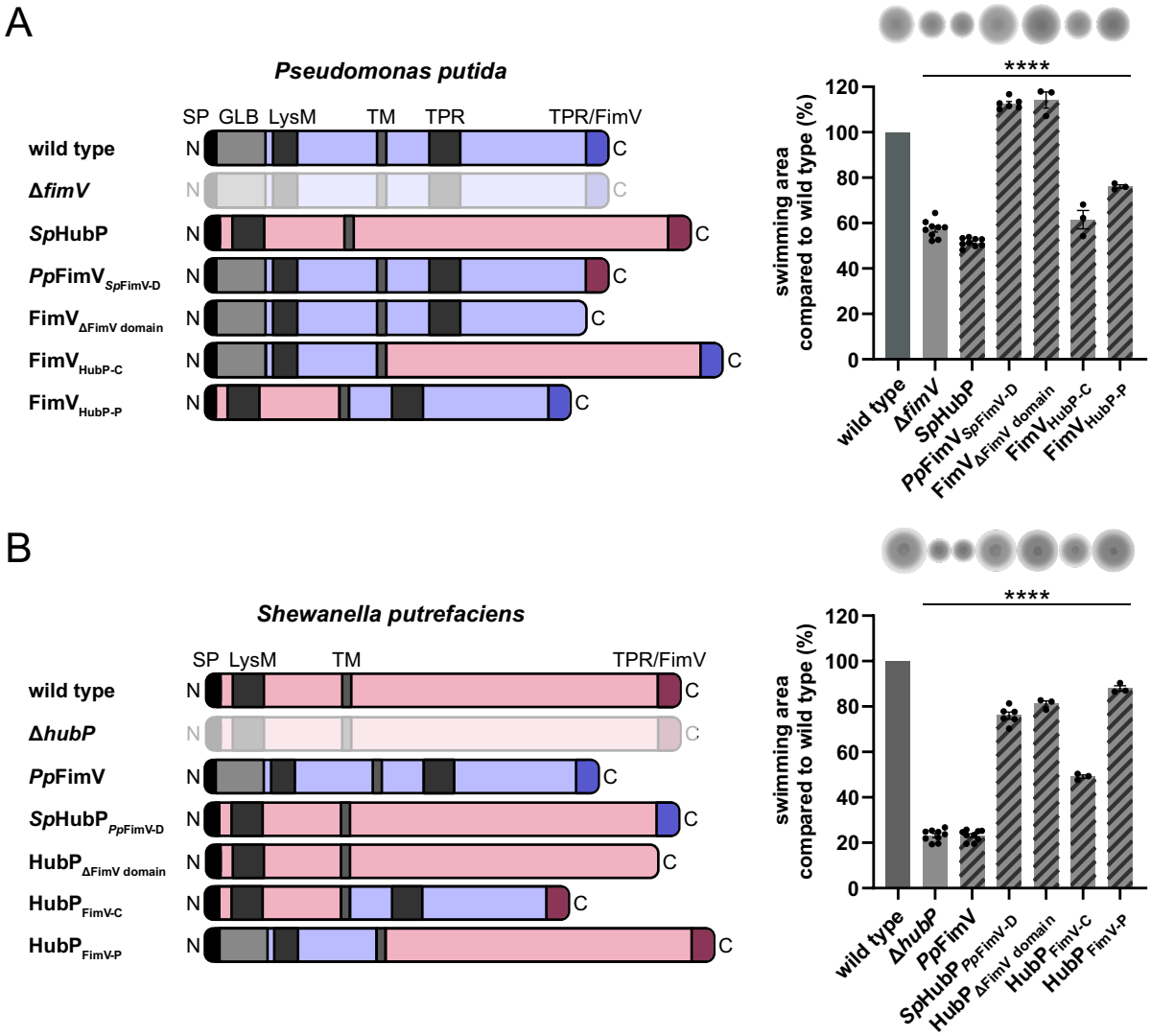

Figure 29. FimV cannot be functionally complemented by *Sp*HubP or its domains. Left panels: schematic representation of the domain architectures of FimV and its variants expressed in *P. putida* (**A**) or HubP and its variants expressed in *S. putrefaciens* (**B**). Right panels: swimming motility of the FimV variants compared to *P. putida* (**A**) or HubP variants compared to *S. putrefaciens* (**B**) wild-type cells (set to 100%). Domains and N- and C-terminal orientations are indicated. Blue coloring represents *P. putida* domain structures, whereas magenta coloring corresponds to *S. putrefaciens* domain structures. The following abbreviations are used: signal peptide (SP), immunoglobulin-like domain (GLB), LysM-like domain (LysM), transmembrane region (TM), tetratricopeptide repeat-like domain, also referred to as FimV domain (TPR/FimV). Strains were spotted onto the same plate to ensure direct comparison. Data from three independent experiments are shown as mean with standard error of the mean. Statistical analysis was performed using one-way ANOVA (****p<0.0001). Adapted from [231].

In conclusion, this chapter demonstrated that FimV acts as a polar organizer in *P. putida* and shares a conserved overall architecture with HubP homologs, while also displaying distinct structural features such as an N-terminal GLB domain. FimV binds peptidoglycan in a LysM-dependent

manner and requires both the LysM-like and GLB domains for proper polar localization. Although deletion of *fimV* does not affect cell growth, morphology, flagellation or chromosome segregation, it results in reduced swimming motility, altered chemotaxis protein positioning and increased biofilm formation. Complementation experiments revealed that *Pp*FimV and *Sp*HubP are not functionally interchangeable, indicating species-specific roles despite structural similarity. Together, these findings establish FimV as a relevant contributor to polar organization in *P. putida*.

2.3 Interaction of the PDE Pch and histidine kinase CheA in *P. putida*

In addition to the polar landmark proteins HubP and FlhF, several further proteins are known to localize to the cell pole in bacteria. As previously mentioned, the main histidine kinase CheA of the chemotaxis machinery shows polar localization in *S. putrefaciens* and *Pseudomonas* species, largely dependent on HubP or FlhF, respectively, and to a lesser extent on FimV [132,134,163,231]. In addition, another protein in *P. aeruginosa* was identified whose polar localization depends on both CheA and FlhF: the PDE Pch [163]. CheA and Pch were found to co-immunoprecipitate, suggesting an interaction and linking c-di-GMP homeostasis to the chemotaxis and flagellar machinery [163]. However, neither the nature of this interaction nor the underlying mechanisms governing polar recruitment of the chemotaxis machinery in *P. putida* have been characterized in detail to date.

This final chapter therefore focuses on the polar localization of CheA, as a representative component of the chemotaxis machinery, and Pch as well as on their potential interaction in *P. putida*. To this end, the polar localization of both proteins was investigated by fluorescence microscopy. Moreover, their interaction was further characterized by attempting to map the interaction interfaces to specific domains within the proteins, using both *in vivo* and *in vitro* experiments with purified Pch and CheA protein domains. Some of these experiments were performed in collaboration with Paul Molis during his master's thesis, which I supervised at Justus Liebig University in Giessen.

2.3.1 Characterization of the PDE Pch and histidine kinase CheA

To investigate Pch and CheA in the context of their interaction and potential roles in the polar localization of the chemotaxis machinery, the structural properties of both proteins were analyzed using AlphaFold3 predictions [234]. These structural analyses were complemented by phenotypic screening assays to examine the effects of protein deletions and to assess the PDE activity of Pch.

2.3.1.1 Identification of *P. putida* Pch and structural characterization of the domain architectures

While the gene encoding the histidine kinase CheA in *P. putida* has been previously identified (PP_4338), a BLAST search for a potential homolog of *P. aeruginosa* Pch (*Pa*Pch, PA5017) revealed PP_0337 as the most likely candidate in *P. putida*. The protein encoded by PP_0337 (hereafter referred to as *Pp*Pch) shares approximately 71% sequence identity with *Pa*Pch over the full length of the protein, with 83% of the amino acids exhibiting similar physicochemical properties (Supplementary figure 4). AlphaFold3-based structural predictions of Pch proteins yielded in robust domain models, as indicated by consistently high pLDDT values above 80% and pTM values exceeding 0.5 (**Figure 30**, Supplementary figure 5). *Pp*Pch comprises 896 amino acids and has an approximate molecular mass of 100 kDa, closely resembling the size and overall architecture of *Pa*Pch (**Figure 30**). The predicted domain architecture consists of six major protein domains,

beginning with an N-terminal PAS-sensory domain. This is followed by a linker region, a GAF domain and a second PAS domain together with an associated C-terminal PAC motif. The PAS-PAC fold is directly followed by a degenerate GGDEF domain and a C-terminal EAL domain, containing the EAL motif.

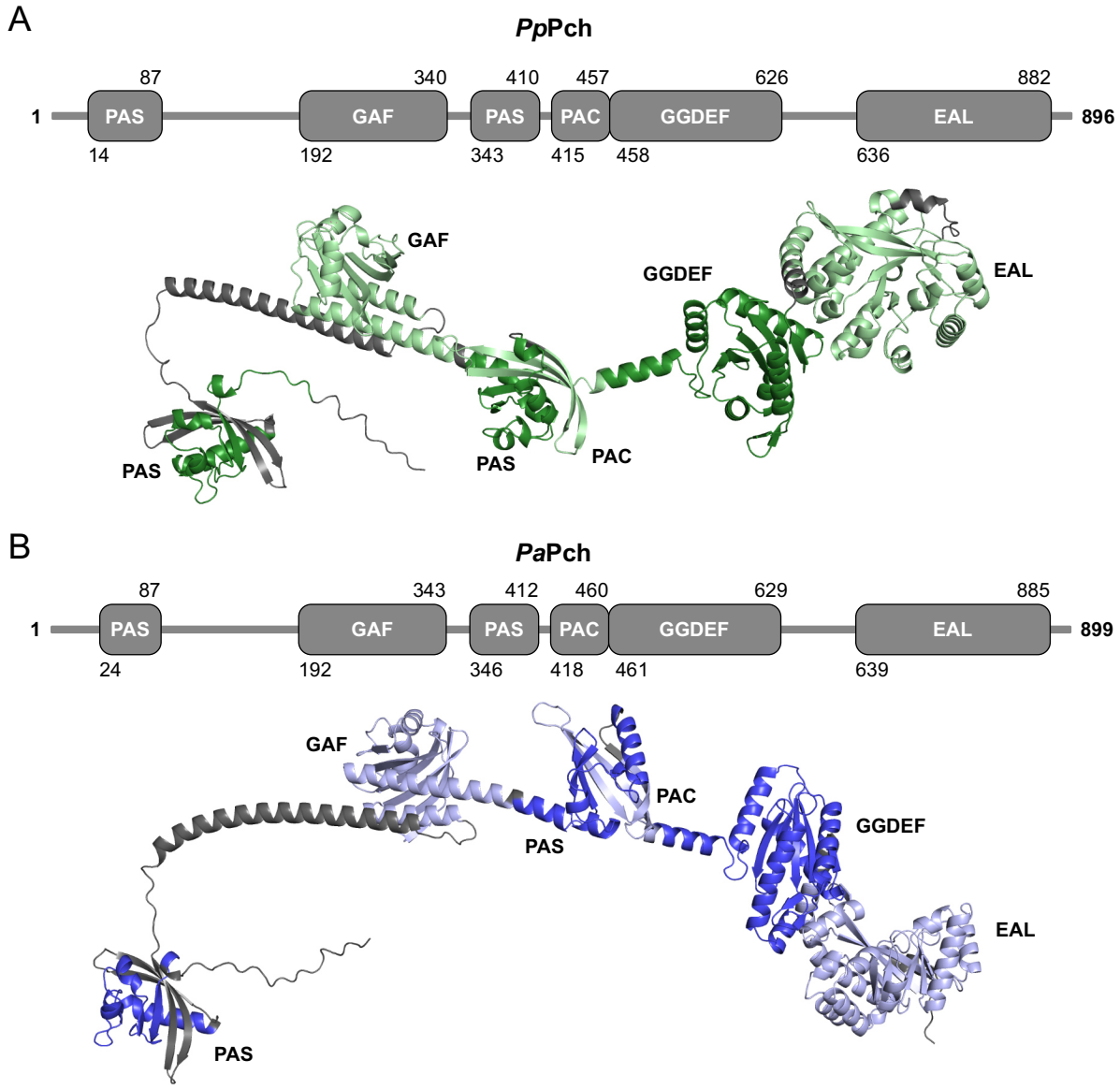

Figure 30. Domain architectures and structural prediction of Pch. Upper panels: schematic representation of the domain architectures of Pch from *P. putida* (*Pp*Pch) (**A**) and *P. aeruginosa* (*Pa*Pch) (**B**). Protein lengths and individual domain boundaries are indicated by amino acid numbers. Pch consists of an N-terminal PAS-sensory domain, followed by a GAF domain, a PAS-PAC module, a GGDEF domain and a C-terminal EAL domain. Lower panels: AlphaFold3-based structural predictions of *Pp*Pch (**A**) and *Pa*Pch (**B**) with domains highlighted in green and blue, respectively. The corresponding calculated pTM scores are 0.6 and 0.57, respectively.

Structural prediction of *P. putida* CheA also revealed a high-confidence model with an overall pLDDT value of 72.5 and a pTM value of 0.64, indicating a robust prediction of both local and global structure (**Figure 31**, Supplementary figure 5). The histidine kinase CheA consists of 747 amino acids and has a molecular weight of approximately 80 kDa (**Figure 31A**). According to the literature [235], *P. putida* CheA exhibits a modular domain architecture comprising five major domains (P1-P5). The

protein starts with an N-terminal Hpt domain (P1), which harbors the conserved histidine residue at position 48 that becomes phosphorylated upon CheA stimulation. This domain is followed by a long, largely unstructured linker region, encompassing five α-helices, that in most organisms corresponds to the second domain (P2). Subsequently, CheA contains a dimerization domain (DIM, P3), the histidine kinase catalytic domain (H-Kinase, P4) responsible for ATP-binding and a C-terminal CheW-like domain (P5). Upon dimerization, CheA forms a stable homodimer that is essential for its kinase activity [127,236]. Following ATP binding, autophosphorylation occurs in trans, whereby the catalytic domain of one CheA subunit phosphorylates the conserved histidine residue located in the Hpt domain of the opposing subunit (**Figure 31B**, Supplementary figure 5). Based on the high sequence similarity and conserved domain architecture, the protein encoded by PP_0337 was identified as the putative PDE Pch in *P. putida* and was selected for further investigation alongside the histidine kinase CheA. Unless stated otherwise, Pch and CheA refer to the *P. putida* proteins throughout this study.

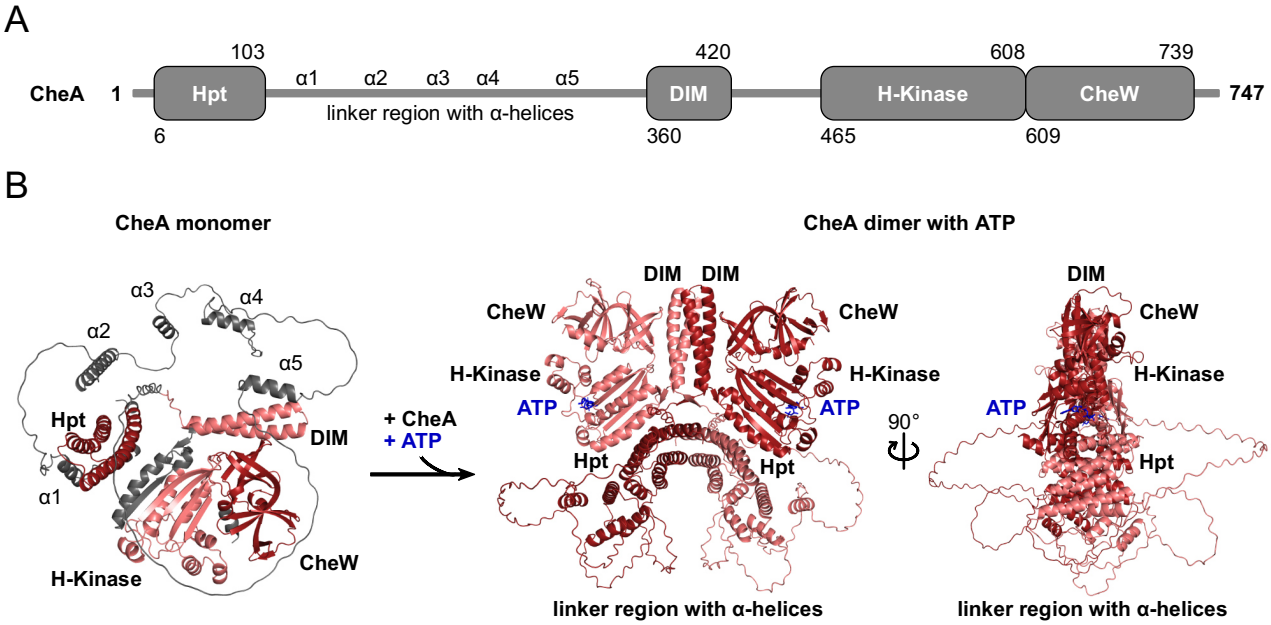

Figure 31. Domain architecture and structural prediction of CheA. A Schematic representation of the domain architecture of CheA from *P. putida*. Protein length and individual domain boundaries are indicated by amino acid numbers. CheA consists of an N-terminal histidine phosphotransfer domain (Hpt), followed by a linker region containing five distinct α-helices, a dimerization domain (DIM), a histidine kinase domain (H-Kinase) and a C-terminal CheW-like domain. **B** AlphaFold3-based structural predictions of the CheA monomer (left) and the CheA homodimer in complex with ATP (right; ATP shown in blue) with domains indicated. The corresponding calculated pTM scores are 0.64 for the monomer and 0.45 for the dimer, with an ipTM score of 0.45.

2.3.1.2 Conservation of Pch and CheA across different *Pseudomonas* species

To assess the conservation of Pch and CheA across different *Pseudomonas* species, multiple sequence alignments were generated and summarized in a phylogenetic tree (**Figure 32**, Supplementary table 1).

Both proteins show a high degree of conservation across the genus, with sequence identities exceeding 70% in all analyzed species. The highest level of conservation was observed between *P. putida* and *Pseudomonas juntendi*, an opportunistic and often multidrug-resistant pathogen belonging to the *P. putida* group [237]. In this comparison, the homologous proteins exhibited 94% identity for Pch and 92% identity for CheA, respectively (**Figure 32**). Overall, the homology analysis demonstrates a high degree of conservation of the putative PDE Pch and the histidine kinase CheA, suggesting preserved functional roles and biological relevance of both proteins across *Pseudomonas* species.

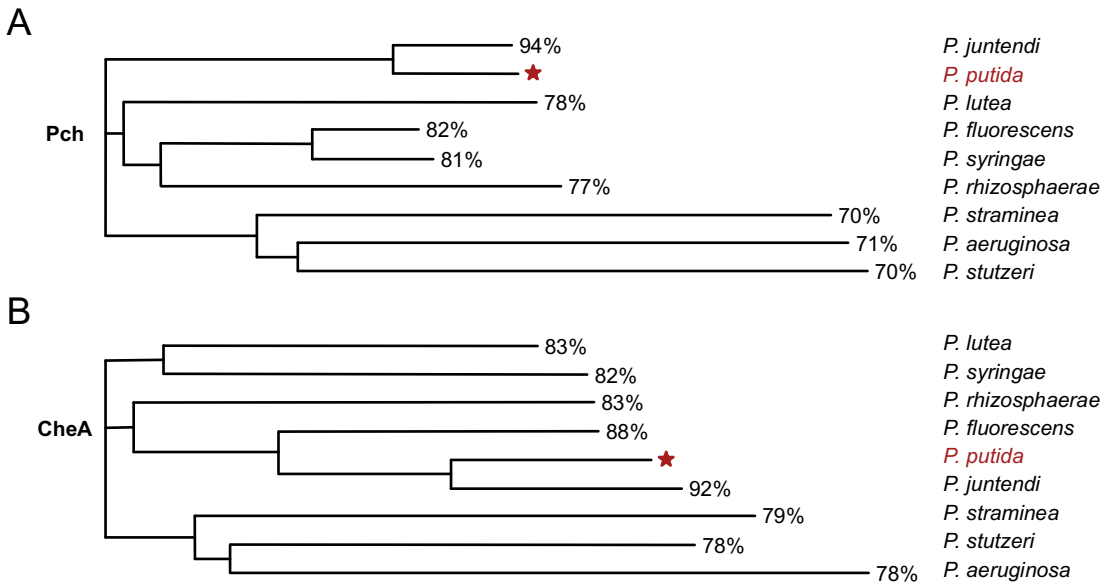

Figure 32. Conservation of Pch and CheA proteins across *Pseudomonas* species. Protein conservation was analyzed by aligning the *P. putida* (**A**) Pch (PP_0337) and (**B**) CheA (PP_4338) sequences with homologous proteins from other *Pseudomonas* species, followed by phylogenetic tree construction using the UniProt alignment tool. Percentages indicate pairwise protein sequence identity. The *P. putida* proteins are highlighted in red and marked with a red star. The conservation analysis was established in collaboration with Paul Molis.

2.3.2 Deletions of *pch* and *cheA* reduce the swimming and increase biofilm formation

Since the flagellar machinery is tightly linked to the chemotaxis system and c-di-GMP homeostasis, the impact of *pch* and *cheA* deletions on swimming motility was investigated. In addition, biofilm formation was analyzed to assess a potential shift from a motile to a sessile lifestyle.

Deletion of *pch* resulted in a moderate but significant reduction in swimming motility to approximately 80-90% compared to wild-type cells (**Figure 33A**). In contrast, deletion of *cheA* caused a severe defect, with cells displaying a non-motile phenotype in swimming assays. Reintegration of either *pch* or *cheA* into their native chromosomal loci fully restored wild-type swimming behavior. Analysis of biofilm formation revealed a significant increase in biofilm formation in the *cheA* deletion mutant, whereas the deletion of *pch* only had minor effects (**Figure 33B**). Despite their pronounced effects on motility or biofilm formation, bacterial growth remained unaffected by deletion of either gene. Growth curves of the *pch* and *cheA* deletion mutants were indistinguishable from wild-type cells in

both LB medium and M9 minimal medium (**Figure 33C**). In summary, loss of *pch* leads to a mild reduction in swimming motility without strongly affecting biofilm formation, whereas deletion of *cheA* completely abolishes swimming motility, while simultaneously promoting biofilm formation. However, neither deletion impacts bacterial growth, suggesting that Pch and CheA specifically regulate flagellar-driven motility and lifestyle transitions, likely through their integration into the chemotaxis machinery and the c-di-GMP signaling network, thereby promoting a shift toward a more sessile state.

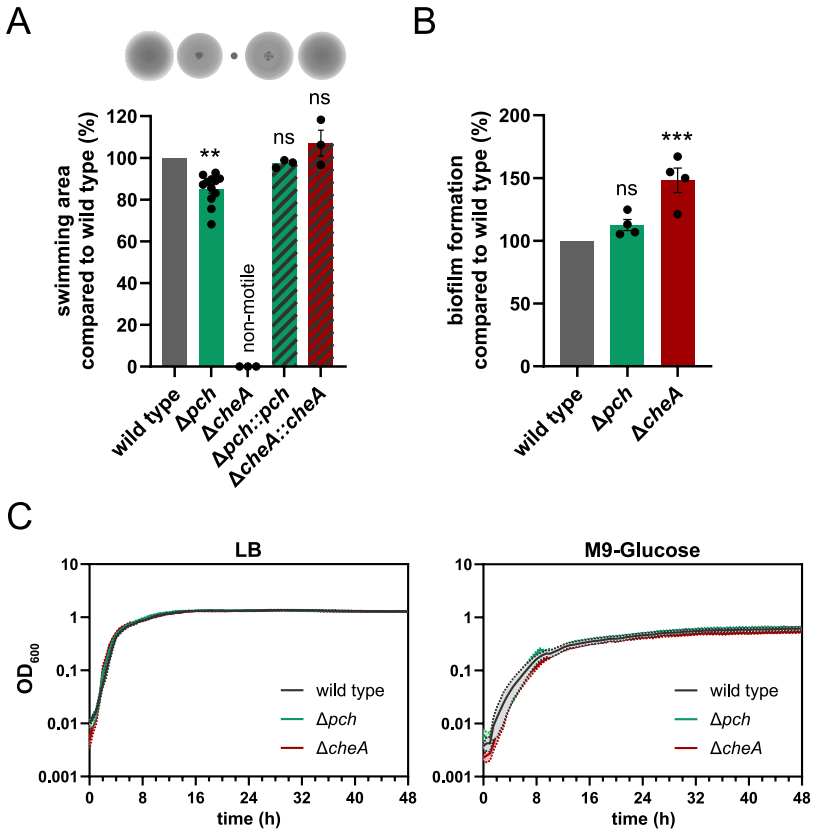

Figure 33. Deletions of *pch* and *cheA* reduce swimming behavior and increase biofilm formation. A Swimming motility of the *pch* and *cheA* deletion mutants and strains carrying reintegrations at the native loci compared to wild-type cells (set to 100%). Strains were spotted onto the same plate to ensure direct comparison. Data from at least three independent experiments are shown as mean with standard error of the mean. Statistical analysis was performed using one-way ANOVA (**p=0.0083, ns = non-significant; here: p=0.9553 and p=0.4836). **B** Biofilm formation of the *pch* and *cheA* deletion mutants compared to wild-type cells (set to 100%). Data from four independent experiments are shown as mean with standard error of the mean. Statistical analysis was performed using one-way ANOVA (***p=0.0007, ns = non-significant; here: p=0.3014). **C** Growth curves of the *pch* and *cheA* deletion mutants and *P. putida* wild type measured at OD_{600} in LB medium (left) and M9 minimal medium (right), supplemented with 0.4% glucose. Data from three independent experiments are shown as mean with standard error of the mean. Growth experiments were performed by Paul Molis.

2.3.3 Absence of Pch influences the c-di-GMP homeostasis

Through their c-di-GMP-degrading activity, PDEs play a central role in maintaining c-di-GMP homeostasis and thereby influence the transition between motile and sessile lifestyles in bacteria [186]. Since *Pa*Pch was previously shown to harbor a functional EAL domain and to exhibit PDE activity [220], the influence of *Pp*Pch on c-di-GMP homeostasis was investigated by measurements of the *in vivo* c-di-GMP levels. For this purpose, a fluorescent reporter system was employed that

comprises three c-di-GMP-binding riboswitches, resulting in c-di-GMP-dependent expression of the red fluorescent protein TurboRFP [238]. Normalization for plasmid copy number and expression variability was achieved by dividing TurboRFP fluorescence values by those of the constitutively expressed AmCyan fluorescent protein.

First, the reliability of the reporter system in *P. putida* wild-type cells was assessed by analyzing the correlation between AmCyan and TurboRFP fluorescence, thereby validating proportional expression and proper normalization. In addition, linear regression analysis was applied to test for potential cell size-dependent effects on the reporter output. The coefficient of determination R^2 for the correlation between red and blue fluorescence was approximately 0.76, indicating a strong proportional relationship that allows reliable normalization to plasmid copy number (**Figure 34A**). In contrast, no correlation was observed between cell length and the normalized TurboRFP/AmCyan fluorescence ratio (R^2 ~0.001), excluding cell-size dependent bias in the reporter signal (**Figure 34B**). Taken together, these results demonstrate that the reporter system can be robustly applied to measure intracellular c-di-GMP levels in *P. putida*.

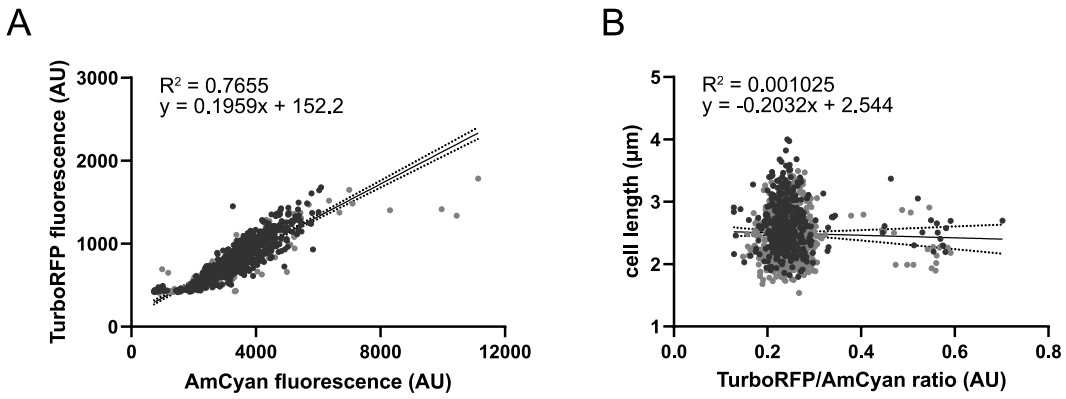

Figure 34. Validation of the c-di-GMP reporter system in *P. putida*. A Correlation between average AmCyan and TurboRFP fluorescence intensities in individual cells. **B** Correlation between cell length and the ratio of TurboRFP to AmCyan fluorescence. Linear regression analysis was performed to assess proportional expression and to detect potential cell-size dependent effects on reporter output. The coefficient of determination (R^2) is indicated. Values close to 1 indicate a strong positive linear correlation, whereas values close to 0 indicate no linear correlation. Experiment was performed by Paul Molis.

Subsequent measurements revealed comparable median c-di-GMP levels in wild-type cells and the *cheA* deletion mutant, with values of approximately 0.24 and 0.25, respectively (**Figure 35**). In contrast, deletion of *pch* resulted in increased intracellular c-di-GMP levels, with a median value of approximately 0.3. These findings indicate that the Pch protein encoded by PP_0337 indeed exhibits c-di-GMP-degrading PDE activity, as loss of Pch leads to an accumulation of c-di-GMP within the cells.

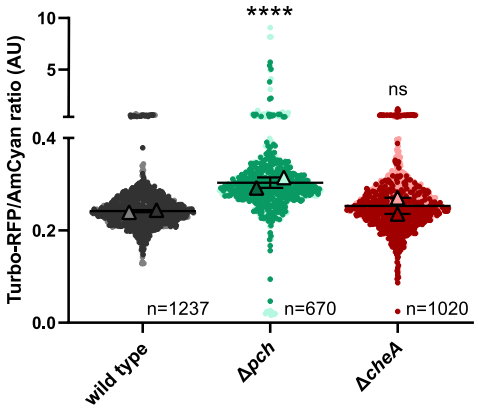

Figure 35. Deletion of *pch* increases intracellular c-di-GMP levels. Intracellular c-di-GMP levels were determined using the fluorescence reporter system. TurboRFP fluorescence, reflecting c-di-GMP levels, was normalized to the constitutively expressed AmCyan fluorescence to account for variations in plasmid copy number. Data from two independent experiments are shown as median with 95% confidence interval. Statistical analysis was performed using one-way ANOVA (****p<0.0001, ns = non-significant; here: p=0.4358). Experiment was performed by Paul Molis.

2.3.4 Pch co-localizes polarly with CheA

Because Pch was previously shown to localize polarly in *P. aeruginosa* [163], the subcellular localization of Pch in *P. putida* was investigated. To this end, a fluorescent Pch fusion as well as two domain variants, either comprising the GGDEF-EAL domains or only the EAL domain, were generated to assess whether these domains contribute to polar localization. Western blot analysis confirmed stable expression of all fusion proteins, and fusion of sfGFP to Pch did not significantly influence the swimming ability of the bacteria (**Figure 36A**, Supplementary figure 6).

Consistent with observations in *P. aeruginosa*, Pch also localizes to the cell pole in *P. putida* (**Figure 36B**). Wild-type cells exhibited a strong polar localization, with a relative distance to the cell center of approximately 0.9. In contrast, Pch mutant variants consisting of the EAL domain alone or in combination with the GGDEF domain showed a significant reduction in polar localization, with relative distances of around 0.5. In addition, the proportion of cells displaying detectable Pch-sfGFP foci appeared reduced in both domain variants (**Figure 36C**). Furthermore, co-localization analysis with CheA-mCherry revealed spatial overlap of both proteins at the cell pole (**Figure 36D**). Taken together, these results indicate that full-length Pch is required for efficient polar localization in *P. putida*, suggesting that domains outside the catalytic GGDEF and EAL regions contribute critically to proper polar targeting of the protein.

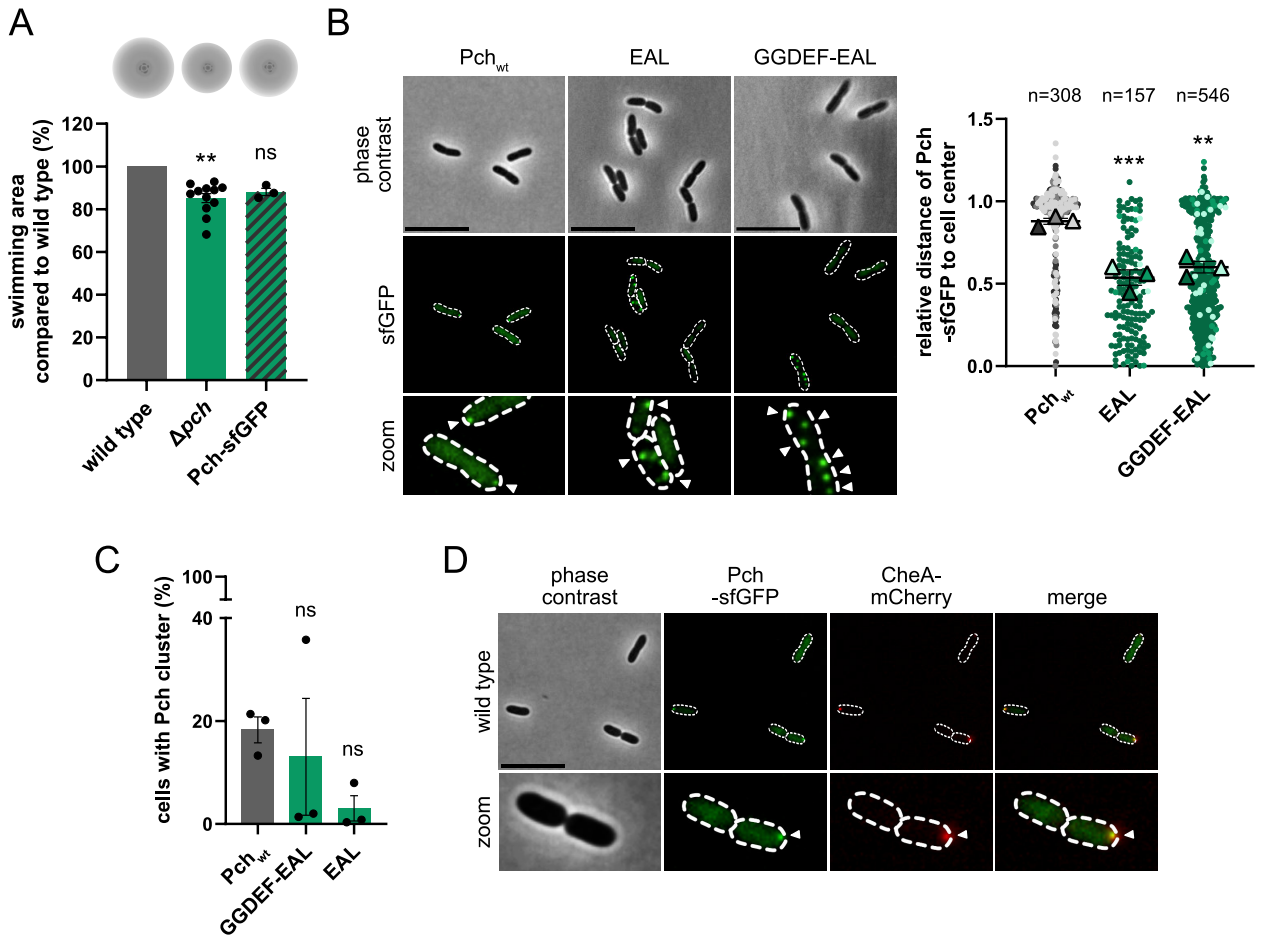

Figure 36. Pch and CheA co-localize at the cell pole. A Swimming motility of the *pch* deletion mutant and the strain harboring the Pch-sfGFP fusion protein compared to wild-type cells (set to 100%). Strains were spotted onto the same plate to ensure direct comparison. Data from at least three independent experiments are shown as mean with standard error of the mean. Statistical analysis was performed using one-way ANOVA (**p=0.0045, ns = non-significant; here: p=0.0611). **B** Left panel: fluorescence microscopy images of wild-type Pch-sfGFP (Pch_{wt}) and the EAL- and GGDEF-EAL domain variants fused to sfGFP expressed in *P. putida* wild-type cells. The upper row shows phase contrast images, followed by the corresponding sfGFP fluorescence (green). The lower row shows magnified regions of the fluorescence images. Fluorescent Pch foci are indicated by white arrows. Scale bar equals 5 µm. Right panel: quantification of the relative distance of Pch cluster to the cell center in wild-type Pch and the domain variants. The relative distance was calculated by dividing the distance between a fluorescent Pch cluster and the cell center (in µm) by the half cell length. Values close to 1 indicate polar localization, whereas values close to 0 correspond to midcell localization. Quantification was performed using the Fiji plugin MicrobeJ. Data from three independent experiments, with total number of cells, are shown as mean values (triangles) together with the mean of the means (horizontal line) and the standard error of the mean. Statistical analysis was performed using one-way ANOVA (***p=0.0009, **p=0.0014). Experiment was performed by Paul Molis. **C** Quantification of cells exhibiting fluorescent Pch-sfGFP cluster (percentage) in *P. putida* wild-type Pch and the domain variants. Quantification was performed using the Fiji plugin MicrobeJ. Data from three independent experiments are shown as mean with standard error of the mean. Statistical analysis was performed using one-way ANOVA (ns = non-significant; here: p=0.8183 and p=0.2733). **D** Fluorescence microscopy images of Pch-sfGFP and CheA-mCherry expressed in *P. putida* wild-type cells. The first column shows the phase contrast image, followed by the corresponding sfGFP (green) and mCherry (red) fluorescence. The last column shows merged fluorescence images. The lower row shows magnified regions of all images. Fluorescent foci are indicated by white arrows. Scale bar equals 5 µm.

2.3.4.1 Polarity of Pch depends on CheA

Since Pch and CheA were previously shown to potentially interact in co-immunoprecipitation assays [163], the effect of deleting one protein on the localization of the other was investigated. In addition, deletions of other proteins known to be polarly localized or involved in polar organization were

analyzed. Stable expression of all fusion proteins was confirmed by western blot analysis (Supplementary figure 6).

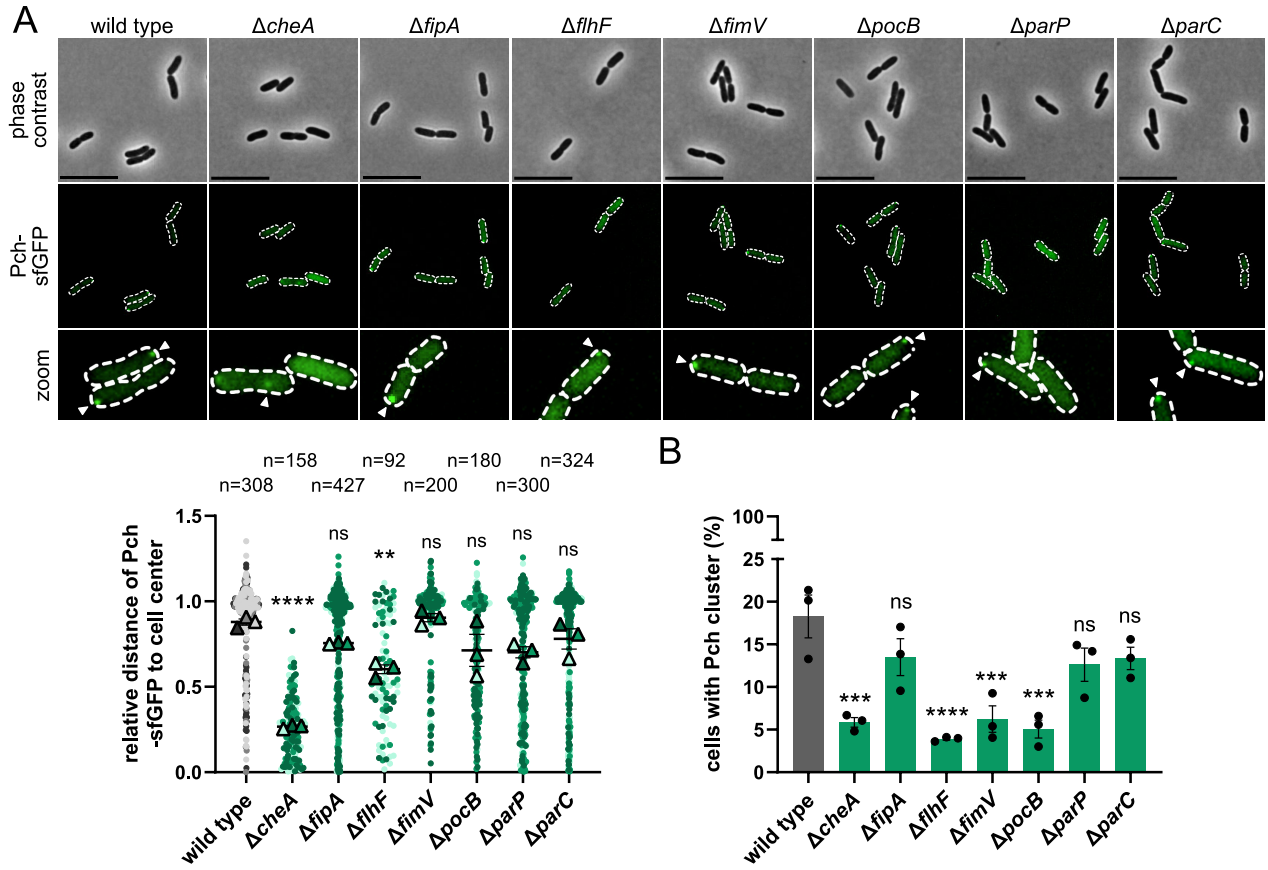

Figure 37. Pch localizes polarly in a CheA-dependent manner. A Upper panel: fluorescence microscopy images of Pch-sfGFP expressed in *P. putida* wild-type cells and deletion mutants. The first row shows the phase contrast images, followed by the corresponding sfGFP fluorescence (green). The lower row shows magnified regions of the fluorescence images. Fluorescent Pch foci are indicated by white arrows. Scale bar equals 5 µm. Lower panel: quantification of the relative distance of Pch cluster to the cell center in wild-type cells and deletion mutants. The relative distance was calculated by dividing the distance between a fluorescent Pch cluster and the cell center (in µm) by the half cell length. Values close to 1 indicate polar localization, whereas values close to 0 correspond to midcell localization. Quantification was performed using the Fiji plugin MicrobeJ. Data from three independent experiments, with total number of cells, are shown as mean values (triangles) together with the mean of the means (horizontal line) and the standard error of the mean. Statistical analysis was performed using one-way ANOVA (****p<0.0001, **p=0.0021, ns = non-significant, here: p>0.05). **B** Quantification of cells exhibiting fluorescent Pch-sfGFP cluster (percentage) in *P. putida* wild-type cells and deletion mutants. Quantification was performed using the Fiji plugin MicrobeJ. Data from three independent experiments are shown as mean with standard error of the mean. Statistical analysis was performed using one-way ANOVA (****p<0.0001, ***p<0.001, ns = non-significant; here: p>0.1).

In wild-type cells, fluorescent Pch clusters were polarly localized, with a mean relative distance to the cell center of approximately 0.9 (**Figure 37A**). Polar localization of Pch was strongly reduced in the absence of CheA and moderately affected by deletion of *flhF*, with relative distances to the cell center of approximately 0.2 and 0.5, respectively. In contrast, deletions of *fipA*, *fimV*, *pocB*, *parP or parC* had no significant effect on the polar localization of Pch. With the exception of *fipA*, *parP* and *parC* deletions, all tested deletions resulted in a reduced fraction of cells exhibiting detectable fluorescent Pch clusters to around 5%, whereas wild-type cells displayed Pch clusters in approximately 20% of the population (**Figure 37B**).

While CheA strongly influenced the polar localization of Pch, its own polar localization was not affected by deletion of *pch*, nor by deletion of *fipA* or *parC* (**Figure 38A**). In contrast, deletion of *flhF*, *fimV, pocB* or *parP* significantly reduced the polar localization of fluorescent CheA foci, resulting in relative distances to the cell center of approximately 0.7-0.8. In addition, deletions of *fipA*, *flhF*, *parP* and *parC* reduced the fraction of cells exhibiting detectable CheA clusters from around 60% to 20-40% (**Figure 38B**). Taken together, these results indicate that CheA acts upstream of Pch in polar recruitment, whereas CheA localization itself depends on multiple polar landmark and scaffolding proteins, like FlhF, PocB and ParP, but is independent of Pch.

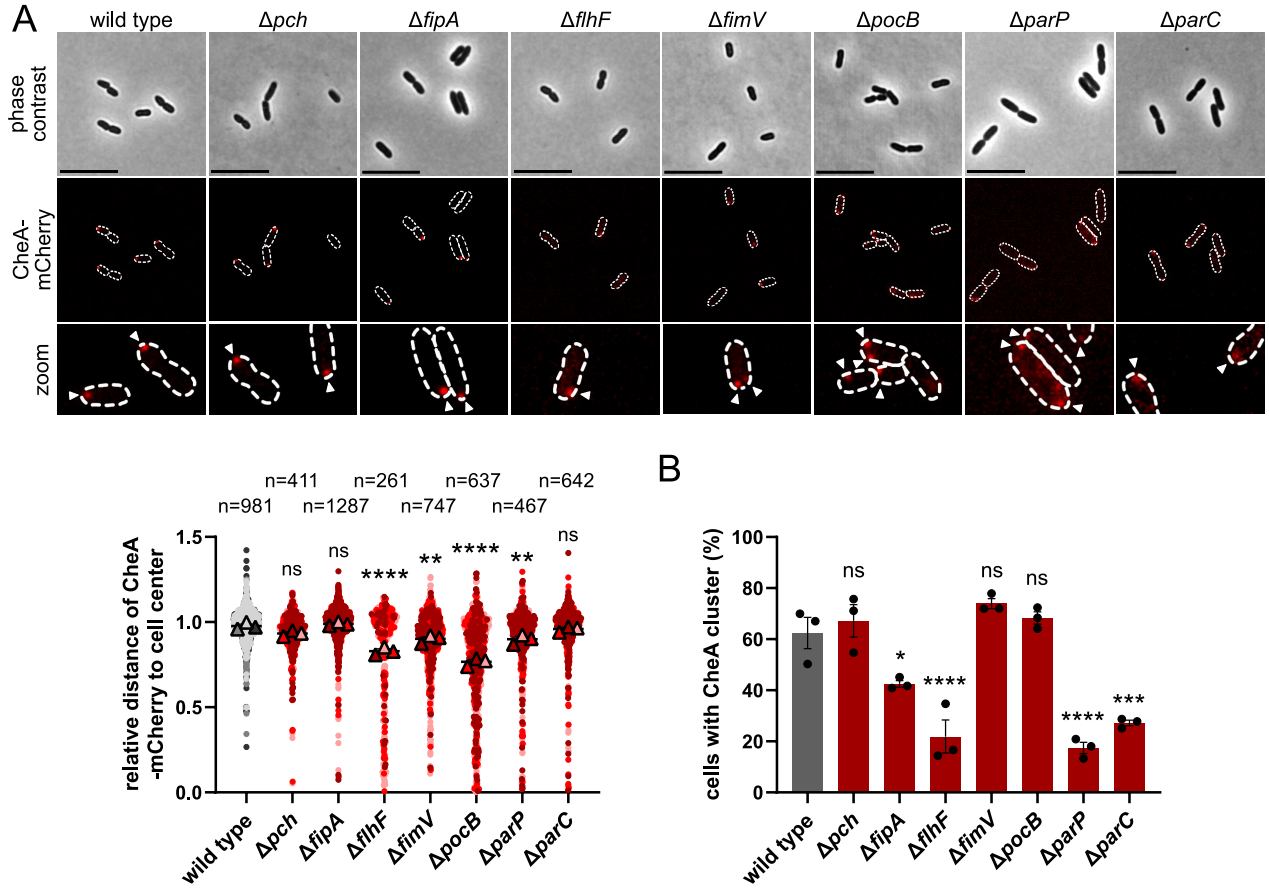

Figure 38. CheA localization depends on the polar organizers FlhF, FimV, PocB and ParP. A Upper panel: fluorescence microscopy images of CheA-mCherry expressed in *P. putida* wild-type cells and deletion mutants. The first row shows the phase contrast images, followed by the corresponding mCherry fluorescence (red). The lower row shows magnified regions of the fluorescence images. Fluorescent CheA foci are indicated by white arrows. Scale bar equals 5 µm. Lower panel: quantification of the relative distance of CheA cluster to the cell center in wild-type cells and deletion mutants. The relative distance was calculated by dividing the distance between a fluorescent CheA cluster and the cell center (in µm) by the half cell length. Values close to 1 indicate polar localization, whereas values close to 0 correspond to midcell localization. Quantification was performed using the Fiji plugin MicrobeJ. Data from three independent experiments, with total number of cells, are shown as mean values (triangles) together with the mean of the means (horizontal line) and the standard error of the mean. Statistical analysis was performed using one-way ANOVA (****p<0.0001, **p<0.01, ns = non-significant, here: p>0.8). **B** Quantification of cells exhibiting fluorescent CheA-mCherry cluster (percentage) in *P. putida* wild-type cells and deletion mutants. Quantification was performed using the Fiji plugin MicrobeJ. Data from three independent experiments are shown as mean with standard error of the mean. Statistical analysis was performed using one-way ANOVA (****p<0.0001, ***p=0.0001, *p=0.0196, ns = non-significant; here: p>0.27).

2.3.5 The EAL domain of Pch interacts *in vivo* with three α-helices of CheA

As shown in the previous chapter, Pch and CheA co-localize at the flagellated cell pole in *P. putida*, with the polar localization of Pch being dependent on CheA. Based on these observations, the potential interaction between both proteins was investigated in more detail using *in vivo* bacterial two-hybrid assays. In addition, as a proof of concept, the interaction between Pch and CheA was examined using the corresponding proteins from *P. aeruginosa* PAO1.

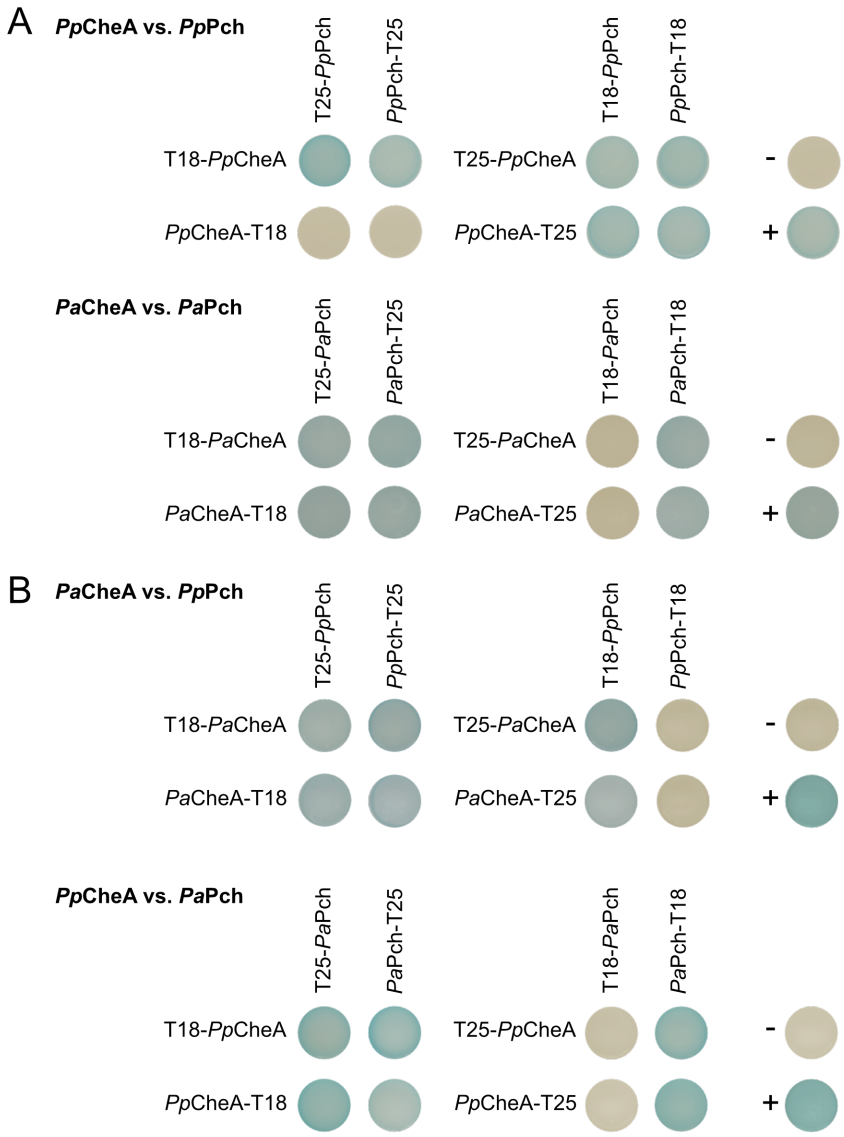

Figure 39. Pch and CheA interact in *P. putida* and *P. aeruginosa*. Bacterial two-hybrid analysis showing interactions between **A** *Pp*CheA vs. *Pp*Pch and *Pa*CheA vs. *Pa*Pch, **B** *Pa*CheA vs. *Pp*Pch and *Pp*CheA vs. *Pa*Pch. Proteins were fused either N- or C-terminally to the T18 or T25 fragment of the catalytic domain of *Bordetella pertussis* adenylate cyclase. Blue coloration of colonies indicates reconstitution of adenylate cyclase activity and subsequent conversion of X-Gal, thereby indicating protein-protein interaction. "+" indicates the positive control and "-" the negative control. Data from at least two independent experiments are shown. Experiments were performed by Paul Molis.

Bacterial two-hybrid assays confirmed a direct protein-protein interaction between Pch and CheA in both *P. putida* and *P. aeruginosa* (**Figure 39**). Moreover, interspecies interaction assays revealed that CheA and Pch from one species were able to interact with their respective partner proteins from the other species, supporting a high degree of functional and structural conservation among *Pseudomonas* homologs.

Domain-resolved interaction analyses using bacterial two-hybrid assays demonstrated that the EAL domain of Pch mediates the interaction with CheA (**Figure 40A**), while the Hpt domain together with the adjacent linker region of CheA is sufficient for binding to Pch (**Figure 40B**, Supplementary figure 7). Direct testing of these domains against each other confirmed the interaction (**Figure 40C**). Further truncation of the linker region revealed that α-helices 3-5 of CheA are required for interaction with the EAL domain of Pch (**Figure 40D**). The interaction pattern between the CheA linker region and the Pch EAL domain was likewise observed for the corresponding proteins from *P. aeruginosa* (**Figure 40E**), indicating a conserved interaction interface across *Pseudomonas* species.

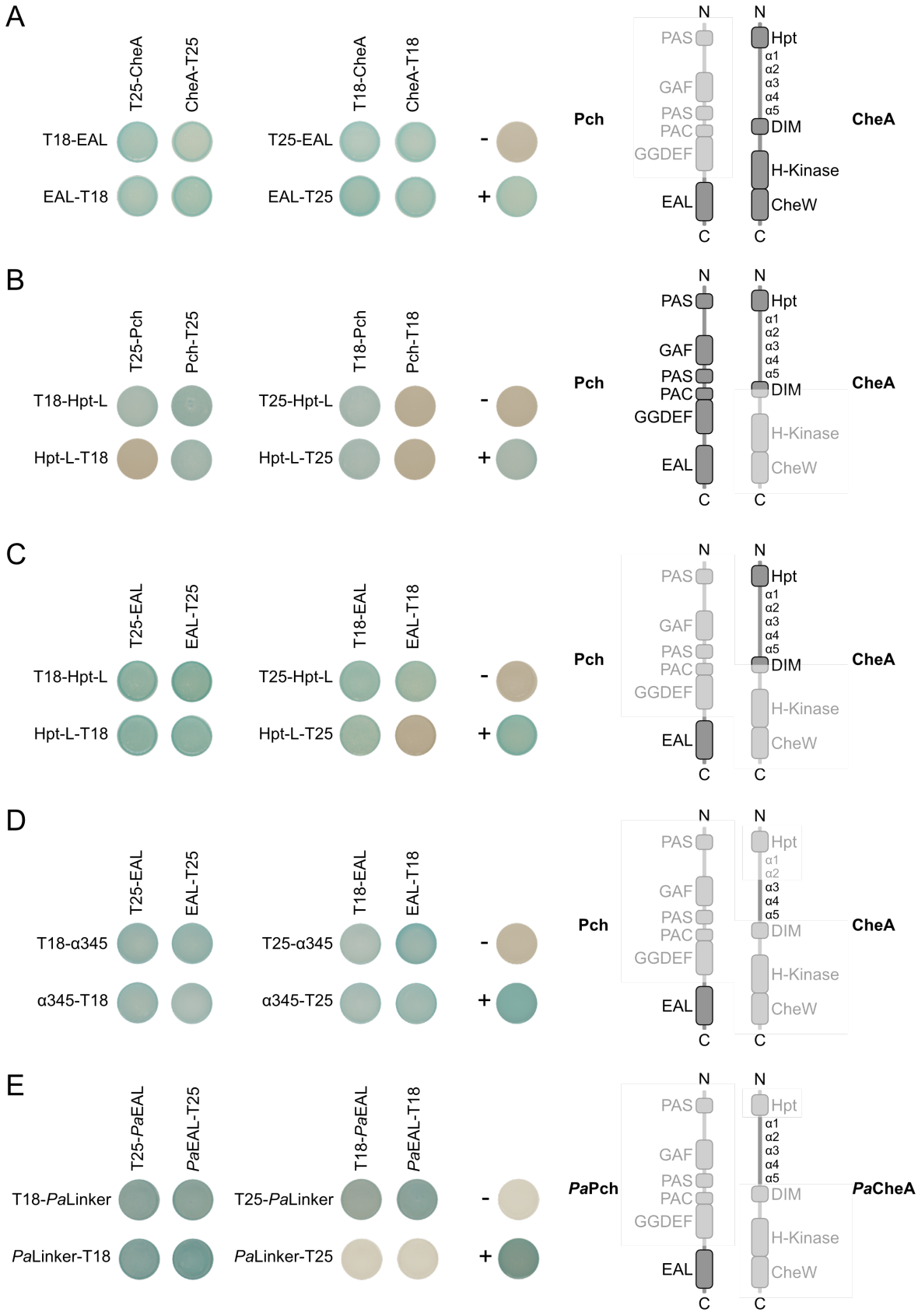

Figure 40. The EAL domain of Pch interacts with three α-helices of CheA. Bacterial two-hybrid analysis showing interactions between **A** the Pch EAL domain and full-length CheA, **B** the CheA Hpt-linker domain and full-length Pch, **C** the CheA Hpt-linker domain and the Pch EAL domain, **D** the Pch EAL domain and CheA α-helices 3-5 and **E** the Pch EAL domain and CheA linker region in *P. aeruginosa*. Left panels: schematic representations of the domain structures indicating the variants used. Proteins were fused either N- or C-terminally to the T18 or T25 fragment of the catalytic domain of *Bordetella pertussis* adenylate cyclase. Blue coloration of colonies indicates reconstitution of adenylate cyclase activity

and subsequent conversion of X-Gal, thereby indicating protein-protein interaction. "+" indicates the positive control and "-" the negative control. Data from at least two independent experiments are shown. Experiments were performed by Paul Molis.

2.3.6 Pch and CheA show an interaction with the partitioning protein ParP

Since the partitioning protein ParP was previously described to prevent dissociation of CheA from the chemotactic signaling arrays [170], the interaction of this polar organizer protein with the *P. putida* proteins CheA and Pch was investigated.

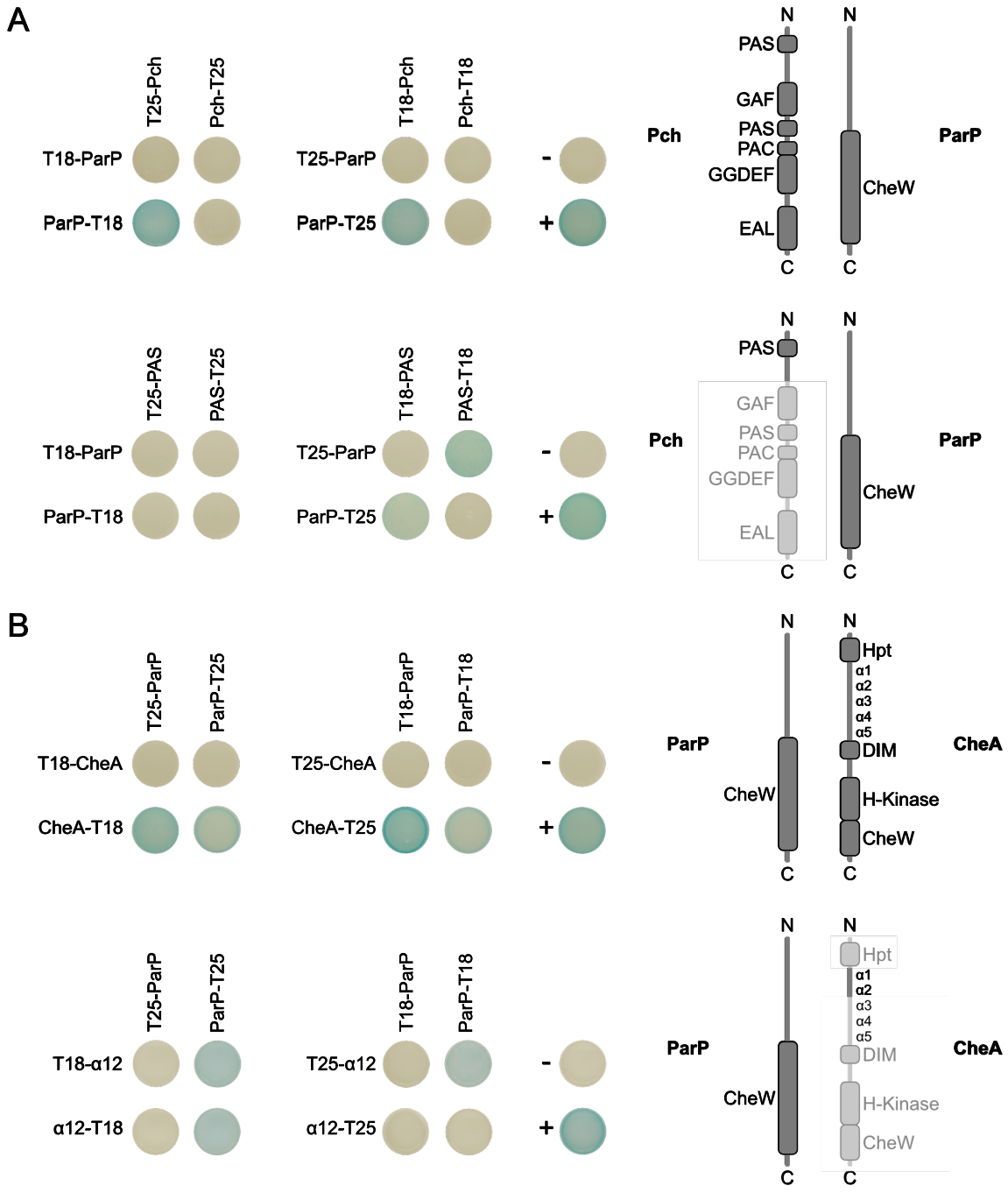

Figure 41. ParP interacts with Pch and CheA. Bacterial two-hybrid analysis showing interactions between **A** Pch vs. ParP and the Pch PAS domain vs. ParP, **B** CheA vs. ParP and CheA α-helices 1-2 vs. ParP. Left panels: schematic representations of the domain structures indicating the variants used. Proteins were fused either N- or C-terminally to the T18 or T25 fragment of the catalytic domain of *Bordetella pertussis* adenylate cyclase. Blue coloration of colonies indicates reconstitution of adenylate cyclase activity and subsequent conversion of X-Gal, thereby indicating protein-protein

interaction. “+” indicates the positive control and “-“ the negative control. Data from at least two independent experiments are shown. Experiments were performed by Paul Molis.

Both proteins exhibited a clear interaction with the partitioning protein ParP (**Figure 41**). Domain-specific bacterial two-hybrid analyses revealed that the interaction between ParP and Pch is mediated by the N-terminal region of Pch, encompassing the PAS fold (**Figure 41A**, Supplementary figure 8). In contrast to the interaction between CheA and Pch, which is mediated by α-helices 3-5 of CheA, the interaction with ParP involved α-helices 1-2 of CheA (**Figure 41B**). Taken together, these results indicate that CheA employs distinct interaction interfaces to bind different polar partners, while Pch interacts with both CheA and ParP via separate domains, suggesting a modular and potentially coordinated role in polar organization.

2.3.6.1 ParP shows polar localization

As an interaction between Pch, CheA and ParP was detected, the localization of ParP was analyzed in more detail. In addition to its effects on swimming motility and growth behavior, polar localization was investigated by generating a stably expressed mCherry-ParP fusion protein (Supplementary figure 6).

Deletion of *parP* resulted in a markedly reduced swimming motility, with cells exhibiting approximately 50% of the swimming area compared to wild-type cells (**Figure 42A**). Reintegration of *parP* into its native chromosomal locus fully restored wild-type swimming behavior. Expression of the mCherry-ParP fusion protein did not impair motility. Growth analysis revealed no significant differences between the *parP* deletion mutant and wild-type cells in either LB or M9 minimal medium (**Figure 42B**). Localization analysis of mCherry-ParP showed distinct fluorescent foci in approximately 45% of the cells (**Figure 42C**), displaying strong polar localization with a relative distance to the cell center of approximately 0.95 (**Figure 42D**). Taken together, these results demonstrate that ParP is required for full swimming motility and localizes predominantly to the cell pole, supporting the hypothesis that ParP, together with CheA and Pch, forms part of a coordinated polar organizer network.

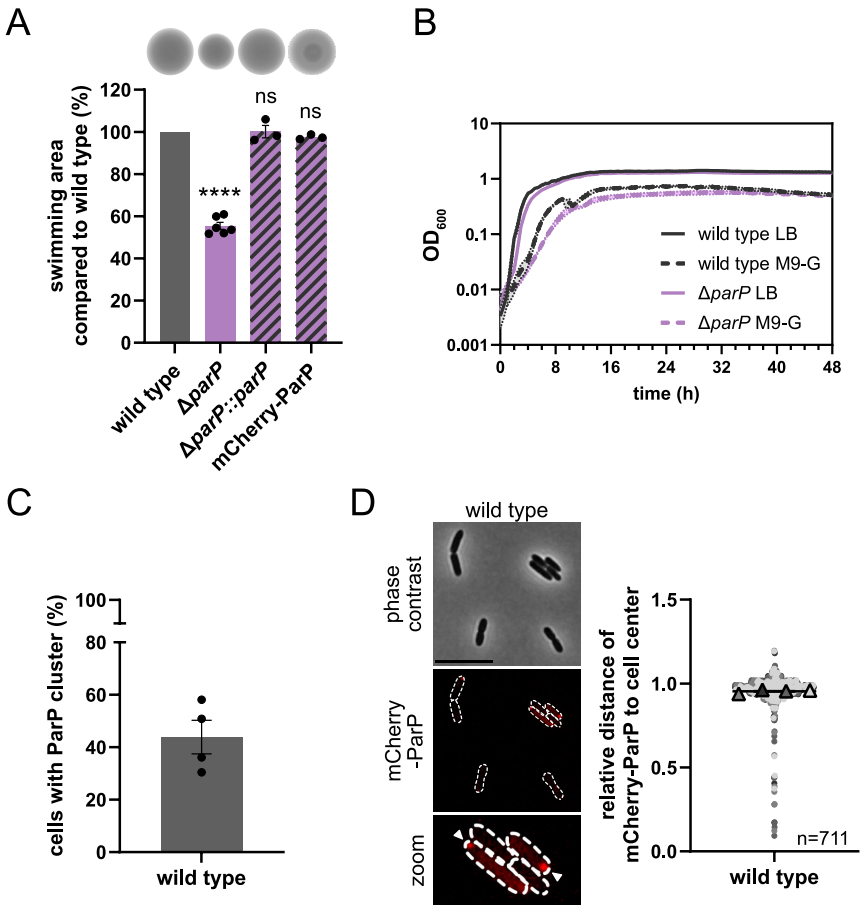

Figure 42. ParP is polarly localized in *P. putida*. A Swimming motility of the *parP* deletion mutant, a strain carrying a reintegration at the native locus and the strain harboring the mCherry-ParP fusion protein compared to wild-type cells (set to 100%). Strains were spotted onto the same plate to ensure direct comparison. Data from at least three independent experiments are shown as mean with standard error of the mean. Statistical analysis was performed using one-way ANOVA (****p<0.0001, ns = non-significant; here: p>0.71). **B** Growth curves of the *parP* deletion mutant and *P. putida* wild type measured as OD_{600} in LB medium and M9 minimal medium, supplemented with 0.4% glucose. Data from three independent experiments are shown as mean with standard error of the mean. **C** Quantification of cells exhibiting fluorescent mCherry-ParP cluster (percentage) in *P. putida* wild-type cells. Quantification was performed using the Fiji plugin MicrobeJ. Data from four independent experiments are shown as mean with standard error of the mean. **D** Left panel: fluorescence microscopy images of mCherry-ParP expressed in *P. putida* wild-type cells. The first row shows the phase contrast image, followed by the corresponding mCherry fluorescence (red). The lower row shows the magnified region of the fluorescence image. Fluorescent ParP foci are indicated by white arrows. Scale bar equals 5 µm. Right panel: quantification of the relative distance of ParP cluster to the cell center in wild-type cells. The relative distance was calculated by dividing the distance between a fluorescent ParP cluster and the cell center (in µm) by the half cell length. Values close to 1 indicate polar localization, whereas values close to 0 correspond to midcell localization. Quantification was performed using the Fiji plugin MicrobeJ. Data from three independent experiments, with total number of cells, are shown as mean values (triangles) together with the mean of the means (horizontal line) and the standard error of the mean. Experiments were performed by Paul Molis.

2.3.7 The Hpt domain of CheA influences the localization of Pch

As previously shown, Pch and CheA interact with each other and co-localize at the cell pole. Since CheA is a histidine kinase that harbors both a catalytic ATP-binding domain and a phosphorylatable histidine residue within its Hpt domain, the functional relevance of this domain was investigated. To this end, a CheA variant lacking the Hpt domain as well as a point mutant carrying a histidine-to-glutamine substitution at position 48 were analyzed. The H48Q substitution has been described to abolish chemotactic activity due to the loss of the phosphorylatable histidine residue [114].

Swimming assays confirmed this functional inactivation, as both CheA variants displayed a non-motile phenotype comparable to the complete *cheA* deletion (**Figure 43A**). In addition to a reduced CheA protein level, localization analysis revealed that deletion of the Hpt domain strongly reduced the fraction of cells exhibiting detectable CheA foci to approximately 4%, although the residual foci remained predominantly polar (**Figure 43B,** Supplementary figure 6). In contrast, deletion of the Hpt domain did not significantly affect the fraction of cells displaying fluorescent Pch foci. However, Pch polarity was markedly impaired, with a relative distance to the cell center of approximately 0.4, resembling the phenotype observed in the *cheA* deletion mutant (**Figure 43C**). Collectively, these findings indicate that while the direct interaction between Pch and CheA is mediated by α-helices 3-5 of CheA, the Hpt domain is essential for proper CheA cluster formation and contributes indirectly to the polar localization of Pch.

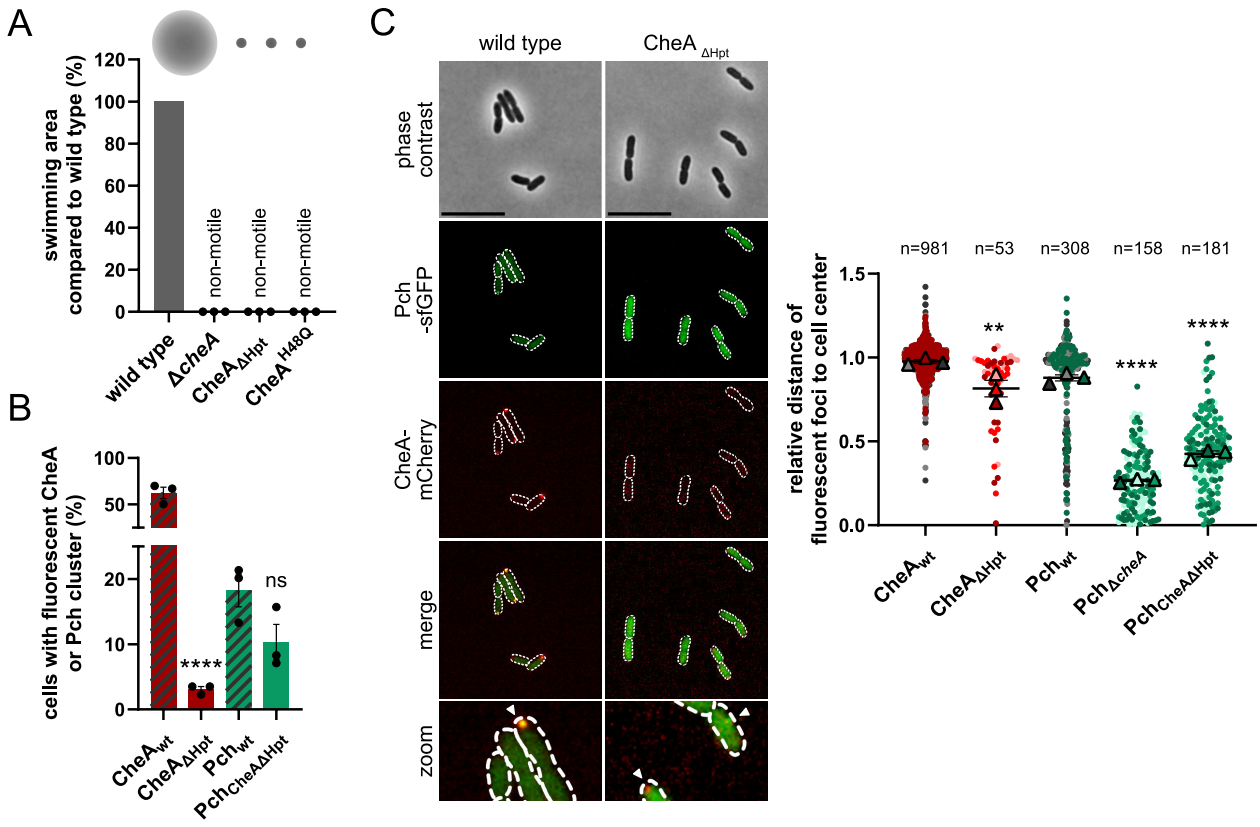

Figure 43. The Hpt domain of CheA influences the localization of Pch. A Swimming motility of the *cheA* deletion mutant, a strain carrying a deletion of the histidine phosphotransfer domain (Hpt) and a strain harboring a histidine-to-glutamine substitution at position 48 (H48Q) compared to wild-type cells (set to 100%). Strains were spotted onto the same plate to ensure direct comparison. Data from at least three independent experiments are shown as mean with standard error of the mean. **B** Quantification of cells exhibiting fluorescent CheA-mCherry (red) or Pch-sfGFP (green) cluster (percentage) in *P. putida* wild-type and protein variants. Quantification was performed using the Fiji plugin MicrobeJ. Data from three independent experiments are shown as mean with standard error of the mean. Statistical analysis was performed using one-way ANOVA (****p<0.0001, ns = non-significant; here: p=0.4493). **C** Left panel: fluorescence microscopy images of Pch-sfGFP and CheA-mCherry expressed in *P. putida* wild-type cells and cells lacking the Hpt domain. The first row shows the phase contrast images, followed by the corresponding sfGFP (green) and mCherry fluorescence (red). The lower row shows the magnified regions of the fluorescence images. Fluorescent Pch and CheA foci are indicated by white arrows. Scale bar equals 5 µm. Right panel: quantification of the relative distance of Pch and CheA cluster to the cell center in wild-type cells and deletion variants. The relative distance was calculated by dividing the distance between a fluorescent Pch or CheA cluster and the cell center (in µm) by the half cell length. Values close to 1 indicate polar localization, whereas values close to 0 correspond to midcell localization. Quantification was performed using the Fiji plugin MicrobeJ. Data from three independent experiments, with total number of cells, are shown as mean values (triangles) together with the mean of the means (horizontal line) and the standard error of the mean. Statistical analysis was performed using one-way ANOVA (****p<0.0001, **p=0.0081).

2.3.8 Purified domains of Pch and CheA show *in vitro* interaction

After confirming the interaction between the PDE Pch and the histidine kinase CheA *in vivo* and restricting the interaction interface to the EAL domain of Pch and α-helices 3-5 of CheA, the interaction was further analyzed using *in vitro* approaches. To this end, the respective interaction domains were purified by affinity chromatography. The influence of the phosphorylatable histidine residue was again examined using the CheA H48Q substitution variant.

Since stable expression of the isolated CheA linker region was not feasible (Supplementary figure 9), the stably expressed Hpt domain together with the linker region (Hpt-Linker), fused to a 6xHis-SUMO tag, was used for purification (**Figure 44A**). The EAL domain was expressed with an N-terminal 6xHis tag and an MBP tag. Both domains were subsequently tested for interaction using MBP-based pulldown assays (**Figure 44**, Supplementary figure 9).

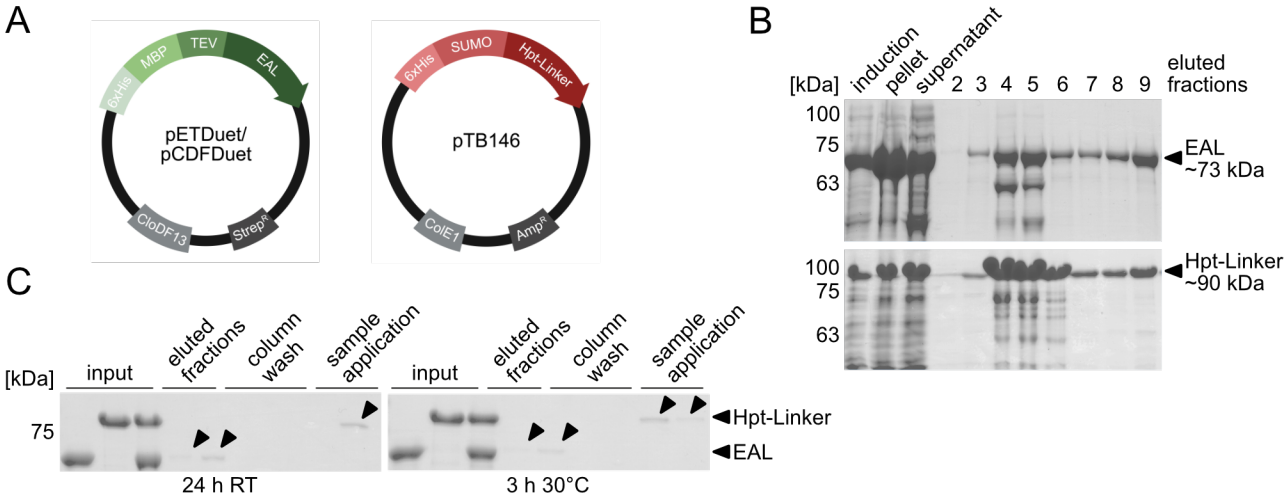

Figure 44. Purification and pulldown analysis of the Pch EAL domain and the CheA Hpt-linker domain. A Schematic representation of plasmids used for overexpression of the 6xHis-MBP-tagged EAL domain of Pch (left) and the 6xHis-SUMO-tagged Hpt-linker domain of CheA (right). Plasmid backbones (pETDuet, pCDFDuet and pTB146), origins of replication (CloDF13 and ColE1) and resistance markers (Amp^R and $Strep^R$) are indicated. Created with BioRender.com. **B** Coomassie-stained SDS-PAGE showing Ni-NTA-based affinity purification of the Pch EAL domain (~73 kDa, upper panel) and the CheA Hpt-linker domain (~90 kDa, lower panel). **C** Coomassie-stained SDS-PAGE of a MBP-based pulldown assay using the MBP-tagged Pch EAL domain as bait and the CheA Hpt-linker domain as prey. Following purification, proteins were incubated together either for 24 hours at room temperature (left panel) or 3 hours at 30°C (right panel).

Using Ni-NTA affinity chromatography, the EAL domain of Pch and the Hpt-Linker construct were successfully purified (**Figure 44B**, Supplementary figure 10). To assess complex formation, purified proteins were incubated either for 24 hours at room temperature or for 3 hours at 30 °C prior to pulldown analysis. However, MBP-based pulldown assays did not reveal co-elution of the proteins under either condition, indicating that no stable complex was formed upon post-purification mixing (**Figure 44C**).

As separate purification followed by *in vitro* incubation did not result in detectable interaction, both protein domains were subsequently co-expressed in the same cells prior to purification (**Figure 45**, Supplementary figure 10). For this approach, both the wild-type Hpt-Linker construct and the H48Q substitution variant were used. Following Ni-NTA purification (**Figure 45A**), MBP-based pulldown assays demonstrated co-elution of the Hpt-Linker and EAL domain, indicating complex formation. Notably, this was observed for both the wild-type and the H48Q variant (**Figure 45B**). In addition, size-exclusion chromatography of the co-expressed proteins revealed a clear shift in elution volume compared to individually expressed domains (Supplementary figure 10C), further supporting the formation of a stable EAL-Hpt-Linker complex. Taken together, these findings indicate that complex formation between the EAL domain of Pch and the Hpt-Linker region of CheA likely requires co-expression, suggesting that additional stabilizing factors may be necessary for stable interaction of the domains, whereas phosphorylation of the conserved histidine residue is not essential for complex formation.

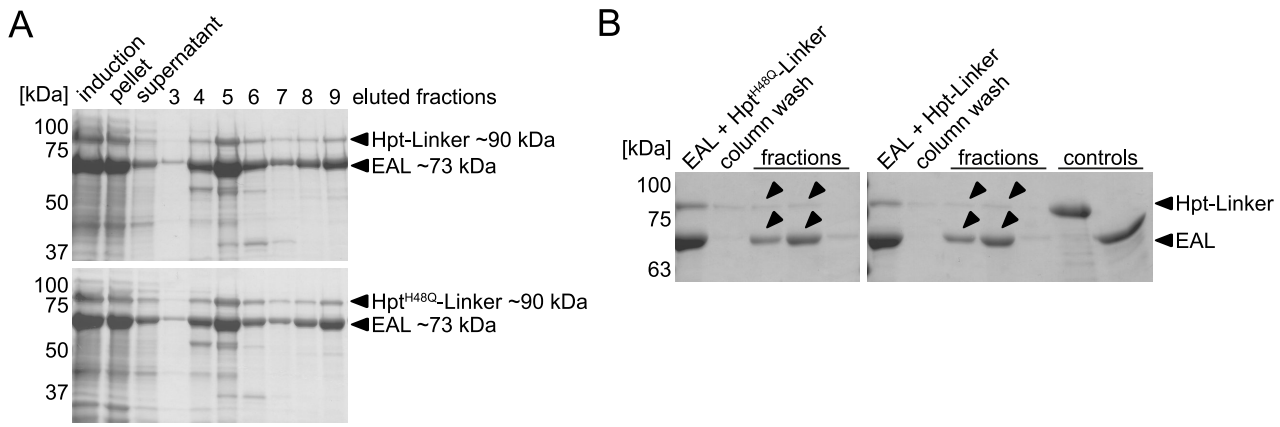

Figure 45. The Pch EAL domain interacts with the CheA Hpt-linker domain upon co-expression and co-purification. **A** Coomassie-stained SDS-PAGE showing Ni-NTA-based affinity chromatography of co-expressed proteins. Upper panel: co-purification of the Pch EAL domain (~73 kDa) together with the CheA Hpt-linker domain (~90 kDa). Lower panel: co-purification of the Pch EAL domain (~73 kDa) together with the CheA Hpt-linker H48Q substitution variant (~90 kDa). **B** Coomassie-stained SDS-PAGE of a MBP-based pulldown assay using the co-expressed proteins shown in **A**. The MBP-tagged Pch EAL domain was used as bait, while the CheA Hpt-linker domain or the H48Q substitution variant served as prey.

2.3.9 Conservation of the interaction interface of Pch and CheA

As shown previously, the interaction between Pch and CheA is mediated by the EAL domain of Pch and a linker region of CheA containing three distinct α-helices. Since there are currently no indications that catalytically active EAL domains directly mediate protein-protein interactions, this interaction interface was investigated in more detail. To this end, the primary amino acid sequence of the *P. putida* Pch EAL domain, spanning residues K637 to P891, was compared with EAL domains from homologous Pch proteins as well as canonical PDEs known to contain either the conserved EAL motif or experimentally validated PDE activity [177,217,239].

Phylogenetic analysis based on sequence identity revealed a close relationship among Pch EAL domains, which shared at least 77% identity with the *P. putida* Pch EAL domain, with most homologs exhibiting even higher similarity (**Figure 46A**). Consistently, all analyzed Pch homologs contained the characteristic conserved EAL motif, starting at residue E672 (Supplementary figure 11). In contrast, canonical PDE EAL domains showed substantially lower sequence identity of only 25-43%, indicating a clear evolutionary divergence from Pch-specific EAL domains (**Figure 46A**, Supplementary figure 12).

A

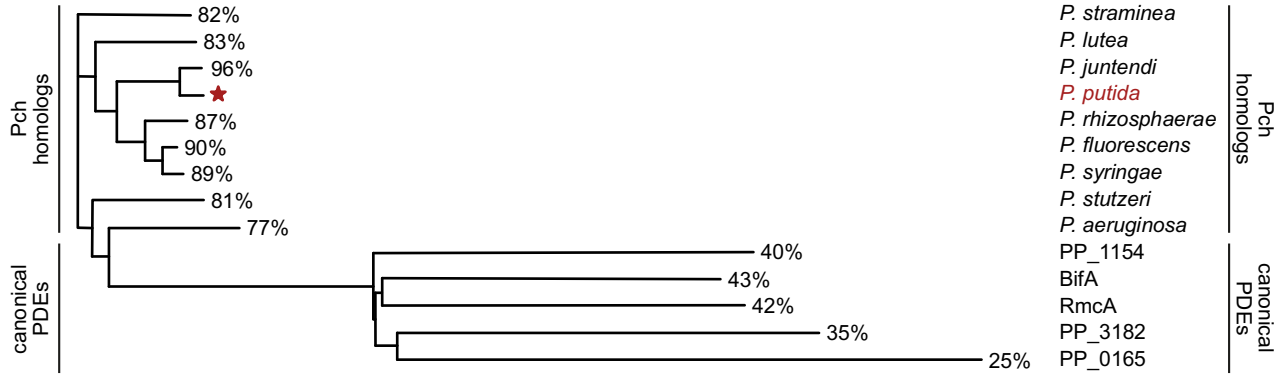

B

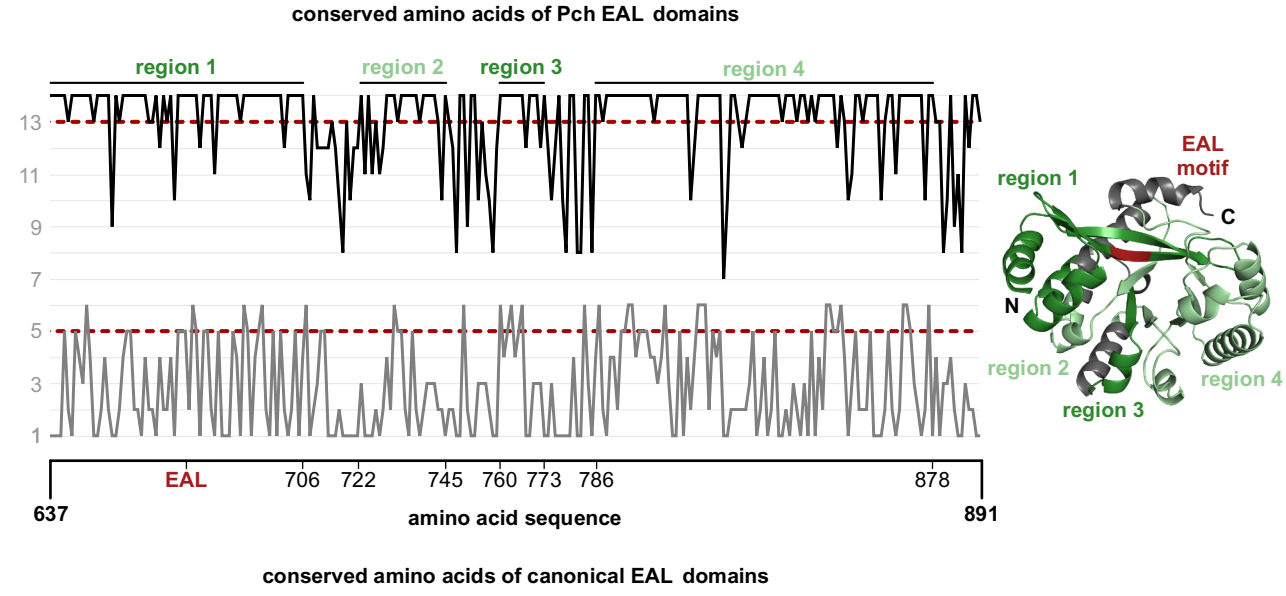

Figure 46. Evolutionary divergence and conservation of Pch-specific EAL domains. A Protein conservation was analyzed by aligning the *P. putida* Pch EAL domain sequence with homologous Pch EAL domains from other *Pseudomonas* species and with EAL domains from canonical PDEs, followed by phylogenetic tree construction using the UniProt alignment tool. Percentages indicate pairwise protein sequence identity. The *P. putida* Pch EAL domain is highlighted in red and marked with a red star. **B** Left: score-based conservation analysis of the Pch EAL domain sequence (amino acids K637 to P891) compared to other Pch EAL domains (upper panel) or canonical PDE EAL domains (lower panel). For each amino acid position of the *P. putida* Pch EAL domain, a conservation score was calculated based on the number of identical residues among aligned sequences (maximum score of 9 for Pch EAL domains and 6 for canonical EAL domains). This score serves as a measure of sequence conservation. To enable direct comparison, scores of the Pch EAL domain alignment were manually increased by 5. The red line indicates the conservation threshold, and conserved regions are marked with their corresponding amino acid positions below the graph. Right: AlphaFold3-based structural prediction of the *P. putida* Pch EAL domain with highly conserved regions highlighted in green and the conserved EAL motif highlighted in red. N- and C-terminal orientations are indicated. The conservation and score-based analyses were established in collaboration with Paul Molis.

A more detailed conservation analysis using a score-based system identified four highly conserved regions within Pch EAL domains when compared across different *Pseudomonas* species (**Figure 46B**). These conserved regions were not observed when canonical EAL domains were compared with the *P. putida* Pch EAL domain, further supporting the presence of Pch-specific sequence features (Supplementary figure 12). Similarly, score-based analysis of the CheA linker region (residues A110 to E360) across different *Pseudomonas* species revealed five conserved regions (**Figure 47**, Supplementary figure 13). Notably, these conserved segments corresponded closely to predicted α-helical elements within the linker region. In particular, α-helices 3 to 5 exhibited near-identical primary sequences, suggesting evolutionary conservation and potential functional importance for structural organization and protein-protein interaction. Taken together, these findings indicate that Pch EAL domains possess distinct sequence features that differentiate them from canonical EAL domains. These conserved regions likely contribute to the specific interaction with the CheA linker region, thereby providing a molecular basis for coupling c-di-GMP homeostasis to the chemotaxis machinery.

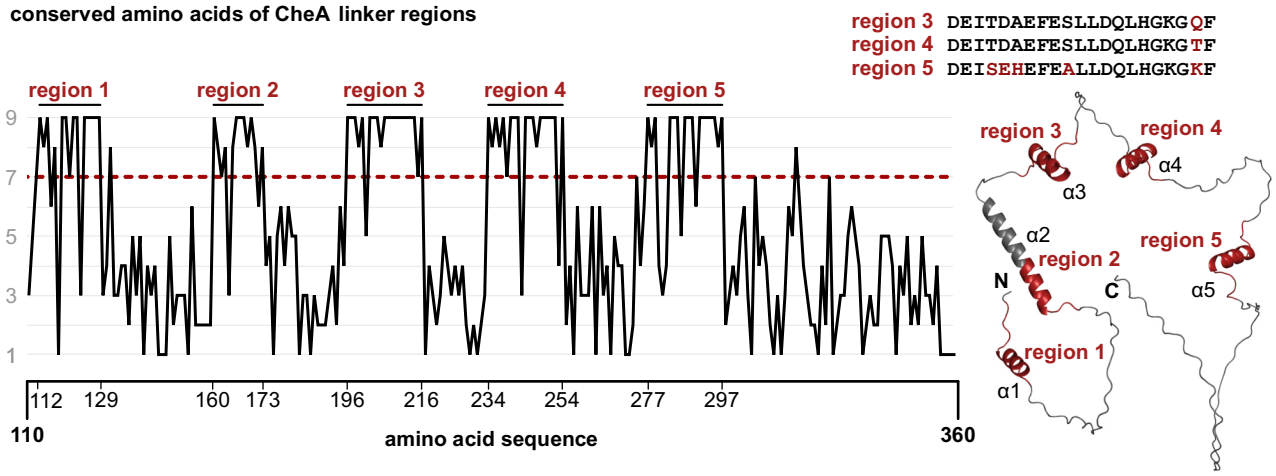

Figure 47. Evolutionary conservation of α-helices within the CheA linker region. Left: score-based conservation analysis of the CheA linker region (amino acids A110 to E360) compared to linker regions from homologous CheA proteins. Based on the amino acid sequence of the CheA linker region, a conservation score was calculated for each position, reflecting the number of identical residues among aligned sequences (maximum score of 9). This score serves as a measure of sequence conservation. The red line indicates the conservation threshold, and conserved regions are marked with their corresponding amino acid positions below the graph. Right: AlphaFold3-based structural prediction of the CheA linker region with conserved regions highlighted in red. N- and C-terminal orientations as well as positions of the α-helices are indicated. The upper panel shows the primary amino acid sequences of conserved regions 3-5, which correspond to highly conserved α-helical elements. The score-based analysis was established in collaboration with Paul Molis.

In summary, this chapter further characterized the interaction between the PDE Pch and the chemotaxis histidine kinase CheA in *P. putida*, providing detailed insight into its molecular basis. Both proteins co-localize at the flagellated cell pole, with Pch localization depending on CheA, and interact via the EAL domain of Pch and a conserved linker region of CheA. Functional analyses demonstrated that deletion of *cheA* abolishes motility, while deletion of *pch* increases intracellular c-di-GMP levels and moderately reduces motility, supporting a role of Pch as a functional PDE.

Additionally, both proteins interact with the polar organizer ParP, indicating their integration into a conserved polar signaling network. Collectively, these findings establish Pch as a polar, CheA-associated PDE that functionally connects chemotaxis signaling with c-di-GMP homeostasis.

3. Discussion

The polar organization of signaling proteins and proteins required for motility is a fundamental principle underlying efficient cellular regulation in many bacteria. The assembly of protein complexes at the cell pole enables spatial coordination of sensory input, signal transduction, and thrust generation, thereby ensuring rapid and precise responses to environmental stimuli. In this context, the findings presented in this work provide new insights into the complex functional signaling networks regarding the proper positioning of flagella in polar flagellated bacteria and protein interaction networks responsible for proper functions of the chemotaxis machinery connected to c-di-GMP homeostasis and lifestyle decisions in both *S. putrefaciens* and *P. putida*.

3.1 Polar flagellar assembly in *S. putrefaciens*

Many studies have contributed to the understanding of polar flagellar assembly in monotrichously flagellated bacteria. Previous studies suggested that the GTPase FlhF plays a key role in initiating polar flagellar assembly by recruiting the MS-ring component FliF to the cell pole during assembly of the polar flagellar machinery [152,229]. However, the precise molecular mechanisms underlying the initiation and regulation of this assembly process have remained largely unclear. Therefore, this study investigated polar flagellar assembly in more detail, with a particular focus on the interaction between FlhF and the C-ring component FliG.

3.1.1 FlhF-bound FliG recruits FliF to the site of polar flagellar assembly

The MS-ring protein FliF is an integral membrane protein containing two transmembrane helices and is inserted into the cytoplasmic membrane early during flagellar assembly, most likely via the canonical SRP-dependent SecYEG translocon, which is uniformly distributed along the cytoplasmic membrane in *S. putrefaciens* [148,240]. As FlhF belongs to the SRP-GTPase family, together with Ffh and FtsY [146], which target nascent membrane proteins to the SecYEG complex for translocation [148], it appeared plausible that FlhF directly recruits FliF to the site of polar flagellar assembly [152]. However, FlhF has not been shown to function as a membrane insertion factor, suggesting that its role is more likely related to spatial regulation of flagellar assembly rather than direct involvement in membrane integration.

In this study, an interaction between *S. putrefaciens* FlhF and the C-ring component FliG was demonstrated, whereas no direct interaction between FlhF and the MS-ring protein FliF was detected (**Figure 8**). Notably, this interaction was mediated specifically by the N-terminal, newly identified FliG interaction domain, FID, of FlhF, while the C-terminal NG-domain was responsible for interaction with HubP (**Figure 9, Figure 11**). Importantly, this recruitment cascade was also reconstituted in the heterologous host *E. coli*, supporting the robustness and transferability of the interaction network (**Figure 15**). These findings support a model in which FliG recruits membrane-diffusing FliF to the

site of flagellar assembly, where the complex is subsequently anchored at the cell pole through the interaction of FliG with FlhF and the association of FlhF with HubP (**Figure 48A**). This anchoring mechanism likely ensures efficient and spatially restricted flagellar assembly at the cell pole in *S. putrefaciens.* Consistent with this model, FlhF variants lacking the FID domain resulted in the formation of laterally positioned flagella (**Figure 13**). In these mutants, the interaction between FlhF and FliG is abolished, preventing stable anchoring of FliF and downstream flagellar components to HubP at the cell pole, thereby leading to mislocalized flagellar assembly [14]. In line with this, it was demonstrated that FliG, in the presence of FlhF, does not interact *in vitro* with the other C-ring components FliM and FliN, whereas interaction with FliF remains possible [14]. These observations led to the hypothesis of a checkpoint mechanism that prevents premature recruitment of downstream C-ring components until FliF has been properly recruited to the site of flagellar assembly. The FliM/FliN complex was shown to interact with FlhG via the N-terminus of FliM in a nucleotide-independent manner [61,224]. It can therefore be hypothesized that integration of the FliM/FliN complex into the assembling flagellar structure occurs only in the presence of FlhG (**Figure 48B**). In this context, FlhG stimulates the ATPase activity of FlhF [132,158,241], which may promote dissociation of FlhF, thereby enabling subsequent recruitment steps and incorporation of additional FliF subunits through interaction with FliG (**Figure 48C**). This proposed model is further supported by the observed coupling of flagellar C-ring assembly to transcriptional regulation mediated by FlhG (**Figure 48D**). In its ATP-bound, dimeric state, FlhG interacts with the master transcriptional activator FlrA [61]. This nucleotide-dependent interaction may enable FlhG to coordinate flagellar gene expression with the progression of polar flagellar assembly, thereby ensuring timely expression of structural components and preventing premature synthesis of proteins that cannot yet be incorporated into the assembling complex [14].

The model is further supported by the existence of homologous polar landmark protein-based systems in other bacteria. For example, *C. crescentus* forms a single polar flagellum at the newly generated cell pole immediately after cell division. In this organism, the polar landmark protein TipN marks the nascent cell pole through re-localization and subsequently recruits the protein TipF. Polar TipF then facilitates recruitment of a third protein, PflI, which is required for guiding the MS- and C-ring components (FliF, FliG and FliM) to the pole [133,173,242]. Thus, this system also relies on a three-protein recruitment cascade, resembling the HubP-FlhF-FliG recruitment pathway proposed in this study [14]. Additionally, another study demonstrated that all three domains of FlhF are required for proper swimming motility in *P. aeruginosa*. Interestingly, deletion of the B-domain (encompassing the first 118 amino acids) resulted in predominantly aflagellated cells, whereas deletion of the G-domain led to cells with a single delocalized flagellum and mislocalized FlhF signals. [243]. Moreover, it was shown that stable complex formation between FlhF and FliG depends on GTP binding and that the B-domain of FlhF is essential for flagellar assembly in *P. aeruginosa*, thereby supporting the results presented here.

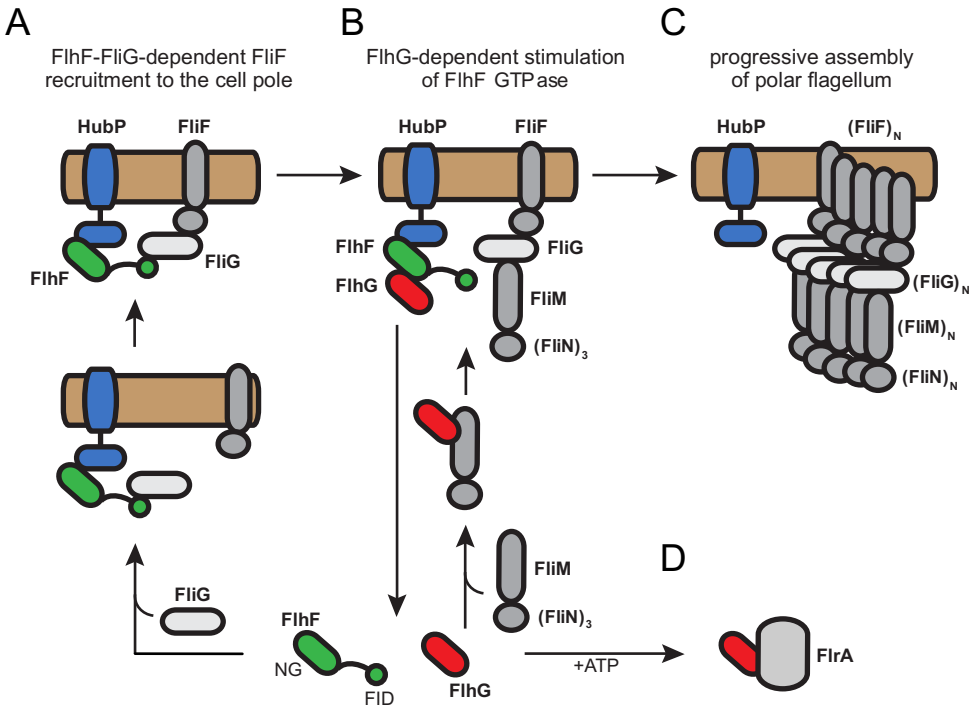

Figure 48. Model of the recruitment cascade responsible for proper polar flagellar assembly. A FlhF (green) binds to FliG (white) via its FID domain, while its NG-domain interacts with the C-terminal region of HubP (blue), thereby anchoring the complex at the cell pole. FliG subsequently captures the membrane-diffusing FliF protein (grey). **B** FlhG (red) stimulates the GTPase activity of FlhF, promoting dissociation and enabling a new cycle of FlhF-FliG-mediated FliF recruitment. **C** This iterative process supports the progressive assembly of the polar flagellum. **D** When not associated with the C-ring components FliM and FliN (grey), FlhG interacts with FlrA, the master transcriptional regulator (light grey), thereby linking flagellar assembly to transcriptional regulation. The cytoplasmic membrane is shown in brown. Adapted from [14].

Besides the involvement of the FID domain in mediating the FlhF-FliG interaction, the central and C-terminal regions of FliG were also reported to interact with FlhF *in vitro* (**Figure 10**). However, the precise molecular interface between the two proteins remains unresolved. Interestingly, deletion of either the N- or C-terminal regions of FliG resulted in bipolar localization and increased foci intensity of FlhF in *S. putrefaciens* cells (**Figure 13**), indicating a loss of strict monopolar localization in these mutants. Whether FlhF retains the ability to interact with these truncated FliG variants remains unknown. However, given that HubP localizes to both cell poles whereas FlhF is normally restricted to the flagellated pole in *S. putrefaciens* [132], it is conceivable that interaction with truncated FliG alters the spatial specificity of FlhF. In this scenario, FlhF may lose its preference for the flagellated pole and instead adopt a bipolar localization pattern resembling that of HubP. This suggests that intact FliG may contribute not only to anchoring flagellar assembly components but also to maintaining the spatial specificity of FlhF localization [14].

Nevertheless, additional proteins were shown to influence the polar localization of FlhF. For instance, deletion of components of the Poc complex in *P. aeruginosa* and *P. putida* resulted in delocalization of both FlhF and the flagellum [166,167]. Furthermore, deletion of the recently identified gene *fipA* led to a more diffuse localization pattern of FlhF in *S. putrefaciens* [165]. These observations suggest

the existence of additional organizer proteins that contribute to the spatial regulation of FlhF localization within the cell and highlight the complexity of the polar recruitment network, which remains subject to ongoing investigation.

3.1.2 The C-terminal region of FlhF interacts with the cytoplasmic region of HubP

Besides its interaction with FliG, FlhF was shown to directly interact *in vitro* with the cytoplasmic region of HubP (**Figure 11**). Notably, the conserved FimV domain of HubP was not required for this interaction. This finding is consistent with previous reports in *V. cholerae*, where protein binding was mediated not by the FimV domain but by the C-terminal region of HubP containing acidic tandem repeats [134]. Furthermore, the C-terminal portion of FlhF, encompassing the NG-domain, was demonstrated to be essential for interaction with HubP. This finding is supported by the polar localization observed for the FlhF FID deletion mutant (**Figure 13**). Despite the absence of the FliG-interacting FID domain, the NG-domain remains intact and mediates the interaction with HubP, resulting in polar FlhF foci even though the flagella themselves are delocalized. These observations indicate that the NG-domain of FlhF is sufficient for anchoring FlhF to HubP at the cell pole, independently of FliG-mediated flagellar recruitment [14]. These results are further supported by observations in *P. aeruginosa*, where deletion of the C-terminal FlhF G-domain resulted in mislocalized FlhF signals [243]. However, the interaction with HubP is not strictly required for the polar localization of FlhF. In *S. putrefaciens*, deletion of *hubP* generally has only minor effects on the polar positioning of FlhF and flagella [132,165]. A similar observation has been reported in *V. cholerae* [134]. In contrast, loss of HubP in *Vibrio parahaemolyticus* resulted in the absence of flagella in approximately half of the population [137,244], whereas deletion of *hubP* in *Vibrio alginolyticus* led to an increased number of flagella [227]. These findings suggest that additional factors contribute to HubP-mediated flagellar assembly and indicate that the underlying mechanisms display species-specific characteristics. One example is the above-mentioned, FlhF-interacting protein FipA protein. FipA is highly conserved among species that employ a FlhF-FlhG-based polar flagellar assembly system [165]. Comparative characterization in *V. parahaemolyticus*, *S. putrefaciens* and *P. putida* revealed fundamentally similar modes of operation. However, deletion of *fipA* had severe consequences in *V. parahaemolyticus*, where cells displayed strongly impaired swimming behavior and lacked flagella almost entirely. In contrast, *fipA* deletion mutants in *P. putida* and *S. putrefaciens* still produced flagella and exhibited only minor reductions in swimming ability. Furthermore, localization studies of FlhF in the absence of HubP or FipA revealed distinct differences among these species, suggesting that HubP and FipA represent separate pathways contributing to FlhF polar localization. Taken together, these findings indicate that a universal recruitment cascade for FlhF - and consequently for polar flagella - cannot be generalized across all species, even though the underlying proteins and mechanisms are largely conserved but adapted to species-specific requirements [14].

3.2 FimV - a polar organizer protein in *P. putida*

Polar landmark proteins serve as orientation points within the cell and are therefore highly important for the spatial control of various networks within the cell. In this study, the polar landmark protein FimV from *P. putida* was characterized in more detail together with its comparison to its potential homolog HubP in *S. putrefaciens* [231].

3.2.1 Polarity of the polar organizer FimV itself

As the well-characterized polar landmark protein HubP was previously shown to exhibit distinct polar localization [132,134,228], the subcellular localization of its homolog FimV was investigated. Using a fluorescent fusion construct, polar localization of FimV in *P. putida* could be clearly confirmed. Similar to HubP, FimV formed discrete clusters at the cell pole (**Figure 18**). Notably, two distinct clusters could be distinguished: a larger cluster located at the old, flagellated cell pole and a smaller cluster at the new cell pole that formed following recruitment of FimV to the division plane during cell division (**Figure 23**). These observations are consistent with findings from a recent study investigating FimV localization, as well as previous localization analyses of the HubP homolog in *S. putrefaciens* [131,132]. Together, these results further support the role of FimV as a polar organizer protein involved in spatial coordination of cellular processes.

The identification and characterization of the periplasmic domain containing an immunoglobulin-like fold suggested a potential role in the polar localization of FimV [231]. In the absence of this domain, FimV was no longer restricted to a distinct polar cluster but instead appeared fragmented into multiple small subclusters, which were frequently delocalized throughout the cell (**Figure 18**). Furthermore, a chimeric FimV variant, in which the periplasmic domain was replaced by that of HubP and which lacked the GLB domain, displayed significantly reduced swimming motility compared to wild-type FimV (**Figure 29**), indicating a functional relevance of proper localization for FimV activity. Deletion of the adjacent LysM domain resulted in a similarly dispersed localization pattern (**Figure 17**), suggesting that both domains contribute to correct polar positioning. Consistent with this observation, the LysM-containing periplasmic domains of HubP homologs in *V. cholerae* and *S. putrefaciens* were previously shown to be essential for proper polar localization [132,134]. Together with the observed interaction between FimV and peptidoglycan (**Figure 17**), these findings support a role for the LysM domain in stabilizing FimV at the cell pole through peptidoglycan binding [231]. However, the delocalization observed upon deletion of the GLB domain suggests that the LysM domain alone is not sufficient to ensure proper recruitment of FimV. Instead, the LysM domain might likely contribute to stabilization rather than initial targeting. This interpretation is further supported by recent findings demonstrating that FimV binds peptidoglycan fragments containing at least two N-acetylglucosamine/N-acetylmuramic acid disaccharide units [231]. Because such structural motifs are present throughout the cell wall, it is unlikely that peptidoglycan binding alone

is sufficient to mediate specific polar localization. Thus, recruitment of FimV to the cell pole likely involves additional factors or mechanisms, potentially including interactions with other polar organizer proteins. In support of this hypothesis, the protein FipA was recently identified as a factor required for proper FlhF function in *V. parahaemolyticus*, *P. putida*, and *S. putrefaciens*, highlighting the existence of additional regulatory components involved in polar organization [165]. GLB domains are well known to mediate protein-protein and ligand interactions, further supporting the idea that this domain may facilitate specific interactions required for correct polar targeting of FimV [245]. In the absence of the GLB domain, such interactions may be disrupted, preventing proper recruitment and resulting in the observed delocalization phenotype. Alternatively, it can be speculated that the GLB domain participates in interactions with the divisome, as *V. cholerae* HubP was shown to fail in polar recruitment in the absence of the cell division proteins FtsZ and FtsI [246]. These findings suggest that the GLB domain may be critical for recruitment in *P. putida*, whereas the LysM domain contributes primarily to stabilization of FimV at the cell pole. Nevertheless, additional studies are required to identify the molecular factors responsible for polar recruitment and stabilization of FimV.

3.2.2 FimV as polar localizer of the chemotaxis machinery

Remarkably, deletion of *fimV* resulted in a marked decrease in swimming motility compared to the wild type (**Figure 18**). Together with the observed increase in biofilm formation **(Figure 19**), these findings suggest a potential shift of the cells toward a sessile lifestyle. Transitions from motile to sessile states can be induced by multiple factors, including altered growth, cell morphology, flagellation, or chemotactic behavior, as previously reported in *P. aeruginosa*, *S. putrefaciens*, and *E. coli* [66,132,247,248]. However, investigation of growth dynamics and the involvement of FimV in chromosome segregation revealed no significant differences between wild-type and *fimV* deletion mutants (**Figure 20**, **Figure 23**). Interestingly, consistent with observations in *P. aeruginosa* [249], the *P. putida* chromosomal *parS* region does not completely localize to the cell pole, as observed in *V. cholerae* or *S. putrefaciens* [132,134,231]. Similarly, microscopic analyses showed that deletion of *fimV* did not noticeably affect cell morphology or flagellation (**Figure 19**). Given that the *P. aeruginosa* homolog FimV has been shown to recruit type IV pilus components to the cell pole [230], it was plausible that FimV functions as a polar organizer in *P. putida* as well. Consistent with this hypothesis, analysis of chemotaxis system localization revealed a reduction in polar clustering of CheA in the absence of FimV (**Figure 21**). A delocalized chemotactic array is likely to compromise signal transduction, providing a mechanistic explanation for the observed decrease in swimming motility. Supporting this notion, *fimV*-deficient cells exhibited shorter and more erratic swimming trajectories, indicative of reduced swimming speed [131].

In addition to FimV, FlhF exerted a strong influence on the polar positioning of the chemotactic array (**Figure 21**). As no direct interaction between CheA and FlhF could be detected in bacterial two-

hybrid experiments (**Figure 22**), this effect is likely indirect, arising from FlhF's role in defining the flagellar assembly site, which is functionally coupled to the chemotaxis machinery [14]. It is also possible that the observed effects arise from transcriptional control by FlhF of the entire chemotaxis machinery, as deletion of *flhF* in *V. cholerae* was shown to alter the transcription of class III flagellar genes [250]. Nevertheless, FimV's influence on FlhF should not be overlooked, as FimV has been shown to stabilize FlhF's association with the cell poles and is essential for proper polar positioning of FleN [131]. A recent preprint further supports the role of FimV in the polar assembly of the chemotaxis system, proposing a hierarchical recruitment cascade in which FimV recruits ParC, which subsequently recruits ParP, thereby ensuring correct assembly of the chemotactic array at the cell pole [178].

3.2.3 Influence of FimV on pilus-mediated motility and swarming-like behavior

FimV was shown to polarly localize various proteins connected to the type IV pilus machinery in *P. aeruginosa*, including the components PilMNOPQ or the membrane-bound sensor kinase PilS that controls *pilA* transcription to place the system at both poles of newly divided cells [136,230]. Since no functional fusion proteins could be created using PilO and PilQ proteins (data not shown), FimV's influence on the localization of the type IV pilus machinery in *P. putida* remains elusive. Moreover, a PilS homolog has not yet been identified in *P. putida*. Besides that, *P. aeruginosa* FimV and its homologs have been shown to be important for proper type IV pili-based twitching motility [132,144,251,252]. Interestingly, twitching motility has not yet been demonstrated for *P. putida*. All attempts to induce twitching motility in *P. putida* using established *P. aeruginosa* protocols were unsuccessful (**Figure 24**). This suggests that twitching motility might be a highly-controlled process that only occurs under certain conditions [231]. For example, the presence of the major pilin PilA could only be detected in *P. putida* cells after 12 hours of static biofilm formation, while the presence of flagella was restricted to planktonic cultures [253]. As demonstrated, structural gene homologs encoding *pil* genes are widely conserved in *P. putida* as well (**Table 1**). Consistent with this, components that are important for the structure and function of the type IV pilus machinery have been identified in *P. putida* WCS358 [254]. However, no pilus structures could be detected under laboratory conditions in *P. putida*, while transfer of *P. putida* PilA to *P. aeruginosa* resulted in production of pili, confirming the functionality of this major pilin. These results indicate a tightly regulated expression of type IV pili or the absence of additional genes required for expression. Accordingly, no *pilB* homolog is found upstream of the *pilA* gene *P. putida*, as in the case in *P. aeruginosa*. Nevertheless, it remains to be determined why some of the *pil* genes are conserved while others were lost. It is thus conceivable that some of the genes encoding important type IV pilus components are located elsewhere in the genome, or that homologous proteins exist that have not yet been identified and can take over these functions [254].

In order to examine the influence on pilus-mediated motility nonetheless, another type of surface motility on PG-agar plates, depending on type IV pili was used. Here, deletion of *fimV* revealed no significant difference on pilus-mediated surface motility in *P. putida* (**Figure 25**). Cells exhibited the characteristic spreading described before [100] with cells from the outer edge of motile fraction showing peritrichous hyper-flagellation. Furthermore, evolvement of motile cells by further passaging revealed more regularly and pronounced motility. Evolutionary experiments with *P. aeruginosa* revealed similar observations, since cells exhibited an increased swarming behavior after a few passages [255]. Those cells were characterized by an increased number of polar flagella triggered by parallel point mutations in the *fleN* gene, locking the bacteria in a multi-flagellated state. However, sequencing of the evolved *P. putida flhF* and *fleN* gene loci did not reveal any mutations in these regions. In addition, the flagellar pattern of the double deletion *flhF fleN* mutant showed a similar pattern of flagellation (**Figure 26**). However, these flagella were significantly shorter and did not appear fully developed, likely resulting from the combined loss of spatial and numerical control of flagellar assembly. While FlhF defines the polar insertion site, FleN restricts flagellar number. Their simultaneous absence leads to uncontrolled and ectopic initiation of flagellar assembly, resulting in inefficient filament elongation and structurally compromised flagella. These results indicate a physiological adaptation rather than a genetic one. However, it would be interesting to see in which phenotypical appearance overproduction mutants of *fleN* and *flhF* would result and if it resembles the peritrichous hyper-flagellation phenotype observed. In conclusion, FimV seems to not influence the functional activity of the pilus machinery, which is in line with previous observations in *Neisseria meningitidis*, where deletion of the FimV homolog TspA had no effects on twitching motility or surface piliation [256].

During investigation of pilus-mediated surface motility of *P. putida*, another type of motility was observed (**Figure 27**). This type of motility resembled the flower-like pattern of swarming motility exhibited by *P. aeruginosa* PA14 strains [233]. Since the typical swarming pattern of *P. aeruginosa* PAO1 was observed using the same experimental setup and the absence of the motility type using strains lacking the *fliC* gene, which is widely described as essential for swarming motility [257,258], the occurrence of *P. putida* showing swarming motility is likely. The *pilA* deletion mutant showing this behavior also supports this hypothesis, since this deletion mutant has been shown to improve swarming motility in *P. aeruginosa* [259]. However, several studies reported differing contributions of flagella and type IV pili to swarming motility, suggesting that their relative importance varies depending on the bacterial species and environmental conditions [258,260]. Interestingly, the flagellar structures observed by electron microscopy in this work were frequently localized at lateral positions along the cell body (**Figure 27**). This is reminiscent of *V. parahaemolyticus*, which normally possesses a Na^+-driven polar flagellum but produces additional H^+-driven lateral flagella encoded by its secondary flagellar system upon surface contact [261,262]. However, lateral structures can

also arise during pilus-mediated surface motility, as described above, and no secondary flagellar system has been identified in *P. putida*. This indicates that the observed lateral filaments in *P. putida* do not represent a dedicated secondary flagellar system, but could instead reflect the alternative swarming mechanisms of surface-associated motility. One might therefore speculate that, under certain circumstances, *P. putida* reverses the polarity of its flagellar system, thereby changing from a lophotrichous to a peritrichous flagellation pattern. Consistent with this, swarming motility relies strongly on the production of surfactants [67]. Since the agar background on these plates often appeared more structured, suggesting the possible production of surfactant-like compounds, this confirms the possibility of observed swarming motility. And since motile/sessile lifestyle decisions are connected to second messenger-dependent signaling networks [186], the influence of proteins involved in this process seems likely. c-di-GMP was shown to be required for swarming motility in *E. coli* by controlling the production of the surfactant colanic acid [263]. However, the origin of this type of motility observed here needs to be further investigated including the participation of second messenger by, for example, using mutants overproducing c-di-GMP.

3.2.4 Functional homologies across bacterial genera

In addition to investigating the functions of FimV in *P. putida*, its structural and functional properties were compared to those of its potential homolog HubP in *S. putrefaciens*. Both proteins exhibit a surprisingly high degree of similarity in domain organization (**Figure 29**). Significant structural differences are primarily restricted to the GLB domain, which is specific to *Pseudomonas* FimV, and to the repeats within the C-terminal region of HubP variants. As described above, the GLB domain is critical for polar localization of FimV [231]. In contrast, HubP homologs lack this domain yet still display robust polar localization [132,134]. Fluorescence microscopy of *Sp*HubP expressed in *P. putida* confirmed its polar positioning in this heterologous host (**Figure 28**), supporting the existence of an alternative, GLB-independent recruitment mechanism. Furthermore, a *Sp*HubP variant harboring the periplasmic domain of *Pp*FimV exhibited slightly but significantly reduced swimming motility (**Figure 29**), suggesting that the GLB domain may represent a *Pseudomonas*-specific feature mediating polar positioning and potentially additional species-specific functions. Regarding the exchange of the C-terminal regions, both HubP and FimV C-terminal regions are enriched in acidic residues, whereas HubP variants contain multiple imperfect repeats, which are often involved in mediating protein-protein interactions via structural flexibility in unstructured linker regions [264,265]. Supporting this notion, deletion of the repeat region in *V. cholerae* HubP abolished its interaction with ParA1, a bacterial plasmid-partitioning protein homolog [134], while experiments in *Legionella pneumophila* showed that the number of repeats influences FimV function [252]. These observations suggest that swapping the cytplasmic domains may disrupt specific interactions between *Sp*HubP and its partners, while introducing novel interactions for FimV, thereby reducing the swimming ability of both species. Exchange of the C-terminal FimV domain did not restore wild-

type swimming, with cells phenocopying a FimV domain deletion mutant (**Figure 29**). These results indicate that, although the secondary structure of the C-terminal FimV domain is highly conserved across species, its functional role remains largely species-specific [231]. This interpretation is consistent with observations from other organisms: the FimV homolog TspA in *N. meningitidis* mediates human cell adhesion rather than twitching motility [256], and FimV influences pigment formation and cell morphology in *L. pneumophila* in addition to motility [252]. Collectively, these findings suggest that FimV and HubP operate within highly species-specific functional contexts, likely reflecting adaptation to distinct environmental-associated constraints. Remarkably, even within a single species, uniform FimV function is not guaranteed: deletion of *fimV* in *P. putida* reduces swimming motility, whereas no comparable deficit is observed in *P. aeruginosa* [136,231].

3.3 Chemotaxis and c-di-GMP-dependent signaling in *P. putida*

Chemotaxis and c-di-GMP signaling constitute two key regulatory systems that coordinate bacterial responses to environmental cues and regulate the transition between motile and sessile lifestyles [186]. While chemotaxis primarily regulates directional motility through the histidine kinase CheA and its downstream signaling cascade [101], c-di-GMP acts as a second messenger coordinating motility, biofilm formation, and cellular adaptation via DGCs and PDEs [190]. Although both systems have been extensively studied individually, increasing evidence suggests that they are functionally interconnected and coordinated at multiple regulatory levels. In this study, the PDE Pch and the histidine kinase CheA from *P. putida* were investigated to elucidate their functional relationship and potential role in linking c-di-GMP homeostasis with the chemotaxis machinery. Using a combination of genetic, cell biological, biochemical, and structural approaches, the interaction between both proteins was reproduced and characterized in detail.

3.3.1 The gene PP_0337 encodes the PDE Pch

In general, PDEs play a central role in maintaining intracellular c-di-GMP homeostasis by catalyzing the hydrolysis of c-di-GMP into linear pGpG, thereby regulating the balance between motile and sessile lifestyles [186,266]. However, the PDE Pch and its homologs represent a specialized subgroup of PDEs, as they form a direct functional and spatial interface between the chemotaxis machinery and c-di-GMP signaling [220]. In this study, the Pch protein from *P. putida*, encoded by the PP_0337 gene, was identified and characterized. Deletion of this gene resulted in reduced swimming motility and increased intracellular c-di-GMP levels (**Figure 33**, **Figure 35**), supporting a role for Pch in c-di-GMP degradation and motility regulation. Consistent with this function, the Pch protein contains the highly conserved EAL motif, which forms part of the catalytic center and is essential for PDE activity. Structural and biochemical studies have demonstrated that residues within and surrounding the EAL motif, including conserved loop regions, coordinate metal ions required for catalysis and substrate binding [216,267]. In contrast, Pch lacks the canonical GGDEF motif, which

is required for DGC activity and c-di-GMP synthesis [200,266], indicating that Pch functions exclusively as a PDE rather than a bifunctional enzyme. These characteristics are consistent with previous findings for the Pch homolog in *P. aeruginosa*, which has been shown to possess PDE activity and to regulate motility and biofilm dispersion, further supporting the functional conservation of this protein family across *Pseudomonas* species [220].

3.3.2 Polarity of Pch and CheA

Together with CheA, the localization patterns of both proteins were analyzed within the cells. The data revealed co-localization of Pch and CheA at the flagellated cell pole using *in vivo* fluorescence microscopy, with Pch's polar localization depending on the presence of CheA (**Figure 36**, **Figure 37**). This observation suggests that CheA functions not only as a signaling kinase but also as a spatial organizer for proteins such as Pch. In addition, the data indicate an important contribution of the Hpt domain to the polar localization of both CheA and Pch, as the fluorescent signal of both proteins was significantly reduced and more diffusely distributed in strains lacking this domain (**Figure 43**). The absence of the Hpt domain may destabilize the structural integrity of CheA, potentially leading to dissociation and destabilization of the entire complex. This could explain the reduced number of detectable CheA clusters within cells, as the signal becomes dispersed rather than concentrated at the pole. Although the Hpt domain is not directly involved in most known interactions between CheA and its binding partners [129,170], it is essential for the functional activity of the histidine kinase, as it contains the phosphorylatable histidine residue H48. Notably, phosphotransfer to CheY was shown to occur even in the absence of the P2 domain - corresponding to the largely unstructured linker region in *P. putida* CheA - despite the lack of the primary CheY binding interface [128]. This finding highlights the functional importance of the Hpt domain and suggests that it may possess additional, yet uncharacterized structural or regulatory roles.

While Pch generally exhibited strong polar cluster formation, only a small proportion of cells displayed a detectable fluorescent signal overall (**Figure 37**). These observations are consistent with previous studies showing that Pch and other proteins involved in c-di-GMP homeostasis in *P. aeruginosa* and other bacterial species exhibit distinct and often heterogeneous localization patterns [163,268–273]. When present, polar localization was observed in most fluorescent cells but was not exclusively restricted to the pole, suggesting a dynamic equilibrium between polar recruitment and cytoplasmic diffusion. This dynamic localization likely reflects reversible interactions with polar chemotaxis complexes, such as the chemotaxis kinase CheA, and may enable rapid modulation of c-di-GMP levels in response to environmental cues. Such transient or reversible recruitment could explain the relatively low number of detectable polar foci as shown in **Figure 37**. However, it remains to be experimentally determined whether Pch is stably retained at the cell pole

through continuous interaction with CheA and incorporation into the chemotaxis array, or whether it undergoes dynamic diffusion within the cell.

Cells expressing only the C-terminal EAL domain or the combined GGDEF-EAL domains failed to localize properly to the cell pole (**Figure 36**). These findings suggest that additional factors are required to stabilize the interaction between CheA and Pch at the cell pole. Since bacterial two-hybrid analysis revealed a potential interaction between ParP and the N-terminal region of Pch, as well as between ParP and CheA (**Figure 41**), it is plausible that ParP contributes to the stabilization of Pch within the chemotaxis array. Previous studies demonstrated that proper positioning of CheA depends on an interaction network involving HubP, ParP, and ParC in *V. parahaemolyticus* [169,170]. In this system, polar localization of HubP is followed by recruitment of ParC, which subsequently recruits ParP to the cell pole. ParP, in turn, stabilizes chemotaxis proteins, for example through interaction with a specific region within the CheA linker, referred to as the LID domain. However, deletion of *parP* did not significantly alter Pch localization (**Figure 37**), suggesting that ParP is not strictly required for proper polar recruitment of Pch. Nevertheless, previous observations showed that chemotaxis complex stability is only partially impaired in *parC* mutants, indicating that ParP can retain functional interactions independently of ParC and highlighting the robustness of the polar recruitment network [134,169,170]. Therefore, it cannot be excluded that ParC may partially compensate for the absence of ParP, and vice versa. This possibility could be tested experimentally by generating a double deletion mutant lacking both proteins.

Interestingly, in *P. putida*, the localization of CheA strongly depends on FlhF and PocB, and to a lesser extent on FimV (**Figure 38**), whereas in *Vibrio* and *Shewanella* species, HubP serves as the primary determinant coordinating the polar recruitment of chemotaxis components [132,134]. Since no direct interaction between FlhF and CheA could be detected (**Figure 22**), the effect of FlhF on the localization of CheA and Pch is likely indirect. This influence may result from the functional and structural coupling of the flagellar and chemotaxis machineries, as FlhF determines the site of flagellar assembly and thereby indirectly defines the spatial context for chemotaxis complex formation [14,131]. Previous studies demonstrated that polar localization of FlhF in *P. putida* and *P. aeruginosa* depends on the polar landmark proteins PocA and PocB, providing a mechanistic explanation for the impaired localization of CheA observed in a *pocB* deletion strain [166,167]. In this scenario, the effect of PocB on CheA localization is likely mediated through its role in positioning FlhF. Consistent with the observations presented here, a recent preprint reported that FimV is required for proper localization of ParC and the subsequent recruitment of ParP, which may explain the altered localization of CheA observed in the absence of FimV [178]. Together, these findings support a model in which CheA and Pch localization depends on a hierarchical polar recruitment network involving flagellar positioning factors and chemotaxis-specific scaffold proteins.

3.3.3 Interaction of Pch with CheA

Previous studies reported an interaction between Pch and CheA in *P. aeruginosa* [163], which was also confirmed in the present study using *P. putida*. Using bacterial two-hybrid analysis, the interaction interface was mapped to the EAL domain of Pch, which interacts with a defined region comprising three α-helices within the linker region corresponding to the P2 domain of *P. putida* CheA (**Figure 40**). This region is predicted to be structurally flexible and may facilitate protein-protein interactions. The interaction between Pch and CheA may functionally link chemotactic signaling with rapid changes in the transition between motile and sessile lifestyles, which are regulated by the second messenger c-di-GMP. This hypothesis is supported by the observed co-localization of both proteins at the flagellated cell pole, suggesting that spatial proximity enables efficient integration of chemotactic and c-di-GMP-dependent regulatory pathways.

3.3.3.1 The conserved interaction interface of CheA and Pch

The results presented in this study demonstrate the involvement of the CheA linker region in mediating the interaction with Pch (**Figure 40**, **Figure 45**). Conservation analysis further revealed that this region is evolutionarily conserved and contains five predicted α-helices, as indicated by AlphaFold3 structural predictions (**Figure 47**). This evolutionary conservation supports the functional importance of the P2 domain, which corresponds to the linker region in *P. putida* CheA.

Consistent with this interpretation, the CheA protein of *E. coli* K-12 contains approximately 10% intrinsically disordered content, as reported in the DisProt database for functionally annotated intrinsically disordered proteins [274]. Proteins containing intrinsically disordered regions are frequently involved in signaling and regulatory processes [275]. High-throughput analyses have shown that approximately 74% of functionally characterized intrinsically disordered regions participate in interactions with proteins, nucleic acids, or other ligands [265]. Intrinsically disordered regions provide structural flexibility and enable the formation of dynamic protein complexes that may not be possible with rigid domains alone. For example, such regions can adapt their conformation upon binding and wrap around interaction partners, thereby facilitating specific and reversible interactions [264]. For proteins such as the CheA histidine kinase within the chemotaxis machinery, structural flexibility is essential to enable interactions with multiple binding partners. In addition to its interactions with ParP and ParC, as described above, the P2 domain of *E. coli* CheA has been shown to mediate interaction with the response regulator CheY [129]. Notably, structural analyses revealed two distinct binding modes for the CheA-CheY heterodimer that involve the same interaction interface, indicating considerable conformational flexibility within this region [276]. This flexibility has also been supported by *in vivo* bacterial two-hybrid analyses in *V. parahaemolyticus*, where CheY was able to interact with CheA variants consisting solely of the P2 domain or truncated versions thereof [170]. Consistent with these findings, AlphaFold3 predictions of the *P. putida* CheY-CheA

heterodimer suggest structural rearrangements within the flexible linker region that facilitate efficient CheY binding (**Figure 49**).

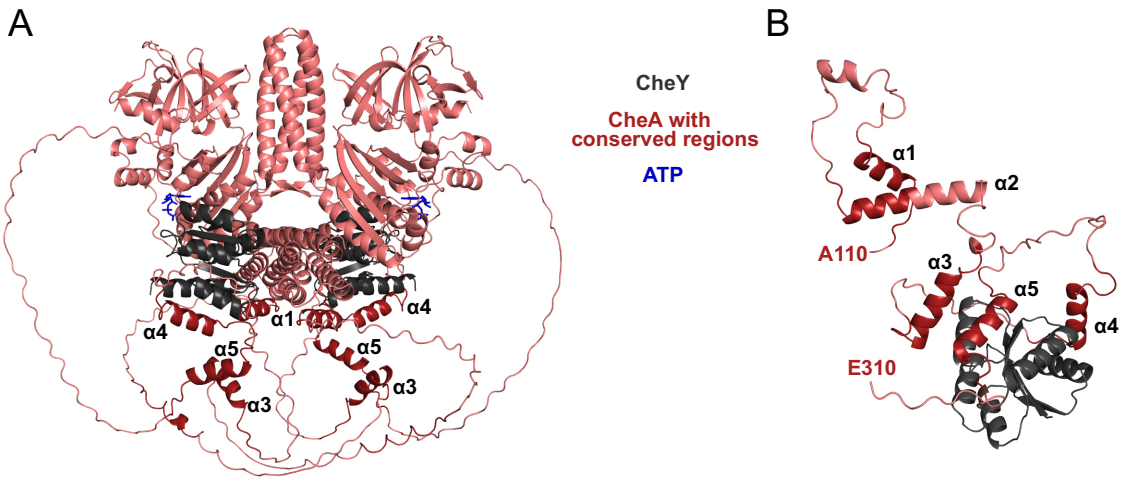

Figure 49. Structural prediction of the interaction between CheY and CheA in *P. putida*. AlphaFold3-based structural predictions of full-length CheY (grey) in complex with either **A** the homodimer of full-length CheA in complex with ATP (pTM score 0.41, ipTM score 0.39) or **B** the CheA linker region (spanning amino acids A110 to E310, pTM score 0.46, ipTM score 0.61). Conserved regions are highlighted in dark red and α-helices 1 and 3-5 within the linker region are indicated.

In contrast to the five highly conserved regions corresponding to predicted α-helices within CheA (**Figure 47**), the EAL domains of Pch PDEs exhibited an overall high level of conservation in their amino acid sequence (**Figure 46**). However, comparison of the *P. putida* Pch EAL domain with those of canonical PDEs revealed only limited conservation, with the exception of the characteristic EAL motif. This observation suggests that Pch EAL domains possess a distinct sequence profile, which may be specifically adapted to mediate interactions with partner proteins such as CheA.

By combining conservation analysis with AlphaFold3-based structural predictions of the interaction interface between the CheA linker region and the Pch EAL domain, amino acid residues potentially critical for this interaction were identified (**Figure 50**). These include four salt bridges, one hydrogen bond and either a π-π or cation-π interaction, depending on the protonation state of the histidine residue. Notably, all predicted interaction residues within CheA are located in conserved regions and frequently coincide with predicted α-helical elements, supporting their structural and functional relevance. Similarly, the predicted interaction residues within the *P. putida* Pch EAL domain are highly conserved among Pch homologs but show little conservation compared to canonical PDEs (**Figure 46**). This finding indicates that these residues may contribute to the specific structural and functional properties of Pch EAL domains, particularly their ability to interact with CheA. Furthermore, the predicted interacting residues are located in close spatial proximity, with inter-residue distances of approximately 3 Å or less, which is consistent with direct molecular interactions. These

observations strongly support the hypothesis that the identified residues play a critical role in mediating the interaction between the CheA linker region and the Pch EAL domain and therefore remain insightful study objects.

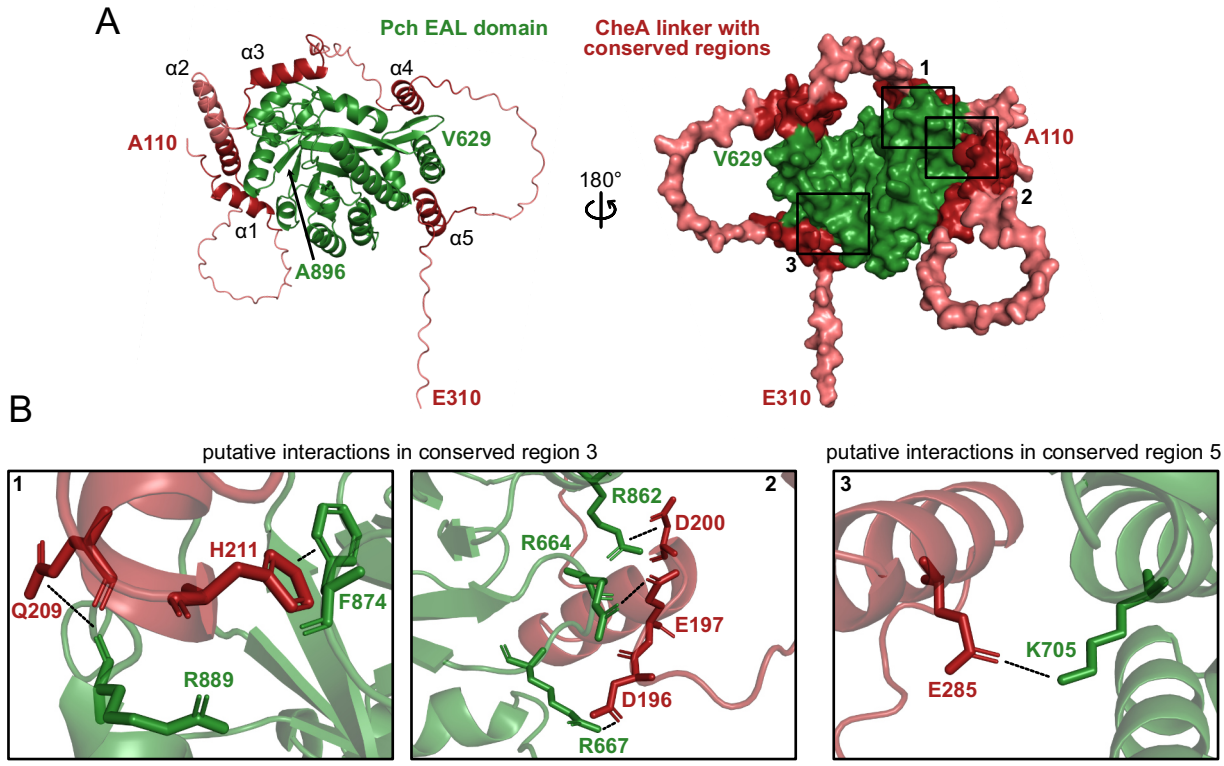

Figure 50. Putative amino acid interactions between the Pch EAL domain and the CheA linker region in *P. putida*. **A** AlphaFold3-based structural prediction of the Pch EAL domain (green; spanning V629 to A896) together in complex with the CheA linker region (spanning A110 to E310), including the α-helices and conserved regions (dark red). The predicted pTM score is 0.63 with an ipTM score of 0.79. Insets indicate the locations of the putative interaction interfaces described in **B**. **B** Close-up views of putative amino acid interactions within conserved region 3 (left) and conserved region 5 (right). Following putative interactions were identified: salt bridges between R862 and D200, R664 and E197, R667 and D196 and K705 and E285; a hydrogen bond between R889 and Q209; and either a π-π or cation-π interaction between F874 and H211, depending on the protonation state of the histidine residue. Amino acid side chains are shown as sticks and are colored according to protein identity (CheA in red, Pch in green). Black dashed lines indicate predicted interacting residues.

3.3.3.2 Interaction dynamics of Pch and CheA in their inactive vs. active states

Since both CheA and, potentially, Pch can exist in active and inactive conformational states [235], the question arises how their interaction influences their respective activities and regulatory states. As described above, the histidine kinase CheA cycles between an inactive, non-phosphorylated state and an active state, in which autophosphorylation of the conserved histidine residue H48 occurs in response to changes in receptor signaling, typically triggered by ligand dissociation [114,277]. For Pch, structural and biochemical studies of other EAL domain-containing PDEs have demonstrated that these enzymes function as homodimers and that substrate binding is directly coupled to dimer formation and catalytic activity [278,279]. Dimerization stabilizes the catalytically competent conformation required for efficient binding and hydrolysis of c-di-GMP. Based on these findings, it is likely that Pch in *P. putida* also functions as a homodimer, with dimerization being essential for its enzymatic activity. The interaction with CheA may therefore influence Pch activity by

modulating its oligomeric state. For example, binding to CheA could shift the equilibrium between monomeric and dimeric forms, potentially stabilizing an inactive monomeric conformation or, alternatively, promoting the formation of an active dimer depending on the regulatory context. At present, it remains unclear in which conformational or activity state CheA interacts with Pch, and whether CheA phosphorylation directly affects this interaction. However, previous findings are consistent with the hypothesis that inactive, non-phosphorylated CheA prevents Pch PDE activity, since measurements in a H48Q mutant resulted in increased intracellular c-di-GMP levels in *P. aeruginosa* [163].

As demonstrated by the protein purification experiments, independent purification of both protein domains followed by subsequent incubation under various conditions did not result in detectable complex formation (**Figure 44**). This observation suggests that additional factors may be required to facilitate or stabilize the interaction between the two domains. One possible factor is the presence of divalent metal ions, which are known to influence kinase activity and protein-protein interactions by stabilizing protein conformations or enhancing substrate binding affinities [280]. For example, CheA from *Thermotoga maritima* was shown to bind ATP analogs in its catalytic center only in the presence of Mg^{2+}, highlighting the essential role of divalent cations for proper catalytic function and structural stabilization [281]. Similarly, Mg^{2+} has been reported to be required for the activity of the c-di-GMP-specific PDE CC3396 from *C. crescentus*, supporting a broader role of divalent metal ions in regulating PDE structure and activity [201]. These findings suggest that Mg^{2+} or other divalent cations may also contribute to stabilizing the interaction between CheA and Pch. In addition, other ligands such as ATP, ADP, c-di-GMP, or cAMP may influence complex formation, as these molecules are known to bind CheA and Pch and can induce conformational changes that affect protein activity and interaction properties. Ligand-induced conformational changes may promote interaction by stabilizing compatible structural states of both proteins. Another possibility is the involvement of an adapter protein that facilitates or stabilizes the interaction between CheA and Pch. Such a mechanism has been described for CheW, which mediates the interaction between CheA and MCPs and is essential for the assembly and stability of the chemotaxis signaling complex [282,283]. A similar adapter-mediated mechanism could contribute to the recruitment or stabilization of Pch within the chemotaxis array.

Notably, co-expression of both protein domains followed by pulldown analysis resulted in detectable co-elution, indicating complex formation (**Figure 45**). These findings suggest that, if additional factors are required for the interaction, they must also be present in *E. coli*, the heterologous expression host used in this study. This would exclude proteins such as the partitioning factor ParP, which is not naturally present in *E. coli*, as an essential mediator of the interaction [284]. However, it cannot be excluded that no additional proteins or ligands are strictly required and that the failure

to detect complex formation in previous experiments was due to suboptimal incubation or purification conditions. Importantly, successful complex formation between the Pch EAL domain and the CheA H48Q substitution variant (**Figure 45**) demonstrates that a non-phosphorylatable CheA variant is still capable of interacting with Pch. This observation suggests that phosphorylation of CheA is not strictly required for the interaction. Conversely, this raises the possibility that CheA phosphorylation may modulate the interaction, potentially reducing or preventing complex formation. In the case of wild-type CheA, a mixed population of phosphorylated and non-phosphorylated proteins is likely present, which cannot be readily distinguished using the experimental approaches applied in this study. Furthermore, expression of both proteins in a heterologous host under non-native conditions may influence their structural and functional states, potentially affecting interaction dynamics. Therefore, it would be important to confirm the interaction under native conditions, for example by co-expression and interaction analysis of the respective protein domains in *P. putida*. Such experiments would provide further insight into the physiological relevance and regulatory context of the CheA-Pch interaction.

To investigate a potential influence of CheA phosphorylation on its interaction with Pch, it would be necessary to increase the proportion of CheA present in the phosphorylated state. One possible approach is to interfere with phosphotransfer to CheY or to prevent CheY dephosphorylation, thereby altering the equilibrium of phosphorylated signaling components. For example, expression of non-phosphorylatable CheY variants, such as CheY S56A/D57N [285], or deletion of the phosphatase CheZ, which normally catalyzes CheY dephosphorylation, would disrupt normal phosphotransfer dynamics and alter the steady-state phosphorylation balance within the chemotaxis system. Another strategy would be to directly modify CheA. However, the generation of a pseudo-phosphorylated CheA variant is challenging, since phosphorylation occurs at a histidine residue, where the phosphate group is bound to the nitrogen atom of the imidazole ring. This type of phosphoramidate linkage cannot be readily mimicked by conventional phosphomimetic substitutions, such as aspartate or glutamate. Alternatively, hyperactive CheA variants could be used to increase the proportion of phosphorylated CheA. For example, the CheA-XD17 mutant from *S. typhimurium* has been reported to exhibit up to a 6.7-fold increase in kinase activity compared to wild-type CheA [286]. Such a hyperactive kinase variant may increase the steady-state level of phosphorylated CheA and could therefore serve as a useful tool to investigate phosphorylation-dependent effects on the interaction with Pch.

3.3.3.3 Involvement of CheY - a potential CheA-binding competitor to Pch?

As previously reported and confirmed in this study, CheY and Pch appear to interact with overlapping regions within the CheA linker region corresponding to the P2 domain (**Figure 49**) [129,170]. This observation raises the possibility that both proteins may compete for binding to CheA. Structural

analyses by AlphaFold3 predictions suggest that binding of CheY induces conformational rearrangements within the flexible linker region of CheA (**Figure 49**), which could disrupt a pre-existing interaction with Pch and result in dissociation of the Pch EAL domain [276]. The affinity between CheA and CheY in *E. coli* has been reported to be in the low micromolar range (Kd ≈ 10-60 µM), consistent with a transient but specific interaction required for efficient phosphotransfer [111,125,127]. Importantly, CheY binding does not strictly require CheA phosphorylation. However, phosphorylation-dependent conformational changes in CheA may influence binding kinetics and interaction stability. More generally, phosphorylation has been shown to alter protein-protein interaction affinities within the chemotaxis signaling network. For example, phosphorylated CheY exhibits reduced affinity for CheA and increased affinity for its downstream interaction partners CheZ and FliM, thereby promoting signal propagation toward the flagellar motor [111,120,287]. Consistent with this, the CheA H48Q substitution variant may still permit CheY binding, although potentially with altered affinity or interaction dynamics due to the absence of phosphorylation. Furthermore, CheY can also be phosphorylated by small phosphodonor molecules, such as acetyl phosphate, independently of CheA [288]. Under such conditions, phosphorylated CheY may exhibit reduced affinity for CheA, favoring interaction with downstream targets instead. This dynamic binding behavior supports a model in which CheY and Pch compete for interaction with CheA in a phosphorylation- and conformation-dependent manner, potentially linking chemotactic signaling to c-di-GMP-mediated lifestyle regulation. Nevertheless, recent results demonstrated that overexpression of CheY leads to increased intracellular c-di-GMP levels and subsequent cell aggregation [130]. One possible explanation is that, despite CheY overexpression, Pch remains bound to CheA in an inactive state, thereby reducing its PDE activity and causing intracellular c-di-GMP levels to rise. Although the underlying mechanism remains unclear, these findings suggest that elevated CheY levels may influence the regulatory balance between chemotaxis signaling and second messenger homeostasis. To determine whether CheY and Pch compete for binding to CheA, comparative interaction studies would be informative. In particular, pulldown assays or bacterial two-hybrid analyses involving all three proteins could clarify whether CheY and Pch share overlapping binding interfaces on CheA or whether their interactions are mutually exclusive.

3.3.4 Interaction and signaling network coordinating lifestyle decisions in polar-flagellated bacteria: a new model

Based on the results of this study and established principles of chemotaxis and flagellar signaling, the data support a model in which CheA, ParP and Pch form a spatially organized regulatory complex at the flagellated cell pole that functionally links chemotaxis activity to c-di-GMP turnover (**Figure 51**). It is well established that CheA forms a homodimer associated with MCPs and CheW at the cell pole, enabling efficient signal transduction in response to environmental stimuli [102,121]. In agreement with this, the localization analyses demonstrate polar co-localization of CheA and Pch

and reveal that polarity of Pch strongly depends on presence of CheA (**Figure 36**, **Figure 37**). The interaction studies further show that CheA directly interacts with the EAL domain of Pch via its linker region, specifically through α-helices 3-5 (**Figure 40**, **Figure 45**). Since EAL domain PDEs typically require dimerization for full catalytic activity [278], binding of Pch to CheA may sterically or conformationally constrain the EAL domain and thereby limit its enzymatic activity (**Figure 51**). Consistent with this interpretation, deletion of *pch* resulted in elevated intracellular c-di-GMP levels, confirming its role as an active PDE, whereas deletion of *cheA* did not result in alterations in c-di-GMP levels (**Figure 35**). These observations raise the possibility that polar sequestration of Pch by CheA may represent a regulatory mechanism to spatially control c-di-GMP degradation.

Upon stimulation of chemotaxis signaling under conditions of low chemoattractant availability (**Figure 51**), CheA undergoes autophosphorylation at the conserved histidine residue within its Hpt domain, followed by phosphotransfer to the response regulator CheY [128,236]. Phosphorylated CheY subsequently dissociates and binds to the flagellar motor, inducing CW flagellar rotation and thereby promoting tumbling or reverse-flick behavior in polar flagellated bacteria [117,118]. It is tempting to speculate that activation of CheA and/or its interaction with CheY may alter the structural organization or binding affinities within the CheA complex (**Figure 49**, **Figure 51**), potentially reducing its affinity for Pch. Such a mechanism would allow Pch to dissociate from the CheA complex, enabling EAL dimerization and activation, thereby promoting c-di-GMP degradation and favoring a motile lifestyle. While this regulatory transition remains to be experimentally demonstrated, it is consistent with the observed inverse relationship between motility and intracellular c-di-GMP levels [186,289]. However, it remains unclear whether CheY directly contributes to the dissociation of Pch from CheA, for example through competitive binding or steric interference, or whether the phosphorylation-dependent conformational changes within CheA itself are sufficient to reduce its affinity for Pch and enable dimerization of EAL domains (**Figure 51**). Both scenarios are plausible and suggest that the activation state of CheA by phosphorylation may function as a molecular switch coordinating chemotaxis signaling with c-di-GMP homeostasis.

In addition to CheA, the partitioning protein ParP was found to interact with both CheA and Pch and to localize at the cell pole (**Figure 41**, **Figure 42**). ParP has previously been implicated in stabilizing and organizing chemotaxis complexes at the pole [170]. The results suggest that ParP may contribute to stabilizing the CheA-Pch complex and thereby facilitate coordinated spatial regulation of chemotaxis signaling and c-di-GMP homeostasis. Furthermore, the dependence of CheA localization on polar organizer proteins such as FlhF, FimV, and PocB (**Figure 38**, **Figure 51**) supports the existence of a larger polar scaffold that integrates flagellar assembly, chemotaxis signaling, and second messenger regulation slightly differing from that of other bacterial species [132,134,170,290].

Taken together, these findings support a model in which CheA not only functions as a central chemotaxis kinase but also serves as a spatial regulator of c-di-GMP homeostasis through its direct interaction with the PDE Pch. This spatial coupling may ensure that changes in environmental sensing are rapidly translated into appropriate alterations in intracellular c-di-GMP levels, thereby coordinating the transition between motile and sessile states in *P. putida* (**Figure 51**). The results presented here provide new insights into the spatial organization, interaction mechanisms and functional implications of the Pch-CheA interaction and support the model of a direct molecular link between c-di-GMP signaling and chemotaxis-dependent motility regulation.

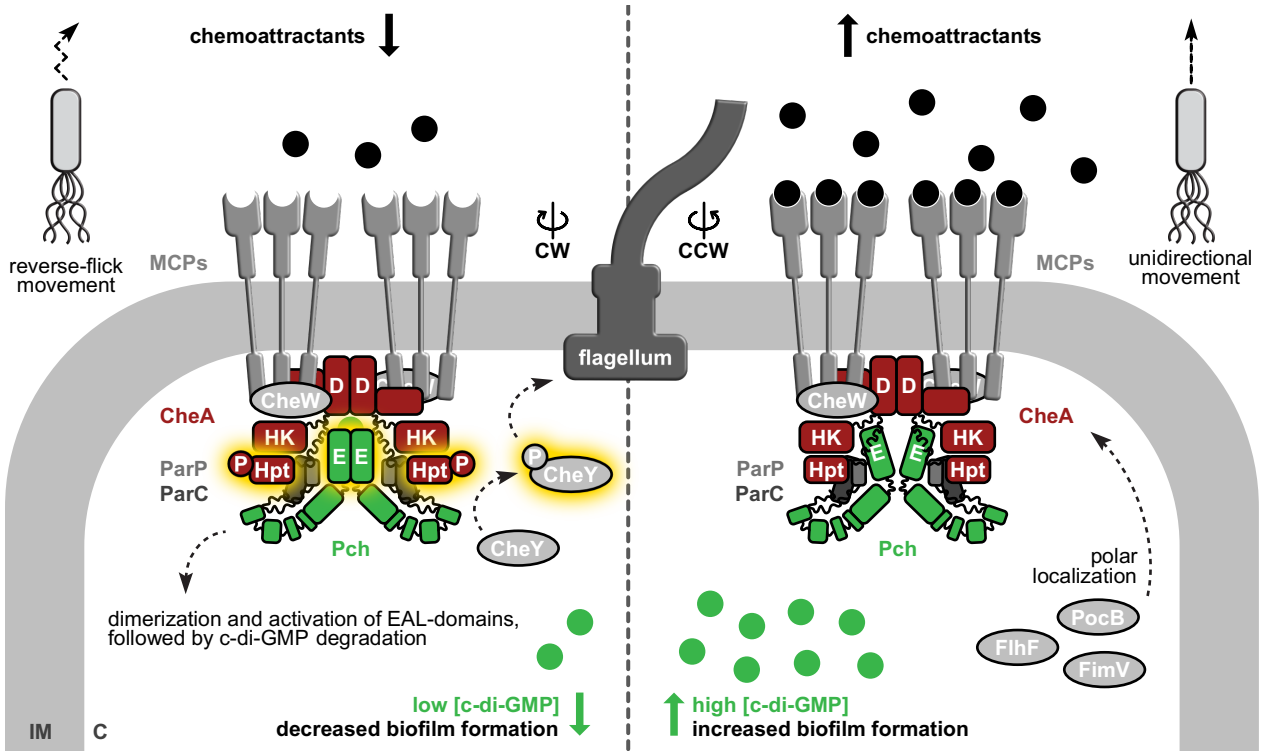

Figure 51. Proposed model of the chemotaxis-flagellum-biofilm-network and underlying protein interactions. Left panel: Two CheA monomers (individual domains and linker regions shown in red) form a homodimer at the methyl-accepting chemotaxis proteins (MCPs, grey) via their dimerization (D) domains localized at the cell pole. This complex is stabilized by two CheW proteins, which bridge CheA and MCPs. CheA interacts via its first linker region with the C-terminal region of ParP (light grey), contributing to proper localization of CheA. ParP further interacts via its N-terminus with ParC (dark grey), supporting polar complex organization. When chemoattractant concentrations decrease, the MCPs are no longer ligand-bound (**left panel**), leading to activation of the CheA homodimer. This activation enables trans-autophosphorylation at the conserved histidine residue H48 within the histidine phosphotransfer (Hpt) domain, mediated by the histidine kinase domain (HK). Subsequently, CheA interacts with CheY, followed by transfer of the phosphoryl group. Phosphorylated CheY dissociates from CheA and diffuses to the flagellar motor. Binding of phosphorylated CheY to FliM and FliN induces a switch in flagellar rotation from counterclockwise (CCW) to clockwise (CW), resulting in reverse-flick movement and reorientation of the cell. Concomitantly, the interaction between CheA and the Pch (green) EAL domains (E) is reduced, allowing EAL domain dimerization and activation of Pch's PDE function. This promotes binding and degradation of c-di-GMP, thereby reducing intracellular c-di-GMP levels, lowering biofilm formation, and favoring a motile lifestyle. When relative chemoattractant concentrations are high (**right panel**), CheA remains in an inactive, non-phosphorylated state, promoting CCW rotation of the bacterial flagellum, resulting in smooth, directional swimming. In this state, the CheA linker region interacts with the C-terminal EAL domains of Pch, thereby preventing EAL dimerization and maintaining Pch in an inactive state. Simultaneously, Pch interacts via its N-terminus with ParP. In this inactive state, reduced PDE activity of Pch contributes to elevated intracellular c-di-GMP levels, promoting biofilm formation. Further details are provided within the discussions section. Generation of new model was inspired by the schematics of [235,291].

4. Materials

4.1 Chemicals

If not mentioned otherwise, all chemicals were purchased from Carl Roth (Germany), New England Biolabs (USA), Sigma-Aldrich (Germany), Thermo Fisher Scientific (USA), Becton Dickinson (BD, USA) and Merck (Germany).

4.2 Devices

Table 2. Used devices.

Device name	Model	Manufacturer
Centrifuge	Sorvall RC 5C Plus	Sorvall
Chemiluminescence Reader	Fusion-SL	PEQLAB Biotechnologie
DNA gel documentation	Intas Photo imager	INTAS science imaging
Elelctroporation device	MicroPulser™	Bio-Rad
Fluorescence Microscope	DMI 6000 B	Leica Microsystems
FPLC device	ÄKTA pure25	Cytiva
Heat block	Mixing Block MB-102	Bioer
Incubator	Sure Temp 70	Benchmark
Microplate spectrophotometer	Epoch2	Biotek Instruments Inc
Microscope camera	pco.edge sCMOS camera	PCO
NanoDrop	1000 Spectrophotometer	PEQLAB Biotechnologie
PCR thermocycler	Mastercycler nexus gradient	Eppendorf
Photometer	Ultrospec 2100 pro	Amersham Bioscience
Pipets	Rainin Pipet-Lite XLS+	Mettler Toledo
Scanner	Epson Perfection V700 Photo	Epson
SDS-PAGE chamber	Mini-PROTEAN® Tetra Vertical Electrophoresis Cell	Bio-Rad
Shaker (room temperature)	Orbi Shaker	Benchmark
Sonification device	UW70, Sonopuls	Bandelin
Table centrifuge	Heraeus Pico 17 Centrifuge	Thermo Scientific
Voltage supplier	Electrophorese Power Supply EV231	PEQLAB Biotechnologie
Western blotter	TE77 ECL Semi-Dry Transfer Unit	Amersham Bioscience

4.3 Enzymes

Table 3. Used enzymes.

Enzyme	Manufacturer	Application
BamHI (Fast digest)	Thermo Fisher Scientific	Linearization of BACTH plasmids
DNase I	PanReac AppliChem	Cell lysis for protein purification
EcoRV (Fast digest)	Thermo Fisher Scientific	Linearization of pNPTS plasmids
NcoI (Fast digest)	Thermo Fisher Scientific	Linearization of pCDF/pETDuet plasmids
Phusion DNA polymerase	Self-made	PCR
SapI	Thermo Fisher Scientific	Linearization of pTB146 plasmids
SmaI (Fast digest)	Thermo Fisher Scientific	Linearization of pBAD/pBBR plasmids
Taq DNA polymerase	Self-made	PCR

4.4 Antibodies

Table 4. Used antibodies.

Antibody	Dilution	Manufacturer
Anti-GFP	1:10,000	Roche
mCherry polyclonal antibody	1:10,000	Invitrogen
Anti-His_6, alkaline phosphatase-coupled, produced in mouse	1:500	Roche
Anti-mouse IgG, alkaline phosphatase-coupled, produced in goat	1:10,000	Invitrogen
Anti-Rabbit IgG, alkaline phosphatase-coupled, produced in goat	1:20,000	Sigma-Aldrich

4.5 Kits

Table 5. Used kits.

Kit	Application	Manufacturer
E.Z.N.A. Plasmid DNA Mini Kit I	Plasmid isolation	Omega Bio-Tek
E.Z.N.A. DNA Probe Purification Kit	PCR product clean-up	Omega Bio-Tek
E.Z.N.A. Gel Extraction Kit	Gel fragments clean-up	Omega Bio-Tek
E.Z.N.A. Bacterial DNA Kit	Isolation of chromosomal DNA	Omega Bio-Tek

4.6 Chemical components

Table 6. Used chemical components.

Component	Application	Manufacturer
AEBSF hydrochloride	Cell lysis for protein purification	Thermo Fisher Scientific
Alexa FluorTM 488 C5 maleimide dye	Flagella staining	Thermo Fisher Scientific
Benzamidin hydrochloride	Cell lysis for protein purification	Carl Roth
CDP-Star Chemiluminscent AP substrate	AP-dependent immunodetection	Roche
GeneRulerTM 1kb	Ladder (agarose gel electrophoresis)	Thermo Fisher Scientific
GelRed® Nucleic Acid Gel Stain	Staining of agarose gels	Biotium
BlueEye Prestained Protein Marker	Ladder (SDS-PAGE)	Jena Bioscience
Instant Blue Coomassie Protein Stain	Staining of SDS gels	Expedeon (Abcam)

4.7 Buffers and other relevant solutions

Table 7. Used buffers and other relevant solutions.

Buffer and application	Components	Concentration
SDS-PAGE		
2x SDS sample buffer	SDS	4%
	ß-mercaptoethanol	10%
	Glycerol	20%
	Bromphenol blue	0.02%
	Tris-HCl (pH 6.8)	125 mM
4x upper buffer (SDS stacking buffer) pH 6.8	SDS	0.4%
	Tris-HCl	0.5 M
4x lower buffer (SDS separating buffer) pH 8.8	SDS	0.4%
	Tris-HCl	1.5 M
10x running buffer SDS-Page	Tris	0.25 M
	Glycine	1.92 M
	SDS	0.25%

Western Blot

10x PBS pH 7.4	NaCl KCl Na_2HPO_4 x 2 H_2O KH_2PO_4	80 g/L 2 g/L 17.8 g/L 2.4 g/L
1x PBS-T	10x PBS Tween	1x 20%
10x Western transfer buffer	Tris Glycine	250 mM 1.92 M
1x Western transfer buffer	10x Western transfer buffer Methanol	1x 100 ml/L
Blocking solution	Milk powder PBS Tween20	5% 1x 0.1%
Antibody solutions	PBS-T Milk powder	1x 2.5%
CDP-Star detection buffer pH 9.5	Tris-HCl NaCl	0.1 M 0.1 M

Agarose gel electrophoresis

6x agarose gel electrophoresis loading buffer	Xylene cyanole Bromphenol blue Gylcerine	0.5% (w/v) 0.5% (w/v) 30% (w/v)
1x TBE-Puffer pH 8.0	Tris Boric acid EDTA	89 mM 89 mM 1 mM

Chromatography

Lysis buffer pH 8.0	Tris-HCl NaCl KCl MgCl2 DNase AEBSF Benzamidin	50 mM 400 mM 50 mM 5 mM 0.3 mg/L 5 mM 5 mM
Buffer A (His affinity chromatography) pH 8.0	Tris-HCl NaCl KCl $MgCl_2$ Glycerol Imidazol	50 mM 400 mM 50 mM 5 mM 10% 20 mM
Buffer B (His affinity chromatography) pH 8.0	Tris-HCl NaCl KCl $MgCl_2$ Glycerol Imidazol	50 mM 400 mM 50 mM 5 mM 10% 600 mM
Size-exclusion chromatography buffer pH 7.4	Tris-HCl NaCl KCl $MgCl_2$ Glycerol	50 mM 400 mM 50 mM 5 mM 5%
Buffer A (MBP affinity chromatography) pH 7.4	Tris-HCl NaCl KCl $MgCl_2$ Glycerol	50 mM 400 mM 50 mM 5 mM 10%
Buffer B (MBP affinity chromatography) pH 7.4	Tris-HCl NaCl KCl $MgCl_2$ Glycerol Maltose	50 mM 400 mM 50 mM 5 mM 10% 10 mM

Gibson Assembly		
5x isothermal reaction buffer	PEG 8000	25% (w/v)
	Tris-HCl pH 7.5	500 mM
	MgCl2	50 mM
	DTT	50 mM
	NAD	5 mM
	dNTPs	1 mM each
Gibson Assembly master mix	5x isothermal reaction buffer	320 µl
	T5 exonuclease	0.64 µl
	Phusion DNA polymerase	20 µl
	Tag DNA ligase	160 µl
	ddH_2O	699.36 µl

4.8 Media

Table 8.Used media.

Bezeichnung	Components	Concentration
Lysogeny Broth (LB) pH 7.0	Tryptone	10 g/L
	Yeast extract	5 g/L
	NaCl	10 g/L
PG-agar 0.5%	Bacto Proteose peptone No. 3	0.5% (w/v)
	Difco agar	0.5% (w/v)
	Glucose	0.2% (w/v)
	ddH_2O	ad. 200 ml
LB swimming soft-agar 0.25%	Invitrogen select agar	0.25% (w/v)
	LB medium	ad. 200 ml
5x M9 minimal salts pH 7.0	KH_2PO_4	15 g/L
	NaCl	2.5 g/L
	Na_2HPO_4	33.9 g/L
	NH_4Cl	5 g/L
1x M9 minimal medium pH 7.0	M9 minimal salts	1x
	$MgSO_4$	2 mM
	Glucose	20 mM
	$CaCl_2$	0.1 mM

4.9 Antibiotics and other additives

Table 9. Used antibiotics and other additives.

Antibiotic	Stock concentration	Final concentration	Solvent
Ampicillin	100 mg/ml	100 µg/ml	ddH_2O
Chloramphenicol	10 mg/ml	10 µg/ml	96% (v/v) EtOH
Crystal violet	0.5% (w/v)	0.5% (w/v)	ddH_2O
2,6-diaminopimelic acid (DAP)	60 mM	300 µM	ddH_2O
Gentamycin	10 mg/ml	10 µg/ml	ddH_2O
Isopropyl-β-D-thiogalactopyranosid (IPTG)	500 mM	0.5 mM	ddH_2O
Kanamycin	50 mg/ml	50 µg/ml	ddH_2O
Lactose	20% (w/v)	1% (w/v)	ddH_2O
L-Arabinose	20% (w/v)	0.05% (w/v)	ddH_2O
Streptomycin	100 mg/ml	100 µg/ml	ddH_2O
Sucrose	80% (w/v)	12% (w/v)	ddH_2O
X-galactosidase (X-Gal)	80 mg/ml	40 µg/ml	Dimethylformamide

4.10 Software

Table 10. Used software.

Software	Usage
Affinity Designer	Figure design
AlphaFold3	AlphaFold predictions
Bacstalk 1.8stable (MPI/University Marburg)	Image analysis
Benchling (Benchling)	Primer design and plasmid construction
BioRender (BioRender)	Figure illustrations
BLAST (NCBI)	Alignment searching
DeepTMHMM 1.0 (DTU Health Tech)	Prediction of transmembrane helices
Fiji (ImageJ)	Image analysis
Gen5 3.10 (BioTek)	Microplate spectrophotometer measurements
GraphPad Prism 10.6.1 (GraphPad)	Graph creation, statistics
Microsoft Excel (Microsoft Corporation)	Data analysis
ProtParam (Expasy)	Protein computations (physical/chemical)
PyMOL 2.5.5 (PyMOL)	Protein structure visualization
SignalP 6.0 (DTU Health Tech)	Prediction of N-terminal signal peptides
SMART (embl)	Protein database
Tm Calculator for Primers (Thermo Fisher Scientific)	Calculation of primer annealing temperatures
Unicorn 7.1 (Cytiva)	Chromatography
UniProt (Uniprot)	Protein database, alignment
VisiView (Visitron)	Fluorescence microscopy

4.11 Bacterial strains

Table 11. Used bacterial strains.

Strain	Abbreviation	Genotype	Reference
Escherichia coli			
DH5αλ*pir*	DH5α	*sup E44, ΔlacU169 (ΦlacZΔM15), recA1, endA1, hsdR17, thi-1, gyrA96, relA1, λpir*phage lysogen.	[292]
WM3064	none	*thrB1004 pro thi rpsL hsdS lacZ ΔM15 RP4-1360 Δ(araBAD) 567ΔdapA 1341: [erm pir(wt)].*	W. Metcalf, University of Illinois, Urbana-Champaign
BL21 (DE3)	none	*fhuA2 [lon] ompT gal (λ DE3) [dcm] ΔhsdS λ DE3 = λ sBamHIo ΔEcoRI-B int::(lacI::PlacUV5::T7 gene1) i21 Δnin5.*	NEB
BTH101	none	*F-, cya-99, araD139, galE15, galK16, rpsL1 (Str r), hsdR2, mcrA1, mcrB1.*	Euromedex, France
E8811	*Sp*HubP	expression of *Sp*HubP (Sputcn32_2442) on pBBR1-MCS2 *Sp*HubP.	[14]
E8812	*Sp*HubP-sfGFP	expression of *Sp*HubP (Sputcn32_2442) fused to sfGFP with Gly, Gly, Ser on pBAD33 *Sp*HubP-GGS-sfGFP.	[14]
E8864	*Sp*FlhF mVenus-*Sp*FliG	expression of FlhF (Sputcn32_2561) and FliG (Sputcn32_2575) fused to mVenus with Gly, Ser, Gly, Gly, Gly on pBAD33 *Sp*FlhF mVenus-GSGGG-*Sp*FliG	[14]
E8865	mVenus-*Sp*FliG	expression of FliG (Sputcn32_2575) fused to mVenus with Gly, Ser, Gly, Gly, Gly on pBAD33 mVenus-GSGGG-*Sp*FliG	[14]
E8877	*Sp*FlhF-mVenus	expression of FlhF (Sputcn32_2561) fused to mVenus with Gly and Ser on pBAD33 *Sp*FlhF-GS-mVenus.	[14]

Shewanella putrefaciens

S757	wild type	wild type strain of *S. putrefaciens* CN-32.	[293]
S2679	*ΔfliG*	deletion of the gene *fliG*$_1$ (Sputcn32_2575).	[14]
S3132	Δ*flhF*	deletion of the gene *flhF* (Sputcn32_2561).	[132]
S3145	*ΔhubP*	deletion of the gene *hubP* (Sputcn32_2442).	[132]
S4063	FlgE^{T183C}	markerless in-frame substitution of Thr183 to Cys in the polar hook protein FlgE$_1$ (Sputcn32_2594).	[218]
S4084	FlgE^{T183C} Δ*flhF*	markerless in-frame substitution of Thr183 to Cys in the polar hook protein FlgE$_1$ (Sputcn32_2594), deletion of the gene *flhF* (Sputcn32_2561).	[14]
S5180	FlhF-mVenus	C-terminal mVenus tag of FlhF (Sputcn32_2561) linked with Gly and Ser.	[165]
S5223	FlaB$_1^{T166C}$ FlaA$_1^{T174C}$ FliG$_{ΔN}$	markerless in-frame substitution of Thr166 to Cys in the polar major flagellin protein FlaB$_1$ (Sputcn32_2585) and Thr174 to Cys in the polar minor flagellin protein FlaA$_1$ (Sputcn32_2586), deletion of the N-terminal domain (Δ2-85) of FliG$_1$ (Sputcn32_2575).	[14]
S5225	FlaB$_1^{T166C}$ FlaA$_1^{T174C}$ FliG$_{ΔC}$	markerless in-frame substitution of Thr166 to Cys in the polar major flagellin protein FlaB$_1$ (Sputcn32_2585) and Thr174 to Cys in the polar minor flagellin protein FlaA$_1$ (Sputcn32_2586), deletion of the C-terminal domain (Δ209-348) of FliG$_1$ (Sputcn32_2575).	[14]
S5292	FlhF-mVenus FliG$_{ΔC}$	C-terminal mVenus tag of FlhF (Sputcn32_2561) linked with Gly and Ser, deletion of the C-terminal domain (Δ209-348) of FliG$_1$ (Sputcn32_2575).	[14]
S5293	FlhF-mVenus FliG$_{ΔN}$	C-terminal mVenus tag of FlhF (Sputcn32_2561) linked with Gly and Ser, deletion of the N-terminal domain (Δ2-85) of FliG$_1$ (Sputcn32_2575).	[14]
S8759	*Pp*FimV	expression of *P. putida fimV* (PP_1993) in *S. putrefaciens hubP* deletion mutant.	[231]
S8953	FlhF$_{ΔFID}$	deletion of first N-terminal 44 amino acids of the gene *flhF* (Sputcn32_2561).	[14]
S8954	FlhF$_{ΔFID}$-mVenus	C-terminal mVenus tag of FlhF without first N-terminal 44 amino acids (Sputcn32_2561) linked with Gly and Ser.	[14]
S9011	FlgE^{T183C} FlhF$_{ΔFID}$	markerless in-frame substitution of Thr183 to Cys in the polar hook protein FlgE$_1$ (Sputcn32_2594) and deletion of first N-terminal 44 amino acids of the gene *flhF* (Sputcn32_2561).	[14]
S9912	*Sp*HubP$_{Pp\text{FimV-D}}$	expression of *S. putrefaciens hubP* (Sputcn32_2442) with *P. putida* FimV domain (PP_1993, P848-V911).	[231]
S10264	HubP$_{FimV-C}$	expression of *S. putrefaciens hubP* (Sputcn32_2442) with *P. putida fimV* C-terminal part (PP_1993, R410-D852).	[231]
S10324	*Pp*FimV-sfGFP	expression of *P. putida fimV* (PP_1993) fused to sfGFP with 3x Gly, Gly and Ser in *S. putrefaciens hubP* deletion mutant.	[231]
S10502	HubP$_{ΔFimV\ domain}$	deletion of C-terminal FimV domain within *hubP* (Sputcn32_2442, ΔE1047-S1097).	[231]
S10504	HubP$_{FimV-P}$	expression of *S. putrefaciens hubP* (Sputcn32_2442) with *P. putida fimV* periplasmic part (PP_1993, L25-N386).	[231]

Pseudomonas putida

P3811	wild type	wild type strain of *P. putida* KT2440.	[177]
P4127	Δ*fliC*	deletion of the gene *fliC* (PP_4378).	[12]
P4135	FliC^{S267C}	markerless in-frame substitution of Ser267 to Cys in the flagellin gene *fliC* (PP_4378).	[12]
P5483	CheA-mCherry	markerless in-frame substitution of Ser267 to Cys in the flagellin gene *fliC* (PP_4378), expression of *cheA* (PP_4338) fused to mCherry with Gly and Ser.	[231]
P6507	Δ*fipA*	deletion of the gene *fipA* (PP_4331).	[165]
P9307	Δ*flhF*	deletion of the gene *flhF* (PP_4343).	This study
P9308	Δ*fimV*	markerless in-frame substitution of Ser267 to Cys in the flagellin gene *fliC* (PP_4378), deletion of the gene *fimV* (PP_1993).	[231]
P9309	CheA-mCherry Δ*flhF*	markerless in-frame substitution of Ser267 to Cys in the flagellin gene *fliC* (PP_4378), expression of *cheA* (PP_4338) fused to mCherry with Gly and Ser, deletion of the gene *flhF* (PP_4343).	[231]
P9310	CheA-mCherry Δ*fimV*	markerless in-frame substitution of Ser267 to Cys in the flagellin gene *fliC* (PP_4378), expression of *cheA* (PP_4338) fused to mCherry with Gly and Ser, deletion of the gene *fimV* (PP_1993).	[231]

P9414	Δ*fimV::fimV*	markerless in-frame substitution of Ser267 to Cys in the flagellin gene *fliC* (PP_4378), complementation of the deleted *fimV* gene (PP_1993) into the native locus.	[231]
P9498	Δ*pocB*	deletion of the gene *pocB* (PP_1899).	This study
P9500	Δ*pch*	deletion of the gene *pch* (PP_0337).	This study
P9520	Pch-sfGFP	markerless in-frame substitution of Ser267 to Cys in the flagellin gene *fliC* (PP_4378), expression of *pch* (PP_0337) fused to sfGFP with 2x Gly, Gly and Ser.	This study
P9533	Δ*cheA*	deletion of the gene *cheA* (PP_4338).	This study
P9539	Δ*pch::pch*	markerless in-frame substitution of Ser267 to Cys in the flagellin gene *fliC* (PP_4378), complementation of the deleted *pch* gene (PP_0337) into the native locus.	This study
P9663	Δ*parP*	deletion of the gene *parP* (PP_4333).	This study
P9746	Δ*cheA::cheA*	markerless in-frame substitution of Ser267 to Cys in the flagellin gene *fliC* (PP_4378), complementation of the deleted *cheA* gene (PP_4338) into the native locus.	This study
P9790	Δ*parP::parP*	markerless in-frame substitution of Ser267 to Cys in the flagellin gene *fliC* (PP_4378), complementation of the deleted *parP* gene (PP_4333) into the native locus.	This study
P9961	*Sp*HubP	markerless in-frame substitution of Ser267 to Cys in the flagellin gene *fliC* (PP_4378), expression of *S. putrefaciens hubP* (Sputcn32_2442) in *P. putida fimV* deletion mutant.	[231]
P9965	*Pp*FimV$_{Sp\text{FimV-D}}$	markerless in-frame substitution of Ser267 to Cys in the flagellin gene *fliC* (PP_4378), expression of *P. putida fimV* (PP_1993) with *S. putrefaciens* HubP FimV domain (Sputcn32_2442, A1034-S1097).	[231]
P9989	p*fimV*	markerless in-frame substitution of Ser267 to Cys in the flagellin gene *fliC* (PP_4378), deletion of the gene *fimV* (PP_1993), harboring cumate-inducible pBBR1 plasmid with *fimV* gene.	[231]
P10067	Δ*pilA*	deletion of the gene *pilA* (PP_0634).	[231]
P10071	FimV-mCherry	markerless in-frame substitution of Ser267 to Cys in the flagellin gene *fliC* (PP_4378), expression of *fimV* (PP_1993) fused to mCherry with 3x Gly, Gly and Ser.	[231]
P10073	sfGFP-ParB	markerless in-frame substitution of Ser267 to Cys in the flagellin gene *fliC* (PP_4378), expression of *parB* (PP_0001) fused to sfGFP with 2x Gly, Gly and Ser.	[231]
P10121	sfGFP-ParB Δ*fimV*	markerless in-frame substitution of Ser267 to Cys in the flagellin gene *fliC* (PP_4378), expression of *parB* (PP_0001) fused to sfGFP with 2x Gly, Gly and Ser, deletion of the gene *fimV* (PP_1993).	[231]
P10152	Δ*fliC* Δ*pilA*	deletion of the gene *fliC* (PP_4378) and deletion of the gene *pilA* (PP_0634).	[231]
P10153	Δ*fliC* Δ*fimV*	deletion of the gene *fliC* (PP_4378) and deletion of the gene *fimV* (PP_1993).	[231]
P10155	sfGFP-ParB FimV-mCherry	markerless in-frame substitution of Ser267 to Cys in the flagellin gene *fliC* (PP_4378), expression of *parB* (PP_0001) fused to sfGFP with 2x Gly, Gly and Ser, expression of *fimV* (PP_1993) fused to mCherry with 3x Gly, Gly and Ser.	[231]
P10160	mCherry-ParP	markerless in-frame substitution of Ser267 to Cys in the flagellin gene *fliC* (PP_4378), expression of *parP* (PP_4333) fused to mCherry with Asp, Ile, Leu, Glu, Leu.	This study
P10229	wild type c-di-GMP	markerless in-frame substitution of Ser267 to Cys in the flagellin gene *fliC* (PP_4378), harboring pMMB-HS-Bc3-5-AAV.	This study
P10230	Δ*cheA* c-di-GMP	markerless in-frame substitution of Ser267 to Cys in the flagellin gene *fliC* (PP_4378), deletion of the gene *cheA* (PP_4338), harboring pMMB-HS-Bc3-5-AAV.	This study
P10231	Δ*pch* c-di-GMP	markerless in-frame substitution of Ser267 to Cys in the flagellin gene *fliC* (PP_4378), deletion of the gene *pch* (PP_0337), harboring pMMB-HS-Bc3-5-AAV.	This study
P10265	FimV$_{HubP\text{-C}}$	markerless in-frame substitution of Ser267 to Cys in the flagellin gene *fliC* (PP_4378), expression of *P. putida fimV* (PP_1993) with *S. putrefaciens* HubP C-terminal part (Sputcn32_2442, L336-G1033).	[231]
P10337	*Sp*HubP-sfGFP	markerless in-frame substitution of Ser267 to Cys in the flagellin gene *fliC* (PP_4378), expression of *S. putrefaciens hubP* (Sputcn32_2442) fused to sfGFP with 3x Gly, Gly and Ser in *P. putida fimV* deletion mutant.	[231]

P10386	EAL-sfGFP	markerless in-frame substitution of Ser267 to Cys in the flagellin gene *fliC* (PP_4378), expression of EAL domain from *pch* (PP_0337, aa 629-896) fused to sfGFP with 2x Gly, Gly and Ser.	This study
P10387	GGDEF-EAL-sfGFP	markerless in-frame substitution of Ser267 to Cys in the flagellin gene *fliC* (PP_4378), expression of GGDEF-EAL domains from *pch* (PP_0337, aa 474-896) fused to sfGFP with 2x Gly, Gly and Ser.	This study
P10398	$FimV_{\Delta GLB}$	markerless in-frame substitution of Ser267 to Cys in the flagellin gene *fliC* (PP_4378), deletion of immunoglobulin-like domain in *fimV* (PP_1993, ΔL30-Q135).	[231]
P10399	$FimV_{\Delta GLB}$-mCherry	markerless in-frame substitution of Ser267 to Cys in the flagellin gene *fliC* (PP_4378), expression of *fimV* (PP_1993) fused to mCherry with 3x Gly, Gly and Ser without immunoglobulin-like domain (ΔL30-Q135).	[231]
P10501	$FimV_{\Delta FimV\ domain}$	markerless in-frame substitution of Ser267 to Cys in the flagellin gene *fliC* (PP_4378), deletion of C-terminal FimV domain within *fimV* (PP_1993, ΔG861-V911).	[231]
P10503	$FimV_{HubP\text{-}P}$	markerless in-frame substitution of Ser267 to Cys in the flagellin gene *fliC* (PP_4378), expression of *P. putida fimV* (PP_1993) with *S. putrefaciens* HubP periplasmic-terminal part (Sputcn32_2442, P34-N313).	[231]

Pseudomonas aeruginosa

PA1	wild type	PAO1	Christian Riedl, Ulm

4.12 Plasmids

Table 12. Used plasmids.

Plasmid	Description	Reference
General plasmids		
pNPTS138-R6KT	mobRP4+ ori-R6K *sacB;* β-galactosidase fragment alpha; suicide vector for *in-frame* deletions or integrations in *S. putrefaciens* or *P. putida*, Kan^R	[294]
pBAD33	*pBAD*, P15A, Cam^R	[295]
pBBR1-MCS2	*plac*, pBBR1, Kan^R	[296]
pBBR1-MCS2-cym	*plac*, pBBR1, integration of *P. putida* F1 cym-system (cymR/*pcym*), Kan^R	[231]
pMMB-HS-Bc3-5-AAV	c-di-GMP reporter plasmid, pMMB-HS backbone, riboswitches Bc3-5, fluorophores TurboRFP with AAV-tag and AmCyan, $Gent^R$	Fitnat Yildiz, UCSC Santa Cruz
pKT25	*plac*, P15A, MCS downstream from T25 fragment encoding region, Kan^R	[297]
pKNT25	*plac*, P15A, MCS upstream from T25 fragment encoding region, Kan^R	[297]
pUT18	*plac*, ColE1, MCS downstream from T18 fragment encoding region, Amp^R	[297]
pUT18C	*plac*, ColE1, MCS upstream from T18 fragment encoding region, Amp^R	[297]
pETDuet-1	*pT7, lac*, ColE1, Amp^R	Novagen
pCDFDuet-1	*pT7, lac,* CloDF13, $Strep^R$	Novagen
pTB146	*pT7*, *lac*, ColE1, N-terminal 6xHis-tag sequence followed by SUMO-tag, Amp^R	Invitrogen

Plasmids for *Escherichia coli*

pBBR1-MCS2 *Sp*HubP	expression of HubP (Sputcn32_2442), Kan^R	[14]
pBAD33 *Sp*HubP-GGS-sfGFP	expression of HubP (Sputcn32_2442) fused to GFP with Gly, Gly and Ser, Cam^R	[14]
pBAD33 *Sp*FlhF mVenus-GSGGG-*Sp*FliG	expression of FlhF (Sputcn32_2561) and $FliG_1$ (Sputcn32_2575) fused to mVenus with Gly, Ser, Gly, Gly, and Gly, Cam^R	[14]

pBAD33 mVenus-GSGGG-*Sp*FliG	expression of $FliG_1$ (Sputcn32_2575) fused to mVenus with Gly, Ser, Gly, Gly, and Gly, Cam^R	[14]
pBAD33 *Sp*FlhF-GS-mVenus	expression of FlhF (Sputcn32_2561) fused to mVenus with Gly and Ser, Cam^R	[14]

Plasmids for *Pseudomonas putida*

pBBR1-MCS2-cym-pFimV	expression of *fimV* upon induction of cumate-inducible cym-system from *P. putida* F1, Kan^R	[231]
pNPTS138-R6KT Δ*fimV*	deletion of the *fimV* gene (PP_1993), Kan^R	[231]
pNPTS138-R6KT $FimV_{\Delta GLB}$	Deletion of immunoglobulin-like domain within *fimV* (PP_1993, ΔL30-Q135), Kan^R	[231]
pNPTS138-R6KT Δ*flhF*	deletion of the *fimV* gene (PP_4343), Kan^R	[231]
pNPTS138-R6KT Δ*flhF::flhF*	in frame complementation of the *flhF* gene (PP_4343), Kan^R	This study
pNPTS138-R6KT Δ*fimV::fimV*	in frame complementation of the *fimV* gene (PP_1993), Kan^R	[231]
pNPTS138-R6KT Δ*fliC*	deletion of the *fliC* gene (PP_4378), Kan^R	[12]
pNPTS138-R6KT Δ*pilA*	deletion of the *pilA* gene (PP_0634), Kan^R	[231]
pNPTS138-R6KT Δ*flhFG*	deletion of the genes *flhF* and *flhG* (PP_4342-43), Kan^R	This study
pNPTS138-R6KT Δ*pocB*	deletion of the *pocB* gene (PP_1899), Kan^R	This study
pNPTS138-R6KT Δ*pch*	deletion of the *pch* gene (PP_0337), Kan^R	This study
pNPTS138-R6KT Δ*pch::pch*	in frame complementation of the *pch* gene (PP_0337), Kan^R	This study
pNPTS138-R6KT Δ*cheA*	deletion of the *cheA* gene (PP_4338), Kan^R	This study
pNPTS138-R6KT Δ*cheA::cheA*	in frame complementation of the *cheA* gene (PP_4338), Kan^R	This study
pNPTS138-R6KT Δ*parP::parP*	in frame complementation of the *parP* (PP_4333), Kan^R	This study
pNPTS138-R6KT mCherry-DILEL-ParP	in frame complementation of *parP* (PP_4333) with mCherry-DILEL-ParP, Kan^R	This study
pNPTS138-R6KT $FliC^{S267C}$	in frame complementation of Ser267 to Cys in the flagellin gene *fliC* (PP_4378), Kan^R	[12]
pNPTS138-R6KT FimV-3xGGS-mCherry	in frame complementation of *fimV* (PP_1993) with FimV-3xGGS-mCherry, Kan^R	[231]
pNPTS138-R6KT CheA-GS-mCherry	in frame complementation of *cheA* (PP_4338) with CheA-GS-mCherry, Kan^R	[231]
pNPTS138-R6KT CheA-Hpt-H48Q	in frame complementation of His48 to Gln in *cheA* (PP_4338), Kan^R	This study
pNPTS138-R6KT sfGFP-2xGGS-ParB	in frame complementation of *parB* (PP_0001) with sfGFP-2xGGS-ParB, Kan^R	[231]
pNPTS138-R6KT Pch-2xGGS-sfGFP	in frame complementation of *pch* (PP_0337) with Pch-2xGGS-sfGFP, Kan^R	This study
pNPTS138-R6KT *Sp*HubP	in frame complementation of the *fimV* gene (PP_1993) with *hubP* (Sputcn32_2442), Kan^R	[231]
pNPTS138-R6KT *Sp*HubP-3xGGS-sfGFP	in frame complementation of the *fimV* gene (PP_1993) with *hubP*-3xGGS-*sfgfp* (Sputcn32_2442), Kan^R	[231]
pNPTS138-R6KT *Pp*$FimV_{SpFimV\text{-}D}$	in frame complementation of the *fimV* gene (PP_1993) with the C-terminal FimV domain of *hubP* (Sputcn32_2442, A1034-S1097), Kan^R	[231]
pNPTS138-R6KT $FimV_{HubP\text{-}C}$	in frame complementation of the *fimV* gene (PP_1993) with the C-terminal part of *hubP* (Sputcn32_2442, L336-G1033), Kan^R	[231]
pNPTS138-R6KT $FimV_{HubP\text{-}P}$	in frame complementation of the *fimV* gene (PP_1993) with the periplasmic part of *hubP* (Sputcn32_2442, P34-N313), Kan^R	[231]
pNPTS138-R6KT $FimV_{\Delta FimV\ domain}$	deletion of the C-terminal FimV domain within *fimV* gene (PP_1993, ΔG861-V911), Kan^R	[231]
pNPTS138-R6KT *Pp*FimV	in frame complementation of the *hubP* gene (Sputcn32_2442) with *fimV* (PP_1993), Kan^R	[231]
pNPTS138-R6KT *Pp*FimV-3xGGS-sfGFP	in frame complementation of the *hubP* gene (Sputcn32_2442) with *fimV*-3xGGS-*sfgfp* (PP_1993), Kan^R	[231]

Plasmids for *Shewanella putrefaciens*

pNPTS138-R6KT FlhF-1xGS-Venus	in frame complementation of *flhF* (Sputcn32_2561) with FlhF-1xGS-mVenus, Kan^R	[165]
pNPTS138-R6KT Δ*flhF*	deletion of the *flhF* gene (Sputcn32_2561), Kan^R	[132]
pNPTS138-R6KT Δ*fliG*	deletion of the $fliG_1$ gene (Sputcn32_2575), Kan^R	[14]
pNPTS138-R6KT FlhF ΔN44	deletion of first 44 N-terminal amino acids in *flhF* (Sputcn32_2561), Kan^R	[14]
pNPTS138-R6KT FliG ΔN	deletion of the N-terminal domain (Δ2-85) in $fliG_1$ (Sputcn32_2575), Kan^R	[14]

pNPTS138-R6KT FliG ΔC	deletion of the C-terminal domain (Δ209-348) in *fliG*$_1$ (Sputcn32_2575), Kan^R	[14]
pNPTS138-R6KT *Sp*HubP$_{Pp\text{FimV-D}}$	in frame complementation of the *hubP* gene (Sputcn32_2442) with the C-terminal FimV domain of *fimV* (PP_1993, P848-V911), Kan^R	[231]
pNPTS138-R6KT HubP$_{\text{FimV-C}}$	in frame complementation of the *hubP* gene (Sputcn32_2442) with the C-terminal part of *fimV* (PP_1993, R410-D852), Kan^R	[231]
pNPTS138-R6KT HubP$_{\text{FimV-P}}$	in frame complementation of the *hubP* gene (Sputcn32_2442) with the periplasmic part of *fimV* (PP_1993, L25-N386), Kan^R	[231]
pNPTS138-R6KT HubP$_{\Delta\text{FimV domain}}$	deletion of the C-terminal FimV domain within *hubP* gene (Sputcn32_2442, ΔE1047-S1097), Kan^R	[231]

BACTH plasmids

	pKT25 plasmids	
pKT25 *Pp*FimV	fusion protein T25-*Pp*FimV (PP_1993, aa 410-911), Kan^R	This study
pKT25 *Pp*FlhF	fusion protein T25-*Pp*FlhF (PP_4343), Kan^R	This study
pKT25 *Pp*CheA	fusion protein T25-*Pp*CheA (PP_4338), Kan^R	This study
pKT25 *Pp*CheA-Hpt	fusion protein T25-*Pp*CheA-Hpt (PP_4338, aa 2-110), Kan^R	This study
pKT25 *Pp*CheA-Linker	fusion protein T25-*Pp*CheA-Linker (PP_4338, aa 111-395), Kan^R	This study
pKT25 *Pp*CheA-α12	fusion protein T25-*Pp*CheA-LinkerA (PP_4338, aa 111-190), Kan^R	This study
pKT25 *Pp*CheA-α345	fusion protein T25-*Pp*CheA-LinkerB (PP_4338, aa 191-360), Kan^R	This study
pKT25 *Pp*CheA-Hpt-Linker	fusion protein T25-*Pp*CheA-Hpt-Linker (PP_4338, aa 2-395), Kan^R	This study
pKT25 *Pp*CheA-Histidine-Kinase	fusion protein T25-*Pp*CheA-Histidine-Kinase (PP_4338, aa 396-609), Kan^R	This study
pKT25 *Pp*CheA-DIM-Kinase	fusion protein T25-*Pp*CheA-Histidine-Kinase (PP_4338, aa 361-609), Kan^R	This study
pKT25 *Pp*CheA-CheW	fusion protein T25-*Pp*CheA-CheW (PP_4338, aa 610-747), Kan^R	This study
pKT25 *Pa*CheA	fusion protein T25-*Pa*CheA (PA1458), Kan^R	This study
pKT25 *Pa*CheA-Linker	fusion protein T25-*Pa*CheA-Hpt (PA1458, aa 110-402), Kan^R	This study
pKT25 *Pp*Pch	fusion protein T25-*Pp*Pch (PP_0337), Kan^R	This study
pKT25 *Pp*Pch-N-terminal	fusion protein T25-*Pp*Pch-N-terminal (aa 2-187), Kan^R	This study
pKT25 *Pp*Pch-Pas-Pac	fusion protein T25-*Pp*Pch-Pas-Pac (aa 188-473), Kan^R	This study
pKT25 *Pp*Pch-GGDEF	fusion protein T25-*Pp*Pch-GGDEF (aa 474-628), Kan^R	This study
pKT25 *Pp*Pch-EAL	fusion protein T25-*Pp*Pch-EAL (aa 629-896), Kan^R	This study
pKT25 *Pa*Pch	fusion protein T25-*Pa*Pch (PA5017), Kan^R	This study
pKT25 *Pa*Pch-EAL	fusion protein T25-*Pa*Pch-EAL (PA5017, aa 631-899), Kan^R	This study
pKT25 *Pp*ParP	fusion protein T25-*Pp*ParP (PP_4333), Kan^R	This study
	pKNT25 plasmids	
pKNT25 *Pp*FimV	fusion protein *Pp*FimV-T25 (PP_1993, aa 410-911), Kan^R	This study
pKNT25 *Pp*FlhF	fusion protein *Pp*FlhF-T25 (PP_4343), Kan^R	This study
pKNT25 *Pp*CheA	fusion protein *Pp*CheA-T25 (PP_4338), Kan^R	This study
pKNT25 *Pp*CheA-Hpt	fusion protein *Pp*CheA-Hpt-T25 (PP_4338, aa 2-110), Kan^R	This study
pKNT25 *Pp*CheA-Linker	fusion protein *Pp*CheA-Linker-T25 (PP_4338, aa 111-395), Kan^R	This study
pKT25 *Pp*CheA-α12	fusion protein *Pp*CheA-LinkerA-T25 (PP_4338, aa 111-190), Kan^R	This study
pKNT25 *Pp*CheA-α345	fusion protein *Pp*CheA-LinkerB-T25 (PP_4338, aa 191-360), Kan^R	This study
pKNT25 *Pp*CheA-Hpt-Linker	fusion protein *Pp*CheA-Hpt-Linker-T25 (PP_4338, aa 2-395), Kan^R	This study
pKNT25 *Pp*CheA-Histidine-Kinase	fusion protein *Pp*CheA-Histidine-Kinase-T25 (PP_4338, aa 396-609), Kan^R	This study
pKNT25 *Pp*CheA-DIM-Kinase	fusion protein *Pp*CheA-Histidine-Kinase-T25 (PP_4338, aa 361-609), Kan^R	This study
pKNT25 *Pp*CheA-CheW	fusion protein *Pp*CheA-CheW-T25 (PP_4338, aa 610-747), Kan^R	This study
pKNT25 *Pa*CheA	fusion protein *Pa*CheA-T25 (PA1458), Kan^R	This study
pKNT25 *Pa*CheA-Linker	fusion protein *Pa*CheA-Hpt-T25 (PA1458, aa 110-402), Kan^R	This study
pKNT25 *Pp*Pch	fusion protein *Pp*Pch-T25 (PP_0337), Kan^R	This study
pKNT25 *Pp*Pch N-terminal	fusion protein *Pp*Pch N-terminal-T25 (aa 1-187), Kan^R	This study
pKNT25 *Pp*Pch Pas-Pac	fusion protein *Pp*Pch Pas-Pac-T25 (aa 188-473), Kan^R	This study
pKNT25 *Pp*Pch GGDEF	fusion protein *Pp*Pch GGDEF-T25 (aa 474-628), Kan^R	This study
pKNT25 *Pp*Pch EAL	fusion protein *Pp*Pch EAL-T25 (aa 629-896), Kan^R	This study
pKNT25 *Pa*Pch	fusion protein *Pa*Pch-T25 (PA5017), Kan^R	This study

pKNT25 *Pa*Pch-EAL	fusion protein *Pa*Pch-EAL-T25 (PA5017, aa 631-899), Kan^R	This study
pKNT25 *Pp*ParP	fusion protein *Pp*ParP-T25 (PP_4333), Kan^R	This study
	pUT18 plasmids	
pUT18 *Pp*FimV	fusion protein *Pp*FimV-T18 (PP_1993, aa 410-911), Amp^R	This study
pUT18 *Pp*FlhF	fusion protein *Pp*FlhF-T18 (PP_4343), Amp^R	This study
pUT18 *Pp*CheA	fusion protein *Pp*CheA-T18 (PP_4338), Amp^R	This study
pUT18 *Pp*CheA-Hpt	fusion protein *Pp*CheA-Hpt-T18 (PP_4338, aa 2-110), Amp^R	This study
pUT18 *Pp*CheA-Linker	fusion protein *Pp*CheA-Linker-T18 (PP_4338, aa 111-395), Amp^R	This study
pKT25 *Pp*CheA-α12	fusion protein *Pp*CheA-LinkerA-T18 (PP_4338, aa 111-190), Amp^R	This study
pUT18 *Pp*CheA-α345	fusion protein *Pp*CheA-LinkerB-T18 (PP_4338, aa 191-360), Amp^R	This study
pUT18 *Pp*CheA-Hpt-Linker	fusion protein *Pp*CheA-Hpt-Linker-T18 (PP_4338, aa 2-395), Amp^R	This study
pUT18 *Pp*CheA-Histidine-Kinase	fusion protein *Pp*CheA-Histidine-Kinase-T18 (PP_4338, aa 396-609), Amp^R	This study
pUT18 *Pp*CheA-DIM-Kinase	fusion protein *Pp*CheA-Histidine-Kinase-T18 (PP_4338, aa 361-609), Amp^R	This study
pUT18 *Pp*CheA-CheW	fusion protein *Pp*CheA-CheW-T18 (PP_4338, aa 610-747), Amp^R	This study
pUT18 *Pa*CheA	fusion protein *Pa*CheA-T18 (PA1458), Amp^R	This study
pUT18 *Pa*CheA-Linker	fusion protein *Pa*CheA-Hpt-T18 (PA1458, aa 110-402), Amp^R	This study
pUT18 *Pp*Pch	fusion protein *Pp*Pch-T18 (PP_0337), Amp^R	This study
pUT18 *Pp*Pch N-terminal	fusion protein *Pp*Pch N-terminal-T18 (aa 1-187), Amp^R	This study
pUT18 *Pp*Pch Pas-Pac	fusion protein *Pp*Pch Pas-Pac-T18 (aa 188-473), Amp^R	This study
pUT18 *Pp*Pch GGDEF	fusion protein *Pp*Pch GGDEF-T18 (aa 474-628), Amp^R	This study
pUT18 *Pp*Pch EAL	fusion protein *Pp*Pch EAL-T18 (aa 629-896), Amp^R	This study
pUT18 *Pa*Pch	fusion protein *Pa*Pch-T18 (PA5017), Amp^R	This study
pUT18 *Pa*Pch-EAL	fusion protein *Pa*Pch-EAL-T18 (PA5017, aa 631-899), Amp^R	This study
pUT18 *Pp*ParP	fusion protein *Pp*ParP-T18 (PP_4333), Amp^R	This study
	pUT18C plasmids	
pUT18C *Pp*FimV	fusion protein T18-*Pp*FimV (PP_1993, aa 410-911), Amp^R	This study
pUT18C *Pp*FlhF	fusion protein T18-*Pp*FlhF (PP_4343), Amp^R	This study
pUT18C *Pp*CheA	fusion protein T18-*Pp*CheA (PP_4338), Amp^R	This study
pUT18C *Pp*CheA-Hpt	fusion protein T18-*Pp*CheA-Hpt (PP_4338, aa 2-110), Amp^R	This study
pUT18C *Pp*CheA-Linker	fusion protein T18-*Pp*CheA-Linker (PP_4338, aa 111-395), Amp^R	This study
pKT25 *Pp*CheA-α12	fusion protein T18-*Pp*CheA-LinkerA (PP_4338, aa 111-190), Amp^R	This study
pUT18C *Pp*CheA-α345	fusion protein T18-*Pp*CheA-LinkerB (PP_4338, aa 191-360), Amp^R	This study
pUT18C *Pp*CheA-Hpt-Linker	fusion protein T18-*Pp*CheA-Hpt-Linker (PP_4338, aa 2-395), Amp^R	This study
pUT18C *Pp*CheA-Histidine-Kinase	fusion protein T18-*Pp*CheA-Histidine-Kinase (PP_4338, aa 396-609), Amp^R	This study
pUT18C *Pp*CheA-DIM-Kinase	fusion protein T18-*Pp*CheA-Histidine-Kinase (PP_4338, aa 361-609), Amp^R	This study
pUT18C *Pp*CheA-CheW	fusion protein T18-*Pp*CheA-CheW (PP_4338, aa 610-747), Amp^R	This study
pUT18C *Pa*CheA	fusion protein T18-*Pa*CheA (PA1458), Amp^R	This study
pUT18C *Pa*CheA-Linker	fusion protein T18-*Pa*CheA-Hpt (PA1458, aa 110-402), Amp^R	This study
pUT18C *Pp*Pch	fusion protein T18-*Pp*Pch (PP_0337), Amp^R	This study
pUT18C *Pp*Pch N-terminal	fusion protein T18-*Pp*Pch N-terminal (aa 1-187), Amp^R	This study
pUT18C *Pp*Pch Pas-Pac	fusion protein T18-*Pp*Pch Pas-Pac (aa 188-473), Amp^R	This study
pUT18C *Pp*Pch GGDEF	fusion protein T18-*Pp*Pch GGDEF (aa 474-628), Amp^R	This study
pUT18C *Pp*Pch EAL	fusion protein T18-*Pp*Pch EAL (aa 629-896), Amp^R	This study
pUT18C *Pa*Pch	fusion protein T18-*Pa*Pch (PA5017), Amp^R	This study
pUT18C *Pa*Pch-EAL	fusion protein T18-*Pa*Pch-EAL (PA5017, aa 631-899), Amp^R	This study
pUT18C *Pp*ParP	fusion protein T18-*Pp*ParP (PP_4333), Amp^R	This study

Plasmids for protein overexpression and purification

pETDuet 6xHis-MBP-TEV-Pch-EAL	fusion of EAL domain (aa 629-896) of Pch (PP_0337) with 6xHis-MBP-TEV, Amp^R	This study
pCDFDuet 6xHis-MBP-TEV-Pch-EAL	fusion of EAL domain (aa 629-896) of Pch (PP_0337) with 6xHis-MBP-TEV, Strep^R	This study

pTB146 6xHis-SUMO-Hpt-Linker	fusion of Hpt and linker region (aa 1-395) of CheA (PP_4338) with 6xHis-SUMO, Amp^R	This study

Kan^R, Kanamycin-resistant; Amp^R, Ampicillin-resistant; Cam^R, Chloramphenicol-resistant, $Gent^R$, Gentamycin-resistant, $Strep^R$, Streptomycin-resistant

4.13 Oligonucleotides

Individual tables can be found in [14] and [231]. The target organism for genetic modification is specified for the respective plasmids.

Table 13. Used Oligonucleotides.

ID	Name oligonucleotide	5' – 3' sequence
General check primer		
M13-rev	check pNPTS138-R6KT rev	CACACAGGAAACAGCTATGACC
M13-fwd	check pNPTS138-R6KT fwd	TGTAAAACGACGGCCAGTCC
LMS-5	check pBAD33 fwd	GCACGGCGTCACACTTTGCTATG
LMS-6	check pBAD33 rev	GCCAGGCAAATTCTGTTTTATCAG
LMS-25	pBBR1 check fwd	ACCATGATTACGCCAAGCGCG
LMS-26	pBBR1 check rev	CGTTGTAAAACGACGGCCAGTG
LMS-91	seq *flhF*	CAGCGCCGAGTGTTGCAAGA
LMS-92	check *hubP* fwd	CAGAAGATTTTCGGTGACGATGAG
LMS-93	check *hubP* rev	TGCACCGCGCGAAAAC
LMS-94	check *fliG* fwd	CAACGGCGTGAACGTGCTG
LMS-95	check *fliG* rev	CCAACCTGTCTGAAGCGCAGTC
JH-460	pKT25 fwd	CACTGACGGCGGATATCGACATGTT
JH-461	pKT25 rev	CCGCCGGACATCAGCGCCATTC
JH-462	pUT18 fwd	CCAGGCTTTACACTTTATGCTTCC
JH-463	pUT18 rev	GACGCGCCTCGGTGCCCACTGC
JH-464	pKNT25 fwd	CCCAGGCTTTACACTTTATGCTTCC
JH-465	pKNT25 rev	GTTTTTTTCCTTCGCCACGGCCTTG
JH-466	pUT18C fwd	CGGCGTGCCGAGCGGACGTTCG
JH-467	pUT18C rev	TCAGCGGGTGTTGGCGGGTGTC
P. putida* - pNPTS138-R6KT Δ*flhF		
TSB-1	EcoRV *flhF* fwd	GAATTCGTGGATCCAGATGAACGAAGCT GACCACAGAGTC
TSB-2	OL *flhF*-KO rev	GCAAGTTAAGGGTTGACCATGAAGCGTGTGC
TSB-3	OL *flhF*-KO fwd	ATGGTCAACCCTTAACTTGCATTATCCCCTACCTC
TSB-4	EcoRV *flhF* rev	CAAGCTTCTCTGCAGGATGCTGCAAGCCCTGTTGTCGG
TSB-5	check *flhF* fwd	CGCGTAGGCGTCGGTAATCG
TSB-6	check *flhF* rev	GCCTAAACTTGCAGAAGAGCTGG
TSB-23	seq *flhF*	GCAATCTTTGACCGCTGCCG
P. putida* - pNPTS138-R6KT Δ*fimV and* Δ*fimV::fimV		
TSB-7	EcoRV *fimV* fwd	GAATTCGTGGATCCAGATCCAGGTGGCATTCAACCTGC
TSB-8	OL *fimV*-KO rev	TCAGACCAGCCGAAGCATGACCTCTTCCCTTG
TSB-9	OL *fimV*-KO fwd	TCATGCTTCGGCTGGTCTGATGCAAGCAGG
TSB-10	EcoRV *fimV* rev	CAAGCTTCTCTGCAGGATCTTGAAGCGGGCATGAAAGTCG
TSB-11	check *fimV* fwd	GCACGGTCATCGACCTGTCC
TSB-12	check *fimV* rev	CGGGTCGTTGTAGATGACATAGC
TSB-13	seq *fimV*	ATAGCGTGCTGCTCGACCAG

TSB-14	seq *fimV*	CGGCTGTGGTTGCCGCTTC
TSB-15	seq *fimV*	CGACTTGCCATCGGACTTCGAC
VK-446	seq *fimV*	ATCAGACAGGTCCACGGC
VK-445	seq *fimV*	TGCCACTTTTTCCGCAGC

pBAD33 *Sp*HubP-GGS-sfGFP

LMS-1	pBAD *hubP* fwd	AATTCGAGCTCGGTACCCAGGAGGGCAAATATGAAATTTCGCACTTCGTA TCTTGTCGGT
LMS-7	seq *hubP*	GCACAATCCGCTGATGTTGTTTC
LMS-8	seq *hubP*	GATATTGCAGTAGCCGATACCGAG
LMS-9	seq *hubP*	ACGGGCTAAATCCAGTTTGGC
LMS-12	pBAD *hubP* rev	CGACTCTAGAGGATCCCCTTAGGATCCTTTGTAGAGCTCATCCATGCC
LMS-23	OL *hubP-sfgfp* rev	TCCTTTGCTGCTACCGCCACTAATCTCTTTTAGTAAACGTCCGGCCTC
LMS-24	OL *hubP-sfgfp* fwd	GAGATTAGTGGCGGTAGCAGCAAAGGAGAAGAACTTTTCACTGGAG

pBBR1-MCS2 *Sp*HubP

LMS-14	pBBR1 *hubP* rev	AGAACTAGTGGATCCCCCTTAACTAATCTCTTTTAGTAAACGTCCGGCCTC
LMS-15	OL *hubP* fwd	ACCATGATTACGCCAAGCGCG
LMS-16	OL *hubP* rev	CGTTGTAAAACGACGGCCAGTG
LMS-22	pBBR *hubP* fwd	ATCGAATTCCTGCAGCCCAGGAGGGCAAATATGAAATTTCGCACTTCGTA TCTTGTCGG

pBAD33 *Sp*FlhF-GS-mVenus

LMS-27	pBAD *flhF* fwd	AATTCGAGCTCGGTACCCAGGAGGGCAAATATGAAGATTAAACGATTTTT TGCCAAAGACATGCG
LMS-28	OL *flhF*-mVenus rev	GCCCTTGCTCACGCTGCCCTCAAATGCACAGGCCATATTATCTGACC
LMS-29	OL *flhF*-mVenus fwd	TGTGCATTTGAGGGCAGCGTGAGCAAGGGCGAGGAGC
LMS-30	pBAD *flhF* rev	CGACTCTAGAGGATCCCCTTACTTGTACAGCTCGTCCATGCCG
LMS-31	seq *flhF*	ATCGCATTGGCGCCTATGAGC

pBAD33 mVenus-GSGGG-*Sp*FliG constructs

LMS-32	*flhF fliG* rev	CACCATATTTGCCCTCCTCTACTCAAATGCACAGGCCATATTATCTGAC
LMS-33	mVenus-*fliG* fwd	TAGAGGAGGGCAAATATGGTGAGCAAGGGCGAGGAGC
LMS-34	mVenus-*fliG* rev	CATGCCGCCGCCGCTGCCCTTGTACAGCTCGTCCATGCCG
LMS-35	*fliG* linker fwd	AAGGGCAGCGGCGGCGGCATGGCTGAGAATAAAACAAAAGAAGCCGC
LMS-36	*fliG* linker rev	CGACTCTAGAGGATCCCCTTAGAGGAACTCATCGCCACCACC
LMS-37	mVenus-*fliG* fwd	AATTCGAGCTCGGTACCCAGGAGGGCAAATATGGTGAGCAAGGGCGAGG AGC
LMS-38	seq mVenus	CGTCTATATCACCGCCGACAAGC

***S. putrefaciens* - pNPTS138-R6KT FlhF ΔN44**

LMS-49	EcoRV *flhF* fwd	CAAGCTTCTCTGCAGGATAACGCGGCTAATTTCGCAGCA
LMS-50	OL *flhF*-N44 KO rev	GTAGAGGACGCATAAGTGGACTACGATGAGCCAAAAGCGAAGG
LMS-51	OL *flhF*-N44 KO fwd	TTTTGGCTCATCGTAGTCCACTTATGCGTCCTCTACTGGCCG
LMS-52	EcoRV *flhF* rev	GAATTCGTGGATCCAGATGGTAGTGTCGTAAAAGTGATGCAAAACCTATT AAATG
JH-152	check *flhF* fwd	GCATCAGTCAATGCAAGCAACC
JH-153	check *flhF* rev	GCACGGATTAATCCAGCATGCT

P. putida* - pNPTS138-R6KT Δ*pocB

LMS-112	EcoRV *pocB* fwd	CAAGCTTCTCTGCAGGATGTATGGATGTGGATCAAGGACAAGCAAC
LMS-113	OL *pocB*-KO rev	ATCGGCGAAAGCCATCAACTTCACGCCTTGCCTCCGG

LMS-114	OL *pocB*-KO fwd	CGGAGGCAAGGCGTGAAGTTGATGGCTTTCGCCGATCGC
TSB-19	EcoRV *pocB* rev	GAATTCGTGGATCCAGATACCAGTTCCAGGTCACGGGC
TSB-20	check *pocB* fwd	GCGGATAATCGGTGGGGAAGC
TSB-21	check *pocB* rev	GTCAGCCTCACGCAAGCGG

***P. putida* - pNPTS138-R6KT Δ*pch*, Δ*pch::pch and* Pch-2xGGS-sfGFP**

LMS-115	EcoRV *pch* fwd	CAAGCTTCTCTGCAGGATGCCGGAGGTGGCTATCCTGG
LMS-116	OL *pch*-KO rev	CCGAGGATTACGCAGCTGCGAAGACTCGCTTGAAGAGGGAAC
LMS-117	OL *pch*-KO fwd	TCTTCAAGCGAGTCTTCGCAGCTGCGTAATCCTCGGGC
LMS-118	EcoRV *pch* rev	GAATTCGTGGATCCAGATTTGTCGAACACCACCAGCACC
LMS-119	check *pch* fwd	GTCGTTGCCCTGGCGCATAC
LMS-120	check *pch* rev	GGCGCCTGCTTCACCATCTC
LMS-121	EcoRV *pch* fwd	CAAGCTTCTCTGCAGGATTCAACCTGTCGCCCAAACAGTTC
LMS-122	OL *pch-sfgfp* rev	GCTACCGCCGCTACCGCCGGCCACCGGGCCACG
LMS-123	OL *sfgfp* fwd	GGCGGTAGCGGCGGTAGCAGCAAAGGAGAAGAACTTTTCACTGGAG
LMS-124	OL *sfgfp* rev	AGGATTACGCAGCTGTTAGGATCCTTTGTAGAGCTCATCCATGC
LMS-125	OL *pch-sfgfp* fwd	CTCTACAAAGGATCCTAACAGCTGCGTAATCCTCGGGC
LMS-126	EcoRV *pch* rev	GAATTCGTGGATCCAGATTTGTCGAACACCACCAGCACCA
LMS-127	seq *pch*	CTGAGCGTGCTCGATGACCAG
LMS-128	seq *pch*	ACGAAGACGTCACCCAGACCAA
LMS-129	EcoRV *pch* rev	GAATTCGTGGATCCAGATTTGTCGAACACCACCAGCACCACTTCG

***P. putida* - pNPTS138-R6KT Δ*cheA*, Δ*cheA*::*cheA* and CheA-Hpt-H48Q**

LMS-130	EcoRV *cheA* fwd	CAAGCTTCTCTGCAGGATACCGCACCATGGACCTGGTC
LMS-131	OL *cheA*-KO rev	CAGGGCGCGCCACCGAAACAAACGTGCTCCTTAAAAACCAAGGCTG
LMS-134	check *cheA* fwd	GCCACCAGTTTGTAGGGTTTGCG
LMS-135	check *cheA* rev	GAGCGCCTGTCGTATGTGGTCA
LMS-136	OL *cheA*-KO fwd	TTTTAAGGAGCACGTTTGTTTCGGTGGCGCGCCCTGG
LMS-137	EcoRV *cheA* rev	GAATTCGTGGATCCAGATTGGCCGGCGCTGGCGC
LMS-177	split *cheA* primer fwd	GGTGATGAAAACCCGTATGCAGCCGA
LMS-178	split *cheA* primer rev	GAAGACCTTCTTGATCGGCTGCATAC
LMS-496	OL *cheA*-H48Q rev	GCCCCCTTTTACAGTCTGGAAACCGCGAAAGATCGCATT
LMS-497S	OL *cheA*-H48Q fwd	ATCTTTCGCGGTTTCCAGACTGTAAAAGGGGGCGCCG
LMS-497L	OL *cheA*-H48Q fwd	ATCTTTCGCGGTTTCCAGACTGTAAAAGGGGGCGCCGGCTTCCTTC

P. putida* - pNPTS138-R6KT Δ*parP*::*parP

LMS-145	EcoRV 4333 fwd	GAATTCGTGGATCCAGATGCTCGGACCACTCTTCCTCG
LMS-146	EcoRV 4333 rev	CAAGCTTCTCTGCAGGATCGATGAGCGCATTTCGCTGTTG
LMS-147	check 4333 fwd	CTGGCGACACCTTTCAGATCG
LMS-148	check 4333 rev	CGCAGTTCGACAGCAAGAGC

BACTH plasmids *Pp*Pch and *Pp*CheA

LMS-153	pUT18/pUT18C/pKNT25 *pch* fwd	CAGGTCGACTCTAGAGATGAAAAGCCAACCCGATGCCG
LMS-155	pKT25 *pch* fwd	AGGGTCGACTCTAGAGATGAAAAGCCAACCCGATGCCG
LMS-161	seq *cheA*	GCCCTGCTGGACCAGTTGC
LMS-162	seq *cheA*	GGCAGCCGAAGCTGTTGCAG
LMS-163	pUT18/pUT18C/pKNT25 *cheA* fwd	CAGGTCGACTCTAGAGATGAGCTTCGGCGCCGATGAAGAAATCCTC
LMS-165	pKT25 *cheA* fwd	AGGGTCGACTCTAGAGATGAGCTTCGGCGCCGATGAAGAAATCCTC
LMS-213	pUT18/pUT18C/pKNT25 *pch* rev	AGCTCGGTACCCGGGGGGCCACCGGGCCACG

LMS-214	pUT18/pUT18C/pKNT25 *cheA* rev	AGCTCGGTACCCGGGGAATACGCCGCGCGGCG
LMS-216	pKT25 *pch* rev	ACTTAGGTACCCGGGGGGCCACCGGGCCACG
LMS-217	pKT25 *cheA* rev	ACTTAGGTACCCGGGGAATACGCCGCGCGGCG

BACTH plasmids *Pp*ParP

LMS-186	pKT25 4333 fwd	AGGGTCGACTCTAGAGATGACTCAAACCCGGCAAAC
LMS-215	pKT25 4333 rev	ACTTAGGTACCCGGGGTTTCTGTTTGGCGTGCATCTG
LMS-188	pUT18/pUT18C/pKNT25 4333 fwd	CAGGTCGACTCTAGAGATGACTCAAACCCGGCAAAC
LMS-212	pUT18/pUT18C/pKNT25 4333 rev	AGCTCGGTACCCGGGGTTTCTGTTTGGCGTGCATCTG

pBBR1 cymR/Pcym

LMS-179	SspI cym fwd	CGCGAATTTTAACAAAATCTAGCGCTTGAATTTCGCGT
LMS-218	cym MCS rev	GAGCTCGAATTCGCTAGCGGCAGTCTCCTTTGATTGTTTTTG
LMS-219	hybr1 MCS fwd	CAATCAAAGGAGACTGCCGCTAGCGAATTCGAGCTCGGTACCCGGGGAT CCTCTAGAG
LMS-220	hybr1 MCS rev	CCACCCCCATGGGCAAATAAGCTTGCATGCCTGCAGGTCGACTCTAGAG GATCCCCGGGTA
LMS-221	hybr2 MCS fwd	CTCTAGAGGATCCCCGGGTACCGAGCTCGAATTCGCTAGCGGCAGTCTC CTTTGATTG
LMS-222	hybr2 MCS rev	TACCCGGGGATCCTCTAGAGTCGACCTGCAGGCATGCAAGCTTATTTGC CCATGGGGGTGG

***S. putrefaciens* - pNPTS138-R6KT *Sp*HubP$_{PpFimV-D}$**

LMS-223	EcoRV *Sp*HubP fwd	CAAGCTTCTCTGCAGGATTGAATGCGACAGCTGTACG
LMS-224	OL *Sp*HubP$_{PpFimV-D}$ rev	GTCGTCCAAAGGCTCAGGACCAACGTCACTCATCTCAATG
LMS-225	OL *Sp*HubP$_{PpFimV-D}$ fwd	GAGATGAGTGACGTTGGTCCTGAGCCTTTGGACGAC
LMS-226	OL *Pp*FimV-D-*Sp*HubP rev	AAACTCGGTTAATCGAGATCAGACCAGCCGGGAG
LMS-227	OL *Pp*FimV-D-*Sp*HubP fwd	CTCTCCCGGCTGGTCTGATCTCGATTAACCGAGTTTCAATCTAAC
LMS-228	EcoRV *Sp*HubP rev	GAATTCGTGGATCCAGATTTACCGTGATAATGGCTTACACC
LMS-229	seq *Sp*HubP$_{PpFimV-D}$	GATGCGAGTGTGAGTGTCTATC
LMS-230	seq *Sp*HubP$_{PpFimV-D}$	GATGATGATCTCGATTTAAGCA

***P. putida* - pNPTS138-R6KT *Pp*FimV$_{SpFimV-D}$**

LMS-231	EcoRV *Pp*FimV fwd	CAAGCTTCTCTGCAGGATTTCAACCTGCTGGCCCAG
LMS-232	OL *Pp*FimV$_{SpFimV-D}$ rev	GGCATCGCCAAGTAAGGCCTCTGGTTGCGCCACC
LMS-233	OL *Pp*FimV$_{SpFimV-D}$ fwd	GCGGTGGCGCAACCAGAGGCCTTACTTGGCGATGCC
LMS-234	OL *Sp*FimV-D-*Pp*FimV rev	AGGCCTGACCTGCTTGCATTAACTAATCTCTTTTAGTAAACGTCCGG
LMS-235	OL *Sp*FimV-D-*Pp*FimV fwd	CTAAAAGAGATTAGTTAATGCAAGCAGGTCAGGCC
LMS-236	EcoRV *Pp*FimV rev	GAATTCGTGGATCCAGATCTTGAAGCGGGCATGAAAGTCG
LMS-237	seq *fimV*	TGCCACTTTTTCCGCAGC
LMS-238	seq *fimV*	ATCAGACAGGTCCACGGC

P. putida* - pNPTS138-R6KT Δ*pilA

LMS-260	EcoRV *pilA* fwd	CAAGCTTCTCTGCAGGATTCGCAACCACTGCGG
LMS-261	OL *pilA*-KO rev	TGGTTTATTGCCCTGCCCGAACGTAGTTCCTTTTTGATTCGC
LMS-262	OL *pilA*-KO fwd	CAAAAAGGAACTACGTTCGGGCAGGGCAATAAACCA
LMS-263	EcoRV *pilA* rev	GAATTCGTGGATCCAGATCTTATGCCTGTCGGATCTACGTC
LMS-264	check *pilA* fwd	AGGAATCACCTCCAGCAACA
LMS-265	check *pilA* rev	GGCAAACGTACAGATCTCCCA

***P. putida* - pNPTS138-R6KT FimV-3xGGS-mCherry**

LMS-277	EcoRV *fimV* fwd	CAAGCTTCTCTGCAGGATATTTCGACCTCGACGTCAGC

LMS-278	OL *fimV*-mCherry rev	CGAACCCCCGCTACCGCCGCTACCGCCGACCAGCCGGGAGAGC
LMS-282	EcoRV *fimV* rev	GAATTCGTGGATCCAGATGCGGGCATGAAAGTCG
LMS-283	check *fimV* fwd	GAAGCTCAGCCGGAAGAAC
LMS-284	OL mCherry fwd	GGCGGTAGCGGCGGTAGCGGGGGTTCGGTTTCCAAAGGGGAAGAGGAC
LMS-285	OL mCherry rev	CCTGACCTGCTTGCATCATTTGTATAACTCATCCATACCACCAGTC
LMS-286	OL *fimV*-mCherry fwd	ATGGATGAGTTATACAAATGATGCAAGCAGGTCAGG

***P. putida* - pNPTS138-R6KT sfGFP-2xGGS-ParB**

LMS-276	OL sf*gfp* rev	GCTACCGCCGCTACCGCCGGATCCTTTGTAGAGCTCATCCA
LMS-292	EcoRV *parB* fwd	CAAGCTTCTCTGCAGGATTGCAGGTCAAGGAAAGCC
LMS-295	OL *sfgfp-parB* fwd	GGCGGTAGCGGCGGTAGCATGGCCGTCAAGAAACGG
LMS-296	EcoRV *parB* rev	GAATTCGTGGATCCAGATGCCACAGTCACCCGCG
LMS-297	check *parB* fwd	TGTTCAAGGCGTGCGATATC
LMS-298	check *parB* rev	GTATCAATCTCGCCGCCTC
LMS-299	OL *sfgfp-parB* rev	TTCTTCTCCTTTGCTCATACGGATTCCTTAAGTTGTTTGTGC
LMS-300	OL *sfgfp* fwd	ACAACTTAAGGAATCCGTATGAGCAAAGGAGAAGAACTTTTCAC

pBBR1-MCS2-cym-pFimV

LMS-303	SmaI cym-*fimV* fwd	AATTCGAGCTCGGTACCCATGCTTCGAATTCGCAAACTG
LMS-304	SmaI cym-*fimV* rev	CGACTCTAGAGGATCCCCTCAGACCAGCCGGGAGA
LMS-305	seq *fimV*	GGAAAGCCTGGACACCAG
LMS-306	seq *fimV*	TGCACGATGAGCCCAAAG

***P. putida* - pNPTS138-R6KT $FimV_{HubP\text{-}C}$**

LMS-338	EcoRV *fimV* fwd	CAAGCTTCTCTGCAGGATAGCTGGATGCCACTCGC
LMS-339	OL *hubP*-C rev	ATTACGTTTACGACGAAGCGCCAGCAGCCACAG
LMS-340	*hubP*-C fwd	CTGCTGTGGCTGCTGGCGCTTCGTCGTAAACGTAATAAAGAGCG
LMS-341	*hubP*-C rev	GAAGTCGAAGTCCAGGTCACCAACGTCACTCATCTCAATGT
LMS-342	OL *hubP*-C fwd	GAGATGAGTGACGTTGGTGACCTGGACTTCGACTTCTTCTCC
LMS-343	EcoRV *fimV* rev	GAATTCGTGGATCCAGATAATCGGCTCGTTGGCG
LMS-344	seq *hubP*-C	GAAATGTTTATCGATACAGGCAG
LMS-345	check *fimV* fwd	GACCAGCAGCAGATCCAGAG
LMS-346	check *fimV* rev	ATGTCGATATAGGCACGGGC

***S. putrefaciens* - pNPTS138-R6KT $HubP_{FimV\text{-}C}$**

LMS-347	EcoRV *hubP* fwd	CAAGCTTCTCTGCAGGATTTGTTAAGGTTGAACCTAAAACTGAGC
LMS-348	OL *fimV*-C rev	CTGGGCCTTGCGTTTGCGCATCATAAATACAAGTAATAAAATCAGTAGCG C
LMS-349	*fimV*-C fwd	TTACTTGTATTTATGATGCGCAAACGCAAGGCC
LMS-350	*fimV*-C rev	GGCATCGCCAAGTAAGGCGTCCAAAGGCTCAGGCTCTG
LMS-351	OL *fimV*-C fwd	GAGCCTGAGCCTTTGGACGCCTTACTTGGCGATGCC
LMS-352	EcoRV *hubP* rev	GAATTCGTGGATCCAGATATTGCATTCGTATCAAAATGCACC
LMS-353	check *hubP* fwd	GCTAAAGAACCTAACACCACGA
LMS-354	check *hubP* rev	TCCTGTTGGTGTTCATTACCA

BACTH plasmids *Pp*FimV

LMS-355	pKT25 *fimV* fwd	AGGGTCGACTCTAGAGCGCAAACGCAAGGCC
LMS-356	pKT25 *fimV* rev	ACTTAGGTACCCGGGGGACCAGCCGGGAGAGC
LMS-357	pUT18/pUT18C/pKNT25 *fimV* fwd	CAGGTCGACTCTAGAGCGCAAACGCAAGGCC
LMS-358	pUT18/pUT18C/pKNT25 *fimV* rev	AGCTCGGTACCCGGGGGACCAGCCGGGAGAGC

pETDuet 6xHis-MBP-TEV-Pch-EAL

LMS-377	NcoI His-MBP-EAL fwd	AGAAGGAGATATACCATGATGCACCATCACCATCACCATGAAGAAGGTAA ACTGGTAATCTGGATTAAC
LMS-378	OL His-MBP rev	GCCCTGAAAATAAAGATTCTCCCCGAGGTTGTTGTTATTGTTATTG
LMS-379	OL MBP-EAL fwd	GAGAATCTTTATTTTCAGGGCGTGCTCAACGCCGAAGC
LMS-380	NcoI His-MBP-EAL rev	TGATGGCTGCTGCCCATGTCAGGCCACCGGGC
LMS-381	seq His-MBP-EAL fwd	GGGCTGGTAGAACACGTCC
LMS-382	seq His-MBP-EAL rev	TCGGCAGCAGATCTTTGTT

BACTH plasmids *Pa*Pch

LMS-387	pKT25 *Papch* fwd	AGGGTCGACTCTAGAGAAAAGTCATCCCGATGCCG
LMS-388	pKT25 *Papch* rev	ACTTAGGTACCCGGGGGTGCAGGGTGCGGCA
LMS-389	pUT18/pUT18C/pKNT25 *Papch* fwd	CAGGTCGACTCTAGAGAAAAGTCATCCCGATGCCG
LMS-390	pUT18/pUT18C/pKNT25 *Papch* rev	AGCTCGGTACCCGGGGGTGCAGGGTGCGGCA
LMS-391	seq *Papch*	ACTACCTGAGGCCGCTGG

BACTH plasmids *Pa*CheA

LMS-392	pKT25 *PacheA* fwd	AGGGTCGACTCTAGAGAGCTTCGACGCCGATGAA
LMS-393	pKT25 *PacheA* rev	ACTTAGGTACCCGGGGGATGCGCCGTGCGTAAC
LMS-394	pUT18/pUT18C/pKNT25 *PacheA* fwd	CAGGTCGACTCTAGAGAGCTTCGACGCCGATGAA
LMS-395	pUT18/pUT18C/pKNT25 *PacheA* rev	AGCTCGGTACCCGGGGGATGCGCCGTGCGTAAC
LMS-396	seq *PacheA*	GGCAAGTTCGGCGATGT

BACTH plasmids *Pa*Pch-EAL domain

LMS-397	pKT25 *Papch*-EAL fwd	AGGGTCGACTCTAGAGGAGGCGCTGACCGCC
LMS-398	pUT18/pUT18C/pKNT25 *Papch*-EAL fwd	CAGGTCGACTCTAGAGGAGGCGCTGACCGCC

BACTH plasmids *Pa*CheA-Hpt domain

LMS-399	pKT25 *PacheA*-Hpt rev	ACTTAGGTACCCGGGGGGACTGCTCGCGCACC
LMS-400	pUT18/pUT18C/pKNT25 *PacheA*-Hpt rev	AGCTCGGTACCCGGGGGGACTGCTCGCGCACC

***S. putrefaciens* - pNPTS138-R6KT *Pp*FimV-3xGGS-sfGFP**

LMS-405	OL *fimV-sfgfp* rev	CTCGGTTAATCGAGATCAGGATCCTTTGTAGAGCTCATCCAT
LMS-406	OL *fimV* fwd	GAGCTCTACAAAGGATCCTGATCTCGATTAACCGAGTTTCAATC
LMS-407	OL *fimV* rev	GAATTCGTGGATCCAGATCCGTGATAATGGCTTACACCATG
LMS-408	seq *sfgfp*	CTGGAGTTGTCCCAATTCTT

***P. putida* - pNPTS138-R6KT *Sp*HubP-3xGGS-sfGFP**

LMS-279	OL *sfgfp* fwd	GGCGGTAGCGGCGGTAGCGGGGGTTCGATGAGCAAAGGAGAAGAACTT TTCAC
LMS-409	EcoRV *hubP* fwd	CAAGCTTCTCTGCAGGATATCTGAGTGATGACAGTGTTCTTGC
LMS-410	OL *hubP-sfgfp* rev	CGAACCCCCGCTACCGCCGCTACCGCCACTAATCTCTTTTAGTAAACGTC CGGC
LMS-411	OL *sfgfp* rev	CCTGACCTGCTTGCATTAGGATCCTTTGTAGAGCTCATCCAT
LMS-412	OL *fimV-sfgfp* fwd	GAGCTCTACAAAGGATCCTAATGCAAGCAGGTCAGGCC
LMS-413	EcoRV *fimV* rev	GAATTCGTGGATCCAGATAAAGTCGGCCGGCATTG

***P. putida* - pNPTS138-R6KT FimV$_{\Delta GLB}$**

LMS-442	EcoRV GLB fwd	CAAGCTTCTCTGCAGGATCTGGGCCTGCCTGAACTG

LMS-443	OL GLB-KO rev	TGCCGCCGGCTGTTCGCCCTCCCCCAGGCCCAG
LMS-444	OL GLB-KO fwd	GCGCTGGGCCTGGGGGAGGGCGAACAGCCGGC
LMS-445	EcoRV GLB rev	GAATTCGTGGATCCAGATTCTTCGTTGTCGCGACG
LMS-446	check GLB rev	CGTGCCAACTGGTTGTTCTT

***P. putida* - pNPTS138-R6KT FimV$_{\Delta FimV\ domain}$**

LMS-464	EcoRV *Pp*FimV-D fwd	CAAGCTTCTCTGCAGGATTCGCTGAGCCTGTGCTC
LMS-465	OL *Pp*FimV-D-KO rev	CCTGACCTGCTTGCATCAGGAGAAGAAGTCGAAGTCCAGGT
LMS-466	OL *Pp*FimV-D-KO fwd	GACTTCGACTTCTTCTCCTGATGCAAGCAGGTCAGG

***S. putrefaciens* - pNPTS138-R6KT HubP$_{\Delta FimV\ domain}$**

LMS-467	EcoRV *Sp*FimV-D fwd	CAAGCTTCTCTGCAGGATTCACACCAACCCTCGATG
LMS-468	OL *Sp*FimV-D-KO rev	CTCGGTTAATCGAGATTAATCATCGACATCAATTATAGCGG
LMS-469	OL *Sp*FimV-D-KO fwd	ATAATTGATGTCGATGATTAATCTCGATTAACCGAGTTTCAATC
LMS-470	EcoRV *Sp*FimV-D rev	GAATTCGTGGATCCAGATCCGTGATAATGGCTTACACCA
LMS-471	check *Sp*FimV-D rev	GTAAAGAACCCCACGTGCTG

***P. putida* - pNPTS138-R6KT FimV$_{HubP\text{-}P}$**

LMS-472	EcoRV *fimV* fwd	CAAGCTTCTCTGCAGGATGAACTGCGCGTACTGCTGG
LMS-473	OL *hubP*-P rev	TAAAGGTTTTACTTTAGGCGCATTCGCCATGCC
LMS-474	*hubP*-P fwd	TCTGGCATGGCGAATGCGCCTAAAGTAAAACCTTTAAAAATCATGGG
LMS-475	*hubP*-P rev	CACGCCCAGAAGCCACGGATTATTGATAATCTTCCGCCATAAGTCA
LMS-476	OL *hubP*-P fwd	CGGAAGATTATCAATAATCCGTGGCTTCTGGGC
LMS-477	EcoRV *fimV* rev	GAATTCGTGGATCCAGATGGCCGGCAACTGACG
LMS-478	check *Sp*Peri rev	GGGAATGGCAAGCATGAC

***S. putrefaciens* - pNPTS138-R6KT HubP$_{FimV\text{-}P}$**

LMS-479	EcoRV *hubP* fwd	CAAGCTTCTCTGCAGGATTACTGCGTAATGCCGAAGGA
LMS-480	OL *fimV*-P rev	CAGCTCCCCCAGGCCCAGCGTATCTGCAGCAACAGCG
LMS-481	*fimV*-P fwd	GCTGTTGCTGCAGATACGCTGGGCCTGGGGGAG
LMS-482	*fimV*-P rev	TGCAATTAACATTGCAGGGTTGCCCAGGACCGAGTC
LMS-483	OL *fimV*-P fwd	GACTCGGTCCTGGGCAACCCTGCAATGTTAATTGCAGCC
LMS-484	EcoRV *hubP* rev	GAATTCGTGGATCCAGATGCCAAGTCCCGCCAG
LMS-485	seq *fimV*	GGTGCCAGCAGCTACACC

pCDFDuet 6xHis-MBP-TEV-Pch-EAL

LMS-486	check pCDFDuet fwd	GGATCTCGACGCTCTCCCT
LMS-487	check pCDFDuet rev	GATTATGCGGCCGTGTACAA
LMS-488	NcoI His-MBP fwd	ATAAGGAGATATACCATGATGCACCATCACCATCACCA

P. putida* - pNPTS138-R6KT Δ*flhFG

LMS-490	EcoRV *flhFG* fwd	CAAGCTTCTCTGCAGGATAGATCCCGTAGTAATCATCGAGACTC
LMS-491	OL *flhFG*-KO rev	CGGCTGAGGTAGGGGATAGCTGGCCGCTGCC
LMS-492	OL *flhFG*-KO fwd	TGGCTGGCAGCGGCCAGCTATCCCCTACCTCAGCCGTTAG
LMS-493	EcoRV *flhFG* rev	GAATTCGTGGATCCAGATAAGGTGCTGCAAGCCCTG
LMS-494	check *flhFG* fwd	TCATGCAGTCCTTCGTGCTC
LMS-495	seq *flhF*	AGGCCGGCAGTATCGATC

***P. putida* - pNPTS138-R6KT mCherry-DILEL-ParP**		
PM-1	EcoRV *parP* fwd	GCCAAGCTTCTCTGCAGGATCTGGAGCGCCAGTCGC
PM-2	OL *mCherry-parP* rev	TCCTCTTCCCCTTTGGAAACCATCAGGCTACCTGCACTGC
PM-3	OL *mCherry* fwd	GCAGTGCAGGTAGCCTGATGGTTTCCAAAGGGGAAGAGGAC
PM-4	OL *mCherry* rev	GTCATCAGTTCCAGAATATCTTTGTATAACTCATCCATACCACCAGTC
PM-5	OL *mCherry*-parP fwd	AAGATATTCTGGAACTGATGACTCAAACCCGGCAAACC
PM-6	EcoRV *parP* rev	GCGAATTCGTGGATCCAGATCACACCAACGGCACCG

BACTH plasmids *Pp*Pch variants		
PM-21	pUT18/pUT18C/pKNT25 N-terminal fwd	GCAGGTCGACTCTAGAGAAAAGCCAACCCGATGCC
PM-22	pUT18/pUT18C/pKNT25 N-terminal rev	GAGCTCGGTACCCGGGGGTAGCGATGGCGGGC
PM-23	pKT25 N-terminal fwd	CAGGGTCGACTCTAGAGAAAAGCCAACCCGATGCC
PM-24	pKT25 N-terminal rev	TACTTAGGTACCCGGGGGTAGCGATGGCGGGC
PM-25	pUT18/pUT18C/pKNT25 Pas-Pac fwd	GCAGGTCGACTCTAGAGAGCGCGGGCAACTCG
PM-26	pUT18/pUT18C/pKNT25 Pas-Pac rev	GAGCTCGGTACCCGGGGGAGGTTGTCGGTGTAAGCCAG
PM-27	pKT25 Pas-Pac fwd	CAGGGTCGACTCTAGAGAGCGCGGGCAACTCG
PM-28	pKT25 Pas-Pac rev	TACTTAGGTACCCGGGGGAGGTTGTCGGTGTAAGCCAG
PM-29	pUT18/pUT18C/pKNT25 GGDEF fwd	GCAGGTCGACTCTAGAGACCAACCTGGGCAACCG
PM-30	pUT18/pUT18C/pKNT25 GGDEF rev	GAGCTCGGTACCCGGGGTTCGGTAAACACCTGTACCTGGT
PM-31	pKT25 GGDEF fwd	CAGGGTCGACTCTAGAGACCAACCTGGGCAACCG
PM-32	pKT25 GGDEF rev	TACTTAGGTACCCGGGGTTCGGTAAACACCTGTACCTGGT
PM-33	pUT18/pUT18C/pKNT25 EAL fwd	GCAGGTCGACTCTAGAGGTGCTCAACGCCGAAGC
PM-34	pUT18/pUT18C/pKNT25 EAL rev	GAGCTCGGTACCCGGGGGGCCACCGGGCCA
PM-35	pKT25 EAL fwd	CAGGGTCGACTCTAGAGGTGCTCAACGCCGAAGC
PM-36	pKT25 EAL rev	TACTTAGGTACCCGGGGGGCCACCGGGCCA

BACTH plasmids *Pp*CheA variants		
PM-37	pUT18/pUT18C/pKNT25 Hpt-Linker fwd	GCAGGTCGACTCTAGAGAGCTTCGGCGCCGAT
PM-38	pUT18/pUT18C/pKNT25 Hpt-Linker rev	GAGCTCGGTACCCGGGGGCCGCTGTTCAGGCC
PM-39	pKT25 Hpt-Linker fwd	CAGGGTCGACTCTAGAGAGCTTCGGCGCCGAT
PM-40	pKT25 Hpt-Linker rev	TACTTAGGTACCCGGGGGCCGCTGTTCAGGCC
PM-41	pUT18/pUT18C/pKNT25 Histidine-Kinase fwd	GCAGGTCGACTCTAGAGGACGAGGCCATGTCCAAG
PM-42	pUT18/pUT18C/pKNT25 Histidine-Kinase rev	GAGCTCGGTACCCGGGGCGCCAGGGTCAGCG
PM-43	pKT25 Histidine-Kinase fwd	CAGGGTCGACTCTAGAGGACGAGGCCATGTCCAAG
PM-44	pKT25 Histidine-Kinase rev	TACTTAGGTACCCGGGGCGCCAGGGTCAGCG
PM-45	pUT18/pUT18C/pKNT25 CheW fwd	GCAGGTCGACTCTAGAGATCATGCCCACCCTTATGGT
PM-46	pUT18/pUT18C/pKNT25 CheW rev	GAGCTCGGTACCCGGGGAATACGCCGCGCGG
PM-47	pKT25 CheW fwd	GCAGGTCGACTCTAGAGAGCTTCGGCGCCGAT
PM-48	pKT25 CheW rev	GAGCTCGGTACCCGGGGGCCGCTGTTCAGGCC
PM-49	pUT18/pUT18C/pKNT25 Hpt fwd	GCAGGTCGACTCTAGAGAGCTTCGGCGCCGA
PM-50	pUT18/pUT18C/pKNT25 Hpt rev	GCGCGAGCGTGCCCCCCGGGTACCGAGCTC
PM-51	pKT25 Hpt fwd	CAGGGTCGACTCTAGAGAGCTTCGGCGCCGA
PM-52	pKT25 Hpt rev	GCGCGAGCGTGCCCCCCGGGTACCTAAGTA
PM-53	pUT18/pUT18C/pKNT25 Linker fwd	GCAGGTCGACTCTAGAGGAAGTGACACCGGCCACC
PM-54	pKT25 Linker fwd	CAGGGTCGACTCTAGAGGAAGTGACACCGGCCACC

P. putida - pNPTS138-R6KT EAL- and GGDEF-EAL-2xGGS-sfGFP variants		
PM-55	EcoRV EAL fwd	GCCAAGCTTCTCTGCAGGATGCCACATTGGCGGC
PM-56	OL EAL rev	CCTCTTCAAGCGAGTCTTCGATGGTGCTCAACGCCGAAGC
PM-57	OL EAL-*sfgfp* fwd	CTTCAAGCGAGTCTTCGATGGTGCTCAACGCCGAAGC
PM-58	OL *sfgfp* rev	TGGCCCGGTGGCCGGCGGCTCGGGCGGCTCGAG
PM-59	OL *sfgfp* fwd	CCGGCGGCTCGGGCGGCTCGAGCAAAGGAGAAGAACTTTTCACTG
PM-60	OL EAL-*sfgfp* rev	GATGAGCTCTACAAAGGATCCTGACAGCTGCGTAATCCTCGGGC
PM-61	OL EAL fwd	AGCTCTACAAAGGATCCTGACAGCTGCGTAATCCTCGG
PM-62	EcoRV EAL rev	GAACTGCTGGCAATGTTCTGGATCTGGATCCACGAATTCGC
PM-63	OL GGDEF rev	CCCTCTTCAAGCGAGTCTTCGATGACCAACCTGGGCAACCG
PM-64	OL GGDEF-*sfgfp* fwd	CTTCAAGCGAGTCTTCGATGACCAACCTGGGCAACCG
PM-67	sequencing *pch*	CATGGCCCACAACCTGAAG
PM-68	sequencing *pch*	ACACCTGCTGGAGCTGGAG
PM-69	sequencing *pch*	GTTCAAGAGCCGACGCAAA
PM-70	sequencing *pch*	GCCCGGAAAACAAGGC
P. putida - pNPTS138-R6KT CheA ΔHpt		
PM-77	EcoRV *cheA* fwd	GCCAAGCTTCTCTGCAGGATACCGCACCATGGACCTG
PM-78	OL Hpt-KO rev	GGTTTTTAAGGAGCACGTTTGATGGAAGTGACACCGGCCACCCC
PM-79	OL Hpt-KO fwd	TTTAAGGAGCACGTTTGATGGAAGTGACACCGGCCACC
PM-80	EcoRV *cheA* rev	AGCGCAGCCAGCGAATCTGGATCCACGAATTCGC
PM-81	check Hpt-KO fwd	GCATCGAGCGAATCGAGC
pTB146 6xHis-SUMO-Hpt-Linker		
PM-87	SUMO fwd	ACAGAGAACAGATTGGTGGTGAAGTGACACCGGCCACC
PM-88	SUMO rev	TTGTTAGCAGCCGGATCTTAGCCGCTGTTCAGGCC
BACTH *Pp*CheA LinkerA/B and DIM-Kinase		
PM-89	pUT18/pUT18C/pKNT25 LinkerA rev	GAGCTCGGTACCCGGGGAGTCTCGCCCTGCATCTG
PM-90	pKT25 LinkerA rev	TACTTAGGTACCCGGGGAGTCTCGCCCTGCATCTG
PM-91	pUT18/pUT18C/pKNT25 LinkerB fwd	GCAGGTCGACTCTAGAGGTCAGCGGTGCGGGTG
PM-92	pUT18/pUT18C/pKNT25 LinkerB rev	GAGCTCGGTACCCGGGGTTCCGCTTCGCTGGC
PM-93	pKT25 LinkerB fwd	CAGGGTCGACTCTAGAGGTCAGCGGTGCGGGTG
PM-94	pKT25 LinkerB rev	TACTTAGGTACCCGGGGTTCCGCTTCGCTGGC
PM-95	pUT18/pUT18C/pKNT25 DIM-Kinase fwd	GCAGGTCGACTCTAGAGACCACCGTGCGCGTCGAC
PM-96	pUT18/pUT18C/pKNT25 DIM-Kinase rev	GAGCTCGGTACCCGGGGCGCCAGGGTCAGCGGC
PM-97	pKT25 DIM-Kinase fwd	CAGGGTCGACTCTAGAGACCACCGTGCGCGTCGAC
PM-98	pKT25 DIM-Kinase rev	TACTTAGGTACCCGGGGCGCCAGGGTCAGCGGC
BACTH plasmids *Pa*CheA Linker		
PM-99	pUT18/pUT18C/pKNT25 Linker fwd	GCAGGTCGACTCTAGAGTCCGAACCGACCCCG
PM-100	pUT18/pUT18C/pKNT25 Linker rev	GAGCTCGGTACCCGGGGGCCACTGTTCAGGCCCAG
PM-101	pKT25 Linker fwd	CAGGGTCGACTCTAGAGTCCGAACCGACCCCG
PM-102	pKT25 Linker rev	TACTTAGGTACCCGGGGGCCACTGTTCAGGCCCAG

fwd, forward primer; rev, reverse primer

5. Methods

5.1 Microbiological methods

5.1.1 Cultivation of *S. putrefaciens or P. putida* strains

For overnight cultivation, *S. putrefaciens* or *P. putida* strains were incubated at room temperature with shaking at 100 rpm. For daytime cultivation, overnight cultures were diluted in fresh LB medium to an optical density at 600 nm (OD_{600}) of 0.02 and incubated at 30°C with continuous shaking at 180 rpm until the cells reached exponential growth.

5.1.2 Cultivation of *E. coli* or *P. aeruginosa* strains

E. coli or *P. aeruginosa* cells were always incubated at 37°C with constant shaking at 180 rpm. If necessary, additives (Table 9) were added to the cultures.

5.1.3 Long-term storage of strains

For long-term storage, strains from stationary-phase cultures were harvested and mixed with dimethyl sulfoxide (DMSO) to a final concentration of 10% (v/v). The strains were shock-frozen in liquid nitrogen and stored at -70°C.

5.1.4 Electroporation

For ectopic expression of *fimV*, a cumate-inducible expression cassette (*cymR*/P_{cym}), derived from *P. putida* F1, was inserted into the vector pBBR1-MCS2. 2 ml of stationary-phase cultures were harvested and washed twice with 300 mM sorbitol. Subsequently, approximately 200 ng of plasmid DNA were introduced into the cells by electroporation using the following parameters: 2.5 kV voltage, 25 µF capacitance, and 200 Ω resistance. After electroporation, cells were recovered for 2 h at 30°C, followed by plating on LB agar plates supplemented with appropriate antibiotics (Table 9) and incubation overnight at 30°C. Expression of *fimV* was induced by adding cumate to a final concentration of 2 mM.

5.1.5 Conjugation and homologous recombination

Conjugation was performed to introduce pNPTS138-R6KT into *S. putrefaciens* or *P. putida* cells. First, 1 µl of the respective pNPTS138-R6KT plasmid was transformed into 50 µl *E. coli* WM3064. For mating, 2 ml of each *E. coli* WM3064 culture carrying the plasmid and the respective *S. putrefaciens* or *P. putida* recipient culture were harvested, washed twice with LB medium and pelleted by centrifugation at 9,000 x g for 3 min. The washed cultures were combined to a final volume of 200 µl and spotted onto LB agar plates supplemented with DAP to support growth of the DAP-auxotrophic donor strain WM3064. Plates were incubated overnight at 30°C. The following day, cells were washed twice with LB medium to remove DAP and resuspended in 1 ml LB. Dilutions (1:10 and 1:100) were plated onto LB-Kan plates and incubated overnight at 30°C. Subsequently,

kanamycin-resistant colonies were restreaked sequentially onto LB-sucrose and LB-Kan plates using the same toothpick and incubated overnight at 30°C. From these plates, four kanamycin-resistant and sucrose-sensitive colonies were inoculated into 10 ml LB medium and grown for 3.5 hours at 30°C with constant shaking at 180 rpm. Cultures were diluted 1:10 and 1:100 and 100 µl of each dilution was plated onto LB-sucrose plates, followed by incubation overnight at 30°C (for *S. putrefaciens*) or 48 h at room temperature (for *P. putida*). Colonies were again restreaked sequentially onto LB-Kan and LB-sucrose plates and incubated overnight at 30°C. Kanamycin-sensitive and sucrose-resistant colonies were screened by Taq PCR to verify the correct genotype.

5.1.6 Growth experiments

To investigate growth behavior, strains were diluted in fresh LB medium or M9 minimal medium, supplemented with different carbon sources (0.4% glucose, 0.4% fructose, or 5 mM each of L-arginine and L-glutamine) to an OD_{600} of 0.02. Cultures were incubated at 30°C for 48 h in an Epoch2 microplate reader (BioTek) with continuous shaking, and optical density at 600 nm was measured every 30 min.

5.1.7 Motility assays

For swimming motility assays, 2 µl of exponentially growing cultures were spotted onto 0.25% LB soft-agar plates (select agar, Invitrogen). Where required, antibiotics were added to the agar (Table 9). Subsequently, plates were incubated at 30°C for 18 h.

Pilus-mediated surface motility assays were performed on agar surfaces as described previously [100]. Briefly, 2 µl of stationary-phase cultures were spotted onto 0.5% PG-agar plates (0.5% Difco agar, 0.5% Proteose Peptone No. 3, 0.2% glucose (w/v)) and incubated for 48 h at 25°C. After incubation, cells from the edge of the motile zone were subsequently transferred onto fresh PG-agar plates and incubated for an additional 24 h at 25°C.

The protocol established for twitching assays in *P. aeruginosa* was followed for the analysis of putative twitching motility in *P. putida* [233]. Stationary-phase cultures were adjusted to an OD_{600} of 1.5. Plates containing 1% LB-agar (Select Agar, Invitrogen) were pierced with a sterile Pasteur pipette, and 1 µl of the adjusted culture was inoculated at the bottom of the plates. After incubation of the plates for 24 h at 30°C, the agar was removed, and twitching zones were stained with 0.5% (w/v) crystal violet for 30 min. To remove unbound stain, plates were carefully washed with water and air-dried at room temperature.

Strains that were compared were always inoculated on the same plate to ensure direct comparability. Swimming and twitching zones were quantified using ImageJ. All plates were documented using an Epson V700 photo scanner.

5.1.8 Transmission electron microscopy

Transmission electron microscopy was carried out with kind support of Anke Treuner-Lange at the Max-Planck-Institute in Marburg.

For transmission electron microscopy using negative staining, bacterial cells were obtained either from exponentially growing liquid cultures or directly from PG-agar plates. For samples derived from liquid cultures, 10 µl of the cell suspension were applied to glow-discharged Formvar/carbon-coated copper grids (300 mesh) and incubated for 15 min to allow cell attachment. For plate-grown cells, grids were briefly placed on the agar surface for transfer of cells. Excess liquid was removed, and grids were washed three times with distilled water before staining with 2% uranyl acetate for 30 sec. After air-drying, samples were analyzed using a JEM-1400 transmission electron microscope (JEOL), operated at 100 kV.

5.1.9 Staining of extracellular structures or membranes

To enable staining of flagellar filaments, a serine-to-cysteine substitution was introduced at position 267 of the *fliC* gene of *P. putida* ($FliC^{S267C}$). Alternatively, a threonine-to-cysteine substitution was introduced into the gene encoding the polar FlgE hook protein of *S. putrefaciens* ($FlgE^{T183C}$). Cells were harvested from exponentially growing cultures and handled with cut pipette tips to minimize shear stress on extracellular structures. The cultures were centrifuged at 1,200 x g for 5 min, and the pellet was resuspended in 1x PBS. The dye Alexa Fluor 488 C5-maleimide (Thermo Fisher Scientific) was added for staining, and the samples were incubated in the dark for approximately 20 min. Unbound dye was removed by washing the cells twice with 1x PBS. Labeled cells were subsequently analyzed by fluorescence microscopy as described below. When required, membranes were stained by incubating cells in PBS containing 5 µg/mL FM™ 4-64 (Thermo Fisher Scientific) for 5 min in the dark. Membrane staining was conducted by Marta Pulido-Sánchez at Universidad Pablo de Olavide in Seville.

5.1.10 Fluorescence microscopy

Fluorescence microscopy was employed to visualize fusion proteins as well as extracellular structures. Cells were spotted on 1x PBS agarose pads (select agar, Invitrogen). For fluorescence microscopy, a Leica DMI 6000 B inverted microscope equipped with a pco.edge sCMOS camera (PCO), a SPECTRA light engine (Lumencor), an HC PL APO 63x/1.4–0.6 objective (Leica), a custom

filter set (T495lpxr, ET525/50m; Chroma Technology), and VisiView software (Visitron Systems, Puchheim, Germany) was used.

Alternatively, confocal imaging was carried out on an Axio Observer7 microscope (Zeiss) with a CSU-W1 spinning disk module (Yokogawa), an α Plan-Apochromat 100x/1.46 Oil DIC M27 inverted objective (Zeiss), and a Prime 95B CMOS camera (Teledyne Photometrics), together with SlideBook 6 software. For confocal imaging, 488 nm and 514 nm laser lines were used for excitation, combined with 525/50 nm and 617/73 nm emission filters, respectively. Confocal fluorescence microscopy was conducted by Marta Pulido-Sánchez at Universidad Pablo de Olavide in Seville.

5.1.11 c-di-GMP reporter system

For measurements of intracellular c-di-GMP levels, the reporter plasmid HS-Bc3-5-AAV was used. This plasmid harbors three c-di-GMP-binding riboswitches (Bc3-5) that regulate expression of the red fluorescent protein TurboRFP [238]. In addition, the cyan fluorescent protein AmCyan is constitutively expressed and serves as an internal reference, allowing normalization for plasmid copy number and expression variability. To assess the reliability of the reporter system, linear regression analysis and calculation of the coefficient of determination (R^2) were used to evaluate the correlation between AmCyan and TurboRFP fluorescence, confirming proportional expression and proper normalization. In addition, linear regression was applied to test for a potential correlation between cell length and the normalized TurboRFP/AmCyan fluorescence ratio, thereby excluding cell size-dependent effects on the reporter output. Cells were harvested from exponentially growing cultures and analyzed by fluorescence microscopy as described above.

5.1.12 Yeast two-hybrid assay

Yeast two-hybrid analysis was conducted by Anita Dornes at Philipps University in Marburg to investigate protein-protein interactions *in vivo* [14].

To test for protein-protein interactions, plasmids encoding the prey proteins fused to the Gal4 activation domain and the FlhF bait protein, fused to the Gal4 DNA-binding domain were co-transformed into the reporter strain PJ69-4A (*MATa trp1-901 leu2-3,112 ura3-52 his3-200 gal4Δ gal80Δ LYS2::GAL1-HIS3 GAL2-ADE2 met2::GAL7-lacZ*) [298]. Representative transformants were spotted in 10-fold serial dilutions onto plates with synthetic complete media and without distinct amino acids: Leucine-Tryptophan (-LT), Histidine-Leucine-Tryptophan (-HLT; *HIS3* reporter), and Adenine-Leucine-Tryptophan (-ALT; *ADE2* reporter). Afterwards, plates were incubated at 30°C for 3 days. Growth on -HLT plates indicates weak to moderate protein-protein interactions, whereas growth on -ALT plates reflects relatively strong interactions.

5.1.13 Bacterial adenylate cyclase two-hybrid assay (BACTH)

Bacterial two-hybrid analysis was performed as previously described [297] to investigate protein-protein interactions *in vivo*. Plasmids encoding the proteins of interest, fused either N- or C-terminally to the T18 or T25 fragments of the catalytic domain of *Bordetella pertussis* adenylate cyclase were used. For transformation, 1 µl of each plasmid carrying the respective T18- and T25-fusion construct was co-transformed into 20 µl *E. coli* BTH101 competent cells. After recovery for 1 h at 30°C, cells were transferred to 5 ml of fresh LB medium supplemented with the appropriate antibiotics (Table 9) and incubated overnight at 30°C. The following day, cultures were spotted onto LB agar plates containing IPTG and X-Gal (Table 9). Plates were incubated for 24 h at 30°C, followed by an additional 24 h at 4°C before documentation. Blue colonies indicated protein-protein interactions, whereas white colonies indicated no detectable interaction.

5.1.14 Biofilm assay

To investigate Biofilm formation, stationary-phase cultures were diluted to an OD_{600} of 0.15 and 200 µl of the diluted cultures were transferred into each well of a 96-well plate. Plates were incubated for 24 h at 30°C under static conditions. After incubation, OD_{600} was measured to allow normalization for cell growth. Subsequently, 12 µl of crystal violet (0.5% w/v) were added to each well to stain the formed biofilms. Plates were incubated for 10 minutes at room temperature with gentle shaking. After uniform distribution of the crystal violet solution, wells were washed twice with ddH_2O to remove unbound dye. Finally, 100% ethanol was added to solubilize the bound crystal violet and plates were incubated for 5 minutes at room temperature or until the dye was completely dissolved. Absorbance was measured at 580 nm using a Tecan plate reader.

5.2 Molecular biology methods

5.2.1 Polymerase chain reaction

Polymerase chain reaction (PCR) was performed as previously described [299] either to generate DNA fragments suitable for insertion into vector backbones for conjugation or transformation (using Phusion polymerase) or to verify the presence of desired genotypic variants (using Taq polymerase). If appropriate, 1% DMSO was added to the PCR mixture (

Table 14). For Taq PCR, cell material was collected using a sterile toothpick and directly added to the PCR reaction as template.

Table 14. PCR mixture and programs.

Component	Phusion PCR	Taq PCR
ddH_2O	36.65 µl	20.7 µl
5x Reaction buffer	10 µl	2.5 µl
dNTPs	1 µl	0.5 µl
Forward primer (50 µM)	0.6 µl	0.15 µl
Reverse primer (50 µM)	0.6 µl	0.15 µl
Polymerase	0.25 µl	1 µl
Template	1 µl	cell template
Total volume	50 µl	25 µl

Cycle	Temperature	Time
1x	95°C Taq	5 min
	98°C Phusion	30 sec
30-35x	95°C Taq	30 sec
	98°C Phusion	30 sec
	55-65°C	30 sec
	72°C	15 sec - 5 min
1x	72°C	10 min

5.2.2 Agarose gel electrophoresis

Agarose gel electrophoresis was used to separate PCR-amplified DNA fragments according to their size [300]. For this purpose, 3 µl or 8 µl of amplified DNA (from Phusion or Taq PCR, respectively) were mixed with the appropriate amount of 5x DNA loading dye and loaded onto 1% (w/v) TBE agarose gels containing 0.05 µg/ml ethidium bromide or 0.5x GelRed® (Biotium), together with 5 µl GeneRuler™ 1kb (Thermo Fisher Scientific). Gels were run in 0.5x TBE buffer at 140 V for 20-30 min at room temperature. DNA fragments were visualized under UV illumination.

5.2.3 Purification and concentration determination of DNA

Plasmid DNA, PCR-amplified fragments, or chromosomal DNA were purified using E.Z.N.A Kits (Table 5). As a final step, DNA was eluted with ddH_2O at 60°C for 5-15 min. DNA concentrations were determined using a NanoDrop spectrophotometer.

5.2.4 Digestion of vector backbones

Vector backbones were linearized using FastDigest restriction enzymes according to the manufacturer's protocol. Linearized fragments were separated by size on an agarose gel, the desired fragment was excised and DNA was purified using an E.N.Z.A kit (Table 5) following the manufacturer's instructions.

5.2.5 Gibson assembly

Gibson Assembly [301] was used for cloning the plasmids listed in Table 12. DNA fragments were amplified by PCR and inserted into linearized vector backbones as described previously in 5.2.1 and 5.2.4. The required amounts of DNA were calculated using 25 ng of the vector backbone and the following formula:

$$Amount\ of\ insert\ DNA\ (ng) = \frac{vector\ (ng)\ x\ insert\ (bp)}{vector\ (bp)}\ x\ 10$$

If the size of the inserted PCR fragment exceeded 2,000 base pairs, the calculated amount was adjusted by multiplying by five instead of ten. The calculated DNA volumes were added to 15 µl

Gibson assembly master mix and adjusted to a final volume of 20 µl with ddH_2O. The assembly reaction was incubated for 1 h at 50 °C.

5.2.6 Transformation

For transformation into *E. coli*, either the complete Gibson assembly reaction or 1 µl of plasmid DNA was added to chemically competent cells and incubated on ice for 10 min. Cells were then heat-shocked at 42°C for 1 min and immediately returned on ice. Subsequently, 950 µl of LB medium was added, and the cells were allowed to recover for 1 h at 37°C with shaking at 600 rpm (30°C for BTH101 cells). After recovery, cells were centrifuged at 9,000 x g for 3 minutes, the supernatant was discarded and the pellet was resuspended in the remaining liquid. Cells were plated on LB agar plates, supplemented with antibiotics or other additives (Table 9) and incubated overnight at 37°C. The following day, selected colonies were screened for the correct genotype by Taq PCR as described previously in 5.2.1. Positive clones were transferred to long-term storage as described in section 5.1.3.

5.2.7 DNA sequencing

DNA sequencing was performed to verify correct ligation of constructs generated by Gibson assembly. Plasmid DNA (40-100 ng/µl) from the respective clones was submitted to Microsynth Seqlab GmbH (Göttingen, Germany) for Sanger sequencing.

5.2.8 Protein sampling and SDS-PAGE

Protein samples were separated by sodium dodecyl sulphate polyacrylamide gel electrophoresis (SDS-PAGE) as previously described [302]. Late-exponentially growing cells were harvested at an OD_{600} of 10 by centrifugation at 17,000 x g for 10 min. The supernatant was discarded, and the pellet was resuspended in 100 µl of 2x SDS sample buffer. Prior to loading, samples were boiled at 95°C for 10 min to denature proteins. Subsequently, 10 µl of each sample were loaded onto SDS polyacrylamide gels consisting of an 8% resolving gel and a 5% stacking gel together with 5 µl of BlueEye Prestained Protein Marker (Jena Bioscience, Table 15).

Table 15. SDS gel composition.

Component	5% stacking gel	8% resolving gel
ddH_2O	1.4 ml	2.4 ml
4x Upper buffer (pH 6.8)	625 µl	-
4x Lower buffer (pH 8.8)	-	1.25 ml
30% Acrylamide	413 µl	1.3 ml
10% APS (Ammonium peroxydisulfate)	25 µl	40 µl
TEMED (Tetrametyl ethylendiamine)	1.9 µl	3 µl

Electrophoresis was performed in 1x SDS running buffer at 200 V for approximately 1 h. Protein bands were visualized using Instant Blue Coomassie Protein Stain (Abcam). When required, gels were subsequently used for western blot analysis.

5.2.9 Western blot analysis

Western blot analysis was performed to assess the expression and stability of fusion proteins. Proteins separated by SDS-PAGE were transferred onto polyvinylidene difluoride (PVDF) membranes using a semi-dry blotting system. Prior to transfer, PVDF membranes were activated in 100% methanol for 30 sec, rinsed with ddH_2O, and equilibrated in 1x Western transfer buffer for 5 min. The activated membrane and SDS gel were assembled with two layers of three Whatman paper (soaked in 1x transfer buffer) on each side. Semi-dry transfer was conducted at 2 mA/cm^2 for 40 min. Following transfer, membranes were blocked overnight at 4°C in 5% (w/v) milk in 1x PBS-T. The next day, membranes were washed three times with 1x PBS-T and incubated with the primary antibody for 1.5 h at room temperature. After washing, membranes were incubated with alkaline phosphatase-conjugated secondary antibodies for 1 h. Following final washes, detection was carried out using CDP-Star chemiluminescent substrate (Roche, Switzerland) or SuperSignal™ West Pico PLUS substrate (Thermo Fisher Scientific). Chemiluminescent signals were recorded with either a Fusion-SL imager (Peqlab, Erlangen, Germany) or an ImageQuant™ LAS 4000 system (GE Healthcare).

5.2.10 Affinity chromatography and size-exclusion chromatography

Protein overproduction and cell lysis

For protein overexpression, *E. coli* BL21 carrying either pCDFDuet-1, pETDuet-1 or pTB146 encoding the proteins of interest were used. Exponentially growing cultures were induced with 1% (w/v) D-(+)-lactose monohydrate and incubated for 3 h at 37°C. Cells were subsequently harvested by centrifugation at 3,400 x g for 30 min at 4°C, the supernatant was discarded and cell pellets were stored at -70°C until further processing. The morning of the purification start, the cell pellets were carefully resuspended in lysis buffer (Table 7) on ice and lysed by sonication (Sonopuls Bandelin, 30 sec, cycle 6, power 60%) for at least 10 cycles. Cells were centrifuged for 30 min, 4°C at 14,000 x g and supernatant was filtered using 0.2 µm syringe filter before applying to ÄKTA chromatography system.

Affinity chromatography (AC)

For affinity chromatography, proteins were produced with either an N-terminal 6xHis tag or a MBP tag. For buffer compositions, see Table 7 in Materials section. Prior to purification, a 5 ml HisTrap HP or MBPTrap HP (Cytiva, USA) was connected to an ÄKTA pure25 chromatography system. Samples were loaded using a 150 ml Superloop (Cytiva, USA) in combination with an external

peristaltic pump. The purification program started with washing the column with 5 column volumes (CV) of ddH_2O at a flow rate of 5 ml/min, followed by equilibration with 5 CV of buffer A at the same flow rate. Protein samples were applied at a reduced flow rate of 1.5 ml/min to ensure efficient binding to the affinity matrix. After sample application, the column was washed with 6 CV buffer A at 5 ml/min to remove unbound proteins. Proteins bound to Ni-NTA column were eluted using a stepwise gradient consisting of 2 CV of buffer A containing 20% buffer B at 1 ml/min, followed by 4 CV of 50% buffer B and finally 2 CV 100% buffer B to ensure complete elution and removal of residual proteins. Proteins bound to the amylose matrix were eluted directly with 100% buffer B supplemented with 10 mM maltose. Eluted protein fractions were collected and stored at 4°C. After purification, the column was washed with 5 CV of ddH_2O and subsequently with 5 CV of 20% ethanol at 5 ml/min.

Size-exclusion chromatography (SEC)

After affinity chromatography, proteins were further purified regarding to their size. For size exclusion chromatography a Superdex Increase 10 300 gl (Cytiva, USA) was used. Protein fractions (500 µl) were manually loaded onto the ÄKTA chromatography system and eluted with 1 CV SEC buffer at a flow rate of 0.4 ml/min. Afterwards the column was washed with 1 CV SEC buffer at 4 ml/min. Eluted protein fractions were collected and stored at 4°C. All eluted fractions were checked for the presence of proteins using SDS-PAGE as described before (see 5.2.8).

5.2.11 *In vitro* downstream analyses of *S. putrefaciens* proteins

Following protein productions, purifications and analysis were conducted by Anita Dornes at Philipps University in Marburg [14].

Protein production and purification

Gene fragments encoding the proteins of interest were amplified by polymerase chain reaction and cloned into the pET24d vector (Novagen) via NcoI and XhoI restriction sites. Protein production was carried out in *E. coli* BL21 (DE3) (Novagen) grown in LB supplemented with 1.5% (w/v) D-(+)-lactose monohydrate for 16 h at 30°C. Cell pellets were resuspended in lysis buffer (20 mM Na-HEPES, pH 8.0; 250 mM NaCl; 10 mM $MgCl_2$; 10 mM KCl) at a ratio of 10 ml buffer per gram of cells and lysed using an M1-10L Microfluidizer (Microfluidics). The lysate was clarified by centrifugation at 125,000 x g for 30 min at 4°C, and the supernatant was applied to a 1 ml HisTrap HP column (Cytiva, USA). The column was washed with five CV of lysis buffer (40 mM imidazole, pH 8.0), and proteins were eluted with lysis buffer containing 500 mM imidazole (pH 8.0). Eluted proteins were concentrated to ~30 mg/ml using an Amicon Ultracel-10K centrifugal filter unit (Millipore) and further purified by size-exclusion chromatography on either an S75/26-60 or S200/26-60 column (Cytiva, USA) using the same buffer without imidazole.

Streptavidin-based pulldown assays

Pulldown assays were performed to investigate protein-protein interactions using StrepTagII. Cultures expressing StrepII-tagged proteins were combined with cultures expressing the corresponding His-tagged proteins (400 ml total) and lysed as described above. Lysates were incubated with 30 µl of MagStrep Strep-Tactin XT beads (IBA Life Sciences) for 30 min at 4°C with gentle rotation. After centrifugation (4,000 rpm, 5 min, 4°C), the supernatant was discarded, and the beads were washed three times with 500 µl of SEC buffer using a magnetic rack. Bound proteins were eluted with 200 µM D-Biotin in SEC buffer and analyzed using SDS-PAGE (section 5.2.8).

Crystallization and structure determination

Crystallization was performed using the sitting-drop method at 20°C, with 250 nl drops containing an equal mixture of 1 mM protein and the precipitant solution. Optimal crystals were obtained in 1.6 M sodium citrate at pH 6.5. Data were collected under cryogenic conditions at the P13 beamline, Deutsches Elektronen-Synchrotron (DESY, Hamburg, Germany). Data processing was carried out using XDS, and scaling was performed with XSCALE [303]. The structure was determined by molecular replacement using PHASER [304] with an AlphaFold-generated FlhF model [305]. Manual model building was performed in COOT [306], and refinement was carried out using the PHENIX version 1.18.2 [307].

5.2.12 *In vitro* downstream analyses of *P. putida* FimV

Following protein purifications, peptidoglycan preparations and analysis were conducted by Marta Pulido-Sánchez at Universidad Pablo de Olavide in Seville [231].

Protein expression and purification

Staionary-phase cultures were diluted to an OD_{600} of 0.01 and grown to an OD_{600} of 0.3. Protein expression was induced, where appropriate, upon addition of 2 mM sodium salicylate. At an OD_{600} of 1, cells were harvested by centrifugation (5,000 x g, 4°C, 15 min) and resuspended in buffer A (20 mM Tris-HCl, pH 8.0; 500 mM NaCl; 1% Nonidet P-40). Cells were lysed by sonication, and the soluble fraction was incubated overnight at 4°C with GFP-Trap® Agarose beads (ChromoTek), which were previously equilibrated in buffer A. Subsequently, beads were washed 12 times with buffer A without Nonidet P-40. Bound proteins were eluted by vortexing the beads in 200 mM glycine (pH 2.5) for 1 min. The supernatant was collected into a fresh tube and immediately neutralized with 200 mM Tris-HCl (pH 8.0).

Co-precipitation assays

Peptidoglycan sacculi from *E. coli* and *P. putida* were isolated as described previously [308]. 5 µg of purified protein were incubated with 2 mg of sacculi in PBS on ice for 2 h. Proteins present in both the pellet and soluble fractions were subsequently analyzed by western blot.

5.3 Bioinformatic methods

5.3.1 Data analysis

Microscopic and swimming images were analyzed using ImageJ (v1.54p) with the MicrobeJ plugin [309], if necessary. Growth experiments were performed using the software Gen5 3.10. Graph creation and statistics were done using Prism 10.4.2 (GraphPad software) and Affinity Designer v1.10 (Serif). Foci intensity or cell length measurements were done using BacStalk 1.8stable [310].

5.3.2 Prediction and alignment tools

AlphaFold predictions were created with the AlphaFold Monomer v2.0 pipeline [311,312] or with AlphaFold3 [234]. To assess the confidence and accuracy of the AlphaFold3 structure predictions, the metrics predicted Local Distance Difference Test (pLDDT), predicted Template Modeling score (pTM) and interface predicted Template Modeling score (ipTM) were used.

The pLDDT score provides a per-residue confidence estimate of the predicted structure (0-100), with higher values indicating higher local structural accuracy, whereas low pLDDT scores suggest flexible or poorly resolved regions. The pLDDT score was calculated as the mean of all atom-wise pLDDT values provided by AlphaFold3. The pTM score reflects the confidence in the overall fold and domain arrangement of the predicted structure (0-1), with higher values indicating greater confidence in the global structural organization. The ipTM score assesses the confidence of predicted protein-protein interfaces in multimeric models and, similar to pTM, ranges from 0 to 1, with higher values reflecting increased confidence in the predicted interaction interfaces between subunits.

For identification of homologous proteins, the Basis Local Alignment Search Tool (BLAST) from NCBI was used [313].

For generation of protein alignments, the UniProt alignment tool (UniProtKB) was used [314].

6. References

1. Raina, J.B., Fernandez, V., Lambert, B., Stocker, R., and Seymour, J.R. (2019). The role of microbial motility and chemotaxis in symbiosis. Nat. Rev. Microbiol. *17*, 284–294. 10.1038/s41579-019-0182-9.
2. Wadhwa, N., and Berg, H.C. (2022). Bacterial motility: machinery and mechanisms. Nat. Rev. Microbiol. *20*, 161–173. 10.1038/s41579-021-00626-4.
3. Huttenhower, C., Gevers, D., Knight, R., Abubucker, S., Badger, J.H., Chinwalla, A.T., Creasy, H.H., Earl, A.M., Fitzgerald, M.G., Fulton, R.S., *et al.* (2012). Structure, function and diversity of the healthy human microbiome. Nature *486*, 207–214. 10.1038/nature11234.
4. Ochman, H., and Moran, N.A. (2001). Genes Lost and Genes Found: Evolution of Bacterial Pathogenesis and Symbiosis. Science (1979). *292*, 1096–1098.
5. Lane, M.C., Lockatell, V., Monterosso, G., Lamphier, D., Weinert, J., Hebel, J.R., Johnson, D.E., and Mobley, H.L.T. (2005). Role of motility in the colonization of uropathogenic *Escherichia coli* in the urinary tract. Infect. Immun. *73*, 7644–7656. 10.1128/IAI.73.11.7644-7656.2005.
6. Ottemann, K.M., and Lowenthal, A.C. (2002). *Helicobacter pylori* uses motility for initial colonization and to attain robust infection. Infect. Immun. *70*, 1984–1990. 10.1128/IAI.70.4.1984-1990.2002.
7. Henrichsen, J. (1972). Bacterial Surface Translocation: a Survey and a Classification. Bacteriol. Rev. *36*, 478–503.
8. Jarrell, K.F., and McBride, M.J. (2008). The surprisingly diverse ways that prokaryotes move. Nat. Rev. Microbiol. *6*, 466–476. 10.1038/nrmicro1900.
9. Chevance, F.F.V., and Hughes, K.T. (2008). Coordinating assembly of a bacterial macromolecular machine. Nat. Rev. Microbiol. *6*, 455–465. 10.1038/nrmicro1887.
10. Kazmierczak, B.I., and Hendrixson, D.R. (2013). Spatial and numerical regulation of flagellar biosynthesis in polarly flagellated bacteria. Mol. Microbiol. *88*, 655–663. 10.1111/mmi.12221.
11. Nuijten, P.J.M., Van Asten, F.J.A.M., Gaastra, W., and Van Der Zeijst, B.A.M. (1990). Structural and functional analysis of two *Campylobacter jejuni* flagellin genes. Journal of Biological Chemistry *265*, 17798–17804. 10.1016/s0021-9258(18)38234-6.
12. Hintsche, M., Waljor, V., Großmann, R., Kühn, M.J., Thormann, K.M., Peruani, F., and Beta, C. (2017). A polar bundle of flagella can drive bacterial swimming by pushing, pulling, or coiling around the cell body. Sci. Rep. *7*. 10.1038/s41598-017-16428-9.
13. Turner, L., Ryu, W.S., and Berg, H.C. (2000). Real-Time Imaging of Fluorescent Flagellar Filaments. J. Bacteriol. *182*, 2793–2801.
14. Dornes, A., Schmidt, L.M., Mais, C.N., Hook, J.C., Pané-Farré, J., Kressler, D., Thormann, K., and Bange, G. (2024). Polar confinement of a macromolecular machine by an SRP-type GTPase. Nat. Commun. *15*. 10.1038/s41467-024-50274-4.

15. Bubendorfer, S., Held, S., Windel, N., Paulick, A., Klingl, A., and Thormann, K.M. (2012). Specificity of motor components in the dual flagellar system of *Shewanella putrefaciens* CN-32. Mol. Microbiol. *83*, 335–350. 10.1111/j.1365-2958.2011.07934.x.
16. Kühn, M.J., Schmidt, F.K., Eckhardt, B., and Thormann, K.M. (2017). Bacteria exploit a polymorphic instability of the flagellar filament to escape from traps. Proc. Natl. Acad. Sci. U. S. A. *114*, 6340–6345. 10.1073/pnas.1701644114.
17. Kühn, M.J., Edelmann, D.B., and Thormann, K.M. (2022). Polar flagellar wrapping and lateral flagella jointly contribute to *Shewanella putrefaciens* environmental spreading. Environ. Microbiol. *24*, 5911–5923. 10.1111/1462-2920.16107.
18. Bubendorfer, S., Koltai, M., Rossmann, F., Sourjik, V., and Thormann, K.M. (2014). Secondary bacterial flagellar system improves bacterial spreading by increasing the directional persistence of swimming. Proc. Natl. Acad. Sci. U. S. A. *111*, 11485–11490. 10.1073/pnas.1405820111.
19. Nakamura, S. (2020). Spirochete flagella and motility. Biomolecules *10*, 1–16. 10.3390/biom10040550.
20. Sultan, S.Z., Manne, A., Stewart, P.E., Bestor, A., Rosa, P.A., Charon, N.W., and Motaleba, M.A. (2013). Motility is crucial for the infectious life cycle of *Borrelia burgdorferi*. Infect. Immun. *81*, 2012–2021. 10.1128/IAI.01228-12.
21. Charon, N.W., Cockburn, A., Li, C., Liu, J., Miller, K.A., Miller, M.R., Motaleb, M.A., and Wolgemuth, C.W. (2012). The unique paradigm of spirochete motility and chemotaxis. Annu. Rev. Microbiol. *66*, 349–370. 10.1146/annurev-micro-092611-150145.
22. Minamino, T., and Imada, K. (2015). The bacterial flagellar motor and its structural diversity. Trends Microbiol. *23*, 267–274. 10.1016/j.tim.2014.12.011.
23. Minamino, T. (2014). Protein export through the bacterial flagellar type III export pathway. Biochim. Biophys. Acta *1843*, 1642–1648. 10.1016/j.bbamcr.2013.09.005.
24. Liu, R., and Ochman, H. (2007). Stepwise formation of the bacterial flagellar system. PNAS *104*, 7116–7121.
25. Francis, N.R., Sosinsky, G.E., Thomas, D., and DeRosier, D.J. (1994). Isolation, characterization and structure of the bacterial flagellar motors containing the switch complex. J. Mol. Biol. *235*, 1261–1270.
26. Johnson, S., Deme, J.C., Furlong, E.J., Caesar, J.J.E., Chevance, F.F.V., Hughes, K.T., and Lea, S.M. (2024). Structural basis of directional switching by the bacterial flagellum. Nat. Microbiol. *9*, 1282–1292. 10.1038/s41564-024-01630-z.
27. Johnson, S., Furlong, E.J., Deme, J.C., Nord, A.L., Caesar, J.J.E., Chevance, F.F.V., Berry, R.M., Hughes, K.T., and Lea, S.M. (2021). Molecular structure of the intact bacterial flagellar basal body. Nat. Microbiol. *6*, 712–721. 10.1038/s41564-021-00895-y.

28. Johnson, S., Fong, Y.H., Deme, J.C., Furlong, E.J., Kuhlen, L., and Lea, S.M. (2020). Symmetry mismatch in the MS-ring of the bacterial flagellar rotor explains the structural coordination of secretion and rotation. Nat. Microbiol. *5*, 966–975. 10.1038/s41564-020-0703-3.
29. Manson, M.D., Tedesco, P., Berg, H.C., Haroldt, F.M., and Van Der Drift, C. (1977). A protonmotive force drives bacterial flagella. PNAS *74*, 3060–3064.
30. Silverman, M., Matsumura, P., and Simon, M. (1976). The identification of the mot gene product with *Escherichia coli*-lambda hybrids. PNAS *73*, 3126–3130.
31. Dean, G.E., Macnab, R.M., Stader, J., Matsumura, P., and Burks, C. (1984). Gene Sequence and Predicted Amino Acid Sequence of the *motA* Protein, a Membrane-Associated Protein Required for Flagellar Rotation in *Escherichia coli*. J. Bacteriol. *159*, 991–999.
32. Stader, J., Matsumura, P., Vacante, D., Dean, G.E., and Macnab, R.M. (1986). Nucleotide Sequence of the *Escherichia coli motB* Gene and Site-Limited Incorporation of Its Product into the Cytoplasmic Membrane. J. Bacteriol. *166*, 244–252.
33. Wu, Z., Tian, M., Zhang, R., and Yuan, J. (2021). Dynamics of the Two Stator Systems in the Flagellar Motor of *Pseudomonas aeruginosa* Studied by a Bead Assay. Appl. Environ. Microbiol. *87*, e01674-21.
34. Asai, Y., Yakushi, T., Kawagishi, I., and Homma, M. (2003). Ion-coupling determinants of Na+-driven and H+-driven flagellar motors. J. Mol. Biol. *327*, 453–463. 10.1016/S0022-2836(03)00096-2.
35. Asai, Y., Kojima, S., Kato, H., Nishioka, N., Kawagishi, I., and Homma, M. (1997). Putative Channel Components for the Fast-Rotating Sodium-Driven Flagellar Motor of a Marine Bacterium. J. Bacteriol. *179*, 5104–5110.
36. Li, N., Kojima, S., and Homma, M. (2011). Sodium-driven motor of the polar flagellum in marine bacteria *Vibrio*. Genes to Cells *16*, 985–999. 10.1111/j.1365-2443.2011.01545.x.
37. Akiba, T., Yoshimura, H., and Namba, K. (1991). Monolayer Crystallization of Flagellar L-P Rings by Sequential Addition and Depletion of Lipid. Science (1979). *252*, 1544–1546.
38. Yamaguchi, T., Makino, F., Miyata, T., Minamino, T., Kato, T., and Namba, K. (2021). Structure of the molecular bushing of the bacterial flagellar motor. Nat. Commun. *12*. 10.1038/s41467-021-24715-3.
39. Zhu, S., Nishikino, T., Kojima, S., Homma, M., and Liu, J. (2018). The *Vibrio* H-Ring facilitates the outer membrane penetration of the polar sheathed flagellum. J. Bacteriol. *200*, e00387-18. 10.1128/JB.00387-18.
40. Zhu, S., Nishikino, T., Takekawa, N., Terashima, H., Kojima, S., Imada, K., Homma, M., and Liu, J. (2020). *In situ* structure of the *Vibrio* polar flagellum reveals a distinct outer membrane complex and its specific interaction with the stator. J. Bacteriol. *202*, e00592-19. 10.1128/JB.00592-19.

41. Magariyama, Y., Sugiyama, S., Muramoto, K., Maekawa, Y., Kawagishi, K., Imae, Y., and Kudo, S. (1994). Very fast flagellar rotation. Nature *371*, 752.
42. Kudo, S., Magariyama, Y., and Aizawa, S.-I. (1990). Abrupt changes in flagellar rotation observed by laser dark-field microscopy. Nature *346*, 677–680.
43. Blocker, A., Komoriya, K., and Aizawa, S.-I. (2003). Type III secretion systems and bacterial flagella: Insights into their function from structural similarities. PNAS *100*, 3027–3030.
44. Minamino, T., Imada, K., and Namba, K. (2008). Mechanisms of type III protein export for bacterial flagellar assembly. Mol. Biosyst. *4*, 1105–1115. 10.1039/b808065h.
45. Yonekura, K., Maki-Yonekura, S., and Namba, K. (2003). Complete atomic model of the bacterial flagellar filament by electron cryomicroscopy. Nature *424*, 643–650.
46. Samatey, F.A., Matsunami, H., Imada, K., Nagashima, S., Shaikh, T.R., Thomas, D.R., Chen, J.Z., Derosier, D.J., Kitao, A., and Namba, K. (2004). Structure of the bacterial flagellar hook and implication for the molecular universal joint mechanism. Nature *431*, 1062–1068.
47. Shaikh, T.R., Thomas, D.R., Chen, J.Z., Samatey, F.A., Matsunami, H., Imada, K., Namba, K., and DeRosier, D.J. (2004). A partial atomic structure for the flagellar hook of *Salmonella typhimurium*. PNAS *102*, 1023–1028.
48. Hirano, T., Yamaguchi, S., Oosawa, K., and Aizawa, S.-I. (1994). Roles of FliK and FlhB in Determination of Flagellar Hook Length in *Salmonella typhimurium*. J. Bacteriol. *176*, 5439–5449.
49. Doetsch, R.N., and Sjoblad, R.D. (1980). Flagellar structure and function in eubacteria. Ann. Rev. Microbial *34*, 69–108.
50. Zhuang, X.Y., and Lo, C.J. (2020). Construction and loss of bacterial flagellar filaments. Biomolecules *10*, 1–14. 10.3390/biom10111528.
51. Bouteiller, M., Dupont, C., Bourigault, Y., Latour, X., Barbey, C., Konto-Ghiorghi, Y., and Merieau, A. (2021). *Pseudomonas* flagella: Generalities and specificities. Int. J. Mol. Sci. *22*, 1–28. 10.3390/ijms22073337.
52. Kühn, M.J., Schmidt, F.K., Farthing, N.E., Rossmann, F.M., Helm, B., Wilson, L.G., Eckhardt, B., and Thormann, K.M. (2018). Spatial arrangement of several flagellins within bacterial flagella improves motility in different environments. Nat. Commun. *9*, 1–12. 10.1038/s41467-018-07802-w.
53. Echazarreta, M.A., and Klose, K.E. (2019). *Vibrio* flagellar synthesis. Front. Cell. Infect. Microbiol. *9*, 1–11. 10.3389/fcimb.2019.00131.
54. Guo, W., Zhang, S., Park, J.H., Stanton, V., Asp, M., Herrera, H., Tai, J.S.B., Yue, J., Wang, J., Guo, J., *et al.* (2025). Structures of the sheathed flagellum reveal mechanisms of assembly and rotation in *Vibrio cholerae*. Nat. Microbiol. *10*, 3305–3314. 10.1038/s41564-025-02161-x.

55. Homma, M., and Iino, T. (1985). Locations of Hook-Associated Proteins in Flagellar Structures of *Salmonella typhimurium*. J. Bacteriol. *162*, 183–189.

56. Ikeda, T., Asakura, S., and Kamiya, R. (1985). “Cap” on the Tip of *Salmonella* Flagella. J. Mol. Biol. *184*, 735–737.

57. Aldridge, P., and Hughes, K.T. (2002). Regulation of flagellar assembly. Curr. Opin. Microbiol. *5*, 160–165.

58. McCarter, L.L. (2006). Regulation of flagella. Curr. Opin. Microbiol. *9*, 180–186. 10.1016/j.mib.2006.02.001.

59. Dasgupta, N., Wolfgang, M.C., Goodman, A.L., Arora, S.K., Jyot, J., Lory, S., and Ramphal, R. (2003). A four-tiered transcriptional regulatory circuit controls flagellar biogenesis in *Pseudomonas aeruginosa*. Mol. Microbiol. *50*, 809–824. 10.1046/j.1365-2958.2003.03740.x.

60. Chilcott, G.S., and Hughes, K.T. (2000). Coupling of Flagellar Gene Expression to Flagellar Assembly in *Salmonella enterica* Serovar Typhimurium and *Escherichia coli*. Microbiology and Molecular Biology Reviews *64*, 694–708.

61. Blagotinsek, V., Schwan, M., Steinchen, W., Mrusek, D., Hook, J.C., Rossmann, F., Freibert, S.A., Kratzat, H., Murat, G., Kressler, D., *et al.* (2020). An ATP-dependent partner switch links flagellar C-ring assembly with gene expression. PNAS *117*, 20826–20835. 10.1073/pnas.2006470117/-/DCSupplemental.

62. Lowe, G., Meister, M., and Berg, H.C. (1987). Rapid rotation of flagellar bundles in swimming bacteria. Nature *325*, 637–640.

63. Lambert, C., Evans, K.J., Till, R., Hobley, L., Capeness, M., Rendulic, S., Schuster, S.C., Aizawa, S.I., and Sockett, R.E. (2006). Characterizing the flagellar filament and the role of motility in bacterial prey-penetration by *Bdellovibrio bacteriovorus*. Mol. Microbiol. *60*, 274–286. 10.1111/j.1365-2958.2006.05081.x.

64. Berg, H.C., and Brown, D.A. (1972). Chemotaxis in *Escherichia coli* analysed by Three-dimensional Tracking. Nature *239*, 500–504.

65. Xie, L., Altindal, T., Chattopadhyay, S., and Wu, X.-L. (2011). Bacterial flagellum as a propeller and as a rudder for efficient chemotaxis. PNAS *108*, 2246–2251. 10.1073/pnas.1011953108/-/DCSupplemental.

66. Harshey, R.M. (2003). Bacterial Motility on a Surface: Many Ways to a Common Goal. Annu. Rev. Microbiol. *57*, 249–273. 10.1146/annurev.micro.57.030502.091014.

67. Kearns, D.B. (2010). A field guide to bacterial swarming motility. Nat. Rev. Microbiol. *8*, 634–644. 10.1038/nrmicro2405.

68. Caiazza, N.C., Shanks, R.M.Q., and O’Toole, G.A. (2005). Rhamnolipids modulate swarming motility patterns of *Pseudomonas aeruginosa*. J. Bacteriol. *187*, 7351–7361. 10.1128/JB.187.21.7351-7361.2005.

69. Zhang, R., Turner, L., and Berg, H.C. (2010). The upper surface of an *Escherichia coli* swarm is stationary. Proc. Natl. Acad. Sci. U. S. A. *107*, 288–290. 10.1073/pnas.0912804107.

70. Harshey, R.M., and Matsuyamat, T. (1994). Dimorphic transition in *Escherichia coli* and *Salmonella typhimurium*: Surface-induced differentiation into hyperflagellate swarmer cells. Dev. Biol. *91*, 8631–8635.

71. Burrows, L.L. (2012). *Pseudomonas aeruginosa* twitching motility: Type IV pili in action. Annu. Rev. Microbiol. *66*, 493–520. 10.1146/annurev-micro-092611-150055.

72. Bradley, D.E. (1972). Evidence for the retraction of *Pseudomonas aeruginosa* RNA phage pili. Biochem. Biophys. Res. Commun. *47*, 142–149.

73. Semmler, A.B.T., Whitchurch, C.B., and Mattick, J.S. (1999). A re-examination of twitching motility in *Pseudomonas aeruginosa*. Microbiology (N. Y). *145*, 2863–2873.

74. Huang, B., Whitchurch, C.B., and Mattick, J.S. (2003). FimX, a Multidomain Protein Connecting Environmental Signals to Twitching Motility in *Pseudomonas aeruginosa*. J. Bacteriol. *185*, 7068–7076. 10.1128/JB.185.24.7068-7076.2003.

75. Mattick, J.S. (2002). Type IV pili and twitching motility. Annu. Rev. Microbiol. *56*, 289–314. 10.1146/annurev.micro.56.012302.160938.

76. Berry, J.L., and Pelicic, V. (2015). Exceptionally widespread nanomachines composed of type IV pilins: The prokaryotic Swiss Army knives. FEMS Microbiol. Rev. *39*, 134–154. 10.1093/femsre/fuu001.

77. Hospenthal, M.K., Costa, T.R.D., and Waksman, G. (2017). A comprehensive guide to pilus biogenesis in Gram-negative bacteria. Nat. Rev. Microbiol. *15*, 365–379. 10.1038/nrmicro.2017.40.

78. Craig, L., Forest, K.T., and Maier, B. (2019). Type IV pili: dynamics, biophysics and functional consequences. Nat. Rev. Microbiol. *17*, 429–440. 10.1038/s41579-019-0195-4.

79. Pelicic, V. (2008). Type IV pili: *e pluribus unum*? Mol. Microbiol. *68*, 827–837. 10.1111/j.1365-2958.2008.06197.x.

80. O'Toole, G.A., and Kolter, R. (1998). Flagellar and twitching motility are necessary for *Pseudomonas aeruginosa* biofilm development. Mol. Microbiol. *30*, 295–304. 10.1046/j.1365-2958.1998.01062.x.

81. Conrad, J.C., Gibiansky, M.L., Jin, F., Gordon, V.D., Motto, D.A., Mathewson, M.A., Stopka, W.G., Zelasko, D.C., Shrout, J.D., and Wong, G.C.L. (2011). Flagella and pili-mediated near-surface single-cell motility mechanisms in *P. aeruginosa*. Biophys. J. *100*, 1608–1616. 10.1016/j.bpj.2011.02.020.

82. Koo, J., Lamers, R.P., Rubinstein, J.L., Burrows, L.L., and Howell, P.L. (2016). Structure of the *Pseudomonas aeruginosa* Type IVa Pilus Secretin at 7.4 Å. Structure *24*, 1778–1787. 10.1016/j.str.2016.08.007.

83. Koo, J., Tammam, S., Ku, S.Y., Sampaleanu, L.M., Burrows, L.L., and Howell, P.L. (2008). PilF is an outer membrane lipoprotein required for multimerization and localization of the *Pseudomonas aeruginosa* type IV pilus secretin. J. Bacteriol. *190*, 6961–6969. 10.1128/JB.00996-08.

84. Chiang, P., Habash, M., and Burrows, L.L. (2005). Disparate subcellular localization patterns of *Pseudomonas aeruginosa* type IV pilus ATPases involved in twitching motility. J. Bacteriol. *187*, 829–839. 10.1128/JB.187.3.829-839.2005.

85. Takhar, H.K., Kemp, K., Kim, M., Howell, P.L., and Burrows, L.L. (2013). The platform protein is essential for type IV pilus biogenesis. Journal of Biological Chemistry *288*, 9721–9728. 10.1074/jbc.M113.453506.

86. Burrows, L.L. (2005). Weapons of mass retraction. Mol. Microbiol. *57*, 878–888. 10.1111/j.1365-2958.2005.04703.x.

87. Adams, D.W., Pereira, J.M., Stoudmann, C., Stutzmann, S., and Blokesch, M. (2019). The type IV pilus protein PilU functions as a PilT-dependent retraction ATPase. PLoS Genet. *15*, e1008393. 10.1371/journal.pgen.1008393.

88. Ayers, M., Sampaleanu, L.M., Tammam, S., Koo, J., Harvey, H., Howell, P.L., and Burrows, L.L. (2009). PilM/N/O/P Proteins Form an Inner Membrane Complex That Affects the Stability of the *Pseudomonas aeruginosa* Type IV Pilus Secretin. J. Mol. Biol. *394*, 128–142. 10.1016/j.jmb.2009.09.034.

89. Tammam, S., Sampaleanu, L.M., Koo, J., Manoharan, K., Daubaras, M., Burrows, L.L., and Howell, P.L. (2013). PilMNOPQ from the *Pseudomonas aeruginosa* type IV pilus system form a transenvelope protein interaction network that interacts with PilA. J. Bacteriol. *195*, 2126–2135. 10.1128/JB.00032-13.

90. Nguyen, Y., Sugiman-Marangos, S., Harvey, H., Bell, S.D., Charlton, C.L., Junop, M.S., and Burrows, L.L. (2015). *Pseudomonas aeruginosa* minor pilins prime type IVa pilus assembly and promote surface display of the PilY1 adhesin. Journal of Biological Chemistry *290*, 601–611. 10.1074/jbc.M114.616904.

91. Giltner, C.L., Nguyen, Y., and Burrows, L.L. (2012). Type IV Pilin Proteins: Versatile Molecular Modules. Microbiology and Molecular Biology Reviews *76*, 740–772. 10.1128/mmbr.00035-12.

92. Alm, R.A., and Mattick, J.S. (1997). Genes involved in the biogenesis and function of type-4 fimbriae in *Pseudomonas aeruginosa*. Gene *192*, 89–98.

93. Russell, M.A., and Darzins, A. (1994). The *pilE* gene product of *Pseudomonas aeruginosa*, required for pilus biogenesis, shares amino acid sequence identity with the N-termini of type 4 prepilin proteins. Mol. Microbiol. *13*, 973–985. 10.1111/j.1365-2958.1994.tb00489.x.

94. Nunn, D.N., and Lory, S. (1991). Product of the *Pseudomonas aeruginosa* gene *pilD* is a prepilin leader peptidase. PNAS *88*, 3281–3285.

95. Mattick, J.S., Whitchurch, C.B., and Alm, R.A. (1996). The molecular genetics of type-4 fimbriae in *Pseudomonas aeruginosa* -a review. Gene *179*, 147–155.

96. Darzins, A. (1993). The *pilG* Gene Product, Required for *Pseudomonas aeruginosa* Pilus Production and Twitching Motility, Is Homologous to the Enteric, Single-Domain Response Regulator CheY. J. Bacteriol. *175*, 5934–5944.

97. Darzins, A. (1995). The *Pseudomonas aeruginosa pilK* gene encodes a chemotactic methyltransferase (CheR) homologue that is translationally regulated. Mol. Microbiol. *15*, 703–717. 10.1111/j.1365-2958.1995.tb02379.x.

98. Darzins, A. (1994). Characterization of a *Pseudomonas aeruginosa* gene cluster involved in pilus biosynthesis and twitching motility: sequence similarity to the chemotaxis proteins of enterics and the gliding bacterium *Myxococcus xanthus*. Mol. Microbiol. *11*, 137–153. 10.1111/j.1365-2958.1994.tb00296.x.

99. Spormann, A.M. (1999). Gliding Motility in Bacteria: Insights from Studies of *Myxococcus xanthus*. Microbiology and Molecular Biology Reviews *63*, 621–641.

100. Matilla, M.A., Ramos, J.L., Duque, E., De Dios Alché, J., Espinosa-Urgel, M., and Ramos-González, M.I. (2007). Temperature and pyoverdine-mediated iron acquisition control surface motility of *Pseudomonas putida*. Environ. Microbiol. *9*, 1842–1850. 10.1111/j.1462-2920.2007.01286.x.

101. Porter, S.L., Wadhams, G.H., and Armitage, J.P. (2011). Signal processing in complex chemotaxis pathways. Nat. Rev. Microbiol. *9*, 153–165. 10.1038/nrmicro2505.

102. Wadhams, G.H., and Armitage, J.P. (2004). Making sense of it all: Bacterial chemotaxis. Nat. Rev. Mol. Cell Biol. *5*, 1024–1037. 10.1038/nrm1524.

103. Falke, J.J., and Hazelbauer, G.L. (2001). Transmembrane signaling in bacterial chemoreceptors. Trends Biochem. Sci. *26*, 257–265.

104. Hazelbauer, G.L., Falke, J.J., and Parkinson, J.S. (2008). Bacterial chemoreceptors: high-performance signaling in networked arrays. Trends Biochem. Sci. *33*, 9–19. 10.1016/j.tibs.2007.09.014.

105. Alexander, R.P., and Zhulin, I.B. (2007). Evolutionary genomics reveals conserved structural determinants of signaling and adaptation in microbial chemoreceptors. PNAS *104*, 2885–2890.

106. Maddock, J.R., and Shapiro, L. (1993). Polar Location of the Chemoreceptor Complex in the *Escherichia coli* Cell. Source: Science, New Series *259*, 1717–1723.

107. Briegel, A., Ortega, D.R., Tocheva, E.I., Wuichet, K., Li, Z., Chen, S., Müller, A., Iancu, C. V, Murphy, G.E., Dobro, M.J., *et al.* (2009). Universal architecture of bacterial chemoreceptor arrays. PNAS *106*, 17181–17186.

108. Morgan, D.G., Baumgartner, J.W., and Hazelbauer, G.L. (1993). Proteins Antigenically Related to Methyl-Accepting Chemotaxis Proteins of *Escherichia coli* Detected in a Wide Range of Bacterial Species. J. Bacteriol. *175*, 133–140.
109. Djordjevic, S., and Stock, A.M. (1998). Chemotaxis receptor recognition by protein methyltransferase CheR. Nat. Struct. Biol. *5*, 446–450.
110. García-Fontana, C., Reyes-Darias, J.A., Muñoz-Martínez, F., Alfonso, C., Morel, B., Ramos, J.L., and Krell, T. (2013). High specificity in CheR methyltransferase function. Journal of Biological Chemistry *288*, 18987–18999. 10.1074/jbc.M113.472605.
111. Li, J., Swanson, R. V, Simon, M.I., and Weis, R.M. (1995). The Response Regulators CheB and CheY Exhibit Competitive Binding to the Kinase CheA. Biochemistry *34*, 14626–14636.
112. Kehry, M.R., and Dahlquist, F.W. (1982). Adaptation in Bacterial Chemotaxis: CheB-Dependent Modification Permits Additional Methylations of Sensory Transducer Proteins. Cell *29*, 761–772.
113. Borczuk, A., Staub, A., and Stock, J. (1986). Demethylation of bacterial chemoreceptors is inhibited by attractant stimuli in the complete absence of the regulatory domain of the demethylating enzyme. Biochem. Biophys. Res. Commun. *141*, 918–923.
114. Hess, J.F., Bourret, R.B., and Simon, M.I. (1988). Histidine phosphorylation and phosphoryl group transfer in bacterial chemotaxis. Nature *336*, 139–143.
115. Anand, G.S., Goudreau, P.N., and Stock, A.M. (1998). Activation of Methylesterase CheB: Evidence of a Dual Role for the Regulatory Domain. Biochemistry *37*, 14038–14047.
116. Chang, Y., Zhang, K., Carroll, B.L., Zhao, X., Charon, N.W., Norris, S.J., Motaleb, M.A., Li, C., and Liu, J. (2020). Molecular mechanism for rotational switching of the bacterial flagellar motor. Nat. Struct. Mol. Biol. *27*, 1041–1047. 10.1038/s41594-020-0497-2.
117. Sarkar, M.K., Paul, K., and Blair, D. (2010). Chemotaxis signaling protein CheY binds to the rotor protein FliN to control the direction of flagellar rotation in *Escherichia coli*. Proc. Natl. Acad. Sci. U. S. A. *107*, 9370–9375. 10.1073/pnas.1000935107.
118. Welch, M., Oosawa, K., Aizawat, S.-I., and Eisenbach, M. (1993). Phosphorylation-dependent binding of a signal molecule to the flagellar switch of bacteria. Proc. Natl. Acad. Sci. U. S. A. *90*, 8787–8791.
119. Toker, A.S., and Macnab, R.M. (1997). Distinct Regions of Bacterial Flagellar Switch Protein FliM Interact with FliG, FliN and CheY. J. Mol. Biol. *273*, 623–634.
120. Mcevoy, M.M., Bren, A., Eisenbach, M., and Dahlquist, F.W. (1999). Identification of the Binding Interfaces on CheY for Two of its Targets, the Phosphatase CheZ and the Flagellar Switch Protein FliM. J. Mol. Biol. *289*, 1423–1433.
121. Parkinson, J.S., Hazelbauer, G.L., and Falke, J.J. (2015). Signaling and sensory adaptation in *Escherichia coli* chemoreceptors: 2015 update. Trends Microbiol. *23*, 257–266. 10.1016/j.tim.2015.03.003.

122. Porter, S.L., Wadhams, G.H., and Armitage, J.P. (2008). *Rhodobacter sphaeroides*: complexity in chemotactic signalling. Trends Microbiol. *16*, 251–260. 10.1016/j.tim.2008.02.006.

123. Hamer, R., Chen, P.-Y., Armitage, J.P., Reinert, G., and Deane, C.M. (2010). Computational inference and analysis of genetic regulatory networks via a supervised combinatorial-optimization pattern. BMC Syst. Biol. *4*, 1–19. 10.1186/1752-0509-4-3.

124. Wuichet, K., and Zhulin, I.B. (2010). Origins and diversification of a complex signal transduction system in prokaryotes. Sci. Signal. *3*, ra50. 10.1126/scisignal.2000724.

125. Schuster, S.C., Swanson, R. V., Alex, L.A., Bourret, R.B., and Simon, M.I. (1993). Assembly and function of a quaternary signal transduction complex monitored by surface plasmon resonance. Nature *365*, 343–347.

126. Bourret, R.B., Davagnino, J., and Simon, M.I. (1993). The Carboxy-Terminal Portion of the CheA Kinase Mediates Regulation of Autophosphorylation by Transducer and CheW. J. Bacteriol. *175*, 2097–2101.

127. Swanson, R. V., Bourret, R.B., and Simon, M.I. (1993). Intermolecular complementation of the kinase activity of CheA. Mol. Microbiol. *8*, 435–441. 10.1111/j.1365-2958.1993.tb01588.x.

128. Stewart, R.C., Jahreis, K., and Parkinson, J.S. (2000). Rapid phosphotransfer to CheY from a CheA protein lacking the CheY-binding domain. Biochemistry *39*, 13157–13165. 10.1021/bi001100k.

129. McEvoy, M.M., Muhandir, D.R., Kay, L.E., and Dahlquist, F.W. (1996). Structure and Dynamics of a CheY-Binding Domain of the Chemotaxis Kinase CheA Determined by Nuclear Magnetic Resonance Spectroscopy. Biochemistry *35*, 5633–5640.

130. Wu, Z., Tian, M., Fu, S., Chen, M., Zhang, R., and Yuan, J. (2025). Spatial integration of sensory input and motor output in *Pseudomonas aeruginosa* chemotaxis through colocalized distribution. Elife *13*. 10.7554/elife.97514.

131. Pulido-Sánchez, M., Leal-Morales, A., López-Sánchez, A., Cava, F., and Govantes, F. (2025). Spatial, temporal and numerical regulation of polar flagella assembly in *Pseudomonas putida*. Microbiol. Res. *292*. 10.1016/j.micres.2024.128033.

132. Rossmann, F., Brenzinger, S., Knauer, C., Dörrich, A.K., Bubendorfer, S., Ruppert, U., Bange, G., and Thormann, K.M. (2015). The role of FlhF and HubP as polar landmark proteins in *Shewanella putrefaciens* CN-32. Mol. Microbiol. *98*, 727–742. 10.1111/mmi.13152.

133. Schuhmacher, J.S., Thormann, K.M., and Bange, G. (2015). How bacteria maintain location and number of flagella? FEMS Microbiol. Rev. *39*, 812–822. 10.1093/femsre/fuv034.

134. Yamaichi, Y., Bruckner, R., Ringgaard, S., Möll, A., Cameron, D.E., Briegel, A., Jensen, G.J., Davis, B.M., and Waldor, M.K. (2012). A multidomain hub anchors the chromosome segregation and chemotactic machinery to the bacterial pole. Genes Dev. *26*, 2348–2360. 10.1101/gad.199869.112.

135. Ringgaard, S., Yang, W., Alvarado, A., Schirner, K., and Briegel, A. (2018). Chemotaxis Arrays in *Vibrio* Species and Their Intracellular Positioning by the ParC/ParP System. J. Bacteriol. *200*, e00793-17. 10.1128/JB.0079.

136. Buensuceso, R.N.C., Daniel-Ivad, M., Kilmury, S.L.N., Leighton, T.L., Harvey, H., Howell, P.L., and Burrows, L.L. (2017). Cyclic AMP-independent control of twitching motility in *Pseudomonas aeruginosa*. J. Bacteriol. *199*, e00188-17. 10.1128/JB.00188-17.

137. Altinoglu, I., Abriat, G., Carreaux, A., Torres-Sánchez, L., Poidevin, M., Krasteva, P.V., and Yamaichi, Y. (2022). Analysis of HubP-dependent cell pole protein targeting in *Vibrio cholerae* uncovers novel motility regulators. PLoS Genet. *18*, e1009991. 10.1371/journal.pgen.1009991.

138. Inclan, Y.F., Persat, A., Greninger, A., Von Dollen, J., Johnson, J., Krogan, N., Gitai, Z., and Engel, J.N. (2016). A scaffold protein connects type IV pili with the Chp chemosensory system to mediate activation of virulence signaling in *Pseudomonas aeruginosa*. Mol. Microbiol. *101*, 590–605. 10.1111/mmi.13410.

139. Wehbi, H., Portillo, E., Harvey, H., Shimkoff, A.E., Scheurwater, E.M., Howell, P.L., and Burrows, L.L. (2011). The peptidoglycan-binding protein FimV promotes assembly of the *Pseudomonas aeruginosa* type IV pilus secretin. J. Bacteriol. *193*, 540–550. 10.1128/JB.01048-10.

140. Garvey, K.J., Saedi, M.S., and Ito, J. (1986). Nudeotide sequence of *Bacillus* phage ϕ29 genes 14 and 15: homology of gene 15 with other phage lysozymes. Nucleic Acids Res. *14*, 10001–10008.

141. Buist, G., Steen, A., Kok, J., and Kuipers, O.P. (2008). LysM, a widely distributed protein motif for binding to (peptido)glycans. Mol. Microbiol. *68*, 838–847. 10.1111/j.1365-2958.2008.06211.x.

142. Akcapinar, G.B., Kappel, L., Sezerman, O.U., and Seidl-Seiboth, V. (2015). Molecular diversity of LysM carbohydrate-binding motifs in fungi. Curr. Genet. *61*, 103–113. 10.1007/s00294-014-0471-9.

143. Gough, C., Cottret, L., Lefebvre, B., and Bono, J.J. (2018). Evolutionary history of plant LysM receptor proteins related to root endosymbiosis. Front. Plant Sci. *9*. 10.3389/fpls.2018.00923.

144. Semmler, A.B.T., Whitchurch, C.B., Leech, A.J., and Mattick, J.S. (2000). Identification of a novel gene, *fimV*, involved in twitching motility in *Pseudomonas aeruginosa*. Microbiology (N. Y). *146*, 1321–1332.

145. Buensuceso, R.N.C., Nguyen, Y., Zhang, K., Daniel-Ivad, M., Sugiman-Marangos, S.N., Fleetwood, A.D., Zhulin, I.B., Junop, M.S., Lynne Howell, P., and Burrows, L.L. (2016). The conserved tetratricopeptide repeat-containing C-Terminal domain of *Pseudomonas aeruginosa* FimV is required for its cyclic AMP-dependent and -independent functions. J. Bacteriol. *198*, 2263–2274. 10.1128/JB.00322-16.

146. Leipe, D.D., Wolf, Y.I., Koonin, E. V., and Aravind, L. (2002). Classification and evolution of P-loop GTPases and related ATPases. J. Mol. Biol. *317*, 41–72. 10.1006/jmbi.2001.5378.

147. Veenendaal, A.K.J., Van Der Does, C., and Driessen, A.J.M. (2004). The protein-conducting channel SecYEG. Biochim. Biophys. Acta *1694*, 81–95. 10.1016/j.bbamcr.2004.02.009.

148. Grudnik, P., Bange, G., and Sinning, I. (2009). Protein targeting by the signal recognition particle. Biol. Chem. *390*, 775–782. 10.1515/BC.2009.102.

149. Dornes, A., Mais, C.N., and Bange, G. (2024). Structure of the GDP-bound state of the SRP GTPase FlhF. Acta Crystallogr. *80*, 53–58. 10.1107/S2053230X24000979.

150. Bange, G., Petzold, G., Wild, K., Parlitz, R.O., and Sinning, I. (2007). The crystal structure of the third signal-recognition particle GTPase FlhF reveals a homodimer with bound GTP. PNAS *104*, 13621–13625.

151. Bange, G., Petzold, G., Wild, K., and Sinning, I. (2007). Expression, purification and preliminary crystallographic characterization of FlhF from *Bacillus subtilis*. Acta Crystallogr. *63*, 449–451. 10.1107/S1744309107020180.

152. Green, J.C.D., Kahramanoglou, C., Rahman, A., Pender, A.M.C., Charbonnel, N., and Fraser, G.M. (2009). Recruitment of the Earliest Component of the Bacterial Flagellum to the Old Cell Division Pole by a Membrane-Associated Signal Recognition Particle Family GTP-Binding Protein. J. Mol. Biol. *391*, 679–690. 10.1016/j.jmb.2009.05.075.

153. Freymann, D.M., Keenan, R.J., Stroud, R.M., and Walter, P. (1997). Structure of the conserved GTPase domain of the signal recognition particle. Nature *385*, 361–1517364.

154. Montoya, G., Svensson, C., Luirink, J., and Sinning, I. (1997). Crystal structure of the NG domain from the signal-recognition particle receptor FtsY. Nature *385*, 365–368.

155. Saraste, M., Sibbald, P.R., and Wittinghofer, A. (1990). The P-loop - a common motif in ATP- and GTP-binding proteins. Trends Biochem. Sci. *15*, 430–434.

156. Focia, P.J., Shepotinovskaya, I. V, Seidler, J.A., and Freymann, D.M. (2004). Heterodimeric GTPase Core of the SRP Targeting Complex. Science (1979). *303*, 373–377.

157. Egea, P.F., Shan, S., Napetschnig, J., Savage, D.F., Walter, P., and Stroud, R.M. (2004). Substrate twinning activates the signal recognition particle and its receptor. Nature *427*, 215–221. 10.1038/nature02250.

158. Bange, G., Kümmerer, N., Grudnik, P., Lindner, R., Petzold, G., Kressler, D., Hurt, E., Wild, K., and Sinning, I. (2011). Structural basis for the molecular evolution of SRP-GTPase activation by protein. Nat. Struct. Mol. Biol. *18*, 1376–1380. 10.1038/nsmb.2141.

159. Bange, G., Wild, K., and Sinning, I. (2007). Protein translocation: checkpoint role for SRP GTPase activation. Current Biology *17*, 980–982. 10.1016/j.cub.2007.09.007.

160. Navarrete, B., Leal-Morales, A., Serrano-Ron, L., Sarrió, M., Jiménez-Fernández, A., Jiménez-Díaz, L., López-Sánchez, A., and Govantes, F. (2019). Transcriptional organization,

regulation and functional analysis of *flhF* and *fleN* in *Pseudomonas putida*. PLoS One *14*, e0214166. 10.1371/journal.pone.0214166.

161. Pandza, S., Baetens, M., Park, C.H., Au, T., Keyhan, M., and Matin, A. (2000). The G-protein FlhF has a role in polar flagellar placement and general stress response induction in *Pseudomonas putida*. Mol. Microbiol. *36*, 414–423. 10.1046/j.1365-2958.2000.01859.x.
162. Murray, T.S., and Kazmierczak, B.I. (2006). FlhF Is required for swimming and swarming in *Pseudomonas aeruginosa*. J. Bacteriol. *188*, 6995–7004. 10.1128/JB.00790-06.
163. Kulasekara, B.R., Kamischke, C., Kulasekara, H.D., Christen, M., Wiggins, P.A., and Miller, S.I. (2013). c-di-GMP heterogeneity is generated by the chemotaxis machinery to regulate flagellar motility. Elife *2013*, e01402. 10.7554/eLife.01402.
164. Kusumoto, A., Shinohara, A., Terashima, H., Kojima, S., Yakushi, T., and Homma, M. (2008). Collaboration of FlhF and FlhG to regulate polarflagella number and localization in *Vibrio alginolyticus*. Microbiology (N. Y). *154*, 1390–1399. 10.1099/mic.0.2007/012641-0.
165. Arroyo-Pérez, E.E., Hook, J.C., Alvarado, A., Wimmi, S., Glatter, T., Thormann, K., and Ringgaard, S. (2024). A conserved cell-pole determinant organizes proper polar flagellum formation. Elife *13*. 10.7554/elife.93004.
166. Ainsaar, K., Tamman, H., Kasvandik, S., Tenson, T., and Hõrak, R. (2019). The TonB m-PocAB System Is Required for Maintenance of Membrane Integrity and Polar Position of Flagella in *Pseudomonas putida*. J. Bacteriol. *201*, e00303-19. 10.1128/JB.
167. Cowles, K.N., Moser, T.S., Siryaporn, A., Nyakudarika, N., Dixon, W., Turner, J.J., and Gitai, Z. (2013). The putative Poc complex controls two distinct *Pseudomonas aeruginosa* polar motility mechanisms. Mol. Microbiol. *90*, 923–938. 10.1111/mmi.12403.
168. Jalal, A.S.B., and Le, T.B.K. (2020). Bacterial chromosome segregation by the ParABS system. Open Biol. *10*. 10.1098/rsob.200097.
169. Ringgaard, S., Schirner, K., Davis, B.M., and Waldor, M.K. (2011). A family of ParA-like ATPases promotes cell pole maturation by facilitating polar localization of chemotaxis proteins. Genes Dev. *25*, 1544–1555. 10.1101/gad.2061811.
170. Ringgaard, S., Zepeda-Rivera, M., Wu, X., Schirner, K., Davis, B.M., and Waldor, M.K. (2014). ParP prevents dissociation of CheA from chemotactic signaling arrays and tethers them to a polar anchor. Proc. Natl. Acad. Sci. U. S. A. *111*. 10.1073/pnas.1315722111.
171. Huitema, E., Pritchard, S., Matteson, D., Radhakrishnan, S.K., and Viollier, P.H. (2006). Bacterial birth scar proteins mark future flagellum assembly site. Cell *124*, 1025–1037. 10.1016/j.cell.2006.01.019.
172. Lam, H., Schofield, W.B., and Jacobs-Wagner, C. (2006). A landmark protein essential for establishing and perpetuating the polarity of a bacterial cell. Cell *124*, 1011–1023. 10.1016/j.cell.2005.12.040.

173. Davis, N.J., Cohen, Y., Sanselicio, S., Fumeaux, C., Ozaki, S., Luciano, J., Guerrero-Ferreira, R.C., Wright, E.R., Jenal, U., and Viollier, P.H. (2013). De- and repolarization mechanism of flagellar morphogenesis during a bacterial cell cycle. Genes Dev. *27*, 2049–2062. 10.1101/gad.222679.113.

174. Heidelberg, J.F., Eisen, J.A., Nelson, W.C., Clayton, R.A., Gwinn, M.L., Dodson, R.J., Haft, D.H., Hickey, E.K., Peterson, J.D., Umayam, L., *et al.* (2000). DNA sequence of both chromosomes of the cholera pathogen *Vibrio cholerae*. Nature *406*, 477–484.

175. Stover, C.K., Pham, X.Q., Erwin, A.L., Mizoguchi, S.D., Warrener, P., Hickey, M.J., Brinkman, F.S.L., Hufnagle, W.O., Kowalik, D.J., Lagrou, M., *et al.* (2000). Complete genome sequence of *Pseudomonas aeruginosa* PAO1, an opportunistic pathogen. Nature *406*, 959–964.

176. Heidelberg, J.F., Paulsen, I.T., Nelson, K.E., Gaidos, E.J., Nelson, W.C., Read, T.D., Eisen, J.A., Seshadri, R., Ward, N., Methe, B., *et al.* (2002). Genome sequence of the dissimilatory metal ion-reducing bacterium *Shewanella oneidensis*. Nat. Biotechnol. *20*, 1118–1123. 10.1038/nbt749.

177. Nelson, K.E., Weinel, C., Paulsen, I.T., Dodson, R.J., Hilbert, H., Martins dos Santos, V.A.P., Fouts, D.E., Gill, S.R., Pop, M., Holmes, M., *et al.* (2002). Complete genome sequence and comparative analysis of the metabolically versatile *Pseudomonas putida* KT2440. Environ. Microbiol. *4*, 799–808. 10.1046/j.1462-2920.2002.00366.x.

178. Pulido-Sánchez, M., López-Sánchez, A., and Govantes, F. (2025). FimV, ParC and ParP coordinate polar location of the chemosensory arrays in *Pseudomonas putida*. bioRxiv. 10.1101/2025.10.27.684771.

179. Sharma, S., Mohler, J., Mahajan, S.D., Schwartz, S.A., Bruggemann, L., and Aalinkeel, R. (2023). Microbial Biofilm: A Review on Formation, Infection, Antibiotic Resistance, Control Measures, and Innovative Treatment. Microorganisms *11*. 10.3390/microorganisms11061614.

180. Stoodley, P., Sauer, K., Davies, D.G., and Costerton, J.W. (2002). Biofilms as complex differentiated communities. Annu. Rev. Microbiol. *56*, 187–209. 10.1146/annurev.micro.56.012302.160705.

181. Uruén, C., Chopo-Escuin, G., Tommassen, J., Mainar-Jaime, R.C., and Arenas, J. (2021). Biofilms as promoters of bacterial antibiotic resistance and tolerance. Antibiotics *10*, 1–36. 10.3390/antibiotics10010003.

182. Donlan, R.M. (2001). Biofilms and Device-Associated Infections. Emerg. Infect. Dis., 277–281.

183. Bernal, P., Allsopp, L.P., Filloux, A., and Llamas, M.A. (2017). The *Pseudomonas putida* T6SS is a plant warden against phytopathogens. ISME Journal *11*, 972–987. 10.1038/ismej.2016.169.

184. Römling, U., Gomelsky, M., and Galperin, M.Y. (2005). C-di-GMP: The dawning of a novel bacterial signalling system. Mol. Microbiol. *57*, 629–639. 10.1111/j.1365-2958.2005.04697.x.

185. Bridges, A.A., Prentice, J.A., Wingreen, N.S., and Bassler, B.L. (2022). Signal Transduction Network Principles Underlying Bacterial Collective Behaviors. Annu. Rev. Microbiol. *76*, 235–257. 10.1146/annurev-micro-042922.

186. Hengge, R. (2009). Principles of c-di-GMP signalling in bacteria. Nat. Rev. Microbiol. *7*, 263–273.

187. Jenal, U. (2004). Cyclic di-guanosine-monophosphate comes of age: A novel secondary messenger involved in modulating cell surface structures in bacteria? Curr. Opin. Microbiol. *7*, 185–191. 10.1016/j.mib.2004.02.007.

188. Jenal, U., and Malone, J. (2006). Mechanisms of cyclic-di-GMP signaling in bacteria. Annu. Rev. Genet. *40*, 385–407. 10.1146/annurev.genet.40.110405.090423.

189. Camilli, A., and Bassler, B.L. (2006). Bacterial Small-Molecule Signaling Pathways. Science (1979). *311*, 1113–1116.

190. Schirmer, T., and Jenal, U. (2009). Structural and mechanistic determinants of c-di-GMP signalling. Nat. Rev. Microbiol. *7*, 724–735. 10.1038/nrmicro2203.

191. Cotter, P.A., and Stibitz, S. (2007). c-di-GMP-mediated regulation of virulence and biofilm formation. Curr. Opin. Microbiol. *10*, 17–23. 10.1016/j.mib.2006.12.006.

192. Dow, J.M., Fouhy, Y., Lucey, J.F., and Ryan, R.P. (2006). The HD-GYP Domain, Cyclic Di-GMP Signaling, and Bacterial Virulence to Plants. Molecular Plant-Microbe Interactions *19*, 1378–1384. 10.1094/MPMI.

193. Ryan, R.P., Fouhy, Y., Lucey, J.F., Jiang, B. Le, He, Y.Q., Feng, J.X., Tang, J.L., and Dow, J.M. (2007). Cyclic di-GMP signalling in the virulence and environmental adaptation of *Xanthomonas campestris*. Mol. Microbiol. *63*, 429–442. 10.1111/j.1365-2958.2006.05531.x.

194. Tamayo, R., Pratt, J.T., and Camilli, A. (2007). Roles of cyclic diguanylate in the regulation of bacterial pathogenesis. Annu. Rev. Microbiol. *61*, 131–148. 10.1146/annurev.micro.61.080706.093426.

195. Duerig, A., Abel, S., Folcher, M., Nicollier, M., Schwede, T., Amiot, N., Giese, B., and Jenal, U. (2009). Second messenger-mediated spatiotemporal control of protein degradation regulates bacterial cell cycle progression. Genes Dev. *23*, 93–104. 10.1101/gad.502409.

196. Paul, R., Abel, S., Wassmann, P., Beck, A., Heerklotz, H., and Jenal, U. (2007). Activation of the diguanylate cyclase PleD by phosphorylation-mediated dimerization. Journal of Biological Chemistry *282*, 29170–29177. 10.1074/jbc.M704702200.

197. Paul, R., Weiser, S., Amiot, N.C., Chan, C., Schirmer, T., Giese, B., and Jenal, U. (2004). Cell cycle-dependent dynamic localization of a bacterial response regulator with a novel di-guanylate cyclase output domain. Genes Dev. *18*, 715–727. 10.1101/gad.289504.

198. Chan, C., Paul, R., Samoray, D., Amiot, N.C., Giese, B., Jenal, U., and Schirmer, T. (2004). Structural basis of activity and allosteric control of diguanylate cyclase. PNAS *101*, 17084–17089.

199. Malone, J.G., Williams, R., Christen, M., Jenal, U., Spiers, A.J., and Rainey, P.B. (2007). The structure-function relationship of WspR, a *Pseudomonas fluorescens* response regulator with a GGDEF output domain. Microbiology (N. Y). *153*, 980–994. 10.1099/mic.0.2006/002824-0.

200. Ryjenkov, D.A., Tarutina, M., Moskvin, O. V., and Gomelsky, M. (2005). Cyclic diguanylate is a ubiquitous signaling molecule in bacteria: Insights into biochemistry of the GGDEF protein domain. J. Bacteriol. *187*, 1792–1798. 10.1128/JB.187.5.1792-1798.2005.

201. Christen, M., Christen, B., Folcher, M., Schauerte, A., and Jenal, U. (2005). Identification and characterization of a cyclic di-GMP-specific phosphodiesterase and its allosteric control by GTP. Journal of Biological Chemistry *280*, 30829–30837. 10.1074/jbc.M504429200.

202. Schmidt, A.J., Ryjenkov, D.A., and Gomelsky, M. (2005). The ubiquitous protein domain EAL is a cyclic diguanylate-specific phosphodiesterase: Enzymatically active and inactive EAL domains. J. Bacteriol. *187*, 4774–4781. 10.1128/JB.187.14.4774-4781.2005.

203. Rao, F., Yang, Y., Qi, Y., and Liang, Z.X. (2008). Catalytic mechanism of cyclic di-GMP-specific phosphodiesterase: A study of the EAL domain-containing RocR from *Pseudomonas aeruginosa*. J. Bacteriol. *190*, 3622–3631. 10.1128/JB.00165-08.

204. Tschowri, N., Busse, S., and Hengge, R. (2009). The BLUF-EAL protein YcgF acts as a direct anti-repressor in a blue-light response of *Escherichia coli*. Genes Dev. *23*, 522–534. 10.1101/gad.499409.

205. Newell, P.D., Monds, R.D., and O'toole, G.A. (2009). LapD is a bis-(3,5)-cyclic dimeric GMP-binding protein that regulates surface attachment by *Pseudomonas fluorescens* Pf0-1. PNAS *106*, 3461–3466.

206. Suzuki, K., Babitzke, P., Kushner, S.R., and Romeo, T. (2006). Identification of a novel regulatory protein (CsrD) that targets the global regulatory RNAs CsrB and CsrC for degradation by RNase E. Genes Dev. *20*, 2605–2617. 10.1101/gad.1461606.

207. Tomb, J.-F., White, O., Kerlavage, A.R., Clayton, R.A., Sutton, G.G., Fleischmann, R.D., Ketchum, K.A., Klenk, H.P., Gill, S., Dougherty, B.A., *et al.* (1997). The complete genome sequence of the gastric pathogen *Helicobacter pylori*. Nature *388*, 539–547.

208. Nambu, J.F., Lewis, J. 0, Wharton, K.A., and Crews, S.T. (1991). The *Drosophila* single-minded Gene Encodes a Helix-Loop-Helix Protein That Acts as a Master Regulator of CNS Midline Development. Cell *67*, 1157–167.

209. Hefti, M.H., Françoijs, K.J., De Vries, S.C., Dixon, R., and Vervoort, J. (2004). The PAS fold: A redefinition of the PAS domain based upon structural prediction. Eur. J. Biochem. *271*, 1198–1208. 10.1111/j.1432-1033.2004.04023.x.

210. Taylor, B.L., and Zhulin, I.B. (1999). PAS Domains: Internal Sensors of Oxygen, Redox Potential, and Light. Microbiology and Molecular Biology Reviews *63*, 479–506.

211. Xing, J., Gumerov, V.M., and Zhulin, I.B. (2023). Origin and functional diversification of PAS domain, a ubiquitous intracellular sensor. Sci. Adv. *9*, eadi4517.

212. Brüderlin, M., Böhm, R., Fadel, F., Hiller, S., Schirmer, T., and Dubey, B.N. (2023). Structural features discriminating hybrid histidine kinase Rec domains from response regulator homologs. Nat. Commun. *14*. 10.1038/s41467-023-36597-8.

213. Granovsky, A.E., Natochin, M., Mcentaffer, R.L., Haik, T.L., Francis, S.H., Corbin, J.D., and Artemyev, N.O. (1998). Probing Domain Functions of Chimeric PDE6/PDE5 cGMP-Phosphodiesterase. J. Biol. Chem. *273*, 24485–24490.

214. Turko, I. V., Haik, T.L., McAllister-Lucas, L.M., Burns, F., Francis, S.H., and Corbin, J.D. (1996). Identification of key amino acids in a conserved cGMP-binding site of cGMP-binding phosphodiesterases: A putative NKX(n)D motif for cGMP binding. Journal of Biological Chemistry *271*, 22240–22244. 10.1074/jbc.271.36.22240.

215. Ho, S.J., Burden, L.M., and Hurley, J.H. (2000). Structure of the GAF domain, a ubiquitous signaling motif and a new class of cyclic GMP receptor. EMBO *19*, 5288–5299.

216. Rao, F., Qi, Y., Chong, H.S., Kotaka, M., Li, B., Li, J., Lescar, J., Tang, K., and Liang, Z.X. (2009). The functional role of a conserved loop in EAL domain-based cyclic di-GMP-specific phosphodiesterase. J. Bacteriol. *191*, 4722–4731. 10.1128/JB.00327-09.

217. Kuchma, S.L., Brothers, K.M., Merritt, J.H., Liberati, N.T., Ausubel, F.M., and O'Toole, G.A. (2007). BifA, a cyclic-di-GMP phosphodiesterase, inversely regulates biofilm formation and swarming motility by *Pseudomonas aeruginosa* PA14. J. Bacteriol. *189*, 8165–8178. 10.1128/JB.00586-07.

218. Rossmann, F.M., Rick, T., Mrusek, D., Sprankel, L., Dörrich, A.K., Leonhard, T., Bubendorfer, S., Kaever, V., Bange, G., and Thormann, K.M. (2019). The GGDEF Domain of the Phosphodiesterase PdeB in *Shewanella putrefaciens* Mediates Recruitment by the Polar Landmark Protein HubP. J. Bacteriol. *201*, e00534-18. 10.1128/JB.

219. Nicastro, G.G., Kaihami, G.H., Pulschen, A.A., Hernandez-Montelongo, J., Boechat, A.L., de Oliveira Pereira, T., Rosa, C.G.T., Stefanello, E., Colepicolo, P., Bordi, C., *et al.* (2020). c-di-GMP-related phenotypes are modulated by the interaction between a diguanylate cyclase and a polar hub protein. Sci. Rep. *10*. 10.1038/s41598-020-59536-9.

220. Roy, A.B., Petrova, O.E., and Sauer, K. (2012). The phosphodiesterase DipA (PA5017) is essential for *Pseudomonas aeruginosa* biofilm dispersion. J. Bacteriol. *194*, 2904–2915. 10.1128/JB.05346-11.

221. Li, Y., Xia, H., Bai, F., Xu, H., Yang, L., Yao, H., Zhang, L., Zhang, X., Bai, Y., Saris, P.E.J., *et al.* (2007). Identification of a new gene PA5017 involved in flagella-mediated motility,

chemotaxis and biofilm formation in *Pseudomonas aeruginosa*. FEMS Microbiol. Lett. *272*, 188–195. 10.1111/j.1574-6968.2007.00753.x.

222. Edelmann, D.B., Jakob, A.M., Wilson, L.G., Colin, R., Brandt, D., Eck, F., Kalinowski, J., and Thormann, K.M. (2025). Role of a single MCP in evolutionary adaptation of *Shewanella putrefaciens* for swimming in planktonic and structured environments. Appl. Environ. Microbiol. *91*, e00229-25. 10.1128/aem.00229-25.
223. Parales, R.E., Luu, R.A., Chen, G.Y., Liu, X., Wu, V., Lin, P., Hughes, J.G., Nesteryuk, V., Parales, J. V., and Ditty, J.L. (2013). *Pseudomonas putida* F1 has multiple chemoreceptors with overlapping specificity for organic acids. Microbiology (N. Y). *159*, 1086–1096. 10.1099/mic.0.065698-0.
224. Schuhmacher, J.S., Rossmann, F., Dempwolff, F., Knauer, C., Altegoer, F., Steinchen, W., Dörrich, A.K., Klingl, A., Stephan, M., Linne, U., *et al.* (2015). MinD-like ATPase FlhG effects location and number of bacterial flagella during C-ring assembly. Proc. Natl. Acad. Sci. U. S. A. *112*, 3092–3097. 10.1073/pnas.1419388112.
225. Regenhardt, D., Heuer, H., Heim, S., Fernandez, D.U., Strömpl, C., Moore, E.R.B., and Timmis, K.N. (2002). Pedigree and taxonomic credentials of *Pseudomonas putida* strain KT2440. Environ. Microbiol. *4*, 912–915. 10.1046/j.1462-2920.2002.00368.x.
226. Harwood, C.S., Fosnaugh, K., and Dispensa, M. (1989). Flagellation of *Pseudomonas putida* and Analysis of Its Motile Behavior. J. Bacteriol. *171*, 4063–4066.
227. Takekawa, N., Kwon, S., Nishioka, N., Kojima, S., and Homma, M. (2016). HubP, a polar landmark protein, regulates flagellar number by assisting in the proper polar localization of FlhG in *Vibrio alginolyticus*. J. Bacteriol. *198*, 3091–3098. 10.1128/JB.00462-16.
228. Park, S., Yoon, J., Lee, C.R., Lee, J.Y., Kim, Y.R., Jang, K.S., Lee, K.H., and Seok, Y.J. (2019). Polar landmark protein HubP recruits flagella assembly protein FapA under glucose limitation in *Vibrio vulnificus*. Mol. Microbiol. *112*, 266–279. 10.1111/mmi.14268.
229. Fukushima, Y., Homma, M., and Kojima, S. (2023). Interaction of FlhF, SRP-like GTPase with FliF, MS ring component assembling the initial structure of flagella in marine *Vibrio*. J. Biochem. *174*, 125–130. 10.1093/jb/mvad029.
230. Carter, T., Buensuceso, R.N.C., Tammam, S., Lamers, R.P., Harvey, H., Howell, P.L., and Burrows, L.L. (2017). The type IVa pilus machinery is recruited to sites of future cell division. mBio *8*, e02103-16. 10.1128/mBio.02103-16.
231. Schmidt, L.M., Pulido-Sánchez, M., Treuner-Lange, A., Zehner, L., López-Sánchez, A., Cava, F., Govantes, F., and Thormann, K.M. (2026). Functional characterization of the polar organizer protein FimV in *Pseudomonas putida*. J. Bacteriol. *208*, e00497-25. 10.1128/jb.00497-25.

232. Mesnage, S., Dellarole, M., Baxter, N.J., Rouget, J.B., Dimitrov, J.D., Wang, N., Fujimoto, Y., Hounslow, A.M., Lacroix-Desmazes, S., Fukase, K., *et al.* (2014). Molecular basis for bacterial peptidoglycan recognition by LysM domains. Nat. Commun. *5*. 10.1038/ncomms5269.

233. Ha, D.-G., Kuchma, S.L., and O'Toole, G.A. (2022). Plate-based assay for swarming motility in *P. aeruginosa*. In *Pseudomonas* Methods and Protocols, A. Filloux and J.-L. Ramos, eds., pp. 67–72.

234. Abramson, J., Adler, J., Dunger, J., Evans, R., Green, T., Pritzel, A., Ronneberger, O., Willmore, L., Ballard, A.J., Bambrick, J., *et al.* (2024). Accurate structure prediction of biomolecular interactions with AlphaFold 3. Nature *630*, 493–500. 10.1038/s41586-024-07487-w.

235. Muok, A.R., Briegel, A., and Crane, B.R. (2020). Regulation of the chemotaxis histidine kinase CheA: A structural perspective. Biochim. Biophys. Acta Biomembr. *1862*, 183030. 10.1016/j.bbamem.2019.183030.

236. Bilwes, A.M., Alex, L.A., Crane, B.R., and Simon, M.I. (1999). Structure of CheA, a Signal-Transducing Histidine Kinase. Cell *96*, 131–141.

237. Tohya, M., Watanabe, S., Teramoto, K., Shimojima, M., Tada, T., Kuwahara-Arai, K., War, M.W., Mya, S., Tin, H.H., and Kirikae, T. (2019). *Pseudomonas juntendi* sp. nov., isolated from patients in Japan and Myanmar. Int. J. Syst. Evol. Microbiol. *69*, 3377–3384. 10.1099/ijsem.0.003623.

238. Zhou, H., Zheng, C., Su, J., Chen, B., Fu, Y., Xie, Y., Tang, Q., Chou, S.H., and He, J. (2016). Characterization of a natural triple-tandem c-di-GMP riboswitch and application of the riboswitch-based dual-fluorescence reporter. Sci. Rep. *6*. 10.1038/srep20871.

239. Scribani-Rossi, C., Molina-Henares, M.A., Angeli, S., Cutruzzolà, F., Paiardini, A., Espinosa-Urgel, M., and Rinaldo, S. (2023). The phosphodiesterase RmcA contributes to the adaptation of *Pseudomonas putida* to l-Arginine. FEMS Microbiol. Lett. *370*, 1–9. 10.1093/femsle/fnad077.

240. Mayer, B., Schwan, M., Oviedo-Bocanegra, L.M., Bange, G., Thormann, K.M., and Graumann, P.L. (2021). Dynamics of Bacterial Signal Recognition Particle at a Single Molecule Level. Front. Microbiol. *12*. 10.3389/fmicb.2021.663747.

241. Gulbronson, C.J., Ribardo, D.A., Balaban, M., Knauer, C., Bange, G., and Hendrixson, D.R. (2016). FlhG employs diverse intrinsic domains and influences FlhF GTPase activity to numerically regulate polar flagellar biogenesis in *Campylobacter jejuni*. Mol. Microbiol. *99*, 291–306. 10.1111/mmi.13231.

242. Obuchowski, P.L., and Jacobs-Wagner, C. (2008). PflI, a protein involved in flagellar positioning in *Caulobacter crescentus*. J. Bacteriol. *190*, 1718–1729. 10.1128/JB.01706-07.

243. Raghav, S., Prajapati, R., and Jain, D. (2025). Role of FlhF and its domains in the assembly of a polar flagellum in *P. aeruginosa*. J. Bacteriol. *207*. 10.1128/jb.00332-25.

244. Arroyo-Pérez, E.E., and Ringgaard, S. (2021). Interdependent Polar Localization of FlhF and FlhG and Their Importance for Flagellum Formation of *Vibrio parahaemolyticus*. Front. Microbiol. *12*. 10.3389/fmicb.2021.655239.

245. Bork, P., Holm, L., and Sander, C. (1994). The immunoglobulin fold. J. Mol. Biol. *242*, 309–320.

246. Galli, E., Paly, E., and Barre, F.X. (2017). Late assembly of the *Vibrio cholerae* cell division machinery postpones septation to the last 10% of the cell cycle. Sci. Rep. *7*. 10.1038/srep44505.

247. Pratt, L.A., and Kolter, R. (1998). Genetic analysis of *Escherichia coli* biofilm formation: Roles of flagella, motility, chemotaxis and type I pili. Mol. Microbiol. *30*, 285–293. 10.1046/j.1365-2958.1998.01061.x.

248. Kuchma, S.L., Geiger, C.J., Webster, S.S., Fu, Y., Montoya, R., and O'Toole, G.A. (2025). Genetic analysis of flagellar-mediated surface sensing by *Pseudomonas aeruginosa* PA14. J. Bacteriol. *207*. 10.1128/jb.00520-24.

249. Vallet-Gely, I., and Boccard, F. (2013). Chromosomal Organization and Segregation in *Pseudomonas aeruginosa*. PLoS Genet. *9*, e1003492. 10.1371/journal.pgen.1003492.

250. Correa, N.E., Peng, F., and Klose, K.E. (2005). Roles of the regulatory proteins FlhF and FlhG in the *Vibrio cholerae* flagellar transcription hierarchy. J. Bacteriol. *187*, 6324–6332. 10.1128/JB.187.18.6324-6332.2005.

251. Siewering, K., Jain, S., Friedrich, C., Webber-Birungi, M.T., Semchonok, D.A., Binzen, I., Wagner, A., Huntley, S., Kahnt, J., Klingl, A., *et al.* (2014). Peptidoglycan-binding protein TsaP functions in surface assembly of type IV pili. Proc. Natl. Acad. Sci. U. S. A. *111*, 953–961. 10.1073/pnas.1322889111.

252. Coil, D.A., and Anné, J. (2010). The role of *fimV* and the importance of its tandem repeat copy number in twitching motility, pigment production, and morphology in *Legionella pneumophila*. Arch. Microbiol. *192*, 625–631. 10.1007/s00203-010-0590-8.

253. Sauer, K., and Camper, A.K. (2001). Characterization of phenotypic changes in *Pseudomonas putida* in response to surface-associated growth. J. Bacteriol. *183*, 6579–6589. 10.1128/JB.183.22.6579-6589.2001.

254. De Groot, A., Heijnen, I., De Cock, H., Filloux, A., and Tommassen, J. (1994). Characterization of Type IV Pilus Genes in Plant Growth-Promoting *Pseudomonas putida* WCS358. J. Bacteriol. *176*, 642–650.

255. van Ditmarsch, D., Boyle, K.E., Sakhtah, H., Oyler, J.E., Nadell, C.D., Déziel, É., Dietrich, L.E.P., and Xavier, J.B. (2013). Convergent evolution of hyperswarming leads to impaired biofilm formation in pathogenic bacteria. Cell Rep. *4*, 697–708. 10.1016/j.celrep.2013.07.026.

256. Oldfield, N.J., Bland, S.J., Taraktsoglou, M., Dos Ramos, F.J., Robinson, K., Wooldridge, K.G., and Ala'Aldeen, D.A.A. (2007). T-cell stimulating protein A (TspA) of *Neisseria*

meningitidis is required for optimal adhesion to human cells. Cell. Microbiol. *9*, 463–478. 10.1111/j.1462-5822.2006.00803.x.

257. Rashid, M.H., and Kornberg, A. (2000). Inorganic polyphosphate is needed for swimming, swarming, and twitching motilities of *Pseudomonas aeruginosa*. PNAS *97*, 4885–4890.
258. Patrick, J.E., and Kearns, D.B. (2012). Swarming motility and the control of master regulators of flagellar biosynthesis. Mol. Microbiol. *83*, 14–23. 10.1111/j.1365-2958.2011.07917.x.
259. Yang, A., Tang, W.S., Si, T., and Tang, J.X. (2017). Influence of Physical Effects on the Swarming Motility of *Pseudomonas aeruginosa*. Biophys. J. *112*, 1462–1471. 10.1016/j.bpj.2017.02.019.
260. Köhler, T., Curty, L.K., Barja, F., van Delden, C., and Pechère, J.-C. (2000). Swarming of *Pseudomonas aeruginosa* Is Dependent on Cell-to-Cell Signaling and Requires Flagella and Pili. J. Bacteriol. *182*, 5990–5996.
261. Atsumi, T., McCarter, L., and Imae, Y. (1992). Polar and lateral flagellar motors of marine *Vibrio* are driven by different ion-motive force. Nature *355*, 182–184.
262. Merino, S., Shaw, J.G., and Tomás, J.M. (2006). Bacterial lateral flagella: An inducible flagella system. FEMS Microbiol. Lett. *263*, 127–135. 10.1111/j.1574-6968.2006.00403.x.
263. Hwang, Y.S., Perez, M., Holzel, R., and Harshey, R.M. (2025). c-di-GMP is required for swarming in *E. coli*, producing colanic acid that acts as surfactant. mBio *16*, 1–17. 10.1128/mbio.00916-25.
264. Chakrabarti, P., and Chakravarty, D. (2022). Intrinsically disordered proteins/regions and insight into their biomolecular interactions. Biophys. Chem. *283*. 10.1016/j.bpc.2022.106769.
265. Meng, F., and Kurgan, L. (2016). DFLpred: High-throughput prediction of disordered flexible linker regions in protein sequences. Bioinformatics *32*, i341–i350. 10.1093/bioinformatics/btw280.
266. Römling, U., Galperin, M.Y., and Gomelsky, M. (2013). Cyclic di-GMP: the First 25 Years of a Universal Bacterial Second Messenger. Microbiology and Molecular Biology Reviews *77*, 1–52. 10.1128/mmbr.00043-12.
267. Tchigvintsev, A., Xu, X., Singer, A., Chang, C., Brown, G., Proudfoot, M., Cui, H., Flick, R., Anderson, W.F., Joachimiak, A., *et al.* (2010). Structural insight into the mechanism of c-di-GMP hydrolysis by EAL domain phosphodiesterases. J. Mol. Biol. *402*, 524–538. 10.1016/j.jmb.2010.07.050.
268. Li, H., Xue, D., Tian, F., Yuan, X., Yang, F., Chen, H., Hutchins, W., Yang, C.-H., and He, C. (2019). *Xanthomonas oryzae* pv. *oryzae* Response Regulator TriP Regulates Virulence and Exopolysaccharide Production Via Interacting with c-di-GMP Phosphodiesterase PdeR. Molecular Plant-Microbe Interactions *32*, 729–739. 10.1094/MPMI-09-18-0260-R.
269. Xue, D., Tian, F., Yang, F., Chen, H., Yuan, X., Yang, C.-H., Chen, Y., Wang, Q., and He, C. (2018). Phosphodiesterase EdpX1 Promotes *Xanthomonas oryzae* pv. oryzae Virulence,

Exopolysaccharide Production, and Biofilm Formation. Appl. Environ. Microbiol. *84*, e01717-18. 10.1128/AEM.

270. Jain, R., Sliusarenko, O., and Kazmierczak, B.I. (2017). Interaction of the cyclic-di-GMP binding protein FimX and the Type 4 pilus assembly ATPase promotes pilus assembly. PLoS Pathog. *13*. 10.1371/journal.ppat.1006594.
271. Valentini, M., Laventie, B.J., Moscoso, J., Jenal, U., and Filloux, A. (2016). The Diguanylate Cyclase HsbD Intersects with the HptB Regulatory Cascade to Control *Pseudomonas aeruginosa* Biofilm and Motility. PLoS Genet. *12*. 10.1371/journal.pgen.1006354.
272. Güvener, Z.T., and Harwood, C.S. (2007). Subcellular location characteristics of the *Pseudomonas aeruginosa* GGDEF protein, WspR, indicate that it produces cyclic-di-GMP in response to growth on surfaces. Mol. Microbiol. *66*, 1459–1473. 10.1111/j.1365-2958.2007.06008.x.
273. Feng, Q., Ahator, S. Dela, Zhou, T., Liu, Z., Lin, Q., Liu, Y., Huang, J., Zhou, J., and Zhang, L.H. (2020). Regulation of Exopolysaccharide Production by ProE, a Cyclic-Di-GMP Phosphodiesterase in *Pseudomonas aeruginosa* PAO1. Front. Microbiol. *11*. 10.3389/fmicb.2020.01226.
274. Sickmeier, M., Hamilton, J.A., LeGall, T., Vacic, V., Cortese, M.S., Tantos, A., Szabo, B., Tompa, P., Chen, J., Uversky, V.N., *et al.* (2007). DisProt: The database of disordered proteins. Nucleic Acids Res. *35*, D786-793. 10.1093/nar/gkl893.
275. Wright, P.E., and Dyson, H.J. (2015). Intrinsically disordered proteins in cellular signalling and regulation. Nat. Rev. Mol. Cell Biol. *16*, 18–29. 10.1038/nrm3920.
276. Mcevoy, M.M., Hausrath, A.C., Randolph, G.B., Remington, S.J., and Dahlquist, F.W. (1998). Two binding modes reveal flexibility in kinase/response regulator interactions in the bacterial chemotaxis pathway. PNAS *95*, 7333–7338.
277. Hess, J.F., Oosawa, K., Matsumura, P., and Simon, M.I. (1987). Protein phosphorylation is involved in bacterial chemotaxis. PNAS *84*, 7609–7613.
278. Sundriyal, A., Massa, C., Samoray, D., Zehender, F., Sharpe, T., Jenal, U., and Schirmer, T. (2014). Inherent regulation of EAL domain-catalyzed hydrolysis of second messenger cyclic di-GMP. Journal of Biological Chemistry *289*, 6978–6990. 10.1074/jbc.M113.516195.
279. Minasov, G., Padavattan, S., Shuvalova, L., Brunzelle, J.S., Miller, D.J., Baslé, A., Massa, C., Collart, F.R., Schirmer, T., and Anderson, W.F. (2009). Crystal structures of YkuI and its complex with second messenger cyclic di-GMP suggest catalytic mechanism of phosphodiester bond cleavage by EAL domains. Journal of Biological Chemistry *284*, 13174–13184. 10.1074/jbc.M808221200.
280. Knape, M.J., Ahuja, L.G., Bertinetti, D., Burghardt, N.C.G., Zimmermann, B., Taylor, S.S., and Herberg, F.W. (2015). Divalent Metal Ions Mg2+ and Ca2+ Have Distinct Effects on Protein

Kinase A Activity and Regulation. ACS Chem. Biol. *10*, 2303–2315. 10.1021/acschembio.5b00271.

281. Bilwes, A.M., Quezada, C.M., Croal, L.R., Crane, B.R., and Simon, M.I. (2001). Nucleotide binding by the histdine kinase CheA. Nat. Struct. Biol. *8*.
282. Pawson, T., and Scott, J.D. (1997). Signaling Through Scaffold, Anchoring, and Adaptor Proteins. Science (1979). *278*, 2075–2080.
283. Kentner, D., and Sourjik, V. (2006). Spatial organization of the bacterial chemotaxis system. Curr. Opin. Microbiol. *9*, 619–624. 10.1016/j.mib.2006.10.012.
284. Blattner, F.R., Plunkett, G., Bloch, C.A., Perna, N.T., Burland, V., Riley, M., Collado-Vides, J., Glasner, J.D., Rode, C.K., Mayhew, G.F., *et al.* (1997). The Complete Genome Sequence of *Escherichia coli* K-12. Science (1979). *277*, 1453–1469.
285. Appleby, J.L., and Bourret, R.B. (1999). Activation of CheY mutant D57N by phosphorylation at an alternative site, Ser-56. Mol. Microbiol. *34*, 915–925. 10.1046/j.1365-2958.1999.01653.x.
286. Ding, X., He, Q., Shen, F., Dahlquist, F.W., and Wang, X. (2018). Regulatory role of an interdomain linker in the bacterial chemotaxis histidine kinase CheA. J. Bacteriol. *200*. 10.1128/JB.00052-18.
287. Kentner, D., and Sourjik, V. (2009). Dynamic map of protein interactions in the *Escherichia coli* chemotaxis pathway. Mol. Syst. Biol. *5*. 10.1038/msb.2008.77.
288. Mayover, T.L., Halkides, C.J., and Stewart, R.C. (1999). Kinetic characterization of CheY phosphorylation reactions: Comparison of P-CheA and small-molecule phosphodonors. Biochemistry *38*, 2259–2271. 10.1021/bi981707p.
289. Jenal, U., Reinders, A., and Lori, C. (2017). Cyclic di-GMP: Second messenger extraordinaire. Nat. Rev. Microbiol. *15*, 271–284. 10.1038/nrmicro.2016.190.
290. Kusumoto, A., Kamisaka, K., Yakushi, T., Terashima, H., Shinohara, A., and Homma, M. (2006). Regulation of polar flagellar number by the flhF and flhG genes in *Vibrio alginolyticus*. J. Biochem. *139*, 113–121. 10.1093/jb/mvj010.
291. Zboralski, A., and Filion, M. (2020). Genetic factors involved in rhizosphere colonization by phytobeneficial *Pseudomonas* spp. Comput. Struct. Biotechnol. J. *18*, 3539–3554. 10.1016/j.csbj.2020.11.025.
292. Miller, V.L., and Mekalanos, J.J. (1988). A Novel Suicide Vector and Its Use in Construction of Insertion Mutations: Osmoregulation of Outer Membrane Proteins and Virulence Determinants in *Vibrio cholerae* Requires *toxR*. J. Bacteriol. *170*, 2575–2583.
293. Fredrickson, J.K., Zachara, J.M., Kennedy, D.W., Dong, H., Onstott, T.C., Hinman, N.W., and Li, S.-M. (1998). Biogenic iron mineralization accompanying the dissimilatory reduction of hydrous ferric oxide by a groundwater bacterium. Geochim. Cosmochim. Acta *62*, 3239–3257.

294. Lassak, J., Henche, A.L., Binnenkade, L., and Thormann, K.M. (2010). ArcS, the cognate sensor kinase in an atypical arc system of *Shewanella oneidensis* MR-1. Appl. Environ. Microbiol. *76*, 3263–3274. 10.1128/AEM.00512-10.

295. Guzman, L.-M., Belin, D., Carson, M.J., and Beckwith, J. (1995). Tight Regulation, Modulation, and High-Level Expression by Vectors Containing the Arabinose pBAD Promoter. J. Bacteriol. *177*, 4121–4130.

296. Kovach, M.E., Elzer A, P.H., Steven Hill, D., Robertson, G.T., Farris, M.A., Roop II, R.M., and Peterson, K.M. (1995). Four new derivatives of the broad-host-range cloning vector pBBR1MCS, carrying different antibiotic-resistance cassettes. Gene *166*, 175–176.

297. Karimova, G., Pidoux, J., Ullmann, A., and Ladant, D. (1998). A bacterial two-hybrid system based on a reconstituted signal transduction pathway. PNAS *95*, 5752–5756.

298. James, P., Halladay, J., and Craig, E.A. (1996). Genomic Libraries and a Host Strain Designed for Highly Efficient Two-Hybrid Selection in Yeast. Genetics *144*, 1425–1436.

299. Mullis, K.B., and Faloona, Fred.A. (1987). Specific synthesis of DNA *in vitro* via a polymerase-catalyzed chain reaction. In Methods in Enzymology, H. A. Gelbart and A. K. Riggs, eds., pp. 335–350.

300. Sambrook, J., Fritsch, E.F., and Maniatis, T. (1989). Molecular cloning: a laboratory manual. In Molecular cloning: a laboratory manual (Cold Spring Harbor Laboratory Press).

301. Gibson, D.G., Young, L., Chuang, R.Y., Venter, J.C., Hutchison, C.A., and Smith, H.O. (2009). Enzymatic assembly of DNA molecules up to several hundred kilobases. Nat. Methods *6*, 343–345. 10.1038/nmeth.1318.

302. Laemmli, U.K. (1970). Cleavage of structural proteins during the assembly of the head of bacteriophage T4. Nature *227*, 680–685.

303. Kabsch, W. (2010). XDS. Acta Crystallogr. D Biol. Crystallogr. *66*, 125–132. 10.1107/S0907444909047337.

304. McCoy, A.J., Grosse-Kunstleve, R.W., Adams, P.D., Winn, M.D., Storoni, L.C., and Read, R.J. (2007). Phaser crystallographic software. J. Appl. Crystallogr. *40*, 658–674. 10.1107/S0021889807021206.

305. Senior, A.W., Evans, R., Jumper, J., Kirkpatrick, J., Sifre, L., Green, T., Qin, C., Žídek, A., Nelson, A.W.R., Bridgland, A., *et al.* (2020). Improved protein structure prediction using potentials from deep learning. Nature *577*, 706–710. 10.1038/s41586-019-1923-7.

306. Emsley, P., and Cowtan, K. (2004). Coot: Model-building tools for molecular graphics. Acta Crystallogr. D Biol. Crystallogr. *60*, 2126–2132. 10.1107/S0907444904019158.

307. Liebschner, D., Afonine, P. V., Baker, M.L., Bunkoczi, G., Chen, V.B., Croll, T.I., Hintze, B., Hung, L.W., Jain, S., McCoy, A.J., *et al.* (2019). Macromolecular structure determination using X-rays, neutrons and electrons: Recent developments in Phenix. Acta Crystallogr. D Struct. Biol. *75*, 861–877. 10.1107/S2059798319011471.

308. Alvarez, L., Hernandez, S.B., de Pedro, M.A., and Cava, F. (2016). Ultra-Sensitive, High-Resolution Liquid Chromatography Methods for the High-Throughput Quantitative Analysis of Bacterial Cell Wall Chemistry and Structure. In Bacterial Cell Wall Homeostasis. Methods in Molecular Biology, HJ. Hong, ed., pp. 11–27.

309. Ducret, A., Quardokus, E.M., and Brun, Y. V. (2016). MicrobeJ, a tool for high throughput bacterial cell detection and quantitative analysis. Nat. Microbiol. *1*. 10.1038/nmicrobiol.2016.77.

310. Hartmann, R., van Teeseling, M.C.F., Thanbichler, M., and Drescher, K. (2020). BacStalk: A comprehensive and interactive image analysis software tool for bacterial cell biology. Mol. Microbiol. *114*, 140–150. 10.1111/mmi.14501.

311. Fleming, J., Magana, P., Nair, S., Tsenkov, M., Bertoni, D., Pidruchna, I., Lima Afonso, M.Q., Midlik, A., Paramval, U., Žídek, A., *et al.* (2025). AlphaFold Protein Structure Database and 3D-Beacons: New Data and Capabilities. J. Mol. Biol. *437*, 168967. 10.1016/j.jmb.2025.168967.

312. Jumper, J., Evans, R., Pritzel, A., Green, T., Figurnov, M., Ronneberger, O., Tunyasuvunakool, K., Bates, R., Žídek, A., Potapenko, A., *et al.* (2021). Highly accurate protein structure prediction with AlphaFold. Nature *596*, 583–589. 10.1038/s41586-021-03819-2.

313. Altschul, S.F., Gish, W., Miller, W., Myers, E.W., and Lipman, D.J. (1990). Basic Local Alignment Search Tool. J. Mol. Biol *215*, 403–410.

314. Bateman, A., Martin, M.J., Orchard, S., Magrane, M., Adesina, A., Ahmad, S., Bowler-Barnett, E.H., Bye-A-Jee, H., Carpentier, D., Denny, P., *et al.* (2025). UniProt: the Universal Protein Knowledgebase in 2025. Nucleic Acids Res. *53*, D609–D617. 10.1093/nar/gkae1010.

7. Supplementary material

Supplementary table 1. *Pseudomonas* species used for conservation analyses of Pch and CheA. *Pseudomonas* species together with corresponding gene numbers and UniProt accession numbers are indicated.

Species	Gene	UniProt accession number
Pch proteins		
Pseudomonas putida	PP_0337	Q88QZ7
Pseudomonas syringae	CT157_02420	A0A3T0JNA9
Pseudomonas fluorescens	PS854_04768	A0A5E7NS06
Pseudomonas lutea	LT42_18585	A0A9X0EDK6
Pseudomonas rhizosphaerae	LT40_17940	A0A089YXL7
Pseudomonas straminea	SAMN05216372_10918	A0A1I1XW62
Pseudomonas stutzeri	CXK94_19665	A0A2N8STA9
Pseudomonas juntendi	H4B97_21510	A0A7W2QW13
Pseudomonas aeruginosa	PA5017	Q9HUF2
CheA proteins		
Pseudomonas putida	PP_4338	Q88EW4
Pseudomonas syringae	ALO73_02783	A0A9X0H3Q1
Pseudomonas fluorescens	PS631_01394	A0A5E6R3K3
Pseudomonas lutea	LT42_08705	A0A9X0JKI1
Pseudomonas rhizosphaerae	LT40_02550	A0A089YIZ2
Pseudomonas straminea	SAMN05216372_103538	A0A1I1UR67
Pseudomonas stutzeri	CXK91_16825	A0A2S4AJI0
Pseudomonas juntendi	H4C80_22785	A0A7W2QB31
Pseudomonas aeruginosa	PA1458	G3XCT6
EAL domains of canonical PDEs		
Pseudomonas aeruginosa	PA4367 (BifA)	Q9HW35
Pseudomonas putida	PP_0386 (RmcA)	Q88QU8
Pseudomonas putida	PP_1154	Q88NQ1
Pseudomonas putida	PP_3182	Q88I20
Pseudomonas putida	PP_0165	Q88RG5

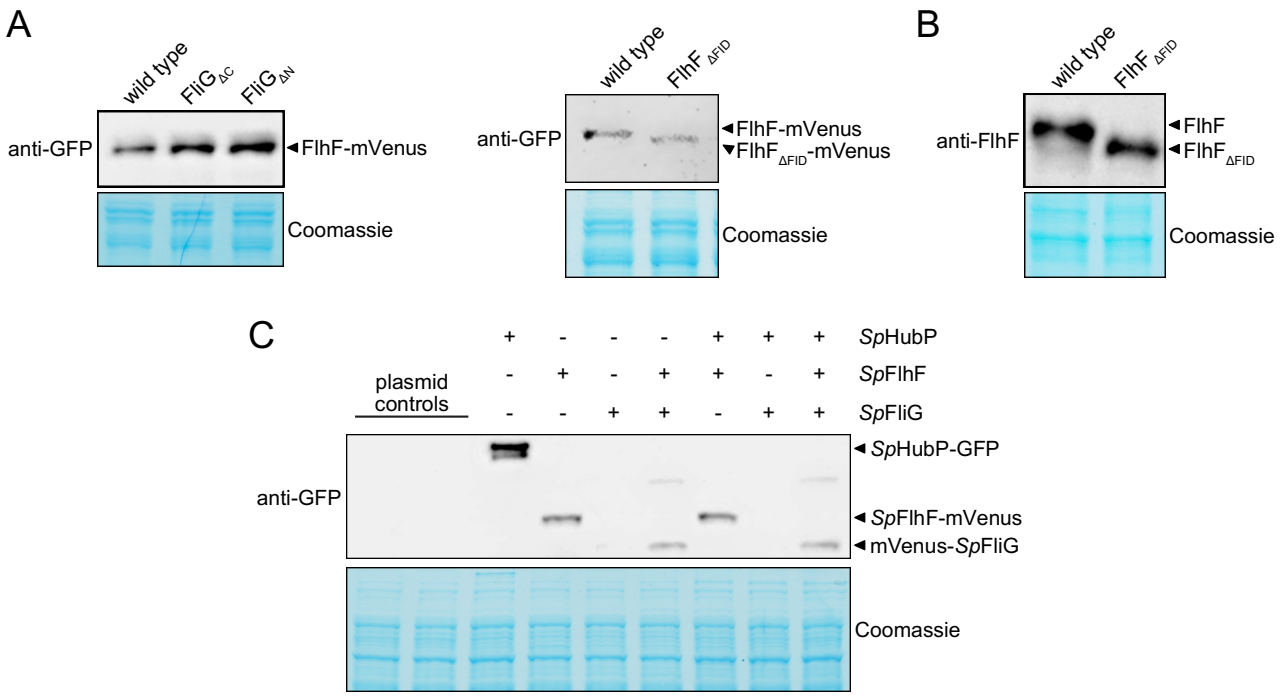

Supplementary figure 1. Expression and stability of *S. putrefaciens* fusion proteins. A Western Blot analysis (upper row) and Coomassie-stained SDS-PAGE (lower row) of the FlhF-mVenus fusion protein (~77 kDa) expressed in *S. putrefaciens* wild-type cells, cells lacking the N- or C-terminal region of FliG (left panel; $FliG_{\Delta N}$ and $FliG_{\Delta C}$, respectively) and cells lacking the FID domain of FlhF (right panel; $FlhF_{\Delta FID}$). An anti-GFP antibody was used to detect the fusion proteins. **B** Western Blot analysis (upper row) and Coomassie-stained SDS-PAGE (lower row) of FlhF (~45 kDa) expressed in *S. putrefaciens* wild-type cells or $FlhF_{\Delta FID}$. An anti-FlhF antibody was used for detection. **C** Western Blot analysis (upper row) and Coomassie-stained SDS-PAGE (lower row) of the *S. putrefaciens* fusion proteins *Sp*HubP-sfGFP (~147 kDa), *Sp*FlhF-mVenus (~77 kDa) and mVenus-*Sp*FliG (~65 kDa) expressed in *E. coli*. Plasmids pBAD33 and pBBR1-MCS2 were loaded as negative controls. An anti-GFP antibody was used to detect the fusion proteins. Adapted from [14].

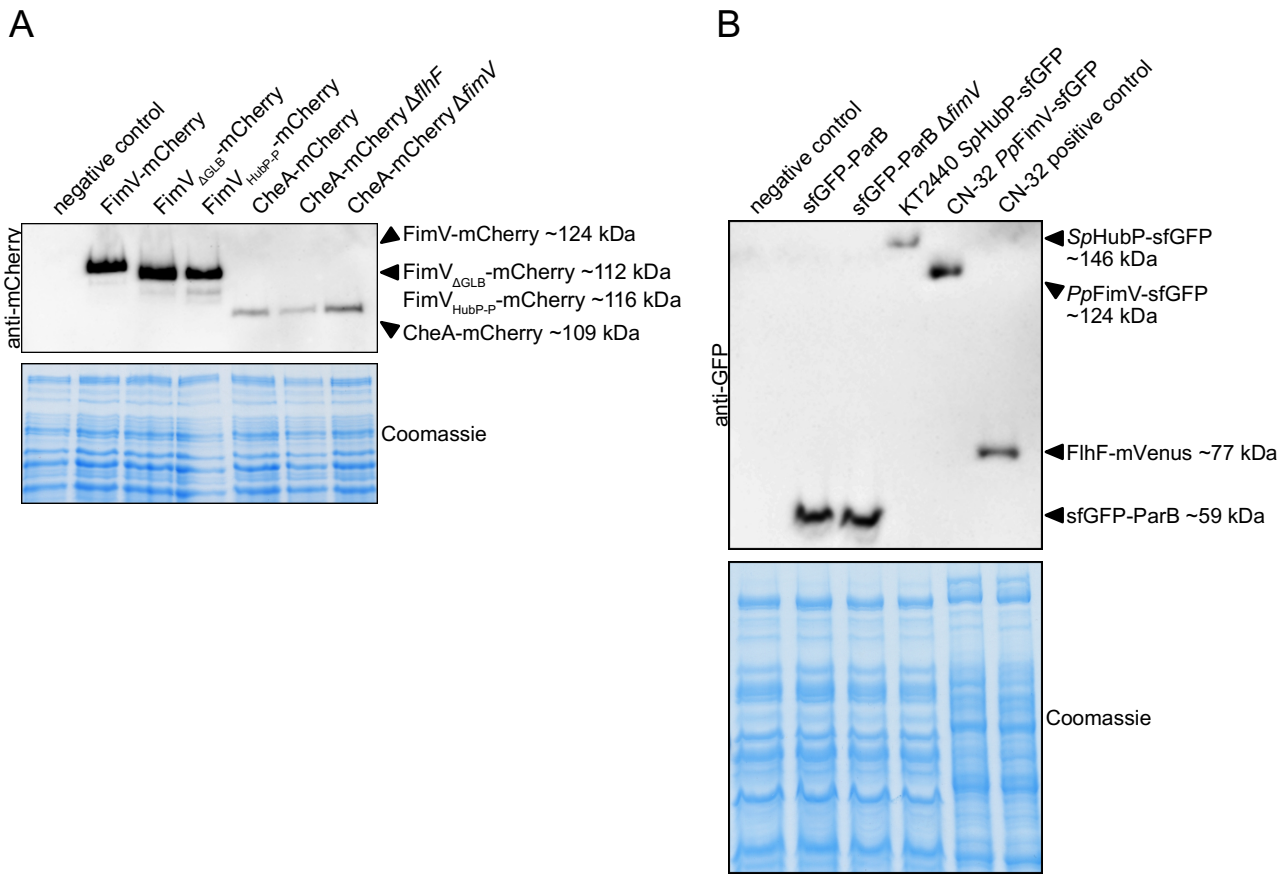

Supplementary figure 2. Expression and stability of *P. putida* fusion proteins. A Western Blot analysis (upper row) and Coomassie-stained SDS-PAGE (lower row) of FimV-mCherry and CheA-mCherry fusion proteins (~124 kDa and ~109 kDa, respectively) and its variants, expressed in *P. putida* KT2440 wild-type cells or deletion mutants. *P. putida* wild type was loaded as negative control. An anti-mCherry antibody was used to detect the fusion proteins. **B** Western Blot analysis (upper row) and Coomassie-stained SDS-PAGE (lower row) of sfGFP-ParB, *Sp*HubP-sfGFP and *Pp*FimV-sfGFP fusion proteins (~59 kDa, 146 kDa and ~124 kDa, respectively) expressed in *P. putida* KT2440 wild-type cells or deletion mutants and *S. putrefaciens* CN-32 wild-type cells. *P. putida* wild type was loaded as negative control and *S. putrefaciens* CN-32 FlhF-mVenus (~77 kDa) as positive control. An anti-GFP antibody was used to detect the fusion proteins. Adapted from [231].

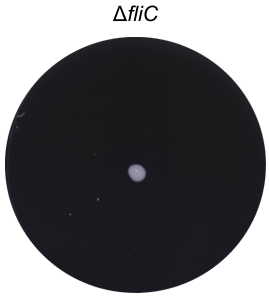

Supplementary figure 3. *fliC* deletion mutants show no swarming-like motility. Swarming-like motility assay of a *P. putida fliC* deletion mutant on a 0.5% PG-agar plate.

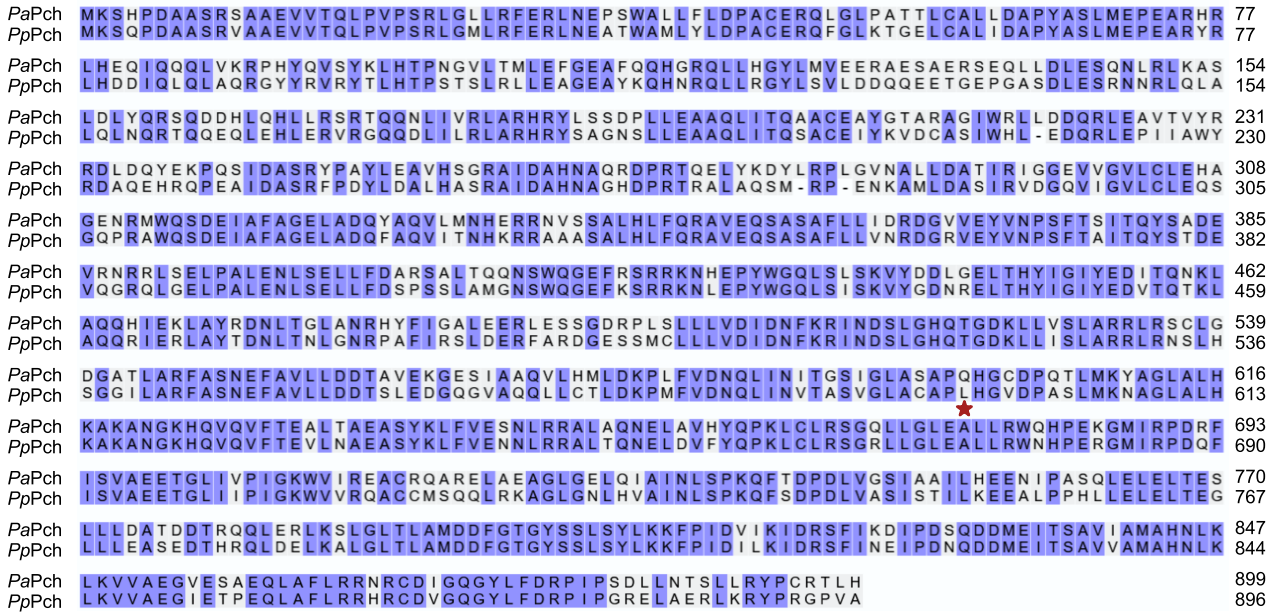

Supplementary figure 4. Sequence alignment of Pch from *P. aeruginosa* and *P. putida*. Sequence alignment of Pch from *P. aeruginosa* (*Pa*Pch, gene PA5017) and *P. putida* (*Pp*Pch, gene PP_0337) was done using the UniProt alignment tool. Identical amino acids are colored violet. Amino acids number are indicated on the right side. The conserved EAL motif is marked with a red star.

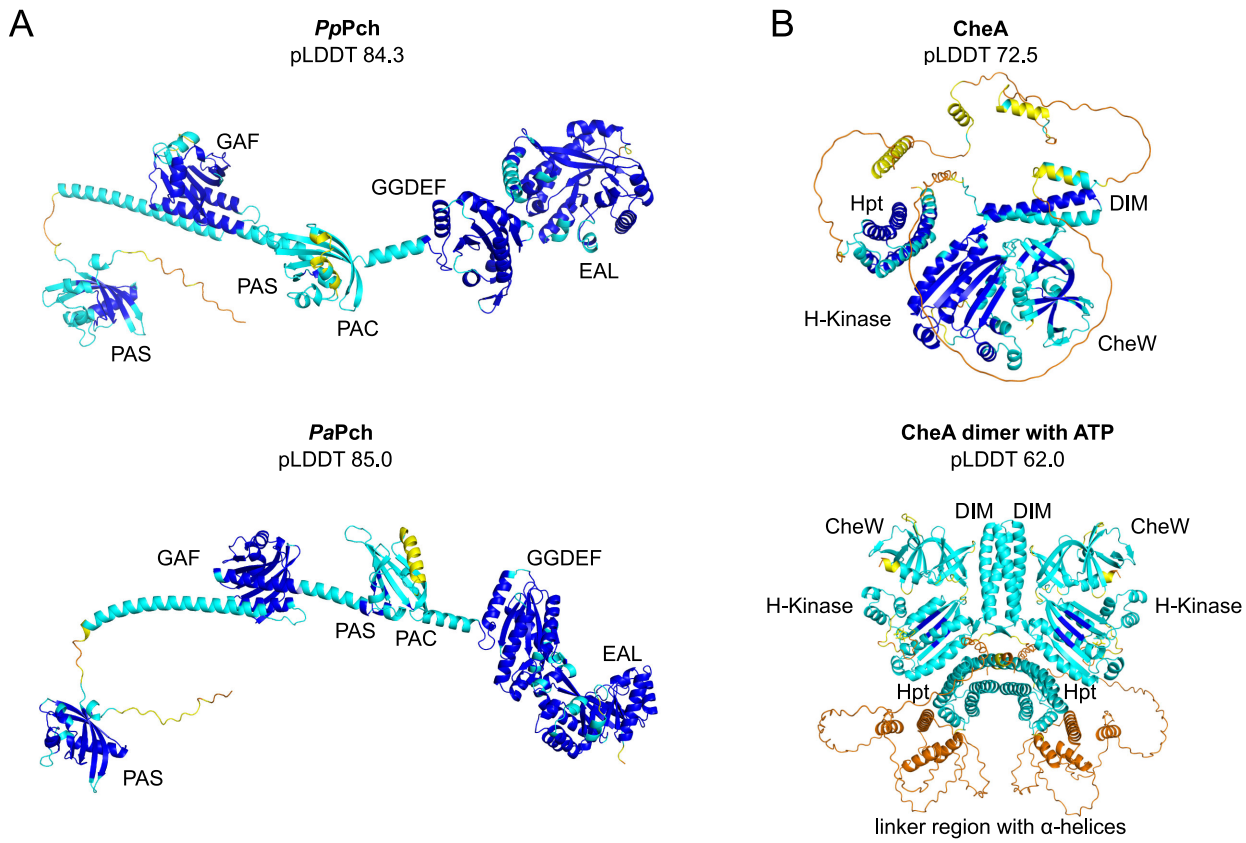

Supplementary figure 5. Structural predictions of Pch and CheA variants colored according to pLDDT score. A Structural prediction of Pch from *P. putida* (*Pp*Pch, upper panel) and *P. aeruginosa* (*Pa*Pch, lower panel). Domain abbreviations are as follows: N-terminal PAS-sensory domain, GAF domain, PAS-PAC module, GGDEF domain and C-terminal EAL domain. **B** Structural prediction of CheA from *P. putida* (upper panel) and the CheA homodimer in complex with ATP (lower panel). Domain abbreviations are as follows: N-terminal histidine phosphotransfer domain (Hpt), dimerization domain (DIM), histidine kinase domain (H-Kinase) and C-terminal CheW-like domain. All structural predictions were generated using AlphaFold3. The overall pLDDT score is indicated and was calculated as the mean of all atom-wise pLDDT values (number of atoms: *Pp*Pch: 7090; *Pa*Pch: 7137; CheA: 5593, CheA dimer with ATP: 11248). Color coding indicates model confidence as follows: very high (dark blue, pLDDT >90), confident (light blue, 90> pLDDT >70), low (yellow, 70> pLDDT >50) and very low (orange, pLDDT <50).

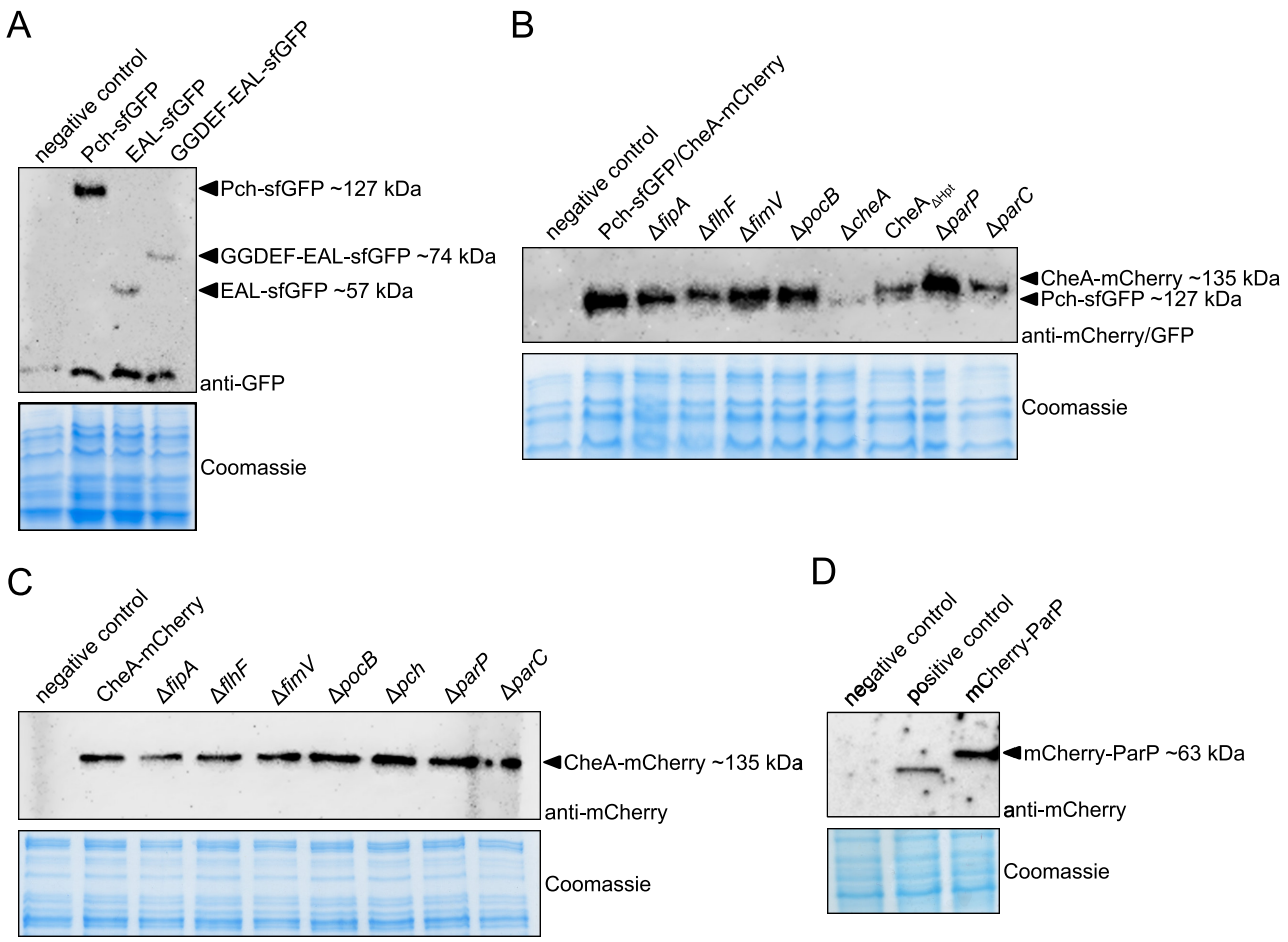

Supplementary figure 6. Expression and stability of *P. putida* fusion proteins. A Western Blot analysis (upper row) and Coomassie-stained SDS-PAGE (lower row) of Pch-sfGFP fusion proteins expressed (~127 kDa, ~74 kDa and ~57 kDa, respectively) in *P. putida* KT2440 wild-type cells. *P. putida* wild type was loaded as negative control. **B** Western Blot analysis (upper row) and Coomassie-stained SDS-PAGE (lower row) of Pch-sfGFP and CheA-mCherry fusion proteins (~127 kDa and ~135 kDa, respectively) expressed in *P. putida* KT2440 wild-type cells or deletion mutants. **C** Western Blot analysis (upper row) and Coomassie-stained SDS-PAGE (lower row) of CheA-mCherry fusion proteins (~135 kDa) expressed in *P. putida* KT2440 wild-type cells or deletion mutants. **D** Western Blot analysis (upper row) and Coomassie-stained SDS-PAGE (lower row) of the mCherry-ParP fusion protein (~63 kDa) expressed in *P. putida* KT2440 wild-type cells. *P. putida* wild type was loaded as negative control. Anti-GFP and anti-mCherry antibodies were used to detect the fusion proteins.

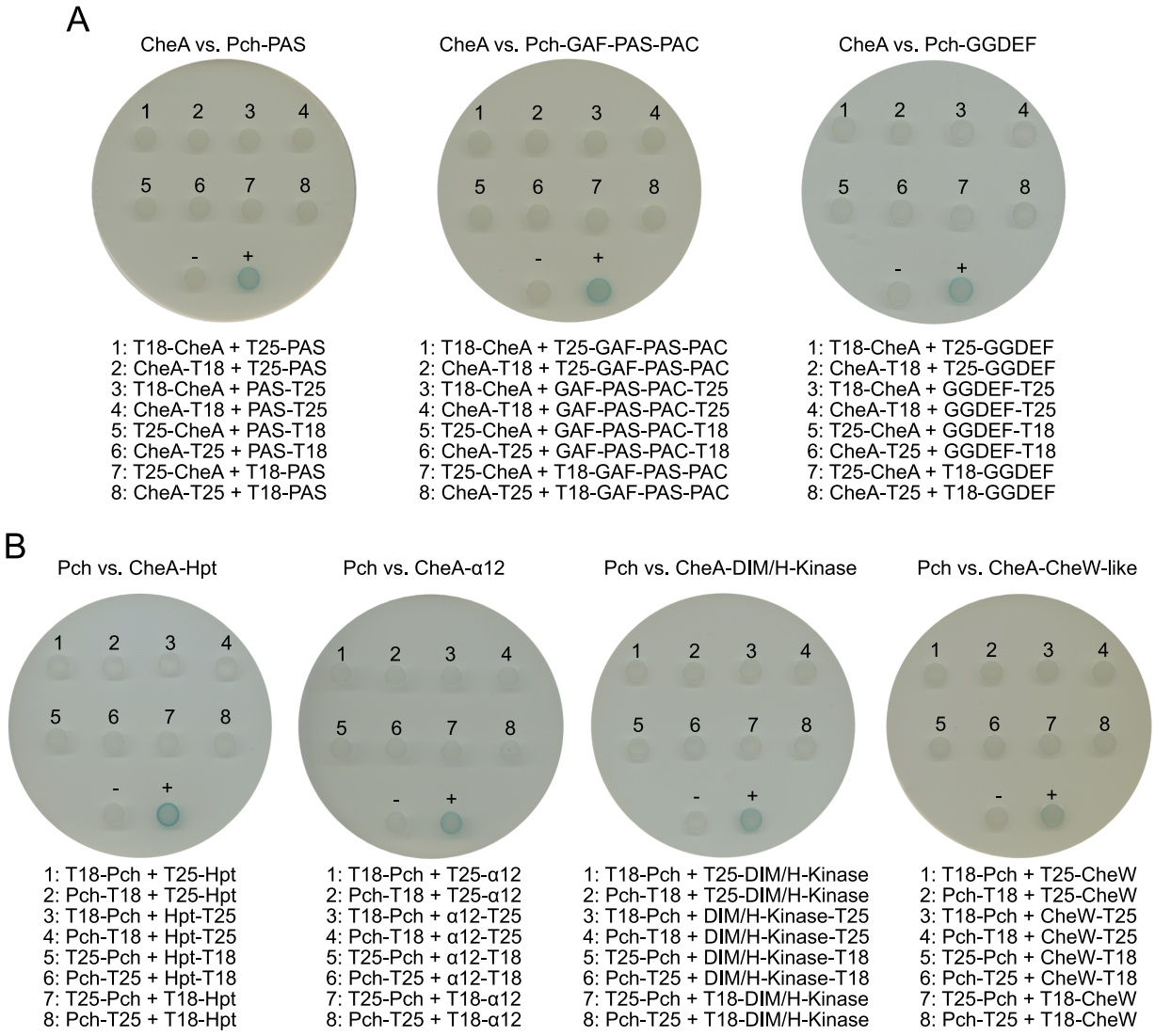

Supplementary figure 7. Non-interacting parts of CheA and Pch. Bacterial two-hybrid analysis showing interactions between **A** CheA and the Pch PAS domain, the Pch GAF-PAS-PAC domains and the GGDEF domain, **B** Pch and the CheA Hpt domain, the linker region with α-helices 1 and 2, the dimerization histidine kinase domain and the CheW-like domain. Proteins were fused either N- or C-terminally to the T18 or T25 fragment of the catalytic domain of *Bordetella pertussis* adenylate cyclase. Blue coloration of colonies indicates reconstitution of adenylate cyclase activity and subsequent conversion of X-Gal, thereby indicating protein-protein interaction. "+" indicates the positive control and "-" the negative control. Data from at least two independent experiments are shown.

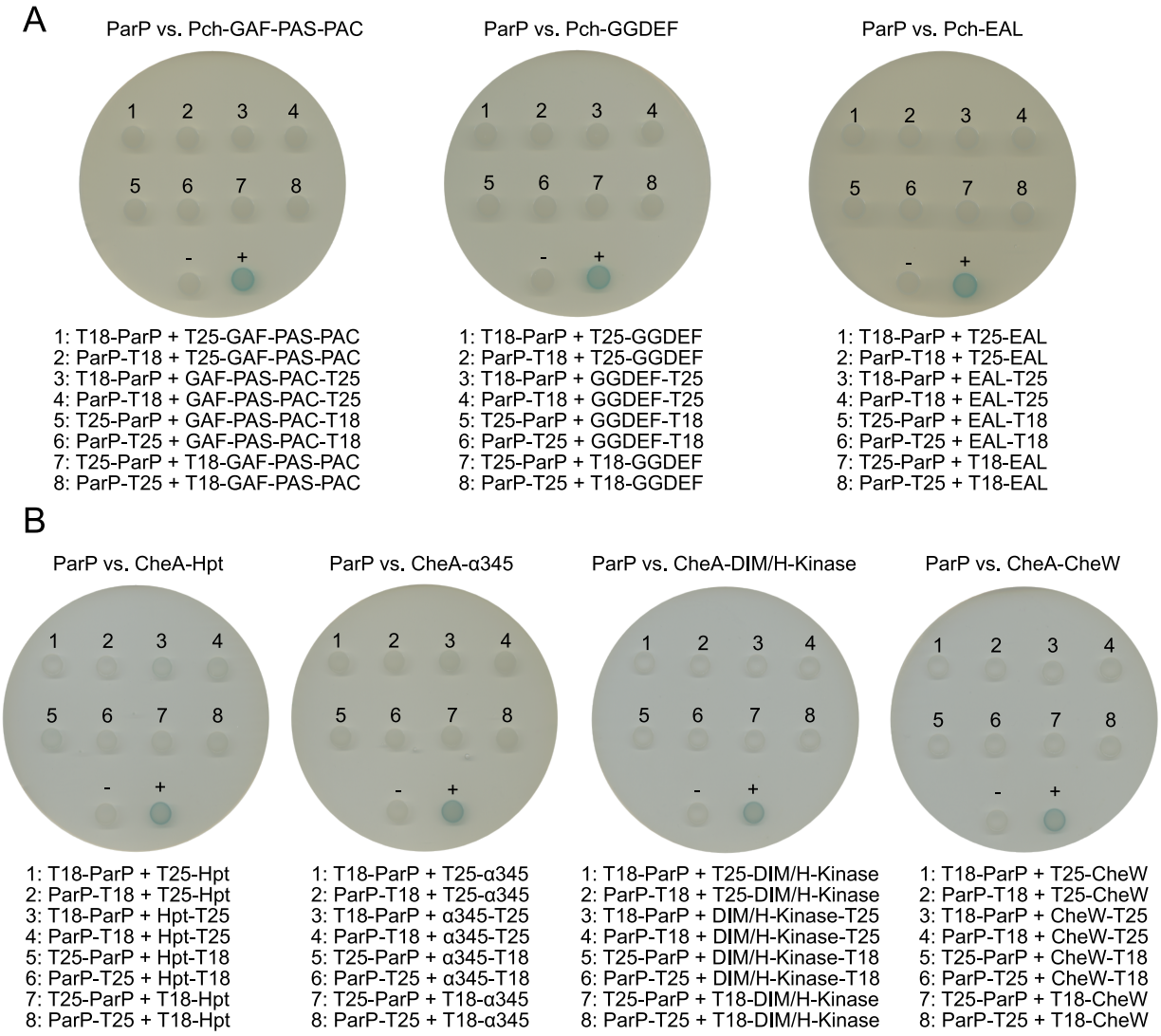

Supplementary figure 8. Non-interacting parts of CheA and Pch with ParP. Bacterial two-hybrid analysis showing interactions between **A** ParP and the Pch GAF-PAS-PAC domains, the GGDEF domain and the EAL domain, **B** ParP and the CheA Hpt domain, the linker region with α-helices 3-5, the dimerization histidine kinase domain and the CheW-like domain. Proteins were fused either N- or C-terminally to the T18 or T25 fragment of the catalytic domain of *Bordetella pertussis* adenylate cyclase. Blue coloration of colonies indicates reconstitution of adenylate cyclase activity and subsequent conversion of X-Gal, thereby indicating protein-protein interaction. "+" indicates the positive control and "-" the negative control. Data from at least two independent experiments are shown.

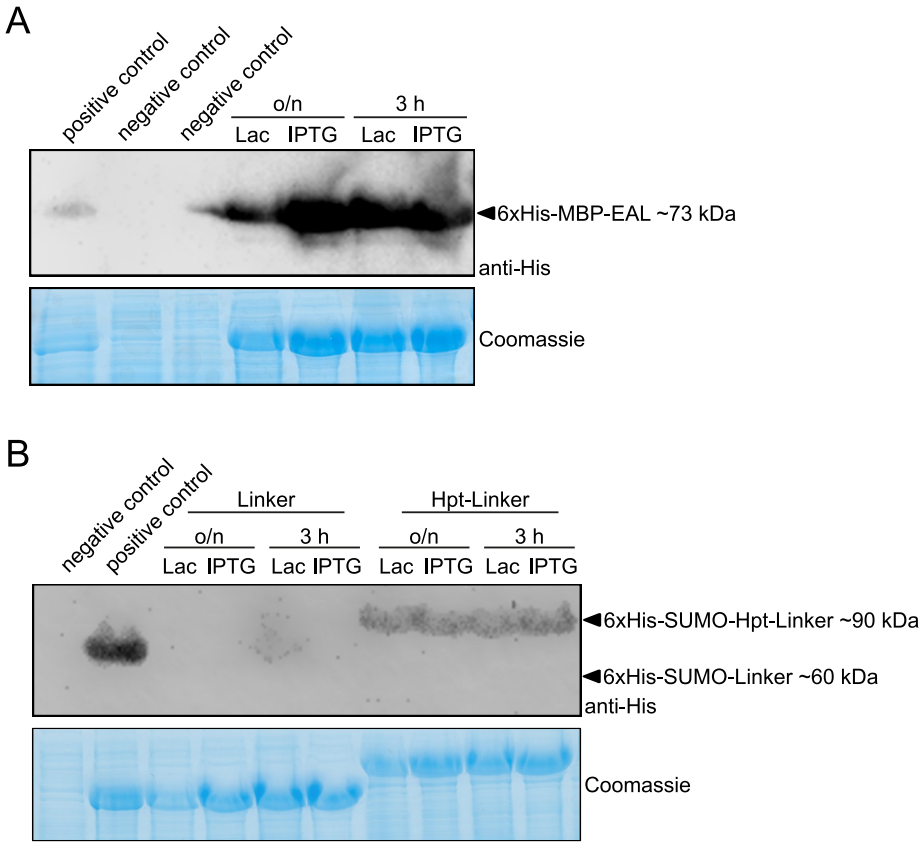

Supplementary figure 9. Expression and stability of overexpressed *P. putida* proteins in *E. coli*. Western Blot analyses (upper panels) and Coomassie-stained SDS-PAGEs (lower panels) of **A** the 6x-His-MBP-tagged Pch EAL domain fusion protein (~73 kDa) and **B** the 6x-His-SUMO-tagged linker or Hpt-linker fusion proteins (~60 kDa and 90 kDa) expressed in *E. coli* BL21. Protein expression was induced either with 1% lactose (Lac) or with 0.5 mM IPTG for three hours at 37°C or overnight at 16°C to identify optimal overexpression conditions. An anti-His antibody was used to detect the fusion proteins.

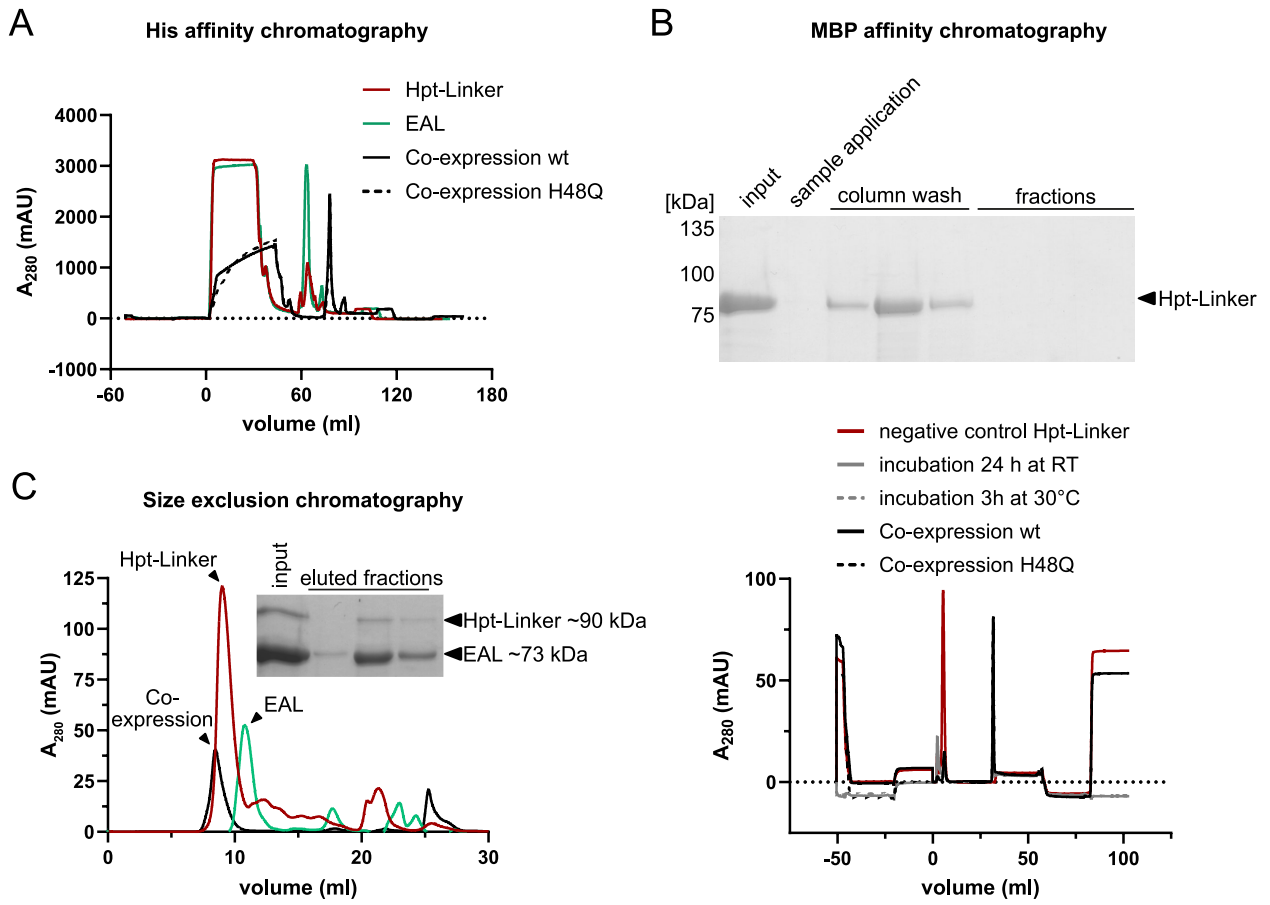

Supplementary figure 10. Purification chromatograms. Chromatograms obtained from **A** Ni-NTA-based affinity chromatography and **B** MBP-based affinity chromatography, including Coomassie-stained SDS-PAGE of the CheA Hpt-linker domain used as negative control. **C** Size-exclusion chromatography chromatogram of co-expressed proteins with corresponding Coomassie-stained SDS-PAGE analysis of peak fractions shown in the inset.

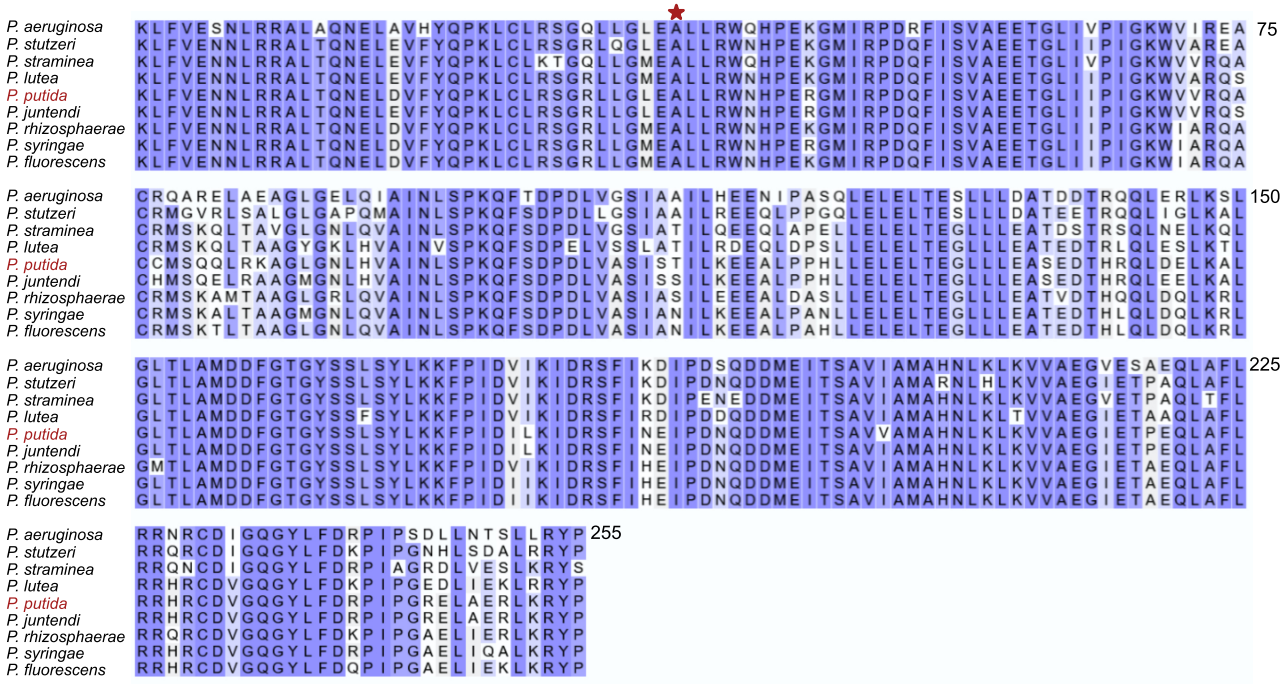

Supplementary figure 11. Sequence alignment of the *P. putida* Pch EAL domain with homologous Pch EAL domains. Sequence alignment of the Pch EAL domain from *P. putida* with homologous Pch EAL domains from other *Pseudomonas* species was performed using the UniProt alignment tool. Identical amino acids are highlighted in violet. Amino acid positions are indicated on the right. The conserved EAL motif is marked with a red star.

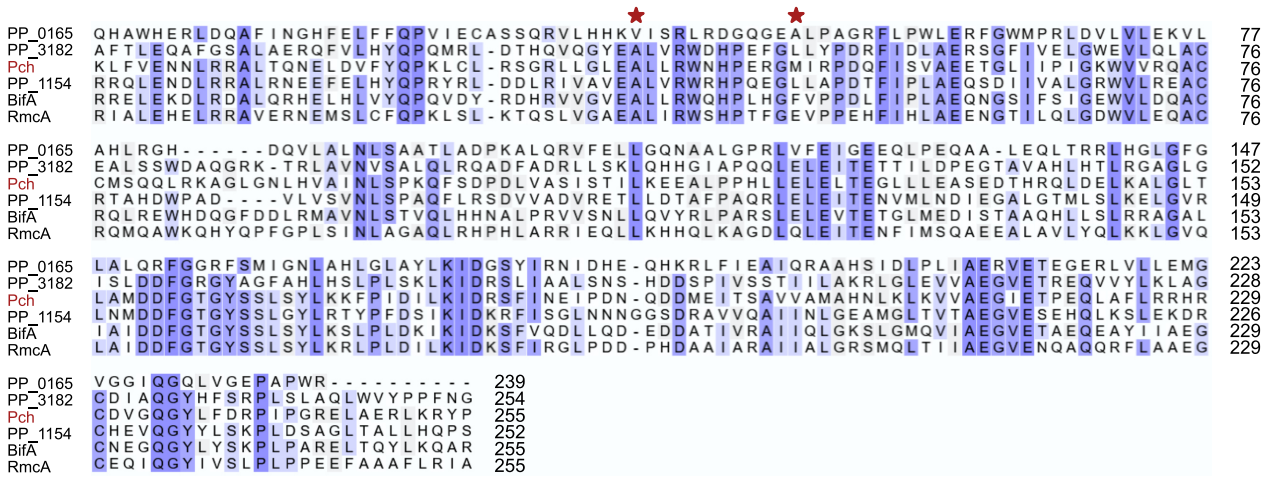

Supplementary figure 12. Sequence alignment of the *P. putida* Pch EAL domain with EAL domains of canonical PDEs. Sequence alignment of the Pch EAL domain from *P. putida* with EAL domains from canonical PDEs was performed using the UniProt alignment tool. Identical amino acids are highlighted in violet. Amino acid positions are indicated on the right. The conserved EAL motif is marked with a red star.

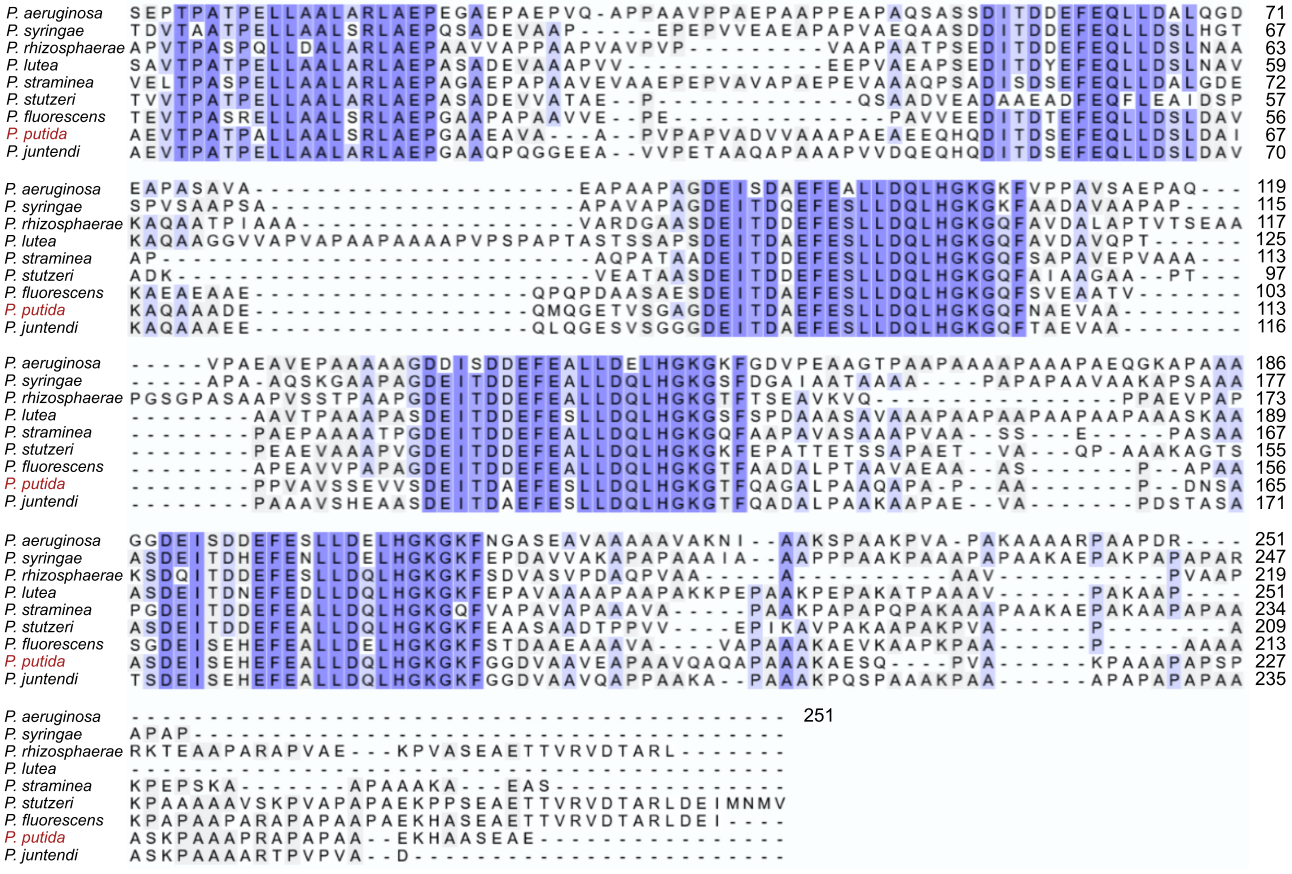

Supplementary figure 13. Sequence alignment of the *P. putida* CheA linker region with CheA linker regions from other *Pseudomonas* species. Sequence alignment of the CheA linker region from *P. putida* with CheA linker regions from other *Pseudomonas* species was performed using the UniProt alignment tool. Identical amino acids are highlighted in violet. Amino acid positions are indicated on the right.

8. Acknowledgements

As with many things in life, a major project such as a doctoral thesis cannot be accomplished alone. It is impossible to adequately thank all the people who have supported me over the past few years as a doctoral candidate, but I would like to try nonetheless.

First and foremost, my deepest gratitude goes to my supervisor, Kai. Having known me since my time as a student, you did not hesitate to welcome me into your research group as a doctoral candidate. Throughout my doctoral studies, you continuously supported me and never doubted my abilities. I greatly valued our collaboration and the many scientific discussions we had, as well as your warm and understanding manner, which I will always remember with a smile. Thank you for giving me this opportunity and for supporting me throughout my doctoral journey!

I would also like to thank Prof. Dr. Till Schäberle for serving as my second examiner, as well as Prof. Dr. Bork Berghoff and PD Dr. habil. Oliver Rossbach for participating in my examination committee.

My thanks also go to the Bange laboratory and Dr. Anke Treuner-Lange in Marburg, and the Govantes laboratory in Seville for the successful collaborations and the resulting publications. I would also like to thank Paul for his valuable support of my research and for the enjoyable and productive collaboration during his Master's studies.

Special thanks also go to the entire Institute of Microbiology and Molecular Biology for the enjoyable and supportive working atmosphere, as well as for the many get-togethers over cake and pizza. I am also very grateful to Sophie and Theresa for the wonderful moments we shared throughout my studies and doctoral years, and for all the unforgettable VAAM parties. I would particularly like to thank all former and current members of the Thormann research group. Thank you, Sandra, for the seamless organization of absolutely everything! Thank you, Nicole, Vanessa, and Svenja, for welcoming me so warmly and supporting me so enthusiastically, especially in the early days, and for the friendships that have developed along the way. Thanks also to Fred, Dodo, and Felix - with you, it was never boring, and even on difficult days you always managed to make me laugh. My thanks also go to Ulrike, Andrea, and Rolf for their tireless support in the lab; without you, I am sure I would have lost a clone or two.

Another heartfelt thank you goes to my friends, who always patiently listened to my endless talk about my doctoral studies and tried to contribute their thoughts and support. I would particularly like to mention my partner in crime in the lab, Alina. I am incredibly grateful that our time together in the Thormann group has made us not only colleagues but true friends. Thank you for our many scientific discussions (even if we often ended up with even more questions), the great musical entertainment

in the lab, and the shared comfort food that kept us going. I have rarely felt so in sync with anyone as I do with you, and your patience, encouragement, and support kept me sane - and laughing - through it all. I am already looking forward to many more concert visits, vacations, and shared plates of mango sticky rice!

Last but not least, I am deeply grateful to my family. Without your support and encouragement, I would not have become the person I am today and would likely have stumbled at one hurdle or another along the way. I would also like to express my deepest gratitude to Daniel. Thank you for being my safe haven, for always listening to me without judgment, and for your patience, love, and unwavering support throughout my doctoral studies and beyond. Finally, I would like to thank my fluffy family members, Freya and Gracie, who faithfully stayed by my side (or directly in front of the computer) while I was writing my dissertation and always manage to put a smile on my face. Especially during the last year, all of you gave me the energy I needed to keep going and truly make it through.

9. Selbstständigkeitserklärung

Ich erkläre: Ich habe die vorgelegte Dissertation selbstständig und ohne unerlaubte fremde Hilfe und nur mit den Hilfen angefertigt, die ich in der Dissertation angegeben habe. Alle Textstellen, die wörtlich oder sinngemäß aus veröffentlichten Schriften entnommen sind, und alle Angaben, die auf mündlichen Auskünften beruhen, sind als solche kenntlich gemacht. Ich stimme einer evtl. Überprüfung meiner Dissertation durch eine Antiplagiat-Software zu. Bei den von mir durchgeführten und in der Dissertation erwähnten Untersuchungen habe ich die Grundsätze guter wissenschaftlicher Praxis, wie sie in der „Satzung der Justus-Liebig-Universität Gießen zur Sicherung guter wissenschaftlicher Praxis“ niedergelegt sind, eingehalten.

Angaben zu auf künstlicher Intelligenz (KI) basierender Hilfen wie ChatGPT oder SchulKI von OpenAI oder Gemini von Google zur Erstellung meiner Dissertation (Zutreffendes angekreuzt):

☐ Ich habe bei der Erstellung dieses Textes kein KI-Tool verwendet.

☐ Ich habe ein KI-Tool in den folgenden Bereichen eingesetzt (Mehrfachnennungen möglich):

- ☐ Ideen finden, meine Kreativität anregen
- ☐ Verstehen von Konzepten, Recherche von Fakten und Definitionen
- ☐ Optimierung eines von mir verfassten Textes
- ☐ Erstellen ganzer Textpassagen nach meinen Vorgaben

Folgende KI-Tools habe ich verwendet, damit aufgeführte Teile meines Textes von dem Tool wie folgt profitiert haben:
DeepL und ChatGPT wurden zur Übersetzung und Verbesserung der englischen Texte sowie zur Literatur- und Informationsrecherche verwendet.

Datum	Unterschrift